



A Multifunctional Design Approach for Sustainable Concrete

With Application to Concrete Mass Products

Götz Hüsken

/ faculty of architecture building and planning tu eindhoven

bouwstenen

148

A MULTIFUNCTIONAL DESIGN APPROACH FOR SUSTAINABLE CONCRETE

With Application to Concrete Mass Products

Götz Hüskens

De promotiecommissie is als volgt samengesteld:

Voorzitter:

prof.ir. J. Westra

Technische Universiteit Eindhoven

Promotor:

prof.dr.ir. H.J.H. Brouwers

Technische Universiteit Eindhoven

Leden (in alfabetische volgorde):

prof.dr.ir. D.A. Hordijk

Technische Universiteit Eindhoven

prof.dr.ir. J.J.N. Lichtenberg

Technische Universiteit Eindhoven

Prof. Dr. rer. nat. B. Meng

Bundesanstalt für Materialforschung und -prüfung

dr.ir. S.P.G. Moonen

Technische Universiteit Eindhoven

Prof. Dr. Dr. H. Pöllmann

Martin-Luther-Universität Halle-Wittenberg

Prof. Dr.-Ing. Prof. h.c. Dr.-Ing. E.h.

H.-W. Reinhardt

Universität Stuttgart



CIP-DATA LIBRARY TECHNISCHE UNIVERSITEIT EINDHOVEN

A Multifunctional Design Approach for Sustainable Concrete - With Application to Concrete Mass Products / by Götz Hüsken.

ISBN 978-90-6814-631-8

Bouwstenen 148

NUR 955

Copyright © 2010 by Götz Hüsken

Ph.D. Thesis, Eindhoven University of Technology, The Netherlands.

Cover design: Grafische Studio Bouwkunde, Eindhoven University of Technology, The Netherlands.

Printed by: Universiteitsdrukkerij, Eindhoven University of Technology, The Netherlands.

All rights reserved. No part of this publication may be reproduced, stored in a retrieval system or transmitted by any means, electronical, mechanical, photocopying, recording or otherwise without the prior written permission of the author.

Cover photograph supplied originally by Lithonplus GmbH & Co. KG - Germany

Typeset with the L^AT_EX Documentation System.

Author e-mail: goetz.huesken@gmx.de

A Multifunctional Design Approach for Sustainable Concrete
With Application to Concrete Mass Products

PROEFSCHRIFT

ter verkrijging van de graad van doctor aan de
Technische Universiteit Eindhoven, op gezag van de
rector magnificus, prof.dr.ir. C.J. van Duijn, voor een
commissie aangewezen door het College voor
Promoties in het openbaar te verdedigen
op woensdag 17 november 2010 om 16.00 uur

door

Götz Hüsken

geboren te Eisenach, Duitsland

Dit proefschrift is goedgekeurd door de promotor:

prof.dr.ir. H.J.H. Brouwers

In honor of my mother, Ingrid Hüskén, née Wilhelm
In honor and in loving memory of my father, Gerd Hüskén

Preface

Basically, most of the people that have done a Ph.D. say that it expands your horizons through a combination of scientific research and gaining experience of life. Both things are not possible without the help of other people. Colleagues, external partners, my family and friends gave me a lot of support during my time in the Netherlands and encouraged me in my work, of which the outcome is this thesis. My sincerest thanks go to all of them but I also want to address some people in particular. First of all, I would like to gratitude my supervisor, Jos Brouwers, for giving me the opportunity to start my Ph.D. research at the Department of Construction, Management and Engineering at the University of Twente. His guidance and critical evaluation helped me to understand the way of scientific work. Thank you for all the support, freedom, trust, and patience to build up this thesis.

I also appreciate the financial support of the European Commission (6th FP Integrated Project “I-STONE”, Proposal No. 515762-2) and the members of our sponsor group who funded my research activities. I would like to express my special gratitude to ing. Jan Smith (Rokramix Enschede B.V.) and ing. Henk ter Welle (Betoncentrale Twenthe B.V.) for their support in practical knowledge, materials and assistance in material testing. Furthermore, I would like to thank drs. Peter Bontrup (Grانيت Import Benelux B.V.) for his creative thinking and the trust he showed in allowing me to present our research at the I-STONE meetings on his behalf, and Mr. Boudewijn Piscaer for his interest in the research of our group and the fruitful discussions on the right definition of the term ‘binder’.

I also want to thank prof.dr.ir. D.A. Hordijk and prof.dr.ir. J.J.N. Lichtenberg (Technische Universiteit Eindhoven) for their comments on the thesis and for agreeing to be on my Ph.D. committee. I would also like to thank my external examiners Prof. Dr. rer. nat. B. Meng (Bundesanstalt für Materialforschung und -prüfung), Prof. Dr. Dr. H. Pöllmann (Martin-Luther-Universität Halle-Wittenberg) as well as Prof. Dr.-Ing. Prof. h.c. Dr.-Ing. E.h. H.-W. Reinhardt (Universität Stuttgart) for their examination of this thesis. Furthermore, I would like to thank Przemek Spiesz for his comments and the careful reading of this thesis.

Ik ben blij dat ik na mijn afstuderen in de vakgroep Bouw/Infra terecht ben gekomen, waar ik nog tot 1 september 2009 werkte. Het was een prettige tijd. Mijn hartelijke dank aan alle mensen in de vakgroep en aan de faculteit. In het bijzonder wil ik bedanken drs. ing. Hans Boes voor de blooper mailtjes, dr. ir. Henny ter Hueme voor zijn discussies over het leven in het algemeen en speciaal, ing. Gerrit Snellink voor zijn technische ondersteuning, ir. Bram Entrop voor de discussies over onze tegengestelde smaak wat betreft films, Yolanda Bosch voor haar introductie “hoe het werkt” en voor de snoep in het secretariaat. Met Maarten Rutten, Erwin Hofman en Roy Visser was het heerlijk fietsen door de bossen rond Enschede. Bedankt! Norbert Spikker, Jacob Dogger en de Theo’s gaven mij een introductie in het frezen, draaien en lassen van staal. Hun vertrouwen in mij, dat ik bij het flansen in de metaalwerkplaats niets kapot zou maken, heb ik ook zeer op prijs gesteld. “Den Supermeister” en voorzitter van de IAF, dr. ir. Laurent Warnet wil ik heel bijzonder bedanken. Mijn dank ook aan alle AIOs van de vakgroep Bouw/Infra voor de gezelligheid en alle activiteiten als klimmen, paintballen en Grolsch drinken, die wij samen ondernomen hebben. De tijd in Enschede was de mooiste ervaring uit mijn leven. Die tijd had ik nooit willen missen.

Hierbij bedank ik ook de mensen van de unit bouwfysica voor de warme ontvangst in Eindhoven en aan de TU/e. In het bijzonder Renée van Geene voor de hulp bij mijn verhuizing, ing. Jan Diepens en Peter Cappon voor de ondersteuning in ons bouwfysisch lab, ir. Hans Lamers en Rien Canters voor de uitstekende faciliteiten om lekker beton te maken in hun materialen-

lab. Ook wil ik prof.dr.ir. D.A. Hordijk en dr.ir. S.P.G. Moonen bedanken voor de mogelijkheid om mijn kennis over beton in hun projecten in te brengen. Het verhuizen van Enschede naar Eindhoven is hierdoor soepel verlopen. Tenslotte mijn excuus aan al die mensen in Enschede, Eindhoven en in de rest van Nederland voor mijn prille Nederlands. Soms was mijn vooruitgang in het Nederlands "schlimm".

Now I would like to thank my friends. Dr. Wei Chen my good friend and colleague during the first one and a half years of my work in Enschede (Wenbin and Wei, I will always remember your hospitality and the open door at your home), Sergei Miller for discovering the similarities of bituminous and cementitious bound composite materials while enjoying Trudy's delicious way to compose foodstuffs in a South African curry, and Jimmy Avendano Castillo for allowing me to convince him that apples are more healthy.

Martin, you started first in Enschede and you finished first – so I can only repeat the words of your acknowledgement with total agreement and say thank you very much for your gratitude. Without hinting me at the vacant position, I probably would not have started a Ph.D. project. So, thank you also for all the trouble involved in doing a Ph.D., but also thanks a lot for all the happy and great moments we shared together at work and in our spare time. Once we were philosophizing "what will be in ten years from now", which is already 12 years ago, and I can state now that this is difficult to predict – like concrete sometimes – but I wish you all the best for the future and hope to see you in more than x times ten years from now still healthy and happy.

Leider sind die vergangenen 5 Jahre und meine Zeit in den Niederlanden nicht nur durch fröhliche Ereignisse geprägt worden. Im November 2008 wurde meine Arbeit zum dritten Mal durch den Tod eines nahen Familienangehörigen überschattet. Viel zu früh und völlig unerwartet verstarb mein Vater, Gerd Hüskén. Er wurde inmitten der Kriegswirren geboren und verbrachte den Großteil seines Lebens in einem Staat, der die Freiheit seiner Bürger nur durch Grenzen zu bewahren wusste. Diese Erfahrung und seine Ausbildung als Ökonom ließen ihn die Bedeutung einer einheitlichen Währung in einem vereinten Europa erkennen und meine Teilnahme an Meetings in Partnerländern des I-STONE Projekts war für ihn so selbstverständlich, wie eine Fahrt von Eisenach nach Herleshausen. Auch wenn er den Tag meiner Verteidigung nicht mehr miterleben durfte, hat er das Entstehen und Erscheinen dieser Arbeit in entscheidendem Maße beeinflusst. Für seine Unterstützung und seinen Einfluss auf meine Person werde ich ihn immer in dankbarer Erinnerung behalten.

Ich möchte mich auch bei meiner Mutter, Ingrid Hüskén, für all ihre Fürsorge und ihr Verständnis, das sie über Jahre hinweg für mich aufgebracht hat, bedanken. Die vergangenen zwei Jahre waren eine schwere Zeit für uns beide. Ein Dank sei an dieser Stelle auch meiner Tante, Sigrid Hüskén, ausgesprochen. Ferner möchte ich Herrn Lutz Böttger für seine tatkräftige Unterstützung bei der Wartung unserer „alten Dame“ und seinen unerschöpflichen Erfahrungsschatz im Bereich der Wasserturbinen danken. Ein Wort des Dankes gilt auch Otto für seine Hilfe, wenn sie dringend gebraucht wurde, und Sylvia für ihre aufmunternde Art.

I wish everyone health and all the best for the future.

Götz Hüskén

Eindhoven, October 2010

Contents

Preface	i
1 Introduction	1
1.1 Concrete mass products	1
1.2 Properties of earth-moist concrete	2
1.2.1 Fresh concrete properties	3
1.2.2 Green-strength	4
1.2.3 Hardened concrete properties	5
1.3 Sustainability in concrete production	6
1.3.1 Use of cement and concrete in the construction industry	6
1.3.2 Sustainability versus durability	9
1.3.3 Application of stone waste materials	11
1.3.4 Utilization of recycled construction rubble in concrete production	12
1.4 Outline of the thesis	13
2 Test procedures and material characterization	15
2.1 Introduction	15
2.2 Characterization techniques for aggregates and fines	16
2.2.1 Particle size analysis	16
2.2.2 Density measurements and related parameters	18
2.2.3 Determination of moisture content	19
2.3 Characteristics of aggregates	19
2.3.1 Coarse aggregates	20
2.3.2 Fine aggregates	20
2.4 Characteristics of recycled aggregates	20
2.4.1 Chemical composition	21
2.4.2 Water absorption	22
2.5 Characteristics of stone waste materials	23
2.5.1 Premix 0-4	23
2.5.2 Filter cake	25
2.5.3 Comparison with conventional materials	26
2.6 Characteristics of fines	28
2.6.1 Cements	28
2.6.2 Fillers	29
2.6.3 Characteristics of photocatalytic materials	30
2.7 Workability tests for earth-moist concrete	30

2.7.1	Degree of compaction	31
2.7.2	Proctor test	33
2.7.3	CemTec test	34
2.7.4	IC-test	35
2.8	Conclusions	38
3	Particle packing – Models and ideas	39
3.1	Introduction	39
3.2	Principles in particle packing	40
3.2.1	General definitions	40
3.2.2	Monosized particles	41
3.2.3	Discrete bimodal mixtures	42
3.2.4	Multimodal mixtures	46
3.2.5	Continuously graded particle	47
3.3	Effects of improved particle packing on mortar and concrete	49
3.3.1	Packing of discrete bimodal aggregate mixtures	50
3.3.2	Utilization of the modified Andreasen and Andersen equation for aggregate mixtures	53
3.3.3	Optimized packing of the fines	56
3.3.4	Discussion	63
3.4	Conclusions	64
4	Mix design concept for earth-moist concrete	65
4.1	Introduction	65
4.2	Mix design concepts and their influence on particle packing	66
4.2.1	Requirements on particle packing and concrete mix design	66
4.2.2	Particle packing in present concrete mix design	68
4.2.3	New mix design concept	70
4.3	Optimization algorithm	73
4.3.1	Target function	74
4.3.2	Variables	75
4.3.3	Constraints	75
4.3.4	Solution	77
4.4	Experimental validation	78
4.4.1	Trial mixes	78
4.4.2	Fresh concrete tests	79
4.4.3	Hardened concrete tests	81
4.4.4	Discussion	82
4.5	Conclusions	84
5	Utilization of alternative materials	85
5.1	Introduction	85
5.2	Stone waste materials	86
5.2.1	Mix design	87
5.2.2	Mortar tests	89

5.2.3	Concrete tests	91
5.3	Recycled concrete fines	94
5.3.1	Composition of tested mortars	94
5.3.2	Mortar tests	95
5.4	Recycled concrete aggregates	98
5.4.1	General aspects on the shrinkage of concrete	98
5.4.2	Mode of action of internal curing agents	100
5.4.3	Composition of tested mortars	101
5.4.4	Mortar tests	102
5.4.5	Shrinkage tests	104
5.5	Conclusions	108
6	Early-age behavior of earth-moist concrete	109
6.1	Introduction	109
6.2	Interparticle forces	110
6.2.1	Electrostatic forces	110
6.2.2	Van der Waals forces	111
6.3	Liquid bridges	111
6.3.1	Surface tension	112
6.3.2	Admixtures and their influence on the surface tension	112
6.3.3	Capillary pressure	113
6.3.4	Formation of liquid bridges	114
6.3.5	Capillary forces	115
6.4	The early-age behavior of earth-moist concrete	117
6.4.1	Experimental procedure	117
6.4.2	Fines	120
6.4.3	Chemical admixtures	121
6.4.4	Grading	123
6.4.5	Discussion	125
6.5	New mix design concept and compaction behavior	126
6.5.1	Mix design	126
6.5.2	Fresh and hardened concrete tests	128
6.5.3	Discussion	133
6.6	Conclusions	134
7	Introduction to photocatalysis	137
7.1	Introduction	137
7.2	Working mechanism of photocatalysts	137
7.2.1	A brief history	137
7.2.2	Photocatalytic principle	139
7.2.3	Degradation of organic compounds	140
7.2.4	Degradation of inorganic compounds	141
7.2.5	Degradation of microorganisms	142
7.2.6	Super-hydrophilicity	143

7.3	Tests for evaluating the efficiency of photocatalysts	144
7.3.1	ISO 22197-1:2007	144
7.3.2	UNI 11247:2007	145
7.4	Development of an experimental setup	146
7.4.1	Reactor	147
7.4.2	Light source	148
7.4.3	Testing gas supply	149
7.4.4	Analyzer	150
7.5	Measurements	150
7.5.1	Measuring protocol	151
7.5.2	Analysis of the measurements	152
7.6	Influencing parameters	153
7.6.1	Irradiance	153
7.6.2	Relative humidity	156
7.6.3	Pollutant concentration	157
7.6.4	Flow rate	157
7.6.5	TiO ₂ related properties	158
7.7	Conclusions	161
8	Application of photocatalysis to concrete products and its modeling	163
8.1	Introduction	163
8.2	Comparative study on concrete paving blocks	165
8.2.1	Patent situation	165
8.2.2	Characteristics of the tested samples	166
8.2.3	Mineralogical composition	167
8.2.4	Experimental results and discussion	167
8.3	Development of new top-layer mixes	169
8.3.1	Composed mixtures	169
8.3.2	Mineralogical composition	170
8.3.3	Experimental results and discussion	170
8.4	Modeling	173
8.4.1	Theoretical model	173
8.4.2	Experimental validation of the model	174
8.4.3	Influencing factors	175
8.4.4	Discussion	182
8.5	Conclusions	183
9	Conclusions and recommendations	185
9.1	Conclusions	186
9.1.1	Mix design concept	186
9.1.2	Application of stone waste materials	186
9.1.3	Application of recycled aggregates	187
9.1.4	Application of photocatalytic materials	188
9.2	Recommendations and future work	188

List of figures	190
List of tables	195
Bibliography	197
List of symbols and abbreviations	205
Appendix A Material properties	209
A.1 Physical properties	209
A.2 Chemical composition	210
Appendix B Sieve data	213
Appendix C Mix design concept	217
Appendix D Mix designs	219
Appendix E Test results	223
E.1 Fresh mortar properties	223
E.2 Hardened mortar properties	224
E.3 Fresh concrete properties	228
E.4 Hardened concrete properties	229
E.5 IC-test	230
Appendix F Comparison of patents on photocatalytic concrete paving products	233
Appendix G Experimental results of NO degradation measurements	235
Summary	242
Samenvatting	243

Introduction

1.1 Concrete mass products

The production of concrete mass products is strongly connected to the developments in concrete technology and advances in machinery and equipment. The first concrete mass products have been produced in the Netherlands at the beginning of the 19th century (De Goey, 1954). In the 1950s, the high demand of cheap products for infrastructural applications and domestic buildings increased the production of prefabricated concrete mass products and the market share on the overall cement consumption in the Netherlands increased to 25% for these products. During the last years, this trend continued and the market of classical concrete mass products, such as sewage pipes, concrete slabs, paving blocks, masonry blocks, roofing tiles, and curbstones, was extended to street furniture, noise barriers, and structural members that can be prefabricated and transported to the construction site. In this context, the advantages of highly automated and mechanized industrial production are combined with the defined and constant boundary conditions of a factory. This manufacturing process allows for cost reduction while obtaining products with constant properties and low reject rates. Furthermore, the production in a closed environment in the factory is not depending on changing weather conditions so that the products can be manufactured over the entire year without weather dependent variations of product properties.

The highly automated production process has a large optimization potential of the individual sub-processes and results in specific concrete mixes that are optimized in terms of product properties and manufacturing technology. Considering the requirements of the production process, three main types of concrete are used by the prefab industry and can be classified according to their workability properties into i) self-compacting concrete (SCC), ii) normal strength, normal weight concrete (NWC), which is also referred to as conventionally vibrated concrete (CVC), and iii) earth-moist concrete (EMC). Examples for the practical application of these types of concrete are given in Table 1.1, which also reflects the two main production methods of concrete mass products that are:

Cast products that are made from concrete with plastic consistency (NWC) or concrete with superior self-flowing and self-compacting properties (SCC). The curing of the concrete takes place in the mold and the product is stripped from the mold after sufficient strength of the hardened concrete is obtained. This technique is used for products with complicated shape or alternating geometry as a production by means of extrusion or other forming processes is not feasible. The production rates of this technique are low which makes it only suitable for complex products such as prefabricated modules, walls, slabs, and components for well shafts and soakaways. The application of light-weight concrete (LWC) containing light-weight aggregates or in the form of autoclaved aerated concrete results in improved thermal properties of the final product and is practiced in the production of wall elements. Accelerated curing of the concrete by means of heat treatment or the use of rapid hardening cements increases the production rate and allows the fast reuse of the mold.

Directly stripped products are produced from stiff concrete (EMC) or concrete with high plastic consistency (NWC). The concrete is rammed to the mold and the fresh product is

stripped from the mold immediately after the compaction process. The so-called green-strength of the fresh concrete results in sufficient strength for transporting the unhardened product to the place where curing takes place. Products that are manufactured by this technique are concrete paving blocks, concrete paving slabs, curbstones, roofing tiles, masonry blocks, and sewage pipes.

Table 1.1: Overview of prefabricated concrete mass products and applied production techniques (VDZ, 2002).

Product type	Curing		Concrete type
	In the mold	Demolded	
Load bearing wall elements, slabs, and beams	x		NWC, SCC, dense LWC
Prefabricated modules	x		NWC, SCC
Wall elements with high insulation value	x [‡]		Highly porous NWC containing light-weight aggregates, autoclaved aerated concrete
Masonry blocks		x	EMC
Aerated concrete blocks	x		Autoclaved aerated concrete
Paving blocks, paving slabs, curbstones		x	EMC with high green-strength and dense structure
Concrete roofing tiles		x	EMC, colored EMC
Non-reinforced sewage pipes		x	NWC with plastic consistency, EMC with high green-strength
Reinforced sewage pipes	x	x	NWC
Components for well shafts and soakaways	x	x	SCC, NWC or EMC depending on the production process
Concrete poles	x		Centrifuged NWC
Prestressed concrete railroad ties	x		High strength NWC

[‡] Autoclaved in the case of aerated concrete

1.2 Properties of earth-moist concrete

Earth-moist concrete, also referred to as no-slump or zero-slump concrete, is characterized by its stiff consistency corresponding to a slump of 6 mm or less (Kosmatka et al., 2002) and is used for the mass production of concrete products. The fresh concrete properties of EMC, caused by its low water content and stiff consistency, are advantageous. Therefore, in contrast to normal strength, normal weight concrete with high plastic consistency, the characteristics of EMC allow for direct stripping of concrete products after filling and vibrating the mold and transportation of the unhardened product to a place with defined curing conditions (Stutech, 2005). As a result, short process times during production can be realized. Further examples for the application of EMC are roller-compacted concrete (RCC) for pavement that is placed by means of slipform pavers and compacted by vibratory rollers. RCC is used for any type of industrial as well as

heavy-duty pavement or in combination with bigger aggregates as roller-compacted concrete for dams (RCD) (Kosmatka et al., 2002). The maximum aggregate size used in RCC has to be limited to 20 mm to achieve a smooth and dense surface of the hardened concrete.

The basic principles of NWC are also applicable to EMC mixes and influence the fresh and hardened concrete properties that are depending on the water content of the mix, mix proportioning, aggregate properties, temperature, and the characteristics of cement and admixtures used (Mindess et al., 2003). This fact is also reflected by the applicable standards, as specific regulations for the composition of EMC mixes do not exist. Requirements are mostly defined by standards that are related to the product, e.g. EN 1338 for specifications on concrete paving blocks or, for some applications, by standards prescribing the performance criteria of concrete such as EN 206-1. These requirements on the composition of EMC mixes in terms of minimum cement content or maximum w/c ratio are defined by the exposition classes given in EN 206-1 and apply to reinforced concrete mass products such as sewage pipes. The production of ordinary concrete mass products, such as concrete paving blocks or curbstones, is not obliged to these limitations as here performance criteria, such as abrasion resistance, freeze-thaw resistance or sufficient mechanical strength of the product, are required.

1.2.1 Fresh concrete properties

Traditional EMC mixes that are used for the production of concrete mass products are characterized by high cement contents ranging from 350 - 400 kg per cubic meter concrete and low content of fine inert particles (Häring, 2002). These high cement contents can be lowered in the case of RCC or RCD with large maximum aggregates size. Kosmatka et al. (2002) give for RCD, depending on the maximum aggregate size, a cement content of 60 - 360 kg per cubic meter concrete, which corresponds to the values reported by Nanni et al. (1996) to meet the specifications of ASTM C33 on aggregate grading. Table 1.2 gives an overview of the mix proportioning of different EMC mixes found in the literature and typical values used in practice.

Table 1.2: Comparison of EMC mix characteristics

	ACI (2002)	Bornemann (2005) [‡]	This research [‡]	Used in practice	
				Stutech (2005)	Sec. 6.5
Cement [kg/m ³]	325	270 - 310	230 - 250	360	262
Filler [kg/m ³]	–	–	120 - 210	–	114
Sand [l/m ³]	206	292 - 313	464 - 512	369	521
Gravel [l/m ³]	531	410 - 435	165 - 173	340	155
Water [l/m ³]	141	100 - 120	112 - 139	115	112
Air content [%]	3.0	4.0 - 9.0	5.0 - 7.5	5.5	7.5
w/c ratio	0.43	0.33 - 0.44	0.45 - 0.56	0.32	0.43
w/p ratio	0.43	0.33 - 0.44	0.30	0.32	0.30
Paste [l/m ³]	244.0	210 - 270	250 - 315	236.0	250.4

[‡] Values taken from experiments for highest packing fractions.

[‡] Considering the mix proportioning of an optimized company mix presented in Section 6.5.

It becomes obvious from the data depicted in Table 1.2 that traditional EMC mixes used for the production of concrete paving blocks (mix Stutech (2005)) are characterized by their high cement contents and the resulting low w/c ratios. In this case, cement is primarily used as binder, but also as filler material. This inappropriate use of a cost and energy intensive material as filler is not

in line with the ideas of sustainable use of natural resources, as materials with low environmental footprint should be used. The workability of EMC mixes, as listed in Table 1.2, is characterized by low water contents that result in low w/c ratios ($w/c < 0.40$). In this respect, the use of the w/p ratio is more appropriate design parameter for the assessment of concrete mixes with high contents of fine materials other than cement. Here, the w/p characterizes concrete mixes with multiple sources of fine materials in a better way regarding their water content and resulting workability.

Håring (2002) defines the workability of uncompacted EMC mixes as free-flowing with a high degree of compaction. This results in high compaction efforts that are needed for sufficient compaction and makes the consolidation of the concrete by means of hand rodding or poker vibrators difficult. However, if pressure and mechanical vibration are combined the material shows adequate workability. The compaction of EMC by combined pressure from the top and mechanical vibration introduced via the mold is referred to as vibropressing and is frequently used for the production of concrete paving blocks on industrial paving block machines. This stiff consistency of EMC makes it difficult to assess the workability of the fresh concrete in an adequate way by means of standard workability tests that are used for NWC. Suitable test method for the evaluation of the workability properties of EMC mixes are given by the degree of compaction test, Proctor test, CemTec test, and the intensive compaction test that will be discussed in detail in Section 2.7.

1.2.2 Green-strength

The so-called green-strength of EMC is a special feature of this type of concrete in its fresh state and is caused by the low water content and the resulting cohesive character of the concrete mix. A definition of the green-strength is given by Bornemann (2005) and can also be found in Stutech (2005) as strength of the product to keep its original shape until the cement starts to set and the hydration products provide sufficient strength. An explanation for the green-strength of the unhardened concrete is given by soil mechanical models that are used for the description of cohesive soils (Bornemann, 2005; Schmidt, 1999). However, it has to be mentioned at this point that the cohesive character of EMC mixes is differing from the *real cohesion* that can be found in soils, like clay. According to Craig (1994), this cohesiveness is only obtained by soils that adhere after wetting and subsequent drying and where significant forces are required for breaking up the structure of the dry material.

The formation of capillary forces and the internal friction of the granular particles cause the cohesive character of EMC mixes in their fresh state. Capillary forces are formed at the contact points of finer particles as a result of the partly saturated void fraction of the granular skeleton. This partial saturation of the void fraction causes the formation of liquid bridges between the smaller particles at their contact points. An attractive force is formed in the liquid bridge that is depending on the surface tension of the wetting liquid and the resulting contact angle between the surface of the liquid and the particle surface. The formation of capillary forces between the fine particles is a rather complex system, which is focused on in Section 6.3.

As mentioned before, the green-strength of EMC mixes is a result of capillary forces that are formed between the fine particles and the internal friction of the granular particles. The grain interlocking of the granular particles causes the internal resistance or friction of the granular skeleton during shearing and is also referred to as angle of shearing resistance (Craig, 1994). The angle of the internal friction of a granular material is depending on the surface roughness of the particles, the particle shape, and the densification of the granular skeleton. Higher surface roughness of the particles increases the internal friction of the granular material in the same way as particles with angular shape. Higher densification of the granular material results in more contact points and increases the angle of shearing resistance as forces are activated that resist the motion of the particles in each contact point. The internal friction of fresh concrete was determined by Ritchie (1962) using the triaxial test and obtained Mohr circles were used for

defining the angle of internal friction in accordance with Coulomb's law.

In soil mechanics, the Mohr-Coulomb failure criterion is used to evaluate the shear resistance of a soil. This failure criterion allows the explanation of the green-strength of EMC based on a soil mechanical model. In this context, the shear strength τ_f of a soil is expressed as a function of the effective normal stresses and follows, according to Craig (1994), from the shear strength parameters. The shear strength parameters c' and ϕ' describe the apparent cohesion and the angle of shearing resistance in terms of effective stresses. The equation of the Mohr-Coulomb failure criterion as a function of normal stresses reads:

$$\tau_f = c' + \sigma'_f \tan \phi' \quad (1.1)$$

Eq. (1.1) results in a line that is tangential to the Mohr circles representing the state of stresses at individual points (see Figure 1.1). The shear parameters of the sample can be derived from standard tests used in soil mechanics, such as triaxial test or direct shear apparatus and determine the inclination and the intercept of the tangent representing the failure envelope of the soil as illustrated in Figure 1.1.

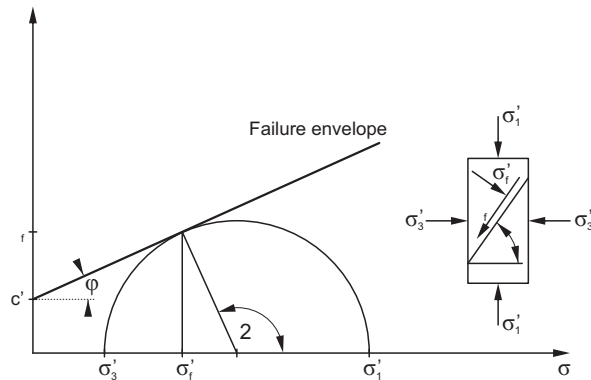


Figure 1.1: Stress conditions at the Mohr-Coulomb failure criterion (Craig, 1994).

1.2.3 Hardened concrete properties

The hardened concrete properties, such as mechanical strength and durability, are dominated by the low w/c ratios that are characteristic for traditional EMC mixes. The mechanical resistance of traditional EMC products is a minor problem as high cement contents are combined with low w/c ratios, which results in high compressive strength. Therefore, the durability of these products attracts more attention under practical conditions and is mainly influenced by the pore structure of the hardened cement paste as most of the problems that are related to durability are caused by transport phenomena in the cement paste.

The low w/c ratios result in a dense structure of the hardened cement paste as the number of capillary pores is reduced. These capillary pores are formed during the hydration process, as excessive mixing water is not involved in the formation of hydration products and, consequently, leaving a void fraction when evaporating. The content of capillary pores with a size

of about 100 nm is essential for the mechanical resistance and durability of the hardened concrete. A denser structure of the hardened cement paste results in higher compressive strength and improved durability as most of the transport phenomena, such as penetration of water and deleterious ions, occur through the capillary pores (Stark and Wicht, 2001). The amount of capillary pores will change over time as the proceeding hydration process generates hydration products that occupy the space of the free water. According to Stark and Wicht (2001), this process is depending on the type of cement used and the degree of hydration. In this context, Häring (2002) demonstrated that the low w/c ratios of EMC mixes and the resulting low degree of hydration after production offer a high potential for reactions that take place in the early age. The data reported by Häring (2002) reveal that the water absorption of a traditional concrete paving block with low w/c ratio is reduced by about 30% in the first two month due to changes of the capillary pore structure and that the resistance to freeze-thaw cycles was improved, too.

The durability of concrete is not only influenced by the capillary pores, but also by the content of micro pores in the range of 10 - 1000 μm . These micro pores provide sufficient space that is required by the expansion of the freezing water. By this, the hydraulic pressure of the freezing water is reduced and prevents that the pressure of the freezing water in the capillary pores exceeds the tensile strength of the hardened cement paste. Furthermore, micro pores have a disconnecting effect on the capillary pores and reduce therefore the capillary suction and the uptake of water. This effect results in a lower saturation of the concrete and improved freezing resistance (Stark and Wicht, 2001). Micro pores in the concrete are either entrained by the use of air-entraining admixtures or entrapped air bubbles that occur as a result of mixing, handling or placing (Kosmatka et al., 2002). A pore size of about 300 μm is recommended by Stark and Wicht (2001) for concretes with high freezing resistance. The minimum air content of concrete with high freezing resistance is given by EN 206-1 with 4% and is usually achieved in NWC by air-entraining admixtures. The data listed in Table 1.2 reveal that this minimum air content of equally distributed voids is obtained by traditional EMC mixes (Häring, 2002). These voids allow the freezing water to expand and give the final product a high resistance against freezing. The deterioration of the concrete in the form of cracking, scaling, or crumbling remains, therefore, only problematic for products that are fully saturated with water and can be caused, for instance, by an insufficient drainage of the sub-base of concrete paving blocks.

1.3 Sustainability in concrete production

The use of natural resources in consideration of ecological and economical aspects forms the basis for sustainable developments. Low energy consumption during production and the use of by-products as well as waste materials are essential to reduce environmental and financial impacts. This thesis gives an overall design approach for the design of sustainable concrete mixes and covers therefore a broad field of relevant subjects in concrete technology. The different subjects show a close relation in terms of sustainability and multifunctional use of raw materials. In this respect, the knowledge from different fields is required nowadays for the design of sustainable concrete as most of these fields form a highly optimized process for its own. However, not only knowledge from concrete technology or cement chemistry is required, but also insights from other fields deliver useful and valuable solutions. In this context, insights from classical design approaches for concrete mixes, particle packing models, material recycling, and photocatalysis are combined.

1.3.1 Use of cement and concrete in the construction industry

Concrete is the second most-used man-made material in the world after drinking-water and its production generates the largest material flow. The wide spread use of concrete as construction material is caused by its low costs (most of the aggregates used in concrete can be obtained locally), ability to be cast into odd shapes, and its high durability and fire resistance compared to other materials. It is assumed that about 1 m^3 of concrete is consumed per person per year,

which corresponds to an annual global production of about 15 billion ton (Aïtcin, 2000). These numbers are also reflected by the global cement production depicted in Figure 1.2. The global cement production was more than doubled in the past 15 years and amounts to about 2800 Mton in 2008, about half being produced in China (CEMBUREAU, 2010). Before the financial crisis in 2008, the cement production remained stable in the U.S. and Europe and a strong regression was recognized by the European cement industry after 2008, which is expected to obtain a stable level in the coming years (CEMBUREAU, 2010). This trend is not in line with the development on the Asian market. Here, the financial crisis resulted in lower growth of the cement production, but still slightly increasing numbers. It is expected that the financial crisis will not stop the development in Asian countries, like China and India, and that the growth of the cement market will continue in the coming decades.

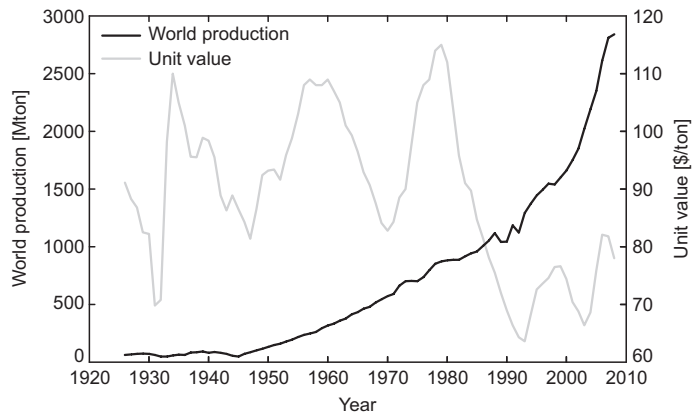


Figure 1.2: World cement production and unit value per metric ton based on the Consumer Price Index with 1998 as base year (U.S. Geological Survey, 2010).

Although the clinker production requires less energy than steel production, the manufacture of cement clinker is still an energy-intensive process. According to CIPEC (2001), the average energy use for clinker production amounts to 5.2 GJ/ton, whereas a value of about 3.6 GJ/ton is reported by VDZ (2002) for operating kilns in Germany. This low value is given in CIPEC (2001) only for highly efficient multi-stage preheater. In comparison, a value of 18.6 GJ/ton is given by Worrell et al. (1999) for steel production.

Considering a standard concrete mix with medium strength and an average cement content of 300 kg ordinary Portland cement (OPC) per cubic meter concrete as well as a fresh concrete density of about 2400 kg/m³, 125 kg of cement are needed to produce 1 ton of concrete, which corresponds to 12.5% of the total concrete mass. The remaining 875 kg are made up of 812.5 kg of aggregates and 62.5 kg of water when a *w/c* ratio of 0.50 is taken as basis for the calculation. Marceau et al. (2007) give a value of 28 MJ/m³ for concrete plant operations, which corresponds to a value of 11.7 MJ/ton. 35.4 MJ/ton are reported by Marceau et al. (2007) for the production of crushed stone or gravel. The production of crushed aggregates is usually a more energy-intensive process than the production of concrete aggregates by extracting sand and gravel from floodplains. Based on the numbers assumed before, the total energy that is consumed by the production of one tone of concrete follows from:

$$\begin{aligned}
 & 125 \text{ kg cement} \times 5,200 \text{ MJ/ton} = 650 \text{ MJ} \\
 & + 812.5 \text{ kg aggregates} \times 35.4 \text{ MJ/ton} = 28.8 \text{ MJ} \\
 & + 11.7 \text{ MJ/ton concrete plant operations} = 11.7 \text{ MJ} \\
 \hline
 & \approx 691 \text{ MJ}
 \end{aligned}$$

This number shows that the total energy consumption of concrete is reduced to about 0.69 GJ/ton, a value in line with the number given by Marceau et al. (2007) for similar cement contents, and is considerably lower than the amount of energy required to produce 1 ton of steel¹ that amounts to 18.6 GJ/ton. However, the tremendous amounts of concrete that are produced per year and the limited recycling of old concrete in the construction industry nowadays, compared to steel, result in a large ecological impact of concrete.

There are different approaches to minimize the environmental impact of concrete production and the most efficient solutions are related to the minimized use of cement in concrete. As illustrated by the aforementioned numbers, about 90% of the energy that is needed to produce 1 ton of concrete is consumed by cement production. It is more than rational to reduce this part in the overall balance by using alternative types of cements with lower energy consumption during production and lower CO₂ footprint. These types of cements are already available on the market in the form of slag-blended cements (Chen, 2007) or composite cements. Depending on the composition of these types of cement, cement clinker is replaced by ground granulated blast furnace slag, a by-product of the steel industry, and the clinker content is reduced up to 95% compared to pure ordinary Portland cement (EN 197-1).

A further solution to lower the environmental impact of concrete production is given by cements with higher fineness and the use of modern admixtures. There is no need to use too much glue in a dense system with low *w/c* ratio or to misuse cement as filler material or for adjusting workability (Aïtein, 2000). Concretes with lower cement contents and comparable performance criteria in terms of mechanical strength and durability can be produced already nowadays, but their cement contents are below the limits given in design codes. This topic will be addressed in a later section of this thesis.

Finally, the recycling of concrete is a topic that is extensively discussed in the literature and on a scientific level, but has not reached until now practical relevance, as it should have. The use of concrete, compared to steel, is still a straight process and the life cycle of concrete is not closed. Here, two possibilities arise to close the life cycle of concrete. First, structures can be designed in such a way that the building can be easily disassembled after use and that the reuse of structural elements in new projects is possible. In case a reutilization of structural parts is not possible, the old concrete should serve as a source to replace aggregates in new concrete. If concrete is recycled nowadays, it is being crushed and used mostly as sub-base and the problem of disposal is shifted from the landfill sites to roads, highways, and other secondary applications. However, several studies have shown that recycled concrete aggregates and fines can be used to replace conventional raw materials in concrete (Kerkhoff and Siebel, 2002; Müller, 2003a,b; Poon and Chan, 2006; Vázquez and Gonçalves, 2005). This utilization of old concrete for the production of new concrete closes the life cycle of concrete.

¹In this context, the energy consumption considers only energy that is consumed during the production of 1 ton of concrete and further energy consumption caused by transport to the construction site and placing was excluded as, in the case of steel, similar numbers accumulate due to rolling and transport.

1.3.2 Sustainability versus durability

It can be stated that durable materials fulfill the aspects of sustainability per definition, as durable materials are the basis for structures with long service life. However, the question arises whether these durable materials are always produced in a sustainable way. In this context, it is worthwhile to give a clear definition of the term *durability* and derived specifications thereof. Stark and Wicht (2001) give an overview of specific definitions for the durability of concrete in terms of:

- Water impermeability in case of structures that are exposed to permanent moisture
- Freeze-thaw resistance and resistance to deicing agent of pavements and bridges
- High carbonation resistance and high chloride impermeability to protect reinforcing bars
- Resistance to deleterious internal reactions such as alkali-silica reaction, alkali-carbonate reaction, and delayed ettringite formation
- Resistance to sulfate attack or other deleterious solutions (acids, waste waters)
- Abrasion resistance to mechanical wear caused by traffic, streaming water, and weathering
- Biological resistance to microorganisms and metabolites thereof
- Prevention of crack formation due to thermal, hygric, mechanical, and dynamic loads
- Fire resistance and resistance to elevated temperatures

In consideration of these definitions, durability is a measure for the concrete's resistance to the aforementioned conditions. This resistance is either stipulated by design specifications, such as maximum crack width and minimum concrete coverage of the reinforcement bars (EC 2, DIN 1045-1), or by material related criteria. In EN 206-1 concrete is considered as durable material for structural applications based on the specification of:

- Mechanical strength that is usually related to the compressive strength
- Minimum cement content
- Maximum water content which is governed by the w/c ratio
- Minimum air content of the fresh concrete adjusted by air-entraining admixtures

The criteria as given in EN 206-1 become applicable for the production of concrete products like sewage pipes or well shafts, whereas concrete mass products, such as concrete paving blocks or slabs, are not constrained by these limitations. In this respect, it is noteworthy to mention that a minimum compressive strength of 50 N/mm^2 was required by DIN 18501 and can be considered as indirect criteria for the durability of concrete paving blocks. However, the specification on the compressive strength was replaced in the German version of EN 1338 (DIN-EN 1338) by the splitting tensile strength, and specified tests on the freeze-thaw resistance or water absorption are required by EN 1338. However, compressive strength and a minimum cement content combined with maximum w/c ratio are still considered by the industry of concrete products to be a common measure for durable concrete and were valid for concretes that have been designed according to classical design approaches.

The primary requirement on the compressive strength of durable² concrete was argued by Neville (1997) in a critical context. In his review on the developments in cement and concrete industry, Neville (1997) states numerous examples that confirm the need for a distinct consideration of both compressive strength and durability. One of these examples is the introduction of finer cements, mainly in the form of classical Portland cements, to the concrete industry, which allowed for cement reduction. However, cement contents were reduced, whereas water contents were increased to maintain constant workability. The higher water contents resulted in more capillary pores, which decreased the durability of the concrete in total. In view of this

²In the following, durability of concrete is considered as resistance to diffusion induced processes of deleterious substances, which are related to the microstructural properties of the hardened cement paste.

fact, the microstructural properties of the cement paste were affected to a larger extent than the paste content was reduced. A further negative effect on the durability of these concretes with the same compressive strength after 28 days, but made with finer Portland cements, was given by the rapid early strength development and their lower potential for long-term reactions and resulting changes in the capillary pore structure. Considering the development of the pore structure of the hardened cement paste, the use of slag-blended cements results in concrete with higher durability, but having same compressive strength. This beneficial effect is caused by a finer pore structure of slag-blended cement pastes compared to that of hardened Portland cement paste. For the same w/c ratios, the hardened paste of slag-blended cements contains more gel pores and fewer capillary pores that are responsible for durability related transport phenomena (Chen, 2007).

The aforementioned detrimental effect of lower cement contents combined with high w/c ratios was compensated by the introduction of modern water reducing admixtures (plasticizers) that increased the workability of concrete mixes while reducing the water content of the paste. The improved rheological properties of the paste combined with the higher fineness of the cement allow now for a reduction in the cement content while maintaining the same workability. The combination of finer cements and plasticizers demonstrated that requirements for minimum cement content are not necessarily favorable from a technical and financial point of view (Wassermann et al., 2009). In this context, it should be mentioned that the concept of minimum cement content applies to a unit volume of concrete, whereas durability depends on the properties of the hardened cement paste (Neville, 1997). Consequently, the question arises whether same durability is obtained when the cement paste, and the amount of capillary pores, in the concrete is reduced. Wassermann et al. (2009) demonstrated that the capillary absorption and chloride ingress reduced with decreasing cement contents for constant w/c ratio. Moreover, it was demonstrated by Wassermann et al. (2009) that carbonation was not affected by decreasing cement contents at given w/c ratios due to two competing process, namely lower penetration and reduction in CO_2 binding. These results demonstrate that cement contents in durable concrete can be reduced efficiently and that cement should be used as a kind of glue in a dense granular structure having low void fraction (Aïtcin, 2000). The influence of a dense granular structure on the concrete properties in fresh and hardened state due to optimized particle packing and resulting potential for cement reduction or cement replacement is also part of this thesis.

As mentioned before, the durability of concrete is influenced to a large extent by the properties of the cement paste. By reason of this as well as financial and environmental aspect, the amount of cement paste should be reduced to a minimum necessary for mechanical strength and durability. This concept requires the aimed composition of all concrete ingredients to obtain a dense granular structure with low void fraction to be filled with cement paste. In doing so, the missing fraction of cement particles has to be replaced by appropriate filler materials with comparable granulometric properties. Inert or reactive filler materials can be used for this purpose. However, the utilization of these materials results in further conflicts with classical durability concepts. Here, the w/c ratio is used to ensure i) durability due to microstructural developments and ii) workability that is adjusted by variations in the cement and water content of the concrete. Considering a concrete mix containing cement and fine inert filler materials only, the w/p ratio is a more appropriate formulation for workability related requirements, which will be demonstrated in this thesis. In view of Neville's critical discussion on the compressive strength as requirement for durable concrete (Neville, 1997), he discusses the suitability of the classical definition of the w/c ratio in modern concrete technology (Neville, 1999, 2006).

In classical systems, which are only based on Portland cement, the w/c ratio is a valid indication for the formation of capillary pores. However, the hydration of Portland cement differs from the hydration of slag-blended cements. The hardened cement paste of slag-blended cements, with same w/c ratio, contains less capillary pores (Chen, 2007). This denser structure of the hardened cement paste reduces the permeability and improves the durability of concrete.

Moreover, more and more concrete mixes will contain additional filler materials with certain reactivity and beneficial effects on the durability due to improvements of the microstructure of the hardened cement paste. This fact is considered by splitting the denominator of the w/c ratio into a term considering the mass of cement used plus a k factored term considering other reactive materials like fly ash or silica fume. Restrictions for the k -value are given and the accountable amount is limited (EN 206-1). Studies have shown that the variation of the properties of different fly ashes decreased and that the average efficiency (k -value) increased to a value higher than restricted by EN 206-1 (Vissers, 1997). Summarizing the above, the w/c ratio gives not a valid characterization for all types of concrete regarding their durability and has a proper meaning only at the time when the concrete is placed and starts to harden.

The literature shows that the durability of modern types of concrete is not only governed by i) compressive strength, ii) minimum cement content and iii) w/c ratio. Complex interactions influence the microstructure of the hardened cement paste. Since the cement paste is influencing the durability properties of the hardened concrete, its content should be reduced to a minimum necessary for giving the granular particles (aggregates and fine fillers) sufficient strength. In this respect, the design of sustainable concrete mixes with low cement contents is not contrary to the aspects of durability.

1.3.3 Application of stone waste materials

Besides the efforts that are made to reduce cement contents, the material with the highest ecological impact in concrete production, natural resources for aggregates and fine fillers should be preserved. Limestone powder is a common material used as fine filler for concretes with low cement contents and the successful application in EMC mixes was demonstrated by Bornemann (2005). However, the embodied energy of limestone powder is given by Keller and Rutz (2010) with about 650 MJ/ton which justifies its substitution by other fine filler materials, such as stone waste powders generated by the processing of natural rock. The stone waste powders originate from two different processes that are i) the processing of natural rock and ii) the production of crushed aggregates.

The processing of ornamental stone by sawing and polishing produces large volume of fine stone waste materials. A rough estimation is given by Calmon et al. (2005), which says that about 30% of the original block turn into fines due to sawing and polishing. Considering the volume of ornamental stone produced per year, these fines turn into an environmental problem in areas with natural stone industry. Consequently, possible fields of application for these fine stone waste materials were investigated and Calmon et al. (2005) used that material successfully for the production of SCC. However, from a sustainable as well as financial point of view, the application of the fine stone waste material is limited to concrete production nearby the quarries or processing companies as the fines are generated by a wet production process, resulting in a slurry like material or filter cake. As a result of the high water content of the waste material, its transport over long distance is not justified under financial and sustainable considerations. In this respect, the fines generated by the production of crushed aggregates are of greater interest for the production of concrete mass products.

The production of crushed concrete aggregates generates fines, which are also referred to as quarry or rock dust, during the crushing and sieving process of rocks. The amount of these fines is given by Ho et al. (2002) with less than about 1% of aggregate production. In standard concrete, the amount of fine materials is limited (DIN 1045-2) or standards on concrete aggregates require a preliminary washing of the material, which removes the fines from the aggregates and generates a fine stone waste material in slurry form. A possible application of this fine stone waste material is found in concretes with a high content of fines (SCC) to replace traditional fillers. The replacement of limestone powder in SCC by fine inert stone waste materials was demonstrated by Ho et al. (2002), Hunger (2010), as well as Hüsken and Brouwers (2010) without detrimental effects on the mechanical resistance of the hardened concrete. Considering the

aspects of sustainability, this concept will be followed within the framework of this thesis and fine stone waste materials will be used for the design of EMC mixes.

1.3.4 Utilization of recycled construction rubble in concrete production

The utilization of construction rubble that is generated by the demolition of buildings and structures forms one of the major pillars of sustainability in concrete production besides cement reduction or replacement. Here, the recycling of building materials helps to reduce the amount of rubble that has to be disposed of in landfill sites and saves energy and raw materials in the production of new building materials. However, the utilization of rubble in concrete production is strongly depending on the composition of recycled material and the applied processing technologies. According to Müller (2003a), the following cases for the composition of building rubble can be distinguished:

Pure concrete rubble that results from the demolition of concrete structures such as concrete roads or bridges. Appropriate processing technologies and the homogeneous composition of the demolition waste generated from pure concrete structures allow for the production of recycled material of high quality that is composed of aggregates and hardened cement paste.

Masonry rubble that is generated by the demolition of mixed structures. This type of rubble contains a variety of building materials such as concrete, lightweight concrete, bricks, mortar, and plaster. The content of the single components varies highly as a carefully separation of the single materials during the demolition process is not possible.

Brick-rich masonry rubble from the demolition of pure brick masonry with high brick content and a low content of mortar and plaster.

Pure brick rubble that contains bricks without any other substances like mortar or plaster. This material is generated by the re-covering of roofs or as production waste from the brick production.

The utilization of recycled concrete aggregate (RCA) is reported manifold in the literature for pure recycled materials such as concrete rubble (Katz, 2003; Kerkhoff and Siebel, 2002; Kou and Poon, 2009; Vázquez and Gonçalves, 2005). It is stated by Vázquez and Gonçalves (2005) that the mechanical properties of concrete with crushed concrete aggregate remain the same when only recycled aggregates larger than 4 mm are used and the amount is restricted to 20% of natural aggregates. The use of coarse recycled concrete aggregates in concrete mass products was investigated by Schießl and Müller (1997) and concrete paving blocks with recycled concrete aggregate and crushed clay brick were produced successfully by Poon and Chan (2006).

Despite the possible use of recycled aggregate in concrete, the utilization rates of recycled concrete aggregates in concrete production are low and most of the material is used for low-level applications like sub-base material for roads and highways (Müller, 2003a). This fact is caused by the negative influence of RCA with high brick content on the mechanical and durability properties of standard concrete (Kerkhoff and Siebel, 2002). These kinds of impurities, originated from clay bricks or other ceramic materials, are difficult to avoid when buildings are demolished. In this case, the lower strength of the clay bricks reduces the mechanical resistance of the concrete and the higher porosity increases the total porosity of standard concrete and reduces its durability. However, the higher porosity and the related potential for water absorption can be beneficial for the internal curing of high strength concretes if the material is applied in low quantities. The fines generated from building rubble offer a further potential for utilization as filler material in concrete. Depending on the chemical composition and fineness, unhydrated cement of the old cement paste can be activated and the pozzolanic properties of the fines generated from clay bricks can contribute to the strength development (Müller, 2003b). In consideration of these aspects, recycled concrete aggregates and fines turn to a multifunctional raw material for concrete production and will, therefore, be incorporated in the design approach for sustainable

concrete mixes.

1.4 Outline of the thesis

This thesis represents a further step in the direction of designing sustainable concrete mixes and, therefore, covers a broad field of relevant subjects in concrete technology. The different subjects show a close relation regarding a sustainable and multifunctional design approach for concrete. In this respect, the knowledge from different fields of concrete technology is required nowadays for the design of sustainable concrete as most of these fields form a highly optimized process for its own. However, not only knowledge from concrete technology or cement chemistry is required, but also insights from other fields deliver useful and valuable solutions. For this purpose, insights from concrete mix design obtained from classical design concepts, particle packing, and photocatalysis are combined.

The relevance to practical problems was always kept in mind to answer also practical questions encountered in the production process of concrete mass products. The early-age behavior of EMC forms one of the leading points with practical relevance for the production of concrete sewage pipes. Higher production rates can be achieved and lower amounts of production wastage are produced if the principles on the early-age behavior of EMC are known and considered in the concrete mix design.

The underlying research framework of this thesis is presented in Figure 1.3 and shows also the relation among the 9 chapters of this thesis. The content of the chapters is briefly described in the following.

Chapter 2 of this thesis gives an overview of test procedures and material characterization techniques with relevance to this research. Based on this overview, the properties of the applied materials are characterized. Furthermore, suitable test methods for evaluating the workability of EMC are introduced and discussed.

Chapter 3 provides deeper insights into particle packing and related models and theories. Relevant findings from the packing of monosized particles, discrete bimodal, multimodal, and continuously graded particle mixtures are discussed and their relevance to concrete mix design is shown. Based on the findings for continuously graded particle mixtures, a design approach for the composition of granular mixtures with optimized and dense particle packing is suggested. The relevance of optimized and dense particle packing is shown by means of experimental results obtained for bimodal aggregate mixtures and extended to continuously graded aggregate mixtures.

Chapter 4 introduces a new mix design concept for earth-moist concrete that is based on optimized particle packing. A mix design tool is developed on the basis of theories for dense geometric packings. The developed design tool allows the composition of granular mixtures that follow a given grading function to obtain dense particle packing. Furthermore, EMC mixes have been designed and tested on laboratory scale using the ideas of the new mix design concept. The experimental results have been used for the validation and calibration of the mix design tool.

Chapter 5 gives an overview of alternative materials that can be used for the production of sustainable concrete mixes. Here, the main attention is paid to cement reduction based on optimized particle packing and cement replacement by inert or reactive fines. Furthermore, the application of recycled concrete aggregates is considered to be a multifunctional application of these materials and will be discussed in detail. In this case, the RCA are used as aggregates and internal water source to prevent autogenous shrinkage.

Chapter 6 investigates the early-age behavior of EMC. The basic principles that govern the behavior of EMC mixes in the fresh state are analyzed in detail. Here, the focus is on the interparticle forces that are formed on micro-level and that influence the behavior of the fresh concrete to a large extent. The influence of the fines, their fineness and content, is investigated and will be related to the ideas of the new mix design concept. By means of the new mix design tool, a

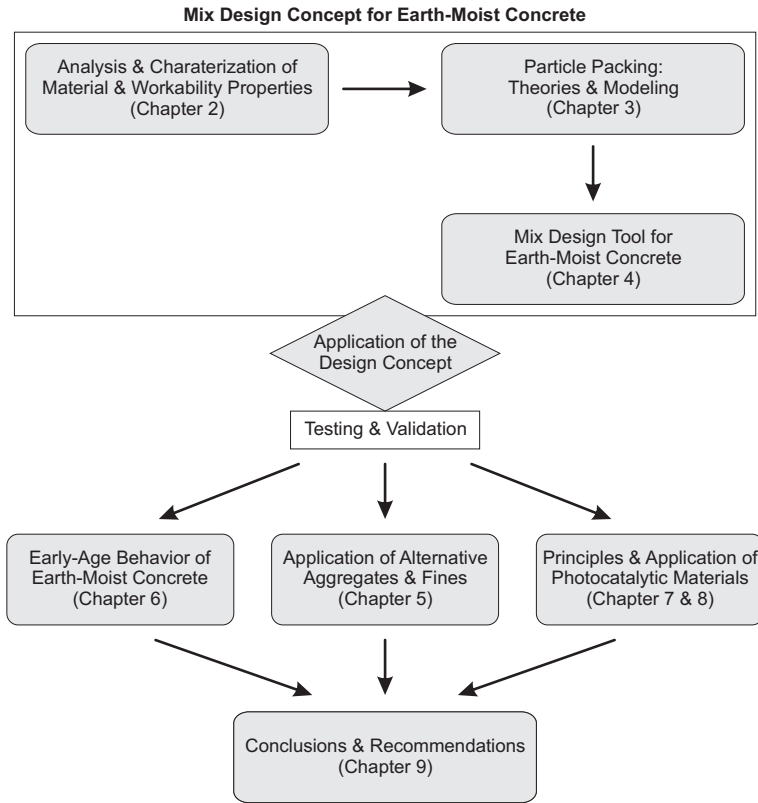


Figure 1.3: Framework of the thesis.

EMC mix used for the production of concrete paving blocks is optimized regarding dense particle packing and compared with the original mix.

Chapter 7 of this thesis focuses on the application of concrete products, mainly applied as concrete paving blocks, with multifunctional properties. Besides their use as classical paving material, these paving blocks possess air-purifying properties based on the photocatalytic reaction of TiO_2 in the anatase modification. Principles of the photocatalytic reaction of TiO_2 are discussed and form the starting point for the development of a suitable test setup and measuring protocol for the evaluation of air-purifying properties of concrete products.

Chapter 8 continues the ideas of air-purification by means of photocatalytic materials and relates them to practical applications. A representative selection of concrete products containing photocatalytic materials was assessed regarding variations in the air-purifying properties. The results of this study are discussed and own developments for new top-layer mixtures of concrete paving blocks with air-purifying properties are presented. A brief introduction to the modeling of the photocatalytic reaction concludes this chapter.

Chapter 9 gives the conclusions of the research with general recommendations for the design of sustainable EMC mixes. Practical applications for the design of sustainable concrete mixes are proposed and starting points for further research being continuation of this work are outlined.

Test procedures and material characterization

2.1 Introduction

The characterization of materials and profound knowledge on the material properties form the basis for both the development of new materials and the improvement of already existing materials. In comparison to other composite materials, a multitude of raw materials with varying properties is combined to form hardened concrete. These raw materials are characterized by their physical and chemical properties and need to be combined in a way that detrimental reactions, such as alkali-silica reaction or alkali-carbonate reaction, do not occur in the final product. The careful characterization of the raw materials regarding their chemical and mineralogical composition helps to prevent these detrimental reactions. The characterization of physical properties, such as particle size distribution (PSD), particle shape, specific density, etc., provides fundamental information for composing concrete aggregates in order to produce concrete with adequate workability when mixed, and appropriate mechanical strength in hardened state.

The testing of the mechanical properties of hardened concrete is standardized by many national and international standards (EN 12390-3, EN 12390-5, EN 12390-6, ASTM C39/C78/C496, CSA A23.2-8C/A23.2-9C/A23.2-13C, etc.), but the objective evaluation of the workability properties of earth-moist concrete on laboratory scale is a critical and frequently discussed issue. Due to the poor workability of the concrete, the material is usually rammed into the mold or the concrete is compacted by high vibration energy in combination with hydraulic pressure. This way of compaction results in high compaction efforts and high stresses in the production machines. The high stresses in the production machines are compensated by the stiff and heavy design of these machines, which is not possible on a laboratory scale without large financial expenses. Nevertheless, concrete paving block machines for the sample production on laboratory scale are available on the market. Within the scope of this research project, it was possible to make use of such a laboratory paving block machine.

Tests carried out on a laboratory paving block machine showed that the conditions of the production process can be realistically simulated on small scale but an adjustment of the machine regarding compaction pressure, vibration energy and compaction time is still necessary in order to meet the properties of industrial production machines (Bilgeri, 2006). Furthermore, the laboratory paving block machine used for own tests on EMC is still heavy and needs special foundation as well as a connection to an industrial air pressure system providing high air pressure and volume flow. This shows that the use of a laboratory paving block machine is still difficult and expensive, as investments in supplementary facilities are needed. For these reasons, several test procedures have been developed in the past or have been adopted from other fields and modified for workability tests on EMC.

Some of the developed test procedures are not only used for workability tests on EMC, but have been designed also for tests on stiff or plastic concretes. The several test methods used for tests on fresh concrete will not be explained in detail as a more comprehensive and detailed explanation of the respective test procedures is given in the literature (Bartos et al., 2002; Ferraris, 1996; Koehler and Fowler, 2003). Therefore, only advantages or disadvantages of the single tests that are important for tests on EMC will be named. The four test procedures discussed in this chapter are frequently used for testing the workability of fresh EMC mixes. The test proce-

dures differ in their applied compaction methods and can be separated in tests using pure impact compaction by tamping a drop weight (classical Proctor test, CemTec test procedure), vibratory compaction combined with a surcharge (vibrated Proctor test), and a combined compaction of pressure and shear (IC-test).

2.2 Characterization techniques for aggregates and fines

The material properties of concrete aggregates, fillers, and binders are important for the design of concrete mixes. The aimed composition of concrete mixes in terms of strength, durability, and sustainability requires the thorough analysis of both physical and chemical material properties by adequate characterization techniques. Therefore, a brief overview of relevant characterization techniques used for determining the physical properties is given in this section.

2.2.1 Particle size analysis

The particle size distribution (PSD) or so-called grading of aggregates and fines is an important parameter for the mix design of concrete as the workability of concrete mixes is influenced by the aggregates grading and the resulting paste requirements. The grading of aggregates is determined by sieve analysis and described in standards (EN 933-1, ASTM C117/C136, CSA A23.2-2A, etc.). The formation of interparticle forces affects the results of the sieve analysis for particles smaller than 100 μm as with decreasing particle diameter interparticle forces prevail over the particles weight (see Section 6.1). In dry particles, electrostatic forces are generated as a result of particle collisions or induced by particle friction and lead to the formation of agglomerates (see Section 6.2.1). These agglomerates influence the results of the sieve analysis of particles smaller than 100 μm to a large extent and the sieve analysis in dry state becomes inappropriate. Consequently, the fine particles have to be dispersed in an appropriate solution and their particle size is measured by the scattering of a laser beam using the principles of laser diffraction analysis (LDA) for particles in the micro range ($1 \mu\text{m} \leq D \leq 100 \mu\text{m}$). Requirements for particle size analysis by means of laser diffraction methods are given in the standard ISO 13320:2009. The principle of LDA becomes unsuitable for particles smaller than 500 nm due to limitations that are related to the wavelength of the applied laser beam. Here, the principles of dynamic light scattering are used for analyzing the grading of nanoparticles ($1 \text{ nm} \leq D \leq 1 \mu\text{m}$).

In the case of classical sieve analysis, the analyzed sample is passed through a stack of sieves that are arranged in order of decreasing sieve openings. An overview of varying sieve sizes and designations is given in Appendix B.1. The grading is usually expressed by the percentage of material passing each sieve, which is also referred to as cumulative finer fraction. The percentage of material passing each sieve can be expressed on mass or volume basis. A volume-based expression is more suitable for the composition of materials that have different density and can be obtained by considering the specific density of each material.

The cumulative finer fraction represents the cumulative distribution function that describes the probability of a variable (particle size) with a given probability function. The probability density function and the cumulative distribution function can be obtained by numerical integration or numerical differentiation of the corresponding cumulative distribution function or probability density function (Alex, 2008). The probability density function is obtained from the frequency distribution considering the interval width. In the considered case, the frequency distribution is given by the mass distribution, which represents the sieve residue in every size class determined by the sieve openings of the sieves used. At this point it is essential to mention that the width of the size classes used for analyzing the raw materials is influencing the mass distribution (sieve residue). Using the mass distribution function, the frequency (sieve residue) is assigned to a mean particle diameter \bar{D} within the size class used. Therefore, the sieve residue in each size class is higher or lower if the range of the size classes used for analysis is large or small (cp. step 1 and step 2 in Figure 2.1).

Contrary to the sieve residue, the cumulative distribution function (cumulative finer) is ex-

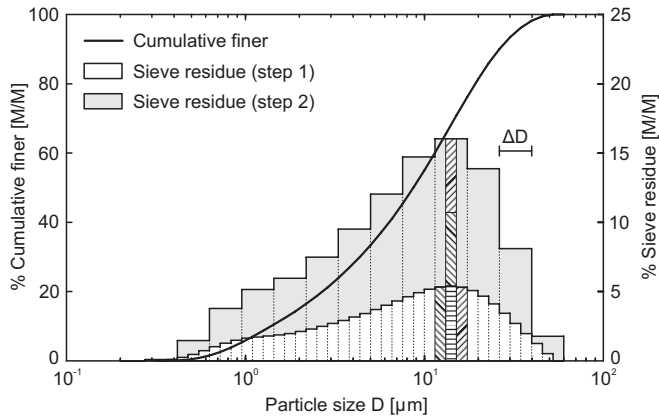


Figure 2.1: Comparison of cumulative finer and sieve residue for varying width ΔD of the sieve classes used for analyzing the grading of CEM I 52.5 N.

actly valid at the upper limit of the size class and is not influenced, as neither the probability density function, by the width of the size classes used for analysis. The width of the size classes (also number of size classes) is only influencing the number of supporting points of the cumulative distribution function. Fixed size classes are used for analyzing the raw materials as the composition of aggregates and fines by means of the optimization algorithm discussed in Section 4.3 is based on the sieve residue obtained in each size class ΔD .

When talking about grading of granular materials, it becomes obvious that the definition of size classes used for concrete ingredients and granular materials differs due to the distinction in different size classes and consideration of the materials' origin. Figure 2.2 gives an overview of common definitions for concrete ingredients and granular materials. It should be mentioned at this point that the definitions given in Figure 2.2 are not considered universally valid, as they can differ from the definitions used in, for instance, soil mechanics.

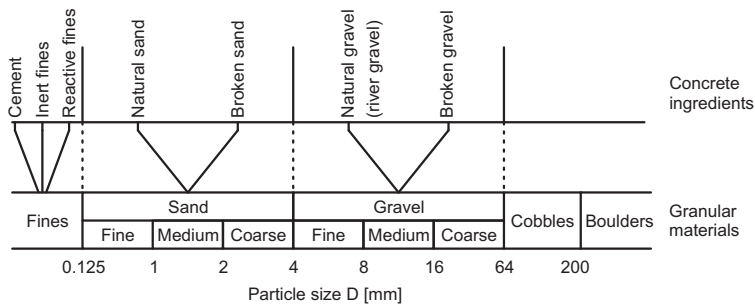


Figure 2.2: Size classes used for the denomination of granular materials and concrete ingredients.

2.2.2 Density measurements and related parameters

The density of the solid concrete ingredients is, besides the grading, a further important parameter for the concrete mix design. The specific density ρ^{spe} of the materials is required to formulate weight-volume relationships and is given by:

$$\rho^{spe} = \frac{M_{sol}}{V_{sol}} \quad (2.1)$$

with M_{sol} as the mass of the solids and V_{sol} as the true volume of the solids. The mass of the solids is determined by weighing, whereas the determination of the true volume of the solids requires more efforts. Here, the true volume of the solids is determined by displacement in water under vacuum. A pycnometer with known volume V_{pyc} is used to determine the true volume of the solids based on Archimedes' law. The measurement using the pycnometer method is described in EN 1097-7 for fines and filler materials and in EN 1097-6 for fine and coarse aggregates. By means of the data obtained using the pycnometer method, the specific density ρ^{spe} follows from:

$$\rho^{spe} = \frac{M_1 - M_0}{V_{pyc} - \frac{M_2 - M_1}{\rho_{liq}}} \quad (2.2)$$

with M_0 as the mass of the empty pycnometer, M_1 as the mass of the pycnometer filled with the dry sample, and M_2 giving the mass of the pycnometer filled with the sample and testing liquid. For testing fine materials, the temperature influence on the liquid density ρ_{liq} has to be considered in Eq. (2.2). Furthermore, an appropriate test liquid that is not dissolving the sample or reacting with single components of the sample has to be selected. In this respect, water was used for inert fillers and other fine materials, whereas cements and binders were measured with isopropyl alcohol.

Besides the specific density, the bulk density of the material is of special interest for storing and transporting materials. In contrast to the specific density, the bulk density considers the total volume that is occupied by the sample. This total volume includes the true volume of the sample V_{sol} , the volume of the remaining void fraction V_{voi} , and, in case of porous materials, the pore volume of the particles V_{por} . The bulk density depends on the densification of the sample as with denser particle packing the remaining void fraction decreases. As a result of the formation of interparticle forces, the bulk density of powders loosely and densely packed varies to a considerable extent. In this research, three types of densification methods are considered:

Loosely packed refers to the bulk density ρ^{loo} of a granular material that is not compacted by any means of vibration or tamping. For determining the bulk density of loosely packed granular materials, a vessel with known volume is carefully filled and the mass of the uncompacted sample in the vessel is measured.

Vibrated corresponds to the bulk density ρ^{vib} of a granular material that is compacted by means of vibration. Similar to the loosely packed bulk density, a vessel with known volume is filled using a filling hopper and the sample is compacted on a vibrating table until a constant volume is reached. After compacting the sample, the filling hopper and surplus material are removed and the mass of the compacted sample in the vessel is measured.

Densely packed is related to the bulk density ρ^{den} of mainly fines and is determined according to the specifications of EN 1097-4 using a Rigden device. The densely packed condition gives the highest bulk density that can be obtained by a granular material.

The bulk density considers the pore volume of particles in the total volume that is occupied by

the sample. The aforementioned measuring techniques are focused only on determining the total volume. However, some applications require more detailed information on the volume of pores that are connected to the surface of the particles (permeable pores). This pore volume is also referred to as open porosity. Using the measures obtained by displacement in water, the open porosity ϕ_{open} is calculated from:

$$\phi_{open} = \frac{M_{sat} - M_{dry}}{M_{sat} - M_{und}} \quad (2.3)$$

with M_{dry} as the mass of the oven dry sample, M_{sat} giving the mass of the saturated sample in surface dry condition, and M_{und} as the mass of the saturated sample determined underwater. The terms *saturated* and *surface dry* condition are explained in detail in the following section.

2.2.3 Determination of moisture content

The moisture content ψ_m of aggregates needs to be known to control the total water content of the concrete and to ensure correct batching of aggregates. The moisture content of aggregates follows from the mass relation of the dry sample (M_{dry}) and the wet sample (M_{wet}):

$$\psi_m = \frac{M_{wet} - M_{dry}}{M_{wet}} \quad (2.4)$$

The dry mass of the sample is given by the mass at oven-dry condition, whereas the mass of the wet sample can refer to different moisture conditions that are given by Mindess et al. (2003) as:

Oven-dry mass which is determined by drying the sample at 105 °C until constant mass is reached. Consequently, all moisture is removed from the sample and the particles are fully absorbent.

Air-dry condition that refers to particles with a dry surface, but with permeable pores that are partially filled with water and can therefore still absorb mixing water from the concrete mix.

Saturated surface dry condition at which all permeable pores are filled with water, but no water is on the surface. Aggregates in saturated surface dry condition neither absorb water from the concrete nor contribute water to the concrete mix.

Damp or wet condition where the permeable pores are completely filled with water and a water film of varying thickness surrounds the particles. The excess water on the particle surface can result in an increase of the mixing water if not considered.

The open porosity of natural and broken rock aggregates is relatively small so that the absorption of mixing water can be ignored in this case and only excessive water of the formed water films has to be considered for concrete batching. The higher open porosity of light-weight aggregates and recycled concrete aggregates requires adjustments in the concrete mix proportioning to account for the higher absorption capacity of these materials. The moisture content and other physical properties of the materials used in this research are addressed in the following sections.

2.3 Characteristics of aggregates

The largest part in concrete is occupied by aggregates (70 - 80% by volume) whose granulometric properties are relevant for the workability of the fresh concrete. An overview of the most relevant materials characteristics of the aggregates used in this research is given in the following section. Most of the concrete aggregates used for the experimental work reported in this thesis are of natural origin. The properties of special types of aggregates, such as recycled concrete aggregates or stone waste materials, are given in Section 2.4 and Section 2.5, respectively.

2.3.1 Coarse aggregates

Different types of river gravel, primarily consisting of quartz and dredged from areas along the Lower Rhine, were used as coarse aggregate fraction. All river gravels that have been used are certified for the use in concrete and fulfill the requirements on concrete aggregates according to EN 12620. The most relevant physical properties were determined by the characterization techniques described in Section 2.2. An overview of the physical properties is given in Appendix A.1 for the medium river gravels, applied in the fraction 4-16 mm and fraction 8-16 mm, and the fine river gravel that was used in the fraction 2-8 mm. Broken aggregates from natural rock were used in addition to the river gravels. The broken aggregate is generated from Scottish granite extracted in the Glensanda Quarry located on the west coast of Scotland. The grading of the broken aggregates, applied in the fraction 2-8 mm, is comparable to the fine river gravel as mentioned before. The use of the broken granite aggregates in concrete is certified and the material fulfills the requirements on concrete aggregates according to EN 12620.

2.3.2 Fine aggregates

Natural river sands were used primarily as fine aggregate fraction of the concrete tests. The river sands are of the same mineralogical origin as the river gravels discussed before and were dredged from areas along the Lower Rhine in Germany and the Netherlands. The sands have been applied in fractions of 0-1 mm, 0-2 mm, and 0-4 mm. Further information on the physical properties are given in Appendix A.1. Besides the natural river sands, sand fractions generated during the production of recycled concrete aggregates and broken aggregates have been applied as fine aggregates with multifunctional properties. These materials are discussed in the following sections.

2.4 Characteristics of recycled aggregates

Since the utilization of recycled materials in concrete production has received a lot of attention during the past years (Kerkhoff and Siebel, 2002; Müller, 2003a,b; Poon and Chan, 2006; Schießl and Müller, 1997; Wassing, 2002), two types of recycled concrete aggregates (RCA) of the fraction 0-2 mm have been selected for this research. In the considered case, the two RCAs that have been used are reprocessed materials obtained from the same type of masonry rubble. The original material is characterized by a minimum concrete content of 50% and the remaining quantity consists of brick, mortar, and plaster. The production of the reprocessed RCAs comprises two different types of treatment:

RCA1 is a reprocessed material obtained from masonry rubble that was screened to a fraction 4-31.5 mm before the secondary crushing. Constituents with a deleterious effect on the concrete properties were removed by means of extracting the fraction smaller than 4 mm from the feed material of the crusher. Substances with a negative effect on the hardened concrete properties are, for instance, clay components, organic matters, and cement paste with high porosity caused by a high w/c ratio of the original concrete. Their low mechanical resistance characterizes all these substances so that particles with a size smaller than 4 mm are generated during the primary crushing of the building rubble. This fact allows for an effective extraction of the deleterious substances by simple screening before the material is reprocessed.

RCA2 is also a reprocessed material from the same source of masonry rubble as RCA1 but with different treatment before the secondary crushing. Deleterious substances smaller than 4 mm were not extracted from the original material so that the entire fraction 0-31.5 mm of the masonry rubble was used as feed material for the crusher.

Regardless of the fact that material RCA1 was screened before the second crushing to remove deleterious substances, impurities like wood fiberboard, plastic, and metal were found in the

delivered material and lead to the conclusion that these deleterious substances are also present in the fines of the reprocessed material. An overview of the contaminants that were contained in the delivered samples is given in Figure 2.3. Similar components were also found in the unscreened material RCA2.

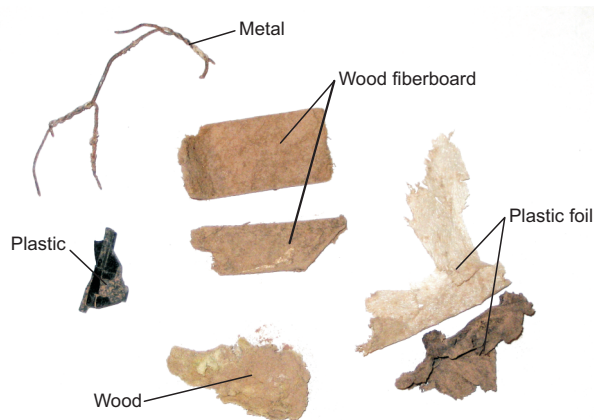


Figure 2.3: Impurities contained in the recycled material RCA1.

The fines smaller than $125\ \mu\text{m}$ have been extracted from both RCA samples by dry screening and are referred to as recycled concrete fines (RCF). In this context, the fines RCF1 and RCF2 refer to the corresponding coarse aggregate fraction RCA1 and RCA2, respectively. The extracted fines have been applied for the experimental work on cement replacement described in Section 5.3 and were therefore analyzed in terms of their chemical composition.

2.4.1 Chemical composition

The aimed application of RCF for cement replacement in concrete requires a thorough material characterization. Besides the physical properties of the material, also the chemical composition of the RCF is a relevant material property for the application as reactive filler material. Furthermore, the careful selection of the raw materials regarding their chemical composition prevents deleterious effects on the properties of the hardened concrete. For this reason, the fines extracted from the selected RCA have been analyzed regarding their elemental composition by means of X-Ray fluorescence (XRF). The major oxides of the analyzed RCF are listed in Table 2.1 and detailed values of the chemical composition are given in Appendix A.2.

The most abundant oxides in the analyzed RCF are silica (SiO_2), alumina (Al_2O_3), lime (CaO), iron (Fe_2O_3), potassium (K_2O), and sodium (Na_2O). Other oxides that have been detected in minor quantities are MnO , and SO_3 (cp. Table A.2). The chemical composition of the material RCF2 listed in Table 2.1 is in good agreement with the average values given by Müller (2003a) for 33 samples of masonry rubble and deviates only to a minor extent. Differences with statistical significance to the values given by Müller (2003a) were only found for the loss on ignition (LOI) and the Al_2O_3 and CaO contents. These variations are explained by Müller (2003a) as a result of variations in the mortar and concrete fraction of the masonry rubble and clarify the difference to the values given by Müller (2003a).

Table 2.1: Major oxides of the recycled concrete fines (RCF) determined by XRF-analysis (Pöllmann, 2007) and values taken from Müller (2003a)

Content [%]	RCF1	RCF2	Wassing (2002)		Müller (2003a)	
			Ra [‡]	Rac [‡]	Masonry	Pure brick
LOI	6.2	1.3	6.6	12.2	5.1	0.9
SiO ₂	69.9	73.3	59.0	55.5	68.0	66.8
Al ₂ O ₃	5.9	10.8	6.3	6.1	9.5	15.5
CaO	11.6	5.1	14.2	15.4	8.0	2.6
Fe ₂ O ₃	1.9	3.8	2.9	2.9	3.6	6.5
K ₂ O	1.2	2.3	1.1	1.1	2.2	3.1
Na ₂ O	0.7	1.0	0.5	0.4	0.7	0.8

[‡] RCF generated from lab-made concrete after 4 months of standard storage

[‡] Same concrete as used for Ra but exposed to accelerated carbonation

Based on the chemical composition of the analyzed materials, it can be stated that the selected sample RCF2 represents a recycled material with a high content of masonry rubble, whereas material RCF1 is considered to be a recycled material that contains higher quantities of the hardened cement paste of the original concrete and lower amounts of masonry rubble. Due to the lower content of masonry rubble, the chemical composition of RCF1 is in good agreement with the data extracted from Wassing (2002) for the material properties of pure RCF generated from concrete samples cast under laboratory conditions. The lower Al₂O₃ content obtained for sample RCF1, which is an indication for a lower content of clay minerals, also confirms this fact. The higher Al₂O₃ content determined for RCF2 results from the high Al₂O₃ content of clay bricks.

The results of the chemical analysis follow the processing of the recycled material. The screening of the reprocessed material RCA1 before the secondary crushing removes a large quantity of the masonry rubble that was contained in the original material. This masonry rubble is characterized by a lower mechanical resistance than the concrete aggregates or the cement paste and is broken to fractions smaller than 4 mm during the primary crushing. During the secondary crushing of the screened material, the hardened cement paste of the original concrete is crushed as the cement paste shows a lower mechanical resistance against the stresses generated during the crushing process than the aggregates of the original concrete.

2.4.2 Water absorption

The water absorption of RCA is an important parameter for the concrete mix design. Due to the porosity of the RCA, part of the mixing water is absorbed by the aggregates during the mixing process and is not available for the formation of a sufficient water layer around the particles. The absorbed water has to be compensated by additional mixing water or the use of plasticizers to allow the production of concrete with comparable workability.

The amount of absorbed water was determined according to the requirements for aggregates larger than 63 µm and smaller than 4 mm as described in EN 1097-6 on saturated surface dry samples. The oven dry samples were immersed in water for 24 hours and dried by a warm air stream until the characteristic cone shape according to Annex F of EN 1097-6 was obtained. Subsequently, the saturated surface dry samples were weighted and dried in a drying oven at 105 °C until constant mass was reached. The mass difference between saturated surface dry and oven dry condition was used to calculate the water absorption as given in Table 2.2.

Table 2.2: Water absorption of recycled concrete aggregates (RCA) of the fraction 0.71-1.4 determined according to EN 1097-6 in saturated surface dry condition.

Material	Water content	
	as delivered	EN 1097-6
	[M.-%]	[M.-%]
RCA 1	3.5	4.9
RCA 2	0.7	6.4

2.5 Characteristics of stone waste materials

Stone waste materials, both in coarse and fine fractions, are generated in large amounts in the natural stone industry or during the production of crushed aggregates from natural rock. The properties of these stone waste materials are strongly depending on their origin and the mineralogical composition of the raw materials. The cutting, drilling and polishing of ornamental stone generates fine stone waste materials under wet process conditions. The granulometric properties of these fine stone waste materials enables their use as fine filler material for concrete production. The sophisticated mechanization of the technological processes like cutting and polishing of ornamental stones results in a high quality of these stone waste materials and constant granulometric properties. Despite the constant granulometric properties, the moisture content of these materials differs to a large extent and makes it difficult to handle and dose these materials in a proper way. Therefore, a possible application of these materials in concrete is recommendable in slurry form. However, the high water content of these stone waste slurries makes the transport over long distances financially unattractive compared to other filler materials, such as limestone powder, and limits the application to concrete production that is located close to the place of origin. A broader application of fine stone waste materials is offered by the production of crushed aggregates from natural rock, as here most of the production processes require dry conditions.

The production of crushed aggregates generates large quantities of fine stone waste materials by crushing and transport of the materials. These fines are partly extracted from the process air by means of filters and cyclones to avoid an emission to the environment. However, a large quantity of fines remains in the aggregate fraction and has to be removed by washing processes as some national standards and application rules in Europe prescribe a maximum fines content of concrete aggregates. These limitations are based on regulations of the past when most of the concrete aggregates were dredged from rivers or former river areas and contained high amounts of fines, such as clay, with detrimental effects on the concrete properties. Considering the granulometric properties of the fine stone waste materials generated during the production of crushed aggregates and the higher requirements of modern concretes, like self-compacting concrete, regarding the fines content, the washing of crushed aggregates becomes unnecessary. In this respect, the focus of this research is on the direct application of the unwashed crushed aggregates to replace conventional filler materials like limestone powder. The unwashed crushed fine aggregate fraction is referred to as Premix 0-4 and detailed information on the material properties are given in the following section.

2.5.1 Premix 0-4

The so-called Premix 0-4 is an intermediate product that is generated during the production of crushed rock aggregates in the Glensanda Quarry, Scotland (UK). The intermediate product is extracted from the coarser aggregate fractions for the production of crushed sands by further conditioning. By means of sieving and washing processes, the fines smaller than 125 μm are ex-

tracted from the crushed sand. The coarser aggregate fractions as well as the crushed sand fulfill the requirements for the use in concrete production prescribed in EN 12620 and the aggregates and sand fraction are tested periodically regarding essential properties for concrete production, such as grading, water absorption, chloride content, etc. It is therefore assumed that also the generated fines are applicable for concrete production and that the granite fines do not affect the concrete properties. In this respect, the elemental composition of the granite fines was determined by XRF-analysis and further information on the mineralogical composition were derived from X-ray diffraction analysis (XRD). Both analyses showed that the granite is mainly composed of SiO_2 (Quartz) and any deleterious substances were not detected (see Appendix A.2).

Besides the required tests for the use as concrete aggregate, the Premix 0-4 was analyzed by sieve analysis for variations in its PSD and the producing company measured regularly the grading for internal quality control. The producing company provided the data of 121 samples over a period of 11 months (January 2006 - November 2006). The results of the quality control are depicted in Figure 2.4 including the coefficient of variation (COV). Detailed values of the granulometric properties are listed in Table 2.3.

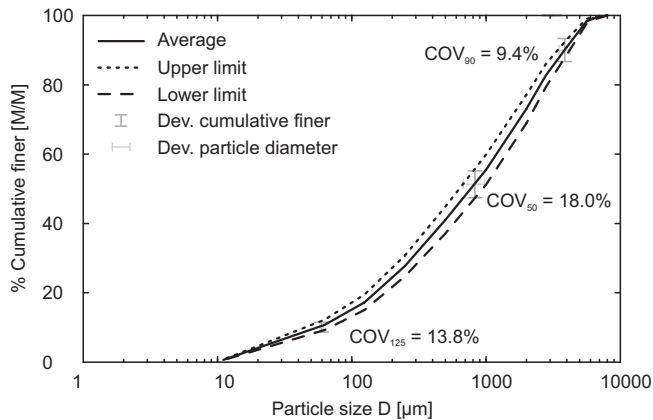


Figure 2.4: PSD of the Premix 0-4 and variations in the grading determined by a monthly quality control conducted over a period of 11 months (January 2006 - November 2006).

The data of the quality control depicted in Figure 2.4 illustrate that the PSD of the Premix 0-4 shows low variation in both the coarse and finer range. The fraction finer than 125 μm amounts to about 11% and showed also no significant variations over the analyzed period of time (cp. Table 2.3). The high content of fines smaller than 125 μm in the Premix 0-4 results from transport processes in the quarry and the treatment in the crushers. In addition to the monthly quality check of the entire grading of the Premix 0-4, the grading of the fines smaller than 125 μm was examined by LDA in monthly intervals over a period of 7 months (June 2006 - September 2006 as well as March 2007 - May 2007). The results of these measurements are depicted in Figure 2.5 and detailed values are given in Table 2.3.

As expected from the data that were obtained for the entire grading of the Premix 0-4, the grading of the fines smaller than 125 μm is also constant and showed no evident fluctuations over the measuring period.

Table 2.3: Granulometric properties of the analyzed stone waste materials (standard deviations are given in parentheses).

Measure	Premix 0-4	Granite fines [‡]	Filter cake
D _{max} [μm]	5600	150	138
D ₉₀ [μm]	3783 (356)	92 (26)	64 (22)
D ₅₀ [μm]	813 (146)	18.7 (5.3)	12.2 (2.6)
D ₁₀ [μm]	–	2.0 (0.3)	1.8 (0.2)
C ₁₂₅ [%]	10.7 (1.5)	–	–
D _{min} [μm]	10	0.5	0.5

[‡] Extracted from the Premix 0-4 by sieving, mesh opening 125 μm.

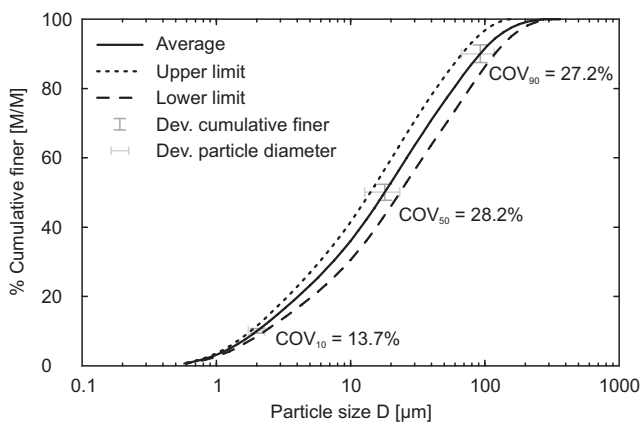


Figure 2.5: PSD of the granite fines contained in the Premix 0-4 and variations in the grading thereof determined by a monthly quality control conducted over a period of 7 months (June 2006 - September 2006 as well as March 2007 - May 2007).

2.5.2 Filter cake

The main object of the application of the generated fines focuses on the direct utilization of the untreated intermediate product in concrete. This concept prevents the generation of fine stone waste materials and reduces the energy consumption during production as the washing process is avoided. However, large quantities of this fine stone waste material have been generated already during the production of the past years and were landfilled in an exploited part of the quarry and only a minor part of these fines is used for the production of calcium silicate blocks or for the grogging of clay bricks. As mentioned before, these fines are extracted from the aggregate fraction by a washing process where the wash water is reused in the process. Wash water and fines are separated by means of a filter press and the resulting filter cake has a moisture content of about 20%. The grading of the generated filter cake was also analyzed monthly by LDA over a period of 13 months (September 2006 - September 2007). The results of these measurements

are depicted in Figure 2.6 and listed in Table 2.3.

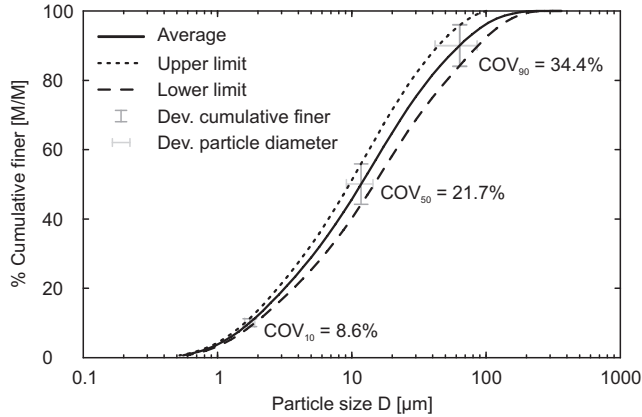


Figure 2.6: PSD of the granite fines of the analyzed filter cake and variations in the grading thereof determined by a monthly quality control conducted over a period of 13 months (September 2006 - September 2007).

The fines of the filter cake differ only slightly in their grading from the fines that were extracted from the Premix 0-4. Both materials have a similar smallest particle size D_{min} of about 0.5 μm and do not differ in their D_{10} values significantly. However, the grading of the filter cake is slightly shifted to the finer range considering the D_{50} and D_{90} values given in Table 2.3 and allows for replacing other filler materials such as limestone powder or fly ash. A comparison with conventional materials is therefore made in the following section.

2.5.3 Comparison with conventional materials

As mentioned in the previous section, the granite fines of the Premix 0-4 as well as the generated filter cake allow for replacing conventional filler materials like limestone powder or fly ash. This research focuses mainly on the application of the unwashed premixed sand as the utilization of the generated filter cake in EMC mixes is not resulting in financial benefits. The high moisture content of the filter cake increases the costs for transport per ton of dry material and the stiff consistency requires investments in special techniques for dosing the material. However, the successful application of the fines generated by the washing of aggregates in SCC is reported by Hunger (2010) and makes the application of the filter cake feasible for concrete production that is closely located to the place of origin.

The direct comparison of the granulometric properties of the granite fines with other filler materials reveals that the grading of the filter cake is comparable to the fly ash that was applied in this research. This fact holds also for the granite fines smaller than 125 μm of the Premix 0-4. Another important issue that is relevant for the composition of concrete aggregates becomes obvious from the data depicted in Figure 2.7. The aimed optimization of the entire grading of the composed solid mix, as discussed in Section 4.2.3, requires a certain overlap of the PSD of the single raw materials to compose a solid mix with the lowest deviation from the given target line. This requirement is fulfilled when the fines (cement and fillers) as well as coarse and fine aggregates are considered separately (see Figure 2.7). However, a gap in the grading of the fines as well as the fine and coarse sand depicted in Figure 2.7 exists. This gap usually ranges from 100

to 180 μm and was observed for several concrete mixes that were designed within this research. The Premix 0-4 contains a sufficient amount of particles in that range to close the gap between the largest cement or filler particles at about 100 μm and the finest sand particles at about 180 μm .

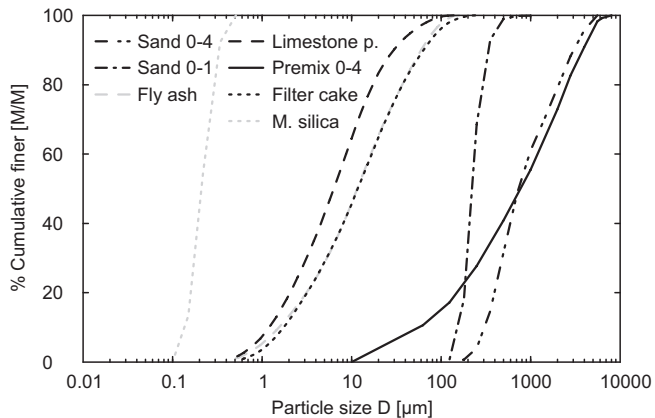


Figure 2.7: Grading of selected fines and sands.

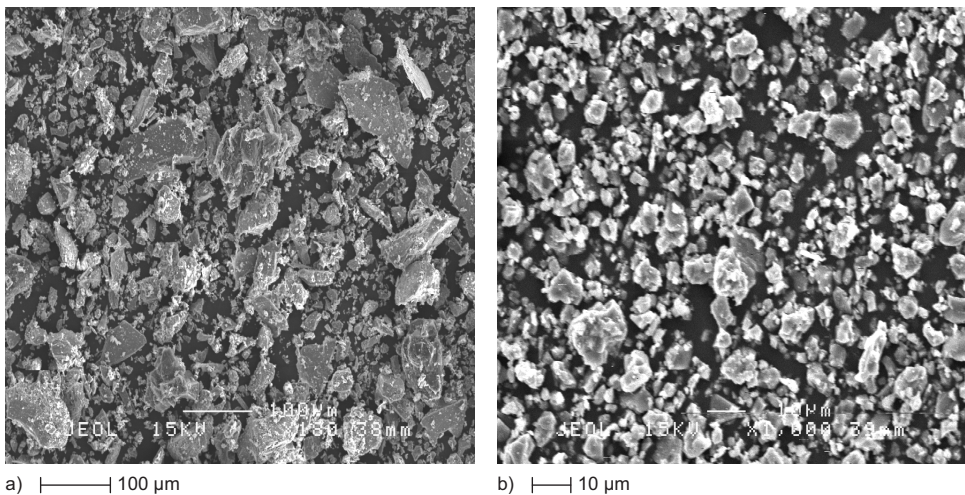


Figure 2.8: SEM micrographs of analyzed powders showing their comparable particle shape: a) granite fines, and b) limestone powder (Hunger, 2010).

Considering the granulometric properties of the raw materials, not only the PSD of the particles is relevant, but also the particle shape influences the properties of fresh and hardened concrete.

The SEM images of the analyzed fines reveal that the granite fines are comparable to limestone powder regarding their particle shape and surface texture. Both types of fines, granite and limestone, are characterized by angular particles with cubical or prismatic shape and high surface roughness, which is caused by the production process by means of grinding and crushing (see Figure 2.8).

2.6 Characteristics of fines

The physical and chemical characteristics of the fines have a large impact on the properties of the paste that is made up of particles smaller than 125 μm and water. In concrete, the paste functions in different modes and determines the fresh and hardened concrete properties. The workability of the fresh concrete is governed by the rheological properties of the paste and in hardened state the mechanical strength and the durability of the concrete are characterized by the microscopic properties of the paste. A first and overall classification of the fines considers the involvement in the hydration process. Following Figure 2.2, the fines are divided into three main categories:

Cement is defined according to EN 197-1 as a fine hydraulic binder that reacts with water to form hydration products. This classical definition refers mainly to ordinary Portland cement (OPC) as here the hydration is the prevailing reaction for curing and strength development. The hydration of OPC is dominated by the reaction of tricalcium silicate (C_3S), also referred to as alite in its mineral phase, and dicalcium silicate (C_2S), whose mineral phase is named belite. The two main clinker phases, C_3S and C_2S , react with water to form fibrous calcium silicate hydrates (CSH) that give the strength to the hardened concrete (Mindess et al., 2003). The requirements on cements used for concrete production are prescribed by international and national standards (EN 197-1, ASTM C150/C595, CSA A5/A8/A362, etc.).

Reactive fines are added to the concrete to improve or influence certain properties, such as workability, strength development, or heat release during hydration. These fines are acting partly as filler material to improve the particle packing in the micro-range, but have also potential for latent-hydraulic or pozzolanic reactions. The reaction of latent-hydraulic materials is similar to the hydration of cement clinker, but calcium hydroxide, alkali-activated reaction, or calcium sulfate, sulfate-activated reaction, are needed to accelerate the reaction (Chen, 2007). The most commonly used latent-hydraulic fines in concrete are ground granulated blast furnace slag (GGBFS) that is blended with OPC to form slag cements. Pozzolanic fines need calcium hydroxide to form CSH phases from the amorphous or glassy silica that are the major components of a pozzolan. Natural pozzolans are trass and pumice, but also industrial by-products, such as fly ash and silica fume, have pozzolanic properties (Mindess et al., 2003).

Inert fines, also referred to as non-reactive fines, do not actively participate in the cement hydration, but can have an accelerating effect on the strength development at early ages as the fines act as nucleation sites for CSH (Domone, 2007; Reschke, 2000). Inert fines, such as ground limestone, silica flour, or hydrated lime, are blended with OPC to form masonry cement with improved workability and water retention (Mindess et al., 2003).

In the following, the most relevant material properties of the fines used for the experimental work of this research are discussed.

2.6.1 Cements

The Dutch construction sector uses mainly slag-blended cements (CEM III) that are followed by ordinary Portland cement (CEM I). The use of so-called Portland composite cements (CEM II) and composite cements (CEM V) is of minor interest for the ready-mix concrete sector or the production of concrete mass products and predominates in the Netherlands, therefore, the market of packed cement.

A slag-blended cement type CEM III/B 42.5 N with low hydration heat release (LH) and high sulfate resistance (HS) was selected for the main experiments on EMC mixes. Furthermore, ordinary Portland cement of the type CEM I 32.5 R and CEM I 52.5 N were used. The CEM I 52.5 N was used for tests on EMC and was blended with the CEM III/B 42.5 N. The blending of ordinary Portland cement with slag-blended cements is a commonly used practice in the Dutch precast concrete industry to increase the early strength of the final products and to obtain a denser microstructure and better durability (Krikhaar, 2010). A OPC with rapid, but low strength development (CEM I 32.5 R) was mainly used for packing experiments and tests on the influence of reactive fines on the strength development of mortars.

Since micro cements show a beneficial effect on the microstructure of the paste and the packing of the fines, an ordinary Portland cement with high fineness (CEM I 52.R), low effective alkali content (LA), and sulfate resistance (HS) was incorporated in this research. The technical specifications of the applied cements are given in Table 2.4 and their physical properties are listed in Appendix A.1.

Table 2.4: Technical specifications of the applied cements (source: Krikhaar (2010) and Cementa AB Sweden (2005)).

Cement	Clinker content	Slag content	Na ₂ O equivalent	Chloride content	Minor constituents	Initial set
	[%]	[%]	[%]	[%]	[%]	[min]
CEM I 32.5 R	99	–	0.7	0.04	1	145
CEM I 52.5 N	97	–	0.7	0.03	3	120
CEM I 52.5 R [‡]	≥ 95	–	≤ 0.6	≤ 0.1	≤ 5	30
CEM III/B 42.5 N	30	70	0.5	0.04	–	230

[‡] Micro cement

2.6.2 Fillers

Fillers are used in concrete to obtain a denser and homogeneous paste structure by adding particles with sizes smaller than 125 µm (Moosberg-Bustnes et al., 2004). Reactive fines can improve the microstructure of the hardened paste, whereas inert fines can function (depending on their fineness) as nucleation sites for the formation of CSH phases. As outlined in Section 1.2, traditional EMC mixes are characterized by a low content of inert fines and the use of fillers is rather uncommon. Since the beneficial effect of fillers, such as limestone powder and fly ash, on the packing density and green-strength was demonstrated by Bornemann (2005), different types of reactive and inert fines have been applied as fillers in this research.

Stone waste powders in the form of premixed sand (Premix 0-4) were used as inert fines to improve the packing of EMC mixes. The properties of the granite fines are addressed in Section 2.5. Furthermore, a hard coal fly ash was used for the experimental work with focus on the early-age behavior of EMC mixes discussed in Section 6.5. The applied fly ash is generated by the combustion of hard coal and fulfills the requirements according to EN 450-1. Quartz flour was used to study the effect of improved particle packing of the fines discussed in Section 3.3.3 and as inert cement replacement for the experimental work on recycled concrete fines outlined in Section 5.3. The composed high strength mortar that was used for the shrinkage tests discussed in Section 5.4 uses the before mentioned fly ash and micro silica as fillers. The colloidal micro silica is based on amorphous silica and was applied as water based suspension that is certified

for the use in high performance concrete. The PSD of the applied filler materials is depicted in Figure 2.7 and their physical properties are listed in Appendix A.1.

2.6.3 Characteristics of photocatalytic materials

The application of photocatalysts in concrete mass products with multifunctional properties is discussed in detail in Chapter 7 and Chapter 8 of this thesis. Five different photocatalysts were selected for the experimental investigations on the influence of powder type and fineness discussed in Section 7.6.5 and were used for further experiments on new developed top-layer mixes addressed in Section 8.3. The selected powders cover four commercially available TiO_2 in the anatase modification (TiO_2 A-D) and one carbon-doped TiO_2 (TiO_2 E) of which the particle size distribution is comparable to the PSD of the undoped powder acting only in the UV-A range (TiO_2 D). As can be seen from the specific properties of the deployed photocatalysts listed in Table 2.5, the selected powders are characterized by their finenesses and high specific surface areas in order to provide a high active area for the photocatalytic reaction. The grading of the photocatalytic powders is considered in the mix design algorithm discussed in Section 4.3, but has only a minor effect on the entire grading of the composed solid mix since the TiO_2 volume is relatively low compared to other filler materials, such as micro or nano silica. In terms of chemical reactivity, the applied photocatalysts are considered to be chemically inert regarding cement hydration, but possessing photocatalytic activity when exposed to UV-A irradiance. This photocatalytic activity remains constant over time as the photocatalyst is participating in the chemical transformations, but is not consumed by the reactions themselves.

Table 2.5: Properties of applied photocatalytic materials.

	TiO_2 A	TiO_2 B	TiO_2 C	TiO_2 D	TiO_2 E [‡]
Anatase	n.s.	> 95%	80%	100%	100%
Rutile	n.s.	< 5%	20%	–	–
Specific density [g/cm^3]	3.90*	3.94	3.90*	3.90*	3.90*
Characteristic particle size [μm]					
D _{0.1}	0.65 [#]	1.193	0.641 [#]	0.593 [#]	0.574 [#]
D _{0.5}	1.245 [#]	2.72	2.104 [#]	2.014 [#]	2.075 [#]
D _{0.9}	2.487 [#]	6.535	7.123 [#]	4.349 [#]	4.92 [#]
Computed specific surface area					
Specific surface [cm^2/g]	15847 [#]	7916	11910 [#]	13139 [#]	13113 [#]
Specific surface [m^2/cm^3]	6181 [#]	3115	4645 [#]	5195 [#]	5114 [#]

[‡] carbon doped TiO_2

* value taken from data sheet

[#] based on measured agglomerates

2.7 Workability tests for earth-moist concrete

The term *workability* is not clearly defined in the literature as the term applies differently to the various types of concrete. In general, fresh concrete properties such as consistency, flowability, mobility, pumpability and compactibility are related to the term workability of concrete (Mindess et al., 2003). For the understanding of EMC, workability is defined as a combination of

compaction behavior, filling behavior of the concrete mix, and demolding behavior of the fresh concrete product after compaction. In the following section, suitable tests for the assessment of the workability of EMC are discussed. As outlined in Section 1.1, NWCs with high plastic consistency or SCCs with self-flowing characteristics are also used for the production of concrete mass products. Characterization methods for these types of concrete will not be explained in this section as a broad overview of workability tests for NWCs with plastic viscosity can be found in Bartos et al. (2002); Ferraris (1996); Koehler and Fowler (2003). In Hunger (2010), suitable tests for the characterization of SCC are discussed and their relevance for practical applications is addressed.

2.7.1 Degree of compaction

The degree of compaction test, also referred to as Walz test or compaction index test, was developed during the 1960s in Germany by Walz (1964) and is standardized in Europe by EN 12350-4 and in Germany by DIN-EN 12350-4. The workability of the tested concrete mix is expressed by the compaction behavior of the concrete sample compacted in a standard container. The square container sizes $a \times a \times H_1$ of $200 \times 200 \times 400$ mm and the sample is compacted by vibration. The volume change of the concrete sample is determined by the distance from the surface of the compacted concrete to the upper edge of the container in the middle of each side (cp. Figure 2.9). In the following, the degree of compaction is calculated as:

$$c_{DIN} = \frac{H_1}{H_1 - \bar{s}} \quad (2.5)$$

$$\text{with } \bar{s} = \frac{1}{4} \sum_{i=1}^4 s_i$$

Typical results of the test range from 1.02 to 1.50. Outside this range the concrete has a workability for which the degree of compaction test is not suitable (Bartos et al., 2002). Walz (1964) gives values around 1.05 for concrete having a high apparent workability, around 1.20 for plastic concrete with medium apparent workability, and 1.40 for stiff concrete with low apparent workability. A compaction curve is obtained by plotting the height of the concrete in the container versus time and allows for determining the time for complete compaction or the compaction behavior of different concretes can be compared using defined compaction efforts (Walz, 1964). The advantages of the test are described by Bartos et al. (2002) in that way that the test is inexpensive and easy to perform. Furthermore, the test provides a useful assessment of concrete tested by normal compaction efforts. According to Walz (1964), the test shows a high repeatability of the measurements. The maximum error (3σ -value) of the measurements conducted by Walz (1964) amounts to less than 10%, whereas the 2σ -value is less than 6%. Nevertheless, an above average size of the sample (approximately 43 kg) is required due to the size of the container and the container is difficult to empty for concrete with low workability.

The above average size of the sample, which is not easy to handle, can be reduced by downsizing the container. In the present case, standard cube molds with a side length a of 150 mm are employed with a filling hopper of 150 mm in height. The total height H_1 of the rectangular cast amounts to 300 mm instead of 400 mm as prescribed in DIN-EN 12350-4. By means of this modification, less sample material is needed and the results of the compressive strength test can directly be related to the degree of compaction, as they are determined using the same sample. A similar downsizing was also suggested by Walz (1964).

It is assumed that the downsizing of the container does not influence the results of the test as a constant scaling factor of 0.75 is used for all dimensions of the container so that the resulting

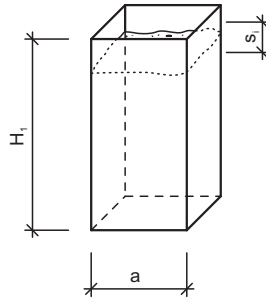


Figure 2.9: Square container used for determining the degree of compaction according to DIN-EN 12350-4.

degree of compaction c_{DIN} will be the same. This fact is also confirmed by the linear relation between the degree of compaction c_{DIN} according to DIN-EN 12350-4 and the computed degree of compaction c_{com} as shown in Figure 2.10. The computed degree of compaction c_{com} uses the densities of the fresh concrete densely and loosely packed in a round vessel having a fixed volume of 8 l and a diameter of 205 mm.

The approach of using the ratio of the fresh concrete densities loosely and densely packed is also mentioned by Walz (1964) in his explanation of the test procedure. The use of a squared container having a side length a of 200 mm and the measurement of the height change s_i is a simplification made by Walz (1964) to meet the demands of test method that is easy to handle on construction sites. Furthermore, cubes having a side length s of 200 mm were standard for tests on concrete at that time.

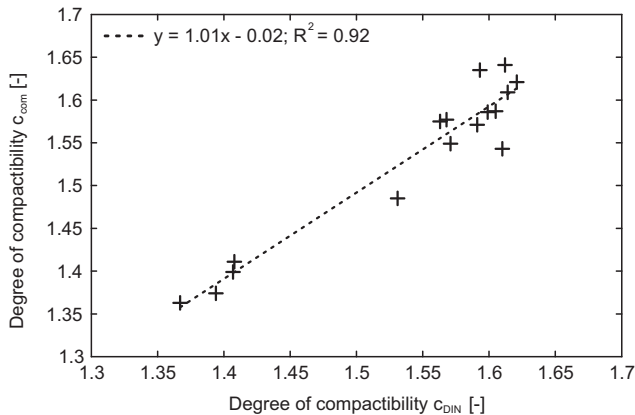


Figure 2.10: Relation between the degree of compaction c_{DIN} and the computed degree of compaction c_{com} using density values.

Considering the determined densities of the fresh concrete mix, the equation of the computed

degree of compaction c_{com} is as follows:

$$c_{com} = \frac{\rho_{con}^{den}}{\rho_{con}^{loo}} = \frac{M_{con}^{den}/V_{ves}}{M_{con}^{loo}/V_{ves}} \quad (2.6)$$

For the experiments discussed in this thesis, the degree of compaction is determined on standard cube molds having a side length a of 150 mm and using a filling hopper of 150 mm in height. These results are referred to as c_{DIN} .

2.7.2 Proctor test

The Proctor test was developed in the early 1930s by Ralph R. Proctor in the U.S. and is a commonly used method for evaluating the compaction behavior of soils in dependence on the water content. The test is standardized by many national standards (EN 13286-2, DIN 18127, ASTM D698/D1557). Using the Proctor test, the dry density of a granular material, primarily soils, is determined as a function of the water content (Craig, 1994). The sample is compacted by means of constant compaction efforts, which is achieved by tamping a drop weight (rammer) with several strokes. Three different weights with different dropping heights and amounts of strokes are prescribed in DIN 18127. The standard Proctor test according to DIN 18127 uses drop weights with 2.5, 4.5, and 15 kg with a dropping height of 300, 450, and 600 mm combined with 25, 22, and 22 strokes, respectively. The modified Proctor test according to DIN 18127 uses drop weights of 4.5 and 15 kg from a dropping height of 450 and 600 mm, respectively. The impact of the drop weight is damped by a spring at the bottom of the rammer. The spring rate that is prescribed in DIN 18127 is depending on the drop weight and the type of drop weight used (A, B, or C). The principle of the standard Proctor test used in soil mechanics is illustrated in Figure 2.11a and resulting compaction curves for different compaction efforts are depicted in Figure 2.11b.

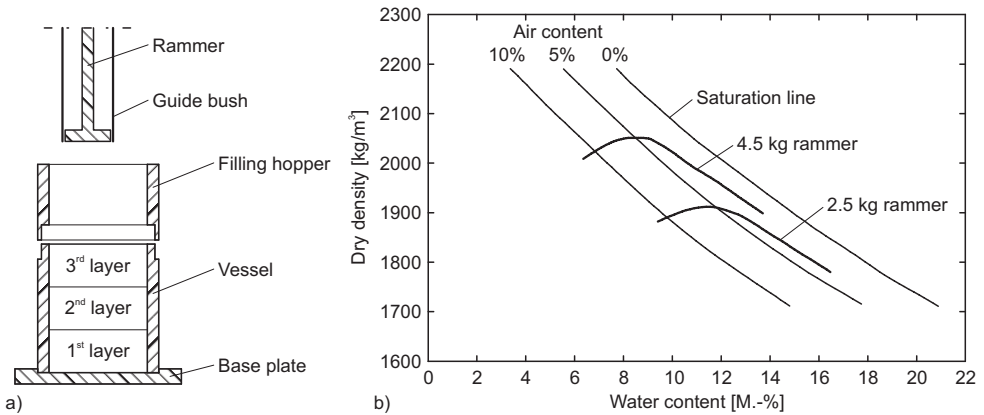


Figure 2.11: Proctor test: a) schematic illustration, and b) compaction curves for different compaction efforts according to Craig (1994).

In addition to the use for testing soils, the test can also be applied to lean and dry concrete mixes as reported by Juvas (1996) and Bartos et al. (2002). For tests on concrete, the results correlate

with the properties of aggregates such as content of fines and shape of coarse aggregates. The precision of the Proctor test is reported by Juvas (1996) as to be sufficient for production and the test is simple to perform under laboratory conditions or in concrete plants. Besides the advantages of the Proctor test and its simple use, the test is strongly depending on the operator and how evenly the strokes are applied to the sample (Juvas, 1996).

An alternative compaction method without tamping is given in ASTM D4253. This standard uses a vibrating table in combination with a surcharge to determine the maximum dry density of free-draining soils. The principle of vibratory compaction can also be found in the modification suggested by Bornemann (2005). The modification of Bornemann considers the requirements on EMC and offers the possibility for further testing of the sample immediately after stripping it from the mold or at a later stage. The apparatus uses a cylindrical mold for standard concrete samples having a height of 300 mm and a diameter of 150 mm. The mold is filled with the concrete sample and a surcharge having a weight of 28 kg is placed on top of the concrete. After placing the surcharge, the concrete is compacted on a vibratory table and inductive displacement transducers measure the displacement of the surcharge. The recorded data show the compaction behavior of the sample over vibrating time and can be used for calculating the packing density.

Both tests, classical Proctor test as well as vibrated Proctor test, are applicable for tests on EMC even if the classical Proctor test is making use of impact compaction. For that reason, the vibrated Proctor test appears to be more suitable for tests on EMC than the classical Proctor test as the compaction of the vibrated Proctor test is not depending on the operator. Unfavorable influences on the compaction of the sample cannot be avoided when the classical Proctor test is done manually and not performed by an automatic Proctor device. Furthermore, an inhomogeneous compaction of the sample can occur when the compaction behavior of the sample is low as it is the case for very dry mixes. Due to the height of the sample, the compaction of the sample in the middle is lower than in the upper and lower region as here the impacts of the tamping have a more concentrated effect. Moreover, the filling of the sample material in layers is also causing inhomogeneous densities over the height of the sample as reported by Bornemann (2005).

Finally, it can be concluded that both versions of the Proctor test provide an easy to handle test method for the workability of EMC. The test device is rather inexpensive and can be used both in the lab and the production plant, as it is transportable. However, the inefficient and deviant compaction of the sample by a manual operation makes the test results doubtful.

2.7.3 CemTec test

The CemTec test procedure was developed by C. Häring to produce EMC samples in a simple and accessible way as the optimization of EMC mixes is usually carried out on large-scale production. The optimization on production machines requires great financial and time expenses (Häring, 2000) and can usually only be carried out when the production volume is low. However, changes of the material properties have to be considered during the production process in order to assure constant product properties. For that reason, the developed CemTec test procedure allows the production of small EMC samples. Different tests can be performed on the produced samples, such as measurement of dry density and compaction behavior, determination of the optimum water content, assessment of the green-strength and surface quality, and characterization of the freeze-thaw resistance.

The test procedure is not standardized, as it is an in-house development of CemTec Beratung GmbH. According to Häring (2000), the test is easy to perform and can be used up to a maximum aggregates size of 16 mm. Samples having a diameter of 60 mm are produced by the test device and the height of the produced samples should not exceed 30 mm to avoid inhomogeneous compaction over the sample height. For determining the strength of the hardened samples, a combined compression/tensile splitting test is suggested by Häring and the results of the strength test are in good agreement with values obtained on production machines.

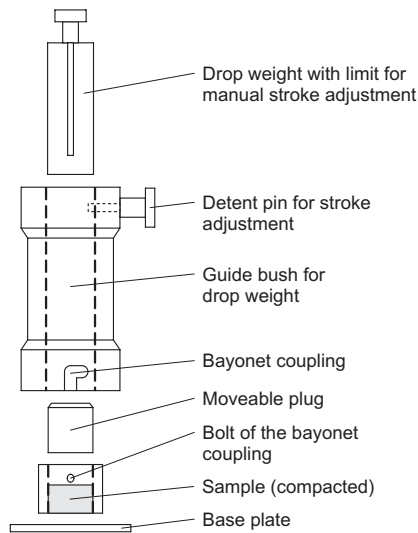


Figure 2.12: Schematic illustration of the CemTec test (Häring, 2003).

2.7.4 IC-test

The method and the equipment of the IC-test were developed by I. Paakkinen in 1984 in Finland (Paakkinen, 1986) and were later adopted by the Nordtest method NT BUILD 427 in 1994. The equipment of the IC-test can be used for testing the compaction behavior of granular materials like zero-slump concrete, soil, asphalt and other granular materials in dry or moisturized conditions. The data of the IC-test give information about the workability of the granular mix in regard to its compaction behavior and the final density after a certain number of working cycles. By means of the IC-test, the optimum water content of a granular mix, e.g. concrete, can be adjusted for achieving maximum density. For that purpose, the sample has to be compacted in multiple measuring cycles using varying water contents. Additional information, such as shear rate, can also be determined by the IC-test. Furthermore, the cylindrical sample obtained after compaction can be tested immediately after removal from the mold for its strength, or cured and tested later. The compressive strength measured immediately after compaction serves as an indicating value for the green-strength of the fresh concrete. The basic principle of the IC-test developed by (Paakkinen, 1986) is illustrated in Figure 2.13.

The sample is compacted by a combination of pressure and shear movement without the use of vibration energy. This principle is referred to as shear-compaction principle (cp. Figure 2.13). The pressure is introduced to the sample by compressing it between the top and bottom plate of the sample cylinder, whereas the gyratory movement of the sample cylinder is resulting in shear forces. The gyratory movement of the sample is caused by the slightly inclined ends of the sample, which are rotating around the central axis of the sample cylinder during the test (Invelop, 2005). One working cycle is defined as a complete rotation of the sample around the fixed axis. The applied pressure, rotation speed, as well as the inclination of the sample to the vertical axis of the device can be adjusted and kept constant during each test. During the test, the IC-tester measures the height of the sample and the shear force and calculates the resulting density based on the sample's mass given to the program. All values can be recorded for later data analysis. Figure 2.14 illustrates the measures obtained by the IC-test for two different EMC mixes.

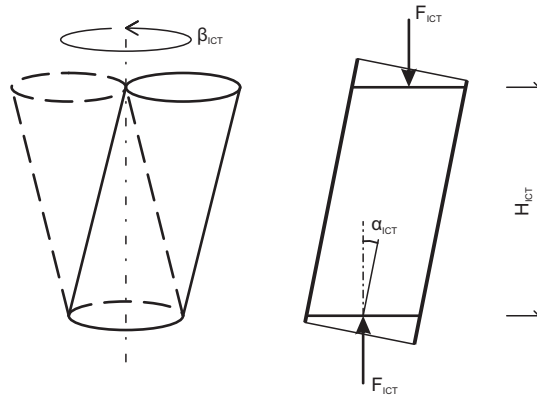


Figure 2.13: Schematic illustration of the working principle of the IC-test (Käppi and Nordenswan, 2007).

The graphs illustrating the compaction behavior obtained by the tests of Bornemann (2005) show a similar run as the results of the IC-test depicted in Figure 2.14. However, the pressure in the sample of the vibrated Proctor test is extremely low as a surcharge of 28 kg is resulting in a pressure of 0.016 N/mm^2 only. Compared to that value, the pressure in the sample of the IC-test can be increased up to 0.32 N/mm^2 which is 20 times higher. The obtained packing densities will also reflect this difference. The vibrated Proctor tests takes up to 15 min until the final packing density is reached, whereas mixes having a high water content achieve no significant density changes already after 10 min. Compared to that, the higher compaction efforts of the IC-test allow for a faster compaction and the maximum packing fraction is obtained already after 2.5 min (depending on the settings).

Käppi and Nordenswan (2007) give an equation for calculating the compaction work W_c from the recorded data by integrating the product of the gyratory angle α_{ICT} , the sample's volume V_{con} , and the measured shear stress τ over the total rotation angle φ_{ICT} that amounts to $2\pi N$ and the corresponding equation reads:

$$W_c = \alpha_{ICT} \int_0^\varphi V_{con} \tau d\beta \quad (2.7)$$

The specific compaction work that allows for comparing different EMC mixes is derived, according to Käppi and Nordenswan (2007), by dividing Eq. (2.7) by the sample's mass M_{con} and follows for N compaction cycles from:

$$\frac{W_c}{M_{con}} = \frac{2\pi\alpha_{ICT}}{M_{con}} \sum_{i=0}^N V_{con,i} \tau_i \quad (2.8)$$

with V_i as average volume of the sample, and τ_i as measured average shear stress in each cycle. Using the specific compaction work, different EMC mixes can be compared and the parameters of the IC-test for compacting the sample can be adjusted to the compaction efforts that are used on industrial scale. For this purpose, a reference mix from the production has to be used and

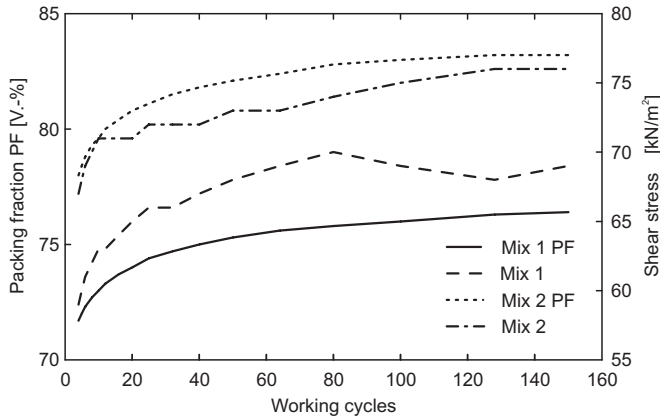


Figure 2.14: Packing fraction and shear rate versus time for two different EMC mixes.

the IC-test has to be adjusted in such a way that the final density of the sample is the same as obtained by the production machine on industrial scale (Käppi and Nordenswan, 2007).

The accurate and constant simulation of the compaction process causes the main advantage of the IC-test. Furthermore, the IC-test is able to identify a change in the water content of three to five liters of water per cubic meter of concrete and the results show a good repeatability and reproducibility (Juvas, 1996). It is questioned by Ferraris (1996) if the applied shear-compaction method can be used for simulating the compaction behavior of EMC products like concrete paving blocks, curbs, etc., as these types of products are compacted using a combined compaction of vibration and pressure.

Nevertheless, the cyclic shear motion combined with the axial compression allows a realignment of the particles in such a way that the packing density is increased and the void content is reduced Juvas (1996). It is also stated by Häring (2000) that the applied compaction method is of lesser importance than the obtained degree of compaction. Compared to other test procedures, e.g. modified Proctor test, or Vebe test, the IC-test is able to apply high compaction efforts as used in the production of EMC products, which makes it favorable for material research conducted on laboratory scale. The experimental tests carried out on EMC mixes in this research are using the following working parameters:

- Cylinder inclination (α_{ICT}): 40 mrad
- Compaction pressure: 250 kPa
- Working speed: 60 rpm

As discussed before, the applied compaction effort can be limited by different criteria. These criteria are either defined by a density limit of the compacted sample or the maximum amount of working cycles used. The applied criteria are as follows:

- Density limit (ρ_{con}): 2.400 g/cm³
- Duration (N): 150 cycles

2.8 Conclusions

The most relevant techniques for material characterization have been discussed in this chapter and have been used for characterizing the properties of the materials used in this research. Besides suitable techniques for material characterization, applicable test procedures for the evaluation of the workability properties of EMC have been discussed. Based on the insights from both material characterization techniques and workability related test procedures, the present chapter can be concluded as follows:

1. A premixed sand, so-called Premix 0-4, is introduced and characterized regarding its granulometric properties. This premixed sand contains a high amount of fines that can be utilized as filler material in concrete for replacing conventional fillers such as limestone powder and fly ash.
2. Recycled masonry rubble, available as both fine aggregate fraction and fines smaller than 125 μm , has been analyzed for its application in concrete. The material characteristics regarding grading and chemical composition reveal that utilization in concrete is possible.
3. The degree of compaction test was selected for preliminary investigations on the compaction behavior of EMC mixes as this test is easy to perform and inexpensive. The experimental results of the degree of compaction test correlate with the results that were obtained using a proportional downsized container that is made up of a standard cube having a side length a of 150 mm and an additional filling hopper. Samples produced that way can be tested for both packing fraction in fresh state and compressive strength of the hardened concrete.
4. The intensive compaction test (IC-test) provides detailed information on the compaction behavior of granular mixes in terms of optimum water content, final density and compaction effort and will be used for investigating the early-age behavior of EMC mixes.

Particle packing – Models and ideas

3.1 Introduction

The packing of solid particles is of essential importance for the understanding of granular materials. These materials are used in many fields of science and industrial processes such as ceramics, chemical engineering, pharmacology and building materials. With the fundamental understanding of the working mechanisms of particle packing it is possible to control the behavior and the characteristics of products based on granular materials. Some examples for the relevance of granular properties in industrial or technical processes are:

- The compressive strength of concrete is depending on the fineness of the cement particles as well as the packing of the aggregates (Mindess et al., 2003; Neville, 2006).
- The potential of fine powders (coal, flour, sugar, etc.) for dust explosion is depending on the fineness and the spatial distribution of the fine particles (Borho et al., 1991).
- The shrinkage of ceramics during their production depends on the packing density and is therefore related to particle size and particle shape (Alex, 2008).
- The permeability of packed beds depends on the particle size and particle shape (Borho et al., 1991).

Due to commercial as well as technical relevance of particle packing, a lot of research into the field of particle packing was carried out in the last century. In particular, this research covers either the physical foundation or empirical investigation of particle packing. Moreover, the complexity in the appearance of particles regarding their size, shape, and surface texture, causes that particle packing applies differently to various systems. According to Funk and Dinger (1994), the subject of particle packing can be divided into the packing of monodisperse (monosized) systems and polydisperse systems. The regular packing of equal spheres represents the simplest form of particle packing and is referred to as packing of monosized particles. A descriptive explanation of this phenomenon becomes more complex when the particles are packed irregularly (randomly) as different densifications are possible now.

More relevant for the practical application in concrete technology is the particle packing of polydisperse systems. The packing of these polydisperse mixtures is much more complex than the packing of monodisperse systems as here particles with different sizes and/or shapes are packed regularly or randomly. If the ratio of particle sizes and the ratio of pertaining quantities are constant, the packing is referred to as geometric packing (Brouwers, 2006). Furthermore, the particle sizes of polydisperse mixtures can be distributed discretely, consisting of two (bimodal) or more components (multimodal), or continuously distributed. The packing of continuously graded particles is also referred to as continuously graded particle size distributions (PSDs) and shows the most relevance to the packing of concrete ingredients. The basic characteristics of different systems and their relevance to concrete mix design will be explained in the following.

3.2 Principles in particle packing

3.2.1 General definitions

In order to avoid ambiguity regarding definitions and use of terminology, some general definitions related to particle packing are introduced and explained in this section. As mentioned in the introduction to this chapter, the main idea of particle packing is controlling the behavior of granular materials. This means, in general, that the packing of particles is used for achieving or controlling the behavior and/or properties of the final granular product. Within the scope of this research, the aim of improved particle packing is characterized by the densest possible packing of the granular ingredients (concrete aggregates inclusive binders). A commonly used terminology for describing how dense particles are packed is the packing density or packing fraction PF . The packing fraction explains the ratio of solids per unit cell to the overall volume of the unit cell and is defined as:

$$PF = \frac{V_{sol}}{V_{uni}} = \frac{V_{sol}}{V_{ves}} \quad (3.1)$$

However, not only the packing fraction itself is of interest when particles are packed, but also the void fraction ϕ of the packing is important. The void fraction is related to the packing fraction and reads:

$$\phi = \frac{V_{wat} + V_{air}}{V_{ves}} = \frac{V_{ves} - V_{sol}}{V_{ves}} = 1 - PF \quad (3.2)$$

In the considered case of concrete and concrete mortars, the term void fraction is used to characterize the void content within the granular structure, whereas the term porosity is related to the pore structure of the hardened cement paste and of particles itself. The packing fraction as well as the void fraction can be used for the characterization of packed particles. In this respect, the aim of improved particle packing is i) to increase the content of solids in a unit cell by increasing the packing fraction PF or ii) to minimize the void fraction ϕ within the granular structure. The void fraction of granular materials can be partly filled by air and water, which is expressed by the degree of saturation S_w . The degree of saturation S_w is given by the liquid volume contained in the void fraction and reads:

$$S_w = \frac{V_{wat}}{V_{tot} - V_{sol}} \quad (3.3)$$

For grading particles in size classes, the terms discretely sized and continuously sized are used. Discretely sized refers to particles that have a uniform size, which is in principle only possible for regularly shaped particles (e.g. equal spheres), or it is assumed that the particles are graded in a single, narrow range. In practice it is impossible to achieve a monodisperse system from natural or broken aggregates as it is not possible to extract particles with a uniform size and shape therefrom. Furthermore, the extraction of particles that represent a discrete distribution by sieving of natural or broken aggregates is very difficult. Such classes or fractions of particles consist of a single and narrowly graded range of continuously sized particles between two sieves and is considered to be a discretely sized distribution. In this context, several researchers have also discussed the span of such a screen-size division and gave values between $\sqrt{2}$ and $\sqrt[4]{2}$. Funk and Dinger (1994) suggest a $\sqrt{2}$ series of sieves to be sufficiently precise.

The term continuously sized applies to systems where the particles cover a range of particle sizes that is continuously from the largest particle size D_{max} to the smallest particle size D_{min} .

Particles generated by comminution processes like crushing, grinding, and milling are continuously sized, but also natural aggregates like river gravel, and river sand.

The difference between discretely and continuously sized, in a strict mathematical context, is that a discrete distribution assigns a probability to one, fixed value such as the particle size. The discrete random variable can only attain values from a certain finite or countable set. Based on that definition, it is not possible to extract particles from natural or broken aggregates with a fixed, discrete size in a strict mathematical meaning.

In contrast to this, a continuous distribution gives the probability for a range of uncountable possible values. Using the mathematical definition, it is called a continuous distribution if the corresponding probability density function is continuous. This is in principle the case for all natural materials as well as artificial materials from crushing or grinding processes. However, it is not possible to determine a continuous distribution when the raw materials are analyzed regarding their particle sizes. In this case, the continuous distribution is substituted by a discrete distribution with size classes between two adjacent sieves and the particles can obtain all possible values within the two sieve sizes (Alex, 2008). These size classes are used to describe the particle size distribution of the analyzed materials.

3.2.2 Monosized particles

Although the packing of monosized spheres represents the simplest form of particle packing, real monosized systems are technologically difficult to obtain. The packing of monosized particles can only be applied to regularly shaped particles that have the same size and shape (spheres, cubes, etc.). The particles are stocked regularly (crystalline) or randomly in an amorphous structure (cp. Figure 3.1). For the packing of monodisperse systems, the size of the particles is not considered, as the size is not influencing the packing behavior of the particles. Therefore the rules for the packing of monodisperse systems are size-independent.

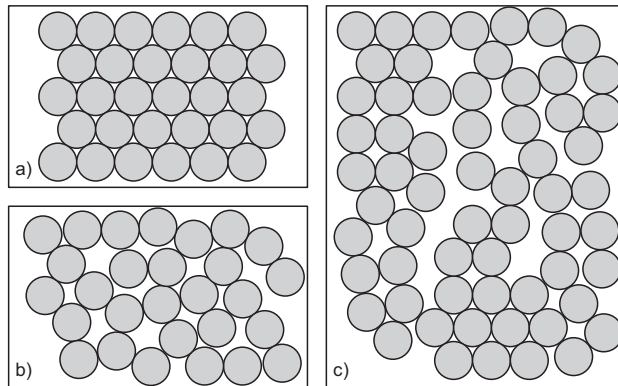


Figure 3.1: Schematic illustration of possible arrangements of monosized particles: a) hexagonal formation, b) ideal amorphous formation, and c) real conditions.

In crystal structures, the atoms are regularly arranged according to the seven crystal systems defining symmetry conditions and the thereof resulting 14 Bravais lattices. The packing fraction of regularly packed particles ranges from $\pi/6 (\approx 0.52)$ for simple cubic (sc) arrangement to

$\pi/6\sqrt{2}(\approx 0.74)$ for hexagonal close packing (hcp)(Rumpf, 1975). The hexagonal close packing represents also the densest possible packing of equal spheres.

However, when particles are packed by filling a container with fixed volume, a regular formation of the particles is not obtained. The particles are arranged in a random and not oriented structure if no compaction is applied (loose packing fraction). Figure 3.1b shows an ideal amorphous structure having no order regarding the arrangement of the particles. The ideal amorphous structure is still not representing the real conditions as shown in Figure 3.1c. Here, the particles are packed in partly regular and partly random arrangements. The packing fraction of these systems is depending on the densification and the interparticle forces and will not exceed the value of $\pi/6\sqrt{2}$ for hexagonal close packing. This value represents the highest possible packing fraction of monosized systems. A further reduction in the void content is only possible by adding particles of a smaller size which will fill the remaining voids within the arrangement of bigger particles without disturbance of their intrinsic packing and leads to the subject of discrete bimodal mixtures of particles.

3.2.3 Discrete bimodal mixtures

A discrete bimodal mix of particles is characterized by two distinct maxima of the cumulative finer fraction. The particles of a discrete bimodal mixture can precisely be classified into two size classes. Figure 3.2 depicts a discrete bimodal mixture of particles having a size of $0.1 \mu\text{m}$ and $10 \mu\text{m}$, respectively.

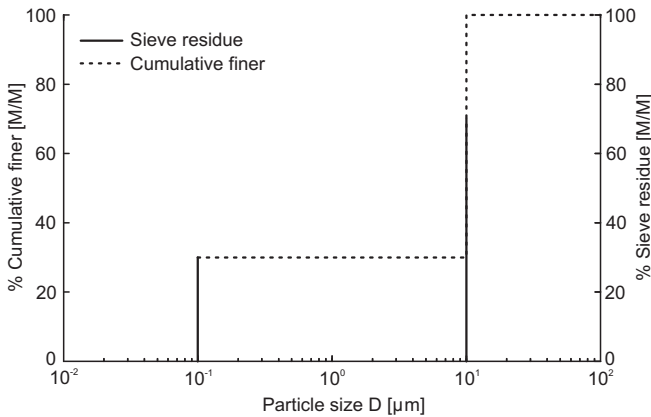


Figure 3.2: Bimodal mix of monodispers particles having a particle size of $0.1 \mu\text{m}$ and $10 \mu\text{m}$ (Funk and Dinger, 1994).

Within this context, not only equal spheres are considered to be discretely sized, but also fractions of particles graded in a single and narrow range are considered to be discretely sized when the distance between the mean particle diameters \bar{D} of the respective fractions are wide and larger than the range of the considered fractions itself. This fact is considered by the size ratio s of large to small particles, here defined as:

$$s = \frac{D_{lar}}{D_{sma}} = \frac{\bar{D}_{lar}}{\bar{D}_{sma}} \quad (3.4)$$

The packing of discrete bimodal mixtures was extensively studied by Furnas (1928, 1931). Based on his investigations, (Furnas, 1928) gives solutions for bimodal mixtures as well as for multimodal systems of more than two components (Furnas, 1931). In this section, the work of Furnas on discrete bimodal mixtures and its later application by Westman and Hugill (1930) is discussed.

The early work of Furnas (1928) is actually based on the void fraction of beds of broken solids as Furnas studied the flow of gases through these systems. As a part of his research, Furnas investigated the void fractions of mixtures of iron ore (angular shape) and lead shot (spherical shape) of varying size classes. Figure 3.3 shows as an example the void fraction of bimodal systems of various size ratios s in dependence of the percentage of coarse material. For these data and similar results given by e.g. Westman and Hugill (1930), the mass fraction of coarse material necessary for obtaining minimum void fraction by filling the voids of the coarse particles with finer material ranges from $2/3$ to $3/4$ depending on the shape and the void fraction of the coarse single sized component.

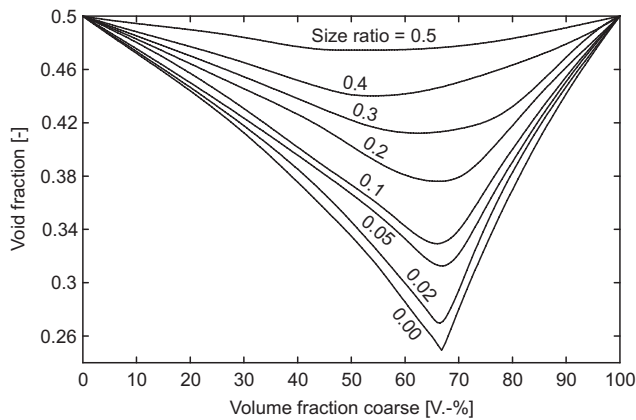


Figure 3.3: Relation between void fraction and size ratio s in bimodal systems of broken solids for solids having a monosized void fraction of 0.50 (Furnas, 1928).

Furnas (1928) discussed the size ratio s between coarse and fine components to be used for decreasing the void fraction of the composed mixture and recommends ratios larger than 2:1. The size ratio between coarse and fine components influences the filling behavior of the fines in the voids of the coarse fraction. This fact is schematically depicted in Figure 3.4 for varying size ratios s . The filling behavior of the fines increases with decreasing particle diameter as the influence of wall effects is also reduced with decreased particle diameter. In Figure 3.4, the arrangement of the finer particles in the voids between the coarse particles is oriented on the densest possible packing of equal spheres in a square as given by Peikert (1994). Here, the densest possible arrangement for $n = 1, 4$ and 8 spheres in a square results in a symmetrical formation.

Ideally, the size ratio s should be infinitely large to optimize the packing as described before. In practice it is not possible to achieve an infinitely large size ratio as the particle size of the coarse and fine components are limited. Funk and Dinger (1994) consider a size ratio s of 100:1 as more realistic, 20:1 to 10:1 as more practical, and less than 10:1 as probably more typical.

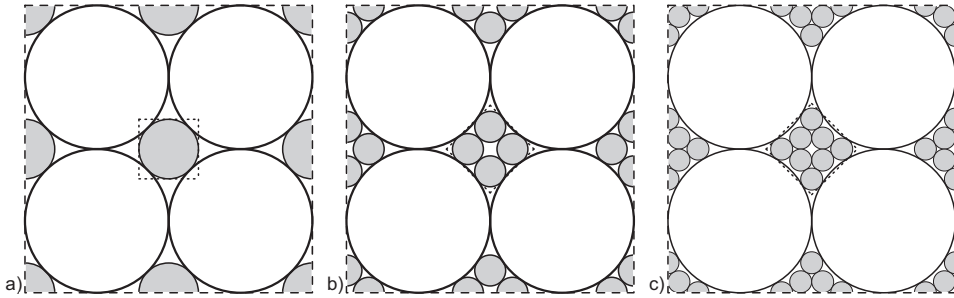


Figure 3.4: Schematic illustration of the influence of the size ratio s on the packing fraction PF of discrete bimodal mixtures in a unit cell: a) $s = 2.4$, b) $s = 4.6$, and c) $s = 6.5$.

This also reflects the conditions for blends of fine sand 0-2 ($\bar{D} \approx 500 \mu\text{m}$) and standard OPC ($\bar{D} \approx 10 \mu\text{m}$), which result in a size ratio s of 50:1.

As already mentioned before, the mass fraction of coarse material for obtaining minimum void fraction ranges from $2/3$ to $3/4$ and the resulting point of minimum void fraction is referred to as saturation point. Furnas (1928) gives a mathematical solution for calculating the saturation point. The mathematical solution of Furnas (1928) is in analogy to the algorithm of Westman and Hugill (1930) for determining the maximum packing fraction. Although the algorithm of Westman and Hugill (1930) was published later, it will be used for explaining some basic phenomena of discrete bimodal mixtures as the graphical solution of the algorithm helps to understand packing phenomena of discrete bimodal mixtures. The algorithm is based on discrete packing theories and is shown in Figure 3.5. The graphical solution of the algorithm depicted in Figure 3.5 is exemplified by values of the modified Puntke test for a mixture of sand 0-1 (coarse component) and a standard OPC (fine component).

The vertical axes symbolize the apparent volume V_{app} of the coarse and fine component, respectively, and the horizontal axis gives their mass fraction. The apparent volume V_{app} , also referred to as specific volume (Furnas, 1928), represents the bulk volume of particles that is necessary for achieving the true volume of particles and which is considered to be unity. For example, a mixture of monosized particles, which packs to a packing density of 0.6, requires a bulk volume of 1.67 m^3 for achieving the true volume of 1.0 m^3 . The definition given by Westman and Hugill (1930) for the apparent volume V_{app} is described by:

$$V_{app} = \frac{1}{PF} = \frac{1}{1 - \phi} \quad (3.5)$$

More lines are plotted in Figure 3.5 than mentioned in the work of Westman and Hugill (1930) to allow a better understanding of the algorithm. The intercepts marked $V_{app,coa}$ and $V_{app,fin}$ are the apparent volumes V_{app} for the pure coarse and fine fraction, respectively. Other lines used in Figure 3.5 are given by Funk and Dinger (1994) as follows:

Line 6 is not a continuous function, but is defined in sections and consists, therefore, of two parts. The first part is formed by the upper part of line 4 from the intercept $V_{app,coa}$ till its intersection with the straight line given by the true volume fraction of 100% coarse particles with the intercept $V_{app,fin}$. The latter line also forms the second part of line 6 till the intercept $V_{app,fin}$. The intersection point A_{opt} gives the composition of optimum packing and minimum void fraction. Some further effects on the packing of bimodal mixtures can be explained in

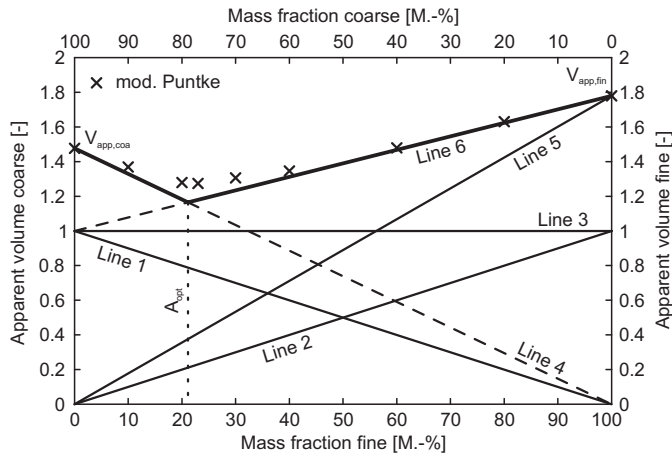


Figure 3.5: Algorithm according to Westman and Hugill (1930) for a mixture of sand 0-1 (coarse fraction) and CEM III/B 42.5 N.

- Line 1:* True volume fraction of coarse particles
- Line 2:* True volume fraction of fine particles
- Line 3:* Total true volume fraction of all particles; the sum of line 1 and line 2 equals a constant value of 1.0
- Line 4:* Apparent volume of the coarse fraction
- Line 5:* Apparent volume of the fine fraction
- Line 6:* Bold V-shaped line which represents the minimum apparent volume for the mixture

principle by the development of line 6. These effects illustrate basic phenomena of discrete bimodal mixtures (Funk and Dinger, 1994):

1. In the first part of line 6, from the intercept $V_{app,coa}$ till the intersection $V_{app,min}$, the apparent volume of the mixture is determined by the coarse fraction. The fines fit into the voids provided by the coarse particles and reduce the void fraction of the mixture, but do not contribute bulk volume to the apparent volume of the mixture. The bold upper left part of line 4 indicates this fact.
2. At the intersection point A_{opt} , the voids between the coarse particles are completely filled with the finer fraction and the minimum void fraction of the composed mixture is obtained. Adding more fines increases the apparent volume of the mixture because their volume is now added to the mixture.
3. For compositions with higher contents of fines than given by the intersection point A_{opt} , the apparent volume of the fine fraction is larger than the void fraction of the coarse fraction. The apparent volume of the mixture results from the summation of the apparent volume of the fine fraction and the true volume of the coarse fraction, which is shown by the bold upper right section of line 6. Line 6 can also be considered as the sum of line 1 and line 5.

These basic phenomena of the packing of discrete bimodal mixtures can also be applied to com-

positions of three or more (multimodal) systems and form the basis for the packing of continuously graded mixtures where the size ratio s between the size classes tends to unity.

3.2.4 Multimodal mixtures

As mentioned before, the basic phenomena of particle packing of discrete bimodal mixtures can also be applied to systems of three or more components. Both Furnas (1931) as well as Westman and Hugill (1930) gave a solution for mixtures of more than two components. Figure 3.6 shows the extension of the algorithm used by Westman and Hugill (1930) for the composition of a discrete bimodal mixture to a mixture consisting of three components (coarse, medium, and fine).

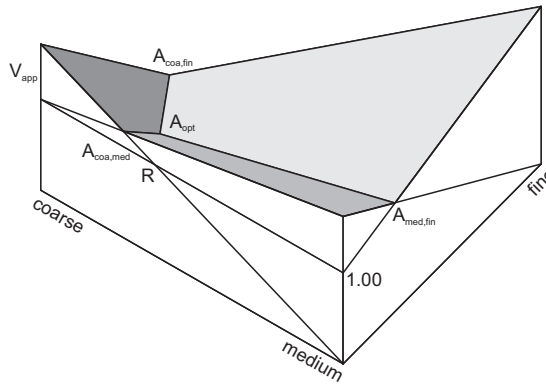


Figure 3.6: Packing of a system consisting of three components with large size ratio (Westman and Hugill, 1930).

For the situation depicted in Figure 3.6, two limiting cases have to be considered which are the same as for discrete bimodal mixtures. The limiting cases are i) that coarse, medium and fine constituents are consisting of particles of the same size or graded in a narrow range, and ii) the size ratio between coarse, medium, and fine particles is large.

The application of the algorithm to systems of three components differs, in principle, not from the approach used for discrete bimodal mixtures (Westman and Hugill, 1930). In the first instance, the points for the bimodal mixtures of coarse and medium, coarse and fine, as well as medium and fine components are constructed on the side of the triangle. By joining the point $A_{med,fin}$ to the point $V_{app} = 1.0$ at the coarse corner, $A_{coa,med}$ to the point $V_{app} = 0$ at the fine corner, and $A_{coa,fin}$ to point R , the final graph of the composed mixture can be drawn.

As a matter of simplicity and practicability, Westman and Hugill (1930) gave an analytical expression for the planes of Figure 3.6. Based on this analytical expression, values for the apparent volume V_{app} are calculated and compared with experimental results. A comparison between both values showed a good agreement of experimental and calculated values (Westman and Hugill, 1930). Considering the positive results obtained for discrete bimodal systems and systems of three components, the analytical expression was extended to mixtures of particles of more sizes, but still considering the limiting case that the size ratio of the particles tends not to unity. If the size ratio between the particles is constant and the finer particles fill the voids between the coarser

particles, the distribution of the particle sizes forms a geometric progression and the cumulative distribution function (cumulative finer) forms a step function. This limits the application of the algorithm given by Westman and Hugill (1930) to discretely sized particle mixtures having a size ratio that tends not to unity. For that reason, ideas for the packing of continuously graded particle mixtures are discussed in the following.

3.2.5 Continuously graded particle

The packing of continuously graded particles shows more relevance to problems that appear in concrete technology. First attempts describing an aimed composition of concrete mixes that generally consist of continuously graded particles, can be found already more than 100 years ago. The fundamental work of Féret (1892), and Fuller and Thompson (1907) showed that the packing of a composed concrete mix is influencing the properties of the produced concrete in fresh and hardened state. Both Féret (1892) as well as Fuller and Thompson (1907) concluded that the continuous grading of the composed concrete mix helps to improve the concrete properties. Andreasen and Andersen (1930) also suggested that the grading of the composed aggregate mix used for concrete production should follow a continuously graded particle size distribution (PSD) as the individual PSDs of the raw materials are also graded continuously. Furthermore, Féret (1892) demonstrated that maximum strength is attained when the void fraction of the granular structure is minimal.

Nevertheless, the packing of discrete multimodal mixtures plays an important role for the packing of continuously graded particle mixtures when the size ratio s of the components tends to unity and the number of size fractions to infinity (Brouwers, 2006). This fact was already shown by Furnas (1931) who extended his work to multimodal systems and gave a solution for continuous distributions as an extension of his solution for multimodal systems. It can be said that the findings presented by Furnas (1931) are in good agreement with the results obtained by Andreasen and Andersen (1930) although the underlying approaches are completely different. According to Furnas (1931), the maximum packing density for a continuous distribution is obtained when the cumulative finer $P(D)$ can be described by the following equation:

$$P(D) = \frac{s^{\log D} - s^{\log D_{sma}}}{s^{\log D_{lar}} - s^{\log D_{sma}}} \quad (3.6)$$

This solution considers already a smallest and largest particle size in the mix and, therefore, covers the width of continuously graded particles. Based on the work of Furnas (1928) as well as Fuller and Thompson (1907), Andreasen and Andersen (1930) studied the packing of continuously graded particles. They related their work to building materials consisting of a graded filling material (aggregates) and a binding medium (cement). Their approach is based on similarity conditions that were defined by granulation images. These granulation images are pictures of packed particles of varying size ranges that are scaled to the same diameter of the coarsest particles in each size range. Adapted from their geometrical considerations, they found that each arrangement of particles can be described by the product of particle fractions. These fractions are increasing in their size according to a mathematical series (geometric progression), which led them to the following semi-empirical equation for the cumulative volume fraction:

$$P(D) = \left(\frac{D}{D_{max}} \right)^q \quad (3.7)$$

In many publications afterwards, a distribution modulus q of 1/2, as given by Eq. (3.8) is referred to as ‘Fuller curve’ or ‘Fuller parabola’, based on the work of Fuller and Thompson (1907), and

recommended by most design codes for normal strength, normal weight concrete.

$$P(D) = \left(\frac{D}{D_{max}} \right)^{1/2} \quad (3.8)$$

At this point, it is worthwhile to mention that the set of curves for proportioning of concrete aggregates given by Fuller and Thompson (1907) can be redrawn by Eq. (3.8) when the cement is excluded from the given data (Hummel, 1959). The curves given by Fuller and Thompson (1907) are purely based on experimental observations and show ideal curves for the grading of concrete mixtures consisting of aggregates and cement and were originally constructed using ellipses with lines tangent to them.

The smallest particle size D_{min} , which is determined by the grading of the fines (binders and fillers), is not considered in Eq. (3.7) and Eq. (3.8) as this equation only accounts for the maximum particle size D_{max} in the system. However, a smallest particle size exists where the cumulative finer fraction of the PSD approaches a value of zero. This smallest particle size is non-zero nor infinitely small as considered by Eq. (3.7) and Eq. (3.8). The asymptotic behavior of Eq. (3.7) shows that the curve approaches, but never reaches, a value of zero. This fact points out that all particle sizes (from the largest to the smallest particle) should be considered in the mix proportioning of concrete aggregates and the related mathematical grading functions.

Not only Funk and Dinger (1994) showed that fine particles have a major influence on the packing of continuously graded particles. This fact was already accounted for many years before by Furnas (1928) and also Plum (1950) considered a minimum particle size in his expression. However, the work of Funk and Dinger (1994) on coal-water suspensions is of major interest for the concrete mix design as both the packing of particles as well as rheological properties are considered. This fact makes their approach and the given solution favorable for the mix design of concrete mixes.

The main intention of Furnas (1928) comprises the extension of Eq. (3.7) to a solution valid for continuously graded particle mixtures considering a minimum particle size D_{min} . This was done by composing a distribution based on Eq. (3.7), but ending on a certain minimum particle diameter. After analyzing the composed distribution, two main problems became obvious:

1. The plot of the cumulative finer ends for the smallest particle size at a certain percentage rather than at zero. The cumulative finer is therefore not a valid distribution.
2. The sum of the size classes of the associated histogram does not add up to 100% as it should. The histogram is therefore not valid either.

To solve the problems, the histogram was normalized to 100% and then the cumulative finer was recalculated. Next, the value of the cumulative finer at D_{min} was equaled to 0% and the values of the cumulative finer of the remaining sizes were adjusted for this. The partially corrected equations were summarized and further simplified by Funk and Dinger (1994) to a modified version of the original equation of Andreasen and Andersen (1930). This modified equation for the PSD (cumulative finer volume fraction) reads:

$$P(D) = \frac{D^q - D_{min}^q}{D_{max}^q - D_{min}^q} \quad (3.9)$$

According to Funk and Dinger (1994), Eq. (3.9) produces constant ratios on all pairs of adjacent sieves between D_{max} and D_{min} and is consistent with Andreasen's similarity condition and includes Furnas' concept of a finite smallest particle size D_{min} . Brouwers (2006) derived an analytical equation for computing the void fraction of an ideal graded mix that obeys Eq. (3.9) in

the range between D_{max} and D_{min} , which reads:

$$\varphi = \varphi_1 \left(\frac{D_{min}}{D_{max}} \right)^{\frac{(1-\varphi_1)\beta}{1+q^2}} \quad (3.10)$$

with φ_1 as void fraction of the monosized particles and a parameter β . Both values, φ_1 and β , are depending on the particle shape and the packing (loose or dense) only. It follows from Brouwers (2006) that for irregular particles, as present in concrete, $\varphi_1^{loo} = 0.52$ and $\beta^{loo} = 0.16$ (loose), and $\varphi_1^{den} = 0.46$ and $\beta^{den} = 0.39$ (dense), respectively.

The modified Andreasen and Andersen equation (Eq. (3.9)) forms the basis of the mix design concept for earth-moist concrete that is explained in detail in Chapter 4. The ideas of the new mix design concept are based on continuous grading curves used for composing all solid concrete constituents. Moreover, other approaches can be found in the literature for the composition of continuous graded particle mixtures that are based on the properties of multimodal, discretely sized particles.

De Larrard (1989) and De Larrard and Sedran (1994, 2002) postulated different approaches for the concrete mix design: the linear packing density model (LPDM), solid suspension model (SSM), and compressive packing model (CPM). Based on the model of Mooney (1951) for multimodal suspensions, De Larrard (1989) developed the linear packing density model for composing multimodal particle mixtures. The functions of the LPDM describe the interactions between the size classes of materials used based on their specific packing densities. Due to the linear character of the LPDM and its similarity to the bimodal models of Furnas (1928) and Westman and Huggill (1930), the designed theoretical curves show angular points in the vicinity of optimal values (cp. Figure 3.5). This defect was improved by De Larrard and Sedran (1994) by introducing the concept of virtual specific packing density that is calculated from the experimental random arrangement. The improvement of the LPDM resulted in the solid suspension model (SSM) that accounts for virtual specific packing density.

In the further development of their models, De Larrard and Sedran (2002) introduced the compaction index to the so-called compressive packing model (CPM). The compaction index considers the difference between actual packing density and virtual packing density. The virtual packing density is the maximum packing density that is only attainable if the particles are placed one by one. The difference between actual packing density and virtual packing density characterizes therefore the placing process and expresses to which extent the actual packing is close to the virtual one. However, also the CPM still uses the packing behavior of size classes that are considered to be monosized particles to predict the packing of the composed mixture made up of different size classes and is not accounting for a geometric distribution of the designed granular mix considering the grading of the single constituents. Based on the concept of De Larrard and Sedran (2002), an alternative concrete mix design method was developed by Fennis et al. (2009) that makes use of the packing fractions of the individual components (cement, sand, gravel, etc.)

Besides the particle packing models that are discussed in this section, also other models have been developed for the mix proportioning of concrete aggregates. A summary of further models, inclusive a comprehensive comparison of designed concrete mixes thereof, is given by Jones et al. (2002). In the following, the positive influence of a dense granular structure due to optimized particle packing is investigated and discussed in detail.

3.3 Effects of improved particle packing on mortar and concrete

The positive influence of dense particle packing on the properties of concrete is a well-known fact and the basis of the most commonly used mix design concepts. Various studies have been published on the proportioning of aggregates and the relation between optimized particle packing

and the concrete properties in fresh and hardened state. The aim of a dense granular structure comprises the achievement of minimum void fraction by maximizing the solids content in a unit volume. It is aimed for a minimum void fraction of the composed aggregate mix in order to i) reduce the cement content of the composed mix, ii) increase the content of free water available as lubricant or iii) to reduce the w/c ratio in the concrete mix, whereas the last two points are connected and depend strongly on the type and the application of the designed concrete mix.

3.3.1 Packing of discrete bimodal aggregate mixtures

The packing of discrete bimodal mixtures provides a demonstrative way for studying the effects of improved particle packing on the concrete properties in fresh and hardened state. It is known that the packing of discrete bimodal mixtures does not represent realistic conditions as they exist when standard concrete aggregates are composed. However, bimodal mixtures are a convenient and illustrative approach for showing the importance of well-graded particle mixtures. To demonstrate the effect of an optimized granular structure on the packing behavior and the compressive strength of concrete mortars, different types of river sand and river gravel were screened to narrow graded fractions that are considered in the following to be discretely sized.

Table 3.1: Material properties of size classes used.

Size class	Sieve size		Source	Density	Loose		Dense	
	D_{min}	D_{max}		ρ^{spe}	PF	ϕ	PF	ϕ
	[mm]	[mm]		g/cm^3	[V.%]	[V.%]	[V.%]	[V.%]
0.125-0.180	0.125	0.180	Sand 0-2	2.641	53.9	46.1	60.2	39.8
0.180-0.250	0.180	0.250		2.641	54.0	46.0	60.9	39.1
0.250-0.355	0.250	0.355		2.641	54.6	45.4	61.1	38.9
0.355-0.5	0.355	0.5	Sand 0-4	2.642	54.5	45.5	61.0	39.0
0.5-0.71	0.5	0.71		2.642	53.7	46.3	60.9	39.1
0.71-1.0	0.71	1.0		2.642	56.3	43.7	61.9	38.1
1.0-1.4	1.0	1.4		2.642	56.0	44.0	60.5	39.5
1.4-2.0	1.4	2.0		2.642	56.2	43.8	60.7	39.3
2.0-2.8	2.0	2.8		2.642	55.4	44.6	59.9	40.1
2.8-4.0	2.8	4.0	Gravel 2-8	2.620	54.5	45.5	63.0	37.0
4.0-5.6	4.0	5.6		2.620	53.1	46.9	62.1	37.9
5.6-8.0	5.6	8.0		2.620	53.5	46.5	62.8	37.2
8.0-11.2	8.0	11.2	Gravel 4-16	2.618	52.6	47.4	62.1	37.9
11.2-16.0	11.2	16.0		2.618	52.2	47.8	61.8	38.2

The materials were selected in such a way that the separated fractions show similar specific density ρ^{spe} and almost constant shape and surface texture of the particles. Table 3.1 gives an overview of the selected size classes and their relevant material properties. The sieve sizes used for screening were chosen in steps of $\sqrt{2}$. More size classes than used for the packing experiments are given in Table 3.1. The remaining fractions were used in later experiments on continuously graded aggregates. The fine fraction 0.71-1.0 was mixed with coarser fractions (1.0-1.4, 1.4-2.0, 2.0-2.8, 4.0-5.6) in varying quantities. The mass fractions of the ingredients were changed in steps of 25% with respect to the total mass of all solids (fine and coarse fraction).

For reducing the influence of the wall effect on the packing, the diameter of the vessel used for determining the packing fraction PF amounts to $D = 100\text{ mm}$ and the height is $H = 120\text{ mm}$.

The vessel was filled with the dry material by means of a filling hopper and a funnel. Surplus material from the uncompacted sample in the vessel was removed carefully in order to prevent the sample to be compacted before determining the packing fraction in loose state. For determining the packing fraction in dense state, the vessel was filled in the same way, but the material was compacted to its densest possible packing before removing surplus material from the vessel. The sample was compacted by a standard vibratory compaction table considering acquirable compaction efforts that can be applied under laboratory conditions. The mass of the material in loose and dense state was determined for calculating the packing fraction PF as described by Eq. (3.1) and the apparent volume as given by Eq. (3.5).

The results obtained for a mix of fine fraction (0.71-1.0) and coarse fraction (4.0-5.6) are depicted in Figure 3.7. The size ratio s of the fractions used in Figure 3.7 amounts to 5.6. Both curves for loosely and densely packed mixes are following the expected curve of the algorithm of Westman and Hugill (1930) as illustrated in Figure 3.5. However, the optimum mix proportioning for obtaining minimum void fraction is shifted to the finer side and is not in line with the value of 27.6% as calculated by the algorithm of Westman and Hugill. This shift is in line with data given in Figure 3.3. Here, the mix proportioning for minimum void fraction is also shifted to finer mixes when the size ratio s obtains values around 5 or lower.

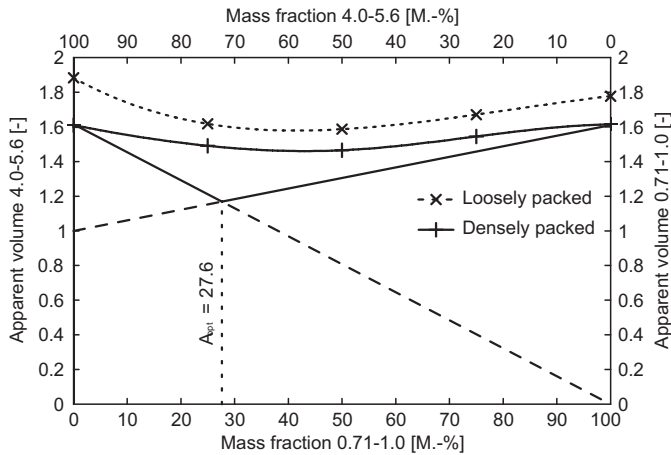


Figure 3.7: Comparison between the algorithm of Westman and Hugill (1930) and experimental results for loose and dense packing of a sand fraction 0.71-1.0 (fine) and a gravel fraction 4.0-5.6 (coarse).

Although the size ratio s is rather small, the results depicted in Figure 3.8 show that packing fraction of mixtures composed of 75% coarse and 25% fine material are increasing with increasing size ratio. This mixing ratio of coarse to fine constituents is assumed to be ideal for bimodal mixtures of particles having the same particle shape. Further lines are given in Figure 3.8 that confirm the positive effect of increasing size ratios s on the packing fraction of bimodal mixtures. Besides the optimum mix proportioning of 75% coarse and 25% fine material, also mixes composed of 25% coarse and 75% fine material show a higher packing fraction when the size

ratio of the constituents is increasing. The same fact applies to the data extracted from Figure 3.3. The extracted data are given for a mass fraction of 67% coarse and 33% fine material. This value is considered to be the optimum for mixing the constituents used in Figure 3.3 for obtaining minimum void fraction. The data are in good agreement and follow a line when plotted in a semi-logarithmic graph.

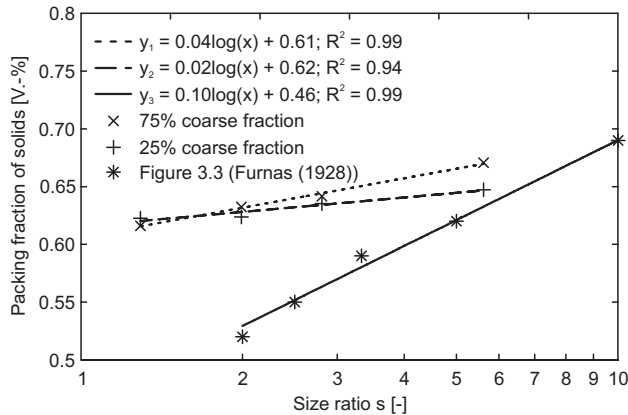


Figure 3.8: Packing fraction for varying size ratios s considering different void fractions of the single components.

The general assumptions, as mentioned in Section 3.2.3, are confirmed by Figure 3.8 and point out that with increasing size ratio an increase of the packing fraction occurs and illustrates that the width of the grading is important for obtaining minimum void fraction. This insight implies for practical applications, such as the mix proportioning of concrete ingredients, that the PSDs of the raw materials should cover a wide range from coarse to fine. However, the increase of the packing fraction proceeds to a minor degree than the increase of the size ratio s and achieves a limit for infinite size ratios.

Next, tests on mortars were performed to show the influence of improved particle packing on the compressive strength. For this purpose, the sand mixtures composed of 25% fine fraction and 75% coarse fraction, as depicted in Figure 3.8, were mixed with a slag blended cement (CEM III B 42.5 N LH/HS). For reasons of comparability, the compressive strength was determined according to the procedure given in EN 196-1. The tailored reference sand (1350 g) as required by the standard EN 196-1 was replaced by the composed sand fractions. The amount of cement (450 g) and water (225 g) were maintained constant as given in EN 196-1. Samples of $40 \times 40 \times 160$ mm were poured and submitted to compressive strength after 28 days. The values of the compressive strength test and the associated packing fractions are depicted in Figure 3.9 and show a clear relation between improved particle packing and compressive strength.

Although the packing of the aggregates, as depicted in Figure 3.9, was increased by 8%, the increase in the compressive strength amounts to 24%. Regardless of the positive effect of improved particle packing on the compressive strength of bimodal mixtures of aggregates, the void fraction of the mix of aggregates used amounts to 33% for a size ratio $s = 5.6$ (mix of fraction 4.0-5.6 and 0.71-1.0). This void fraction can be further reduced when the size ratio s of the composed aggregate mix is increased. However, following the procedure as explained before, the remaining void fraction of the aggregate mix is filled by the cement paste without considering the packing

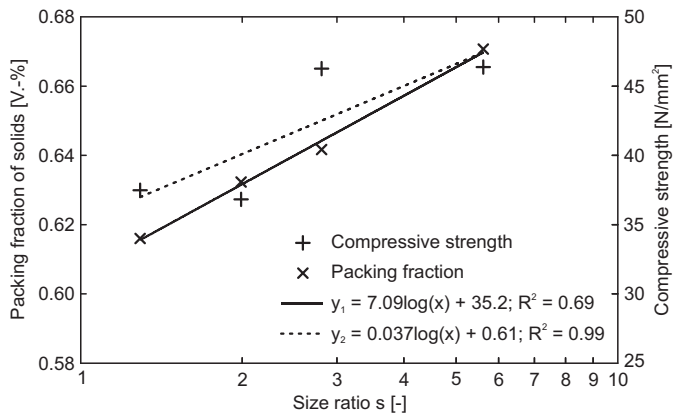


Figure 3.9: Packing fraction and compressive strength of the tested mortar samples for varying size ratios s .

behavior of the binder. Based on the positive effect of improved packing of bimodal mixtures, the influence of particle packing of continuously graded aggregate mixes on the concrete properties in fresh and hardened state is investigated and discussed in the next section.

3.3.2 Utilization of the modified Andreasen and Andersen equation for aggregate mixtures

It was demonstrated in Section 3.2.4 and Section 3.2.5 that highest packing fractions are obtained when the grading of the composed aggregate mix follows a geometric progression. The previous findings on the packing of discretely sized particles and their transformation to continuously sized particle mixtures originate therefore the application of the modified Andreasen and Andersen equation (Eq. (3.9)) for the proportioning of concrete mixes. In this section, the influence of continuously graded aggregate mixes on the particle packing and the mechanical properties is investigated and discussed in detail.

Besides the maximum and minimum particle size D_{max} and D_{min} , the distribution modulus q influences the grading according to Eq. (3.9). Figure 3.10 depicts the computed PSDs for varying distribution modulus q in Eq. (3.9). The plotted graphs are used for the proportioning of aggregate mixes. For each distribution modulus given in Figure 3.10, the corresponding aggregate mix was composed using the separated fractions as given in Table 3.1. The detailed mix proportioning of the composed aggregate mixes is given in Appendix D.1. After composing the aggregate mixes, the mixes were screened again to control the conformance with the computed PSDs. The results of the sieve analysis and the applied grading curves of the distribution moduli q of 0.25, 0.30, 0.35, 0.40 are given in Appendix B.1 - B.4. The composed aggregate mixes were tested for their dry packing fractions PF in loose and dense state in the same way as explained in Section 3.3.1 by filling a vessel with a diameter of $D = 150$ mm and a height of $H = 175$ mm. The corresponding packing fractions were calculated as described in Eq. (3.1). The loose and dense packing fractions are depicted in Figure 3.11.

The values depicted in Figure 3.11 illustrate that with increasing distribution modulus q the packing fractions in loose and dense state are slightly decreasing. The most relevant for concrete experiments is the packing fraction of the densely packed particles, as this condition is assumed to be the packing of compacted normal strength, normal weight concrete (NWC) and earth-moist

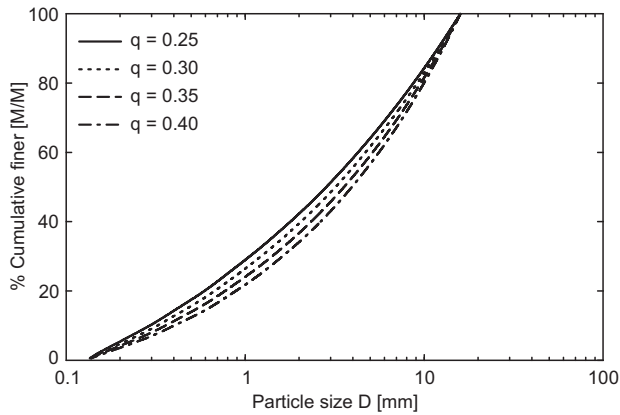


Figure 3.10: Computed PSDs for varying distribution modulus q ($D_{max} = 16$ mm, $D_{min} = 125$ μ m).

concrete (EMC). The average packing fraction of the densely packed aggregates is decreasing from 79.1% for a distribution modulus of $q = 0.25$ to 78.4% for $q = 0.40$. However, the decrease in the packing fraction is, in some cases, smaller than the variation of the measurements. Furthermore, both measurements in loose and dense state demonstrate that the decrease in the packing fraction is larger for an increase of q from 0.25 to 0.30 than for an increase from 0.35 to 0.40. As already mentioned, the decrease in the packing fraction is rather small. This fact is caused by the limited width of the grading of the composed aggregate mix. In the considered case, the grading ranges from 125 μ m to 16 mm and is not considering particles finer than 125 μ m as it was not possible in an appropriate way to separate fine particles smaller than 125 μ m to size classes in steps of $\sqrt{2}$. Although the designed aggregate mixes show only slight differences in their packing fractions PF , they were tested for their compressive strength in order to investigate the influence of varying distribution modulus q on the mechanical properties.

The mix design of the tested concrete is based on the composed aggregate mixes that were discussed before. The concrete mixes of the varying distribution modulus q are designed in such a way that slag-blended cement (CEM III/B 42.5 N LH/HS) and fine filler (limestone powder) were added to the aggregate mix. The volume of the fines (cement and filler) was adjusted to 152 dm^3/m^3 and is oriented on the cumulative volume fraction of fine particles smaller than 125 μ m considering the grading curve according to Eq. (3.9) determined by $D_{max} = 16$ mm, $D_{min} = 0.1$ μ m and $q = 0.325$. The volume of the fines was kept constant for all distribution moduli q in order to achieve constant w/p ratios. Therefore, a distribution modulus of $q = 0.325$ was chosen that represents the middle of the investigated range from 0.25 to 0.4. Furthermore, the cement content was fixed for all mixes to 300 kg per m^3 concrete to account for constant test conditions and to reduce the number of influencing factors on the compressive strength. A polycarboxylic ether based plasticizer was applied to adjust the workability of the concrete mixes in such a way that it was possible to compact the concrete to its densest possible packing by means of a standard vibratory table. The detailed mix proportioning of the concrete mixes is given in Table 3.2.

Cubes having a dimension of 150 \times 150 \times 150 mm were cast, cured sealed during the first day, stripped from the mold after 24 hours, and cured subsequently for 27 days under water according to the prescribed storing conditions given by DIN EN 12390-2. The cubes were tested

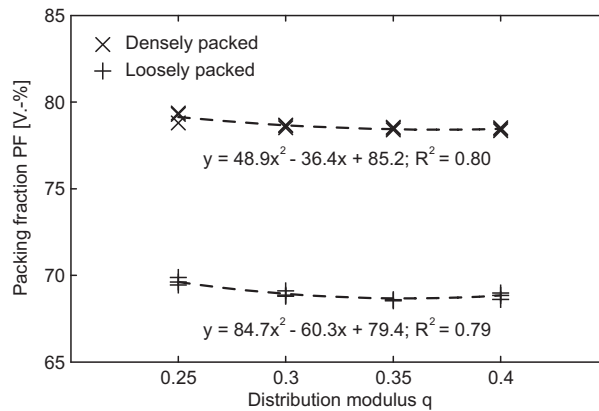


Figure 3.11: Packing fractions PF of designed aggregate mixes for varying distribution modulus q in loose and dense state

Table 3.2: Mix proportioning of the tested concrete mixes using the composed aggregate fractions of varying distribution modulus q (see Appendix D.1).

Material	Volume	Mass
	[dm ³]	[kg]
Aggregate mix	683.4	1797.4
CEM III/B 42.5N LH/HS	101.7	300.0
Limestone	50.8	136.1
Air [‡]	40.0	0.0
Water	120.0	120.0
SP	4.1	4.5
Total	1000.0	2358.0

[‡] Estimated value

for their compressive strength f_c after 28 days according to the test conditions described by DIN-EN 12390-3. The results of the compressive strength test are depicted in Figure 3.12 for the analyzed range of the distribution modulus q and show a similar trend as obtained for the dry packing fractions PF of the composed aggregate mixes. Here, the compressive strength is also decreasing with increasing distribution modulus q and it is obvious, as illustrated before, that the decrease in the compressive strength is larger for increasing q from 0.25 to 0.30 than for an increase from 0.35 to 0.40.

The results of the investigations on varying distribution modulus q show that in the range of $0.25 \leq q \leq 0.40$ the packing fractions of the composed aggregate mixes slightly decrease. This decrease shows also an effect on the compressive strength of the hardened concrete after 28 days. Here, the compressive strength is reduced in the same way as the packing fractions decrease. The

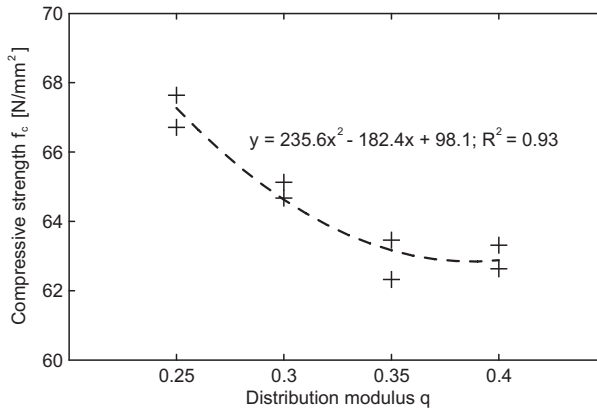


Figure 3.12: Compressive strength f_c of designed aggregate mixes for varying distribution modulus q .

overall reduction of the packing fraction in the investigated range amounts to 0.9%, whereas the compressive strength after 28 days is reduced by 1%. It can be concluded from the minor difference in both packing fraction and compressive strength that the grading in the investigated range of $0.25 \leq q \leq 0.40$ follows an optimum line for densest possible packing of the aggregates. The variation of the distribution modulus influences the ratio of coarse to fine aggregates. Lower values of $q = 0.25$ result in finer aggregate mixes, whereas higher values of $q = 0.40$ produce coarser aggregate mixes. This difference in coarse to fine aggregates ratio influences the workability properties of the fresh concrete and is explained in detail in Section 4.2.3. However, not only the of coarse to fine aggregates ratio (fine sand) is important for the workability properties of the fresh concrete, but also the ratio of coarse aggregates to fines (cement and filler) is relevant.

The granulometric properties of the fines influence the packing and the workability of the designed concrete to a large extent (Geisenhanslüke, 2008; Reschke, 2000). The influence of the granulometric properties of the fines was not considered in this section nor in Section 3.3.1, as it was focused on the packing of the aggregate mix only. For that reason, the beneficial effect of improved particle packing of the fines is investigated in the following section and is related to the requirements on the grading of concrete mixes considering the granulometric properties of all solid ingredients.

3.3.3 Optimized packing of the fines

It was demonstrated in the previous two sections that a close relation between a dense granular structure of the aggregates and the mechanical properties of the designed mortars exists. Due to improved particle packing, the granular structure of the aggregates is denser and results in higher compressive strength. However, the previous findings, as presented in Section 3.3.1 and Section 3.3.2, consider only the packing of aggregates and the influence of the packing of the fines, as listed in Table 3.3, is ignored. The overall optimization of the particle packing in concrete mixes requires also the optimization of the grading of the fines (cement and fillers) since the packing of the fines influences the formation of the microstructure to a large extent (Reschke, 2000).

The packing of the fines and the related void fraction of the cement paste are fundamental properties that can be improved by optimized particle packing. Improved particle packing results in a denser microstructure of the cement paste and less water is needed to produce workable

Table 3.3: Densities and packing fractions of fines for different densification.

Material	Bulk density			Density	Packing fraction			D_{50} [μm]
	ρ^{loo} [g/cm^3]	ρ^{vib} [g/cm^3]	ρ^{den} [g/cm^3]	ρ^{spe} [g/cm^3]	PF^{loo} [%]	PF^{vib} [%]	PF^{den} [%]	
CEM I 32.5 R [‡]	—	—	1.732	3.14	—	—	55.2	7.1
CEM III/B 42.5 N [‡]	0.832	1.166	1.755	2.96	28.1	39.4	59.3	8.1
CEM I 52.5 R	0.804	1.072	1.710	3.15	25.5	34.0	54.3	3.8
Quarz flour 1	0.850	—	1.706	2.65	32.1	—	64.4	3.1

[‡] Values taken from Hunger and Brouwers (2009)

concrete mixes. The lowered water content is not only influencing the w/c ratio of the cement paste and related porosity of the hardened cement stone, but also the interfacial transition zone near the interface paste-aggregate is improved and results in better properties of the hardened concrete (Neville, 2006).

In order to demonstrate the influence of improved particle packing of the fines, two coarse cements (CEM I 32.5 R and CEM III/B 42.5 N LH/HS) were blended with a micro cement (CEM I 52.5 R LA/HS) and a quartz powder of the same fineness as the micro cement to achieve a denser granular structure of the binder. The packing fractions of the materials used are given in Table 3.3 and their PSDs are depicted in Figure 3.13.

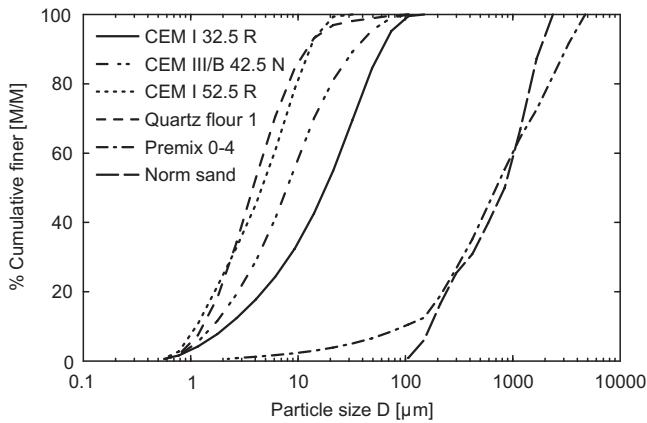


Figure 3.13: PSDs of materials used.

The mix proportion of the coarse and fine constituents is oriented on the optimum value A_{opt} for obtaining minimum void fraction of bimodal mixtures. Due to the small difference of the mean particle diameter D_{50} of the coarse and fine cements, the mix proportioning was shifted to the fines according to the explanation for small size ratio s as given in Section 3.2.3 and amounts to 65% coarse cement and 35% fine cement. In the next step, the micro cement was replaced by an inert filler material (quartz flour) to study the strengthening effect of the finer cement. The

replacement of the micro cement is based on its volume fraction in order to account for the lower density of the quartz flour.

Table 3.4: Mix proportioning of the blended cements.

Material	Cem 1	Cem 2	Cem 3	Blend 1	Blend 2	Blend 3	Blend 4
	[g]	[g]	[g]	[g]	[g]	[g]	[g]
CEM I 32.5 R	450.0	–	–	291.9	291.9	–	–
CEM III/B 42.5 N	–	450.0	–	–	–	291.9	291.9
CEM I 52.5 R	–	–	450.0	158.1	–	158.1	–
Quartz flour	–	–	–	–	133.0	–	133.0
Total	450.0	450.0	450.0	450.0	424.9	450.0	424.9

The blended cements as well as the original cements were tested for their void fraction according to the European standard EN 1097-4 using a Rigden device. The obtained values of the void fraction were used to calculate the corresponding packing fractions PF according to Eq. (3.2). The average values of the obtained packing fractions are depicted in Figure 3.14 and show that the packing of the blended cements is higher than the packing of the original cements.

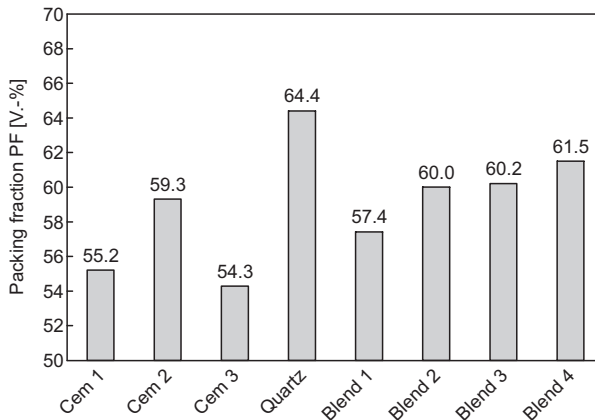


Figure 3.14: Packing fractions PF of the original cements, quartz flour and blends thereof.

The lower packing fractions of the coarser cements were increased by adding 35% of the finer micro cement. The packing fraction of the coarse OPC (CEM I 32.5 R) was increased from 55.2% to 57.4% by adding the finer micro cement (CEM I 52.5 R). This effect became clearer for the blend of 65% slag cement (CEM III/B 42.5 N) and 35% micro cement. Here, the packing fraction was increased from 54.3% of the original coarse cement to 60.2% as obtained for the blended cement. The same increase in the packing was observed for blends of coarse cements and quartz flour. Although the grading of the quartz flour is similar to the grading of the micro

cement, the packing fraction is with 64.4% higher than the value determined for the micro cement. This higher packing fraction increased the packing of the corresponding blends (Blend 2 and Blend 4) to a further extent.

Based on the higher packing fractions of the blended cements, the compressive strength of the blends as well as the original cements was determined to investigate the effect of improved particle packing of the fines on the mechanical properties. The development of the compressive strength was tested according to EN 196-1. Mortars consisting of 450 g cement, 1350 g specified reference sand (CEN-Standard sand), and 225 g water have been produced. Samples of $40 \times 40 \times 160$ mm were poured and submitted to compressive strength after 1, 7 and 28 days. The compressive strength development of the coarse OPC (CEM I 32.5 R) as well as the blended cement thereof is depicted in Figure 3.15 and detailed values are given in Appendix E.2. Figure 3.16 shows the results obtained for the slag cement (CEM III/B 42.5 N) and the blended cements thereof. Both figures contain the compressive strength development of the micro cement (CEM I 52.5 R) for comparison.

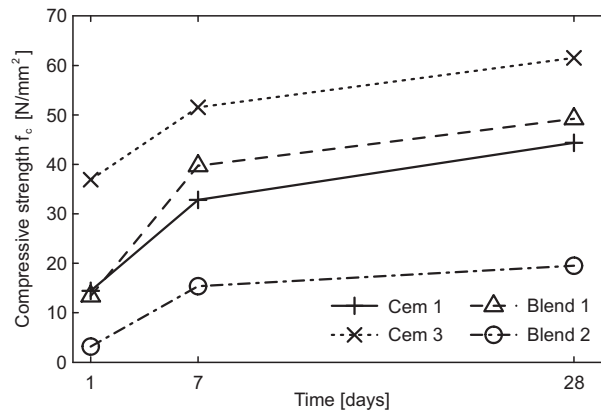


Figure 3.15: Development of the compressive strength according to EN 196-1 for CEM I 32.5 R (Cem 1), CEM I 52.5 R (Cem 3) and blends thereof.

It becomes obvious from the data depicted in Figure 3.15 and Figure 3.16 that the application of a micro cement with high fineness shows a beneficial effect on the strength development of the produced mortars. However, the figures of the strength development show two different effects of the applied micro cement. In the case of the coarser OPC (CEM I 32.5), the 1-day compressive strength was not influenced by the addition of the finer micro cement, whereas the strength after 7 and 28 days increased to a remarkable extent. Here, 7-days strength was increased by about 20% and the 28-days strength by about 10% compared to strength of the coarse OPC. A different behavior was observed for the strength development of the slag-blended cement as here only the 1-day strength increased and the application of the micro cement showed no effect on the 7 and 28-days strength.

The experimental results of the mortar tests carried out according to EN 196-1 revealed that the application of the micro cement with high fineness shows a beneficial effect on the strength development of the coarse OPC. However, it has to be noticed that this effect is not only related to the higher packing fractions of the blended cements, but also influenced by the higher reactivity of the micro cement and the related higher strength. To demonstrate the positive effect of

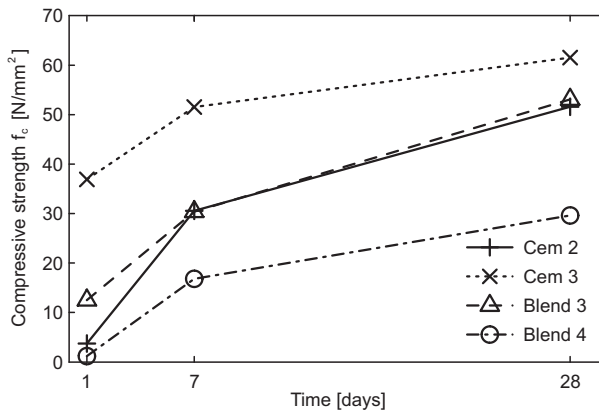


Figure 3.16: Development of the compressive strength according to EN 196-1 for CEM III/B 42.5 N (Cem 2), CEM I 52.5 R (Cem 3) and blends thereof.

improved particle packing of the fines on the mechanical properties, the grading of the fines and aggregates has to be considered entirely, which is not the case in EN 196-1. The test procedure according to EN 196-1 gives standardized conditions for determining the compressive strength of cements and uses therefore a specified aggregate mix (CEN-Standard sand). This reference sand is graded in such a way that the composed mortar follows the grading of the Fuller curve (Eq. (3.8)). The influence of the grading of the fines is not considered and the amount of cement and water used for producing the reference mortars is fixed to maintain constant and representative test conditions for the quality control of cement production. However, the aimed optimization of the grading of concrete mixes requires a more integral approach that is not considering the grading of aggregates and fines separately. Both aspects were considered in the mix design of mortars that combine a dense granular structure of the aggregates with the positive effect of improved particle packing of the fines. For this purpose, mortars were designed that are making use of the blended cements (Blend 1 and Blend 3). The aggregate fraction of the produced mortar was composed in such a way that the grading of the composed mortar follows the modified Andreasen and Andersen equation (Eq. (3.9)) with $q = 0.30$ as closely as possible. The Premix 0-4, as described in Section 2.5.1, proved to be a suitable material for the aggregate fraction as its grading follows a continuous distribution over a wide range. Furthermore, the Premix 0-4 contains fine material that helps to close the gap between the maximum particle size of common cements (around $100 \mu\text{m}$ for the used CEM I 32.5 R) and the smallest aggregate fraction around $250 \mu\text{m}$.

The mix proportioning of the designed mortars aims on equal test conditions for the grading of the composed mix as well as the dosage of cement and aggregate fraction. The dosage of the aggregate fraction was determined by the necessary amount of Premix 0-4 to follow the grading curve, as given by Eq. (3.9), in the range above $125 \mu\text{m}$ as closely as possible. The remaining volume below $125 \mu\text{m}$ is filled up with the blended cements according to the values listed in Table 3.5. The resulting PSDs of the designed mortars is depicted in Figure 3.17 and compared with the grading of a mortar designed according to the European standard EN 196-1. The w/c as well as w/p ratio of the designed mortars was kept constant and their workability was adjusted by means of a polycarboxylic ether based plasticizer to maintain comparable conditions. The workability of the designed mortars was assessed by the Hägermann spread flow test. The values

of the spread flow test of the designed mortars are given in Appendix E.1.

Table 3.5: Mix proportioning of the designed mortars.

	Mix 1	Mix 2	Mix 3	Mix 4
	[g]	[g]	[g]	[g]
CEM I 32.5 R	229.3	229.3	—	—
CEM III/B 42.5 N LH/HS	—	—	227.9	227.9
CEM I 52.5 R LA/SR	124.2	—	123.4	—
Quarz flour 1	—	104.5	—	103.8
Norm sand	—	—	—	—
Premix 0-4	1544.3	1544.3	1534.7	1534.7
Water	191.0	191.0	189.7	189.7
SP	5.0	5.0	4.0	4.0
w/c	0.54	0.83	0.54	0.83
w/p	0.35	0.35	0.35	0.35

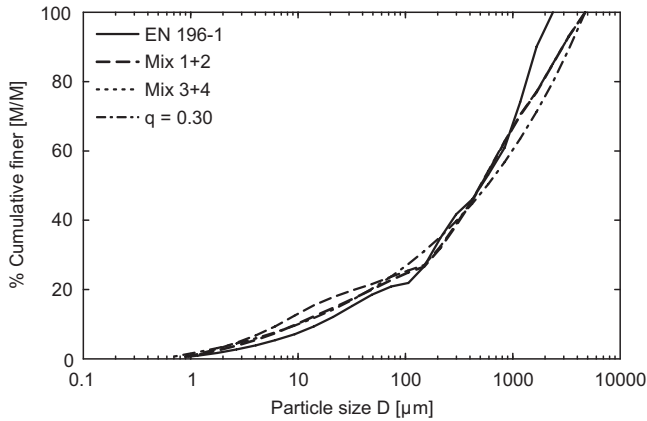


Figure 3.17: PSD of the designed mortar mixes and comparison with the grading of a mortar according to EN 196-1.

Prisms having a dimension of $40 \times 40 \times 160$ mm were poured and submitted to compressive strength after 1, 7 and 28 days. The results of the compressive strength test are depicted in Figure 3.18 for the mixes that are based on the blended OPC (CEM I 32.5 R), whereas Figure 3.19 shows the compressive strength of the blended slag cement mortars. The compressive strength of the corresponding reference cements was determined according to EN 196-1 as explained before and is included in both figures.

The data depicted in Figure 3.18 and 3.19 demonstrate the positive effect of improved particle

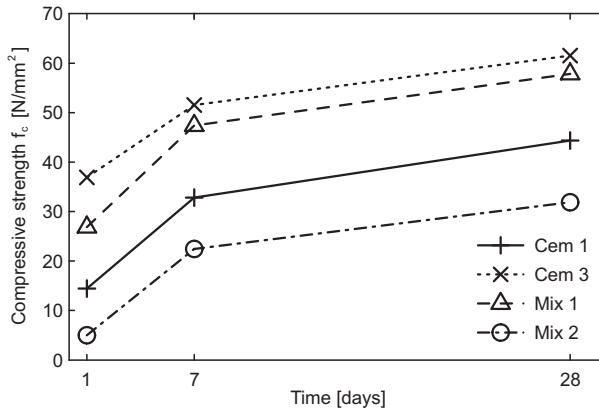


Figure 3.18: Development of the compressive strength for CEM I 32.5 R (Cem 1), CEM I 52.5 R (Cem 3) and blends thereof (see Tables 3.4 and 3.5).

packing on the hardened mortar properties. In this case, not only the grading of the aggregates was considered in the mix proportioning, but also the packing of the fines was accounted for in the mix design process. The designed mortar (Mix 1) contains a blended OPC (Blend 1) that has a higher packing fraction than obtained by the single components (cp. Figure 3.14). Due to the higher packing fraction of the blended cement and the optimized grading of the aggregate fraction, the cement content of the designed mortar was reduced. The designed mortar of Mix 1 contains about 23% less cement than the comparable mortars that have been tested according to the requirements given by EN 196-1 (Cem 1 and Cem 3). Although the cement content of Mix 1 is significantly lower than applied for the comparative mortar Cem 1, its compressive strength is around 30% higher than obtained for the mix Cem 1. It has to be mentioned that the strengthening effect is also caused by the higher fineness and the resulting higher reactivity of the added micro cement (Cem 3) which is indicated by the higher strength in the early age.

At this point it becomes clear that the strengthening effect of improved particle packing is hard to identify when two cements that are characterized by different fineness and reactivity are mixed. Therefore, another parameter is required that helps to assess the effectiveness of cement on more performance-based criteria. For this purpose, the compressive strength is related to the cement content of the mix. The resulting parameter x_{cem} gives the compressive strength in N/mm² provided by each kilogram of cement or reactive binder and is computed as follows:

$$x_{cem} = \frac{f_c}{M_{cem}} \quad (3.11)$$

This parameter for considering the cement efficiency is also used by Brouwers and Radix (2005); Su and Miao (2003) as well as Hunger (2010) for the mix design of self-compacting concretes.

The computation of the cement efficiency factor requires that the mix proportioning, as given in Table 3.5, is related to a fixed volume. In the present case, the mass of ingredients for producing a mortar volume of 1 m³ is considered and the corresponding quantities were recalculated. The recalculated quantities of the mortars given in Table 3.5 are listed in Appendix D.2 and allow for a comparison of the cement efficiency factor of the tested mortars.

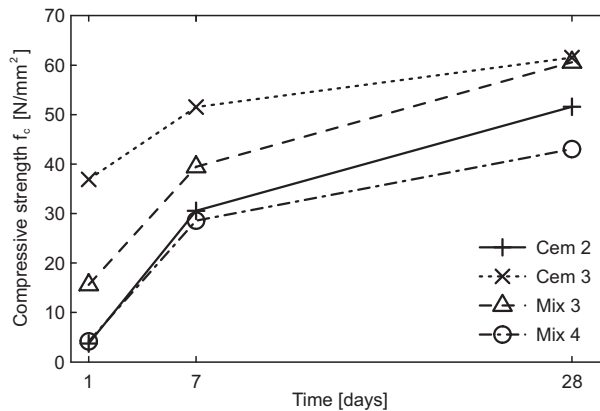


Figure 3.19: Development of the compressive strength for CEM III/B 42.5 N (Cem 2), CEM I 52.5 R (Cem 3) and blends thereof (see Table 3.4 and Table 3.5).

Considering the data depicted in Figure 3.18, the cement efficiency of the coarse OPC (CEM I 32.5 R) increased from $x_{cem} = 0.086 \text{ Nm}^3/\text{kgmm}^2$ (Cem 1) to $x_{cem} = 0.145 \text{ Nm}^3/\text{kgmm}^2$ (Mix 1) and is also higher than $x_{cem} = 0.120 \text{ Nm}^3/\text{kgmm}^2$ as determined for the pure micro cement (Cem 3). This demonstrates clearly that cement is used more efficiently when the entire grading of the composed mix is optimized. The same findings were also noted for the blended slag cement (Blend 3). Also here, the cement content of the designed mortar (Mix 3) that uses the blended slag cement is about 23% lower than for the comparable mortars according to EN 196-1 (Cem 2 and Cem 3). Here, the compressive strength of Mix 2 is about 20% higher than for the mortar that uses the pure slag cement and reaches almost the same compressive strength as the pure micro cement. However, also in the case of the blended slag cement mortars, the performance of the mortars has to be related to their cement efficiency factors to account for their different reactivity. In view of the cement efficiency of the blended slag cement mortar, the effect of optimized particle packing is significant. The cement efficiency of the original coarse slag cement (CEM III/B 42.5 N) increased from $x_{cem} = 0.101 \text{ Nm}^3/\text{kgmm}^2$ (Cem 2) to $x_{cem} = 0.153 \text{ Nm}^3/\text{kgmm}^2$ (Mix 2). This is an increase of more than 50% while the cement content was reduced by 30%.

3.3.4 Discussion

The theoretical and experimental results presented in this chapter demonstrate that the particle packing of granular mixtures can be improved and that a relation between packing fraction and size composition exists. Improved particle packing results in a denser granular structure and better mechanical properties such as compressive strength. The packing of discrete bimodal mixtures provides a simple model to demonstrate the beneficial effects of improved particle packing and shows that the void fraction in granular systems of two components is strongly depending on the size ratio s between coarse and fine fraction. Based on the theoretical and experimental work of Furnas (1928) and Westman and Hugill (1930) bimodal mixtures of aggregates, aggregates and fines, or fines can be composed that have minimum void fraction. These bimodal mixes with higher packing fractions have better mechanical properties due to their denser granular structure.

The basic principles of particle packing of discrete bimodal mixtures were extended by Furnas (1931) to ternary or multimodal discretely sized systems. This extension allows for an in-

tegral approach to optimize the particle packing of the composed mix in consideration of the packing behavior of the single materials or fractions. However, the single constituents are still considered individually and the next finer fraction is used for filling the void fraction of the coarser fraction. This principle leads to similarity conditions for the particle packing of multimodal systems and forms the basis for the theoretical considerations of the packing of continuously sized particle mixtures. Based on the geometric progression of adjacent fractions, Eq. (3.7) was derived by Andreasen and Andersen (1930) for the grading of continuously sized particle mixtures. This equation was later modified by Funk and Dinger (1994) to account for the smallest particle size D_{min} that is present in the mix. The modified Andreasen and Andersen equation results in grading curves that are characterized by high packing fractions and constant ratios of adjacent fractions between D_{max} and D_{min} .

The theoretical considerations on the packing of continuously sized particle mixtures were confirmed by the experimental results. Here, aggregate mixes that are graded according to the modified Andreasen and Andersen equation (Eq. (3.9)) resulted in high packing fractions and high compressive strength. Extending the modified Andreasen and Andersen equation to the grading of the fines allows an integral approach by optimizing the grading of concrete mixes as already mentioned by Féret (1892) and Plum (1950). The optimization of the entire grading of aggregates and fines resulted in mortars with lower cement contents and higher compressive strength. Therefore, the integral approach of optimizing the grading of all solid ingredients that are present in the composed concrete forms the basis of the new mix design concept that is introduced in Chapter 4.

3.4 Conclusions

This chapter focus on theories of particle packing and suitable models for the packing of discretely sized particles and continuously graded particle size distributions have been discussed. Based on the theoretical and experimental investigations presented in this chapter, the following conclusions can be derived:

1. The grading of discrete bimodal mixtures demonstrates that the size ratio s between coarse and fine fraction influences the packing fraction of the composed mix. The same holds for continuously graded mixtures where the packing fraction is influenced by the width of the composed grading. Here, the packing is governed by the difference between largest particle size D_{max} and smallest particle size D_{min} present in the composed mix.
2. The higher packing fractions of bimodal aggregate mixtures with a large size ratio between coarse and fine fraction increased the compressive strength of the produced mortars significantly.
3. The packing of the fines and their granulometric characteristics influence the properties of the designed concrete mix. For that reason, the granulometric properties of the fines should be considered in the concrete mix design. This requires an integral approach for the concrete mix design where the composed mix is considered as a granular mix of aggregates and fines. The fines can be of inert (limestone powder) or reactive nature (cement, slag, fly ash, pozzolans, etc.).
4. Continuously graded particle size distributions (PSDs) show favorable characteristic for the design of concrete mixes. Here, mixes that are characterized by a geometric progression result in higher packing fractions and higher compressive strength.

Mix design concept for earth-moist concrete¹

4.1 Introduction

The proportioning of concrete mixes, also referred to as concrete mix design, covers the combination of different ingredients to produce concrete of appropriate workability, strength, and durability (Mindess et al., 2003). Besides the right proportioning of the concrete ingredients, their proper selection is an important issue. Usual ingredients used for concrete production are aggregates (sand and gravel), cement, water, and mineral or chemical admixtures. Here, the balance between economy and desired requirements has to be found by the proper proportioning of the concrete ingredients and leads in most of the cases to a compromise as, for example, the best workable mix does not have to be economic.

Basic rules for the mix design of concrete are already known since the early beginnings of concrete research and reported manifold in the literature (Andreasen and Andersen, 1930; Féret, 1892; Fuller and Thompson, 1907; Hummel, 1959; Plum, 1950). Although the principles are known for more than one hundred years, the mix design of concrete is still an empirical process as the ingredients itself show material-specific characteristics that will influence the properties of the designed concrete mix in fresh and hardened state. These specific material properties and their complex interaction makes it difficult to predict the properties of concrete purely based on theoretical models. However, these models, such as particle packing models, help to minimize the efforts involved in the empirical design process due to proper assumptions that consider the effects of influencing factors. These influencing factors of the concrete ingredients can be of physical or chemical nature.

In general, physical characteristics of aggregates are granulometric properties², specific density, compressive strength, wear resistance, soundness regarding alternate freezing and thawing or repeated wetting and drying, moisture content, and porosity. Chemical properties of aggregates with influence on the concrete properties are mineral oxide composition (more important for binders and reactive fillers), chemical resistance against alkali-silica reaction as well as alkali-carbonate reaction (Mindess et al., 2003), and deleterious substances such as chloride and sulfur compounds. These characteristics become important for concrete that is exposed to deleterious environmental conditions such as sea water, de-icing salts, or other types of chemical attacks.

Physical as well as chemical properties of the aggregates used have to be considered when concrete mixes are designed and their importance depends on the aimed application of the designed concrete. Usually, most of the concrete mix designs are based on achieving a specified compressive strength at given workability and age (Mindess et al., 2003). In this case, the compressive strength of the aggregates and their proper granulometric composition are important as a strong relation exists between the granulometric properties of the aggregates and the concrete properties in fresh and hardened state (De Larrard and Sedran, 1994; Hüskén and Brouwers, 2008; Schmidt and Geisenhanslüke, 2005). This shows that the concrete properties are strongly influenced by the particle packing of the solid ingredients (aggregates) and their particular gran-

¹Parts of this chapter were published elsewhere (Hüskén and Brouwers, 2008).

²In this respect, the term granulometric properties of aggregates covers the grading of the aggregates as well as particle shape and surface texture of the aggregates and is therefore deviating from other definitions.

ulometric properties.

In the following, a brief introduction to commonly used mix design concepts is given and their relevance for the design of EMC mixes is addressed. Based on theories used for geometric packing of continuously graded particle size distributions, a new mix design concept for EMC is introduced and validated by experimental investigations. Results obtained on laboratory scale are presented and discussed in detail to validate the new mix design concept. Furthermore, the experimental results are used to adjust boundary conditions, such as requirements on the grading of the composed concrete mix and its paste content. Finally, a tool is provided that reduces the efforts in the empirical process of concrete mix designs.

4.2 Mix design concepts and their influence on particle packing

The relations between concrete mix design and particle packing were investigated since the early beginnings of modern concrete technology and have their origin in the early work of Féret (1892). These first attempts were followed by the work of Fuller and Thompson (1907) as well as Andreasen and Andersen (1930). The early work on the relationship between aggregates grading and concrete properties was focused on coarse aggregates, such as gravel and sand, only. This fact is caused by limitations of the characterization techniques that were restricted to sieve analysis at that time. However, first and important conclusions were drawn from the empirical work of Féret (1892) and Fuller and Thompson (1907). Féret (1892) demonstrated that the maximum strength of the composed concrete mix is attained when the porosity of the granular structure is minimal and reflects also the basic approach for the design of high performance and ultra high performance concretes (Schmidt and Geisenhanslüke, 2005). The basic idea of improved concrete properties as a result of an optimized and dense granular structure can also be applied to concretes of standard strength and earth-moist concretes. The positive effect of improved particle packing on the properties of EMC will be demonstrated in the following.

4.2.1 Requirements on particle packing and concrete mix design

As addressed before, the packing of the solid ingredients is influencing the properties of the designed concrete in fresh and hardened state. The workability of the concrete in its fresh state is strongly influenced by the granular composition and the ratio between coarse and fine particles. This fact is depicted in Figure 4.1. The original figure of Okamura and Ouchi (2003) was extended with a standard EMC mix. Figure 4.1 points out clearly that the three main types of concrete require different approaches in their mix design as the ratio between coarse and fine aggregates as well as dissimilar paste contents are necessary to fulfill the requirements on the aimed workability properties. According to the desired workability properties and the related rheological properties, three different types of concrete can be classified:

Flowable concretes or self-compacting concretes (SCC) that are characterized by their specific rheological properties. According to Kordts (2005), these concretes can be defined as a Newtonian fluid with high viscosity that keeps the coarse aggregate fraction at a stable state and prevents them from segregation. The self-flowing and self-compacting behavior of these concretes is based on the high powder content combined with optimum water ratio. The coarse aggregate fraction (gravel content) is limited to 50% of the solids volume and the sand fraction amounts up to 40% of the solids volume. In general, this type of concrete is characterized by its higher content of fine materials.

Plastic concrete like normal weight, normal strength concrete (NWC) has, in contrast to SCC, a higher content of coarse aggregates and sand. Here, up to 70% of the solids volume is occupied by particles having a size larger than 125 μm that form the granular skeleton of the aggregates. The paste, consisting of cement, water and fines, is used to fill up the void fraction of the granular skeleton. The dense packing of the aggregates is obtained due to intensive compaction by means of external energy (vibration). The paste content as well

as the rheological properties of the paste have, compared to SCC, a minor influence on the workability properties of these types of concrete as insufficient workability properties are usually compensated in practice by modifications of the compaction process.

Zero slump concretes, such as EMC, RCC and RCD, are characterized by their low workability. This behavior is caused by the internal friction of the concrete mix and the cohesive behavior of the paste. The internal friction of the concrete is obtained by the high content of coarse aggregates that favor grain interlocking, whereas the low water content of these mixes results in partially saturated voids. The partially saturated voids cause the formation of capillary forces and the cohesive behavior of this type of concrete. High compaction efforts are necessary for compaction and to achieve a dense granular structure.

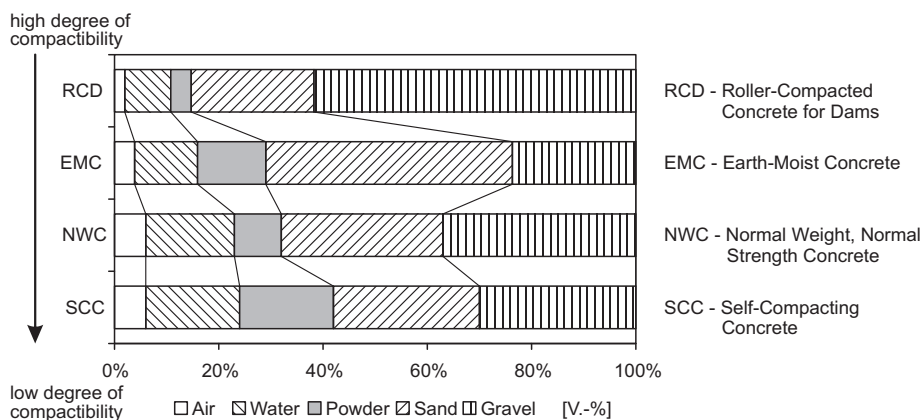


Figure 4.1: Schematic composition of RCD, NWC and SCC taken from Okamura and Ouchi (2003); extended with earth-moist concrete (EMC).

In Figure 4.1, EMC and RCD are representing concretes of the same workability class but showing a difference in the maximum particle size. The influence of the wall effect on the surface texture of the final product is accounted for by the difference in the maximum particle size. Classical EMC mixes used for products like concrete paving blocks are characterized by a maximum aggregate size up to 8 mm in order to achieve a sufficient surface texture. This maximum grain size is higher for RCD mixes without reinforcement bars and can, in special cases, exceed the maximum aggregate size of 40 mm as given by Mindess et al. (2003) for reinforced concrete members. This increase of the maximum particle size is resulting in a shift in the mean particle size of the composed granular mix and is resulting in coarser mixes containing less fine material and less paste – see the difference between EMC and RCD in Figure 4.1.

These lower paste contents for mixes with larger maximum aggregate size are caused by the fact that fewer voids have to be filled by the actually weaker cement paste. This is resulting in concretes with higher compressive strength as the w/c ratio can be lowered. Mindess et al. (2003) point out that the higher strength of concrete caused by an increase of the maximum aggregate size is only noticeable for concretes with low cement contents as applied in EMCs or RCDs. For mixes rich in cement, the increased internal stresses caused by bigger aggregates are compensating the strengthening effect of these aggregates.

However, the beneficial effect of increasing aggregate size and lower paste requirements is only of interest for concretes with plastic behavior and zero-slump concretes. It is obvious from Figure 4.1 that the paste content of SCC is much higher than for other types of concrete to achieve a self-flowing and stable SCC. The higher paste contents of SCCs are required in order to reduce the internal stresses of the mix as the flow energy is consumed by them. The internal stress of the mix increases when the relative distance between the bigger particles decreases and the frequency of collisions and contacts increases (Okamura and Ouchi, 2003). The energy consumption of coarse aggregates caused by their movement relative to each other during compaction or flow is particularly intensive. This fact is also reflected by the different compaction efforts that have to be applied to SCC, NWC or EMC for obtaining concrete that shows similar packing fractions. Hence, the internal stress or friction of the granular mix has to be reduced to improve the flow behavior of SCC and can only be realized by a larger distance between the coarse aggregates.

The use of high paste contents in EMC mixes, as applied for SCC, makes it difficult to achieve densest packing combined with high green-strength values as the green-strength of EMC mixes is a result of adhesive forces between the fine particles and the internal friction of the mix. In the first instance, the apparent cohesion will be influenced positively by an increasing content of fine particles as well as their fineness since the capillary forces are depending to a large extent on the particle size and the number of grain-to-grain contacts in the finer range. Particles smaller than 100 μm have, in particular, the most important influence on the capillary forces in a granular system as with decreasing particle size the capillary force between two particles increases. Therefore, a large number of grain-to-grain contacts in the range of particles smaller than 100 μm is desirable.

As mentioned before, the internal friction will be reduced by higher paste contents as the coarser particles are spread out by finer particles and the grain-to-grain contacts between the coarse particles are reduced. Since the green-strength is a result of the interaction of apparent cohesion as well as internal friction, also the green-strength is reduced. Furthermore, a disproportion in the ratio of coarse to fine particles results in a grading that is not continuous anymore. Such a gap graded PSD leads to insufficient properties of the concrete in the hardened state as the load bearing capacity of the granular structure is not activated completely due to missing grain contacts of the coarser particles. The influence of the grading on the early-age behavior of EMC and the resulting green-strength are discussed in detail in Chapter 6. The following points can be concluded from the before mentioned requirements on the concrete mix design and will be used as basic framework within the new mix design concept:

- High packing fractions should be achieved regardless the way of compaction or self-flowing properties of the composed concrete mix.
- The composed aggregate mix should follow a continuously graded PSD.
- Different types of workability classes should be accounted for by the mix design concept and a simple variation of the ratio coarse to fine particles as well as the paste content should be possible.
- The designed concrete mixes must be robust against small variations in the material properties of the raw materials and the main characteristics of the designed concrete in fresh and hardened state should not be affected by possible variations in the grading of the raw materials.

4.2.2 Particle packing in present concrete mix design

According to Mindess et al. (2003), the theoretical work of concrete mix design is influenced by two main aspects that are still reflected by modern design concepts. The w/c ratio as well as the aggregate grading is known to be the most important factors in concrete mix design. The influence of the w/c ratio on the concrete properties is manifold discussed in the literature (Abrams, 1922; Neville, 1999; Powers and Brownyard, 1947). Limiting values of the w/c ratio

as given in many standards and design recommendations are based on the observation that the strength of the concrete is inversely proportional to the w/c ratio. This fact is explained by Powers and Brownard (1947) in that way that the w/c ratio determines the porosity of the cement paste during hydration. In this context, other concrete properties are also related to the porosity of the hardened cement paste, which limits the w/c ratio for concretes of certain exposition classes or if stricter requirements on the durability are made.

However, not only restrictions on the w/c ratio are given by the most design codes for concrete, but also requirements on the grading of the composed concrete mix are given. These requirements are expressed by so-called grading curves that are usually based on the Fuller curve (Eq. (3.8)). Three different grading curves can be found in the European design codes. These curves are depicted in Figure 4.2 using the example of the Dutch standard NEN 5950 for aggregates having a maximum size of 16 mm. The grading curves A, B, and C are representing specified grading limits for coarse and fine aggregates in dependence of the maximum aggregate size. These curves are available for different maximum aggregate sizes that are commonly used for concrete production. Grading curve A is the limit for coarse sized aggregate mixes that contain less fine material, whereas grading curve C gives the limit for aggregate mixes that have higher contents of fine materials. The optimum grading of the aggregate mix, as also recommended by Hummel (1959), is given by grading curve B that approximates the Fuller curve and is located between curve A and C. The grading curves A, B, and C depicted in Figure 4.2 are comparable to the German standard DIN 1045-2.

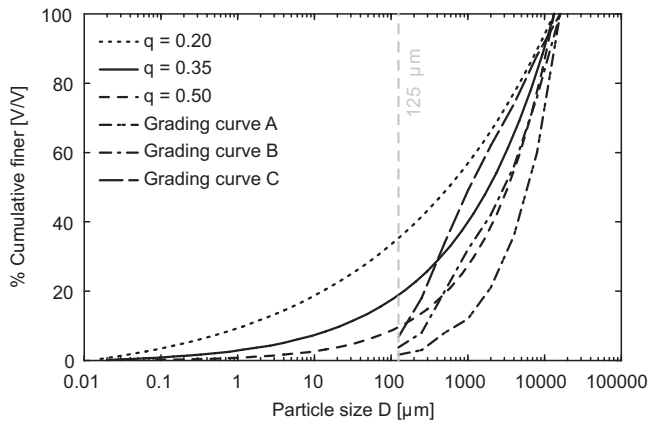


Figure 4.2: Grading curves for varying distribution moduli q of the modified A&A equation using $D_{max} = 16$ mm, $D_{min} = 0.01$ μm and grading curves A, B and C according to NEN 5950.

Figure 4.2 illustrates that the grading curves A, B, and C are applied to aggregates only and that the grading of the fines is not considered in the mix design. The grading curves are given by the Dutch and German standard for aggregates that have a particle size larger than 125 μm . This limitation leads to the consequence that minimum and maximum amounts of fines are prescribed. The granulometric properties of the fines as well as their positive effect on the particle packing are not considered. Table 4.1 gives an overview of the minimum volume fraction of fines that is required by the Dutch standard NEN 5950 for the mix design of NWC.

Limiting values are not only given for the minimum content of fine material, but also for the maximum content of fines. The German standard DIN 1045-2 gives limits for the maximum

Table 4.1: Minimum amount of fine material smaller than 250 μm as defined by NEN 5950.

Largest grain size (D_{\max})	Min. vol. fraction
[mm]	[dm^3]
8	140
11.2	130
16	125
22.4	120
31.5	115

content of fines in order to reduce the water demand of the concrete and should account for requirements in respect to durability. Here, the maximum content of fines is limited for concrete up to a strength class C55/67, depending on the cement content, to 600 kg per m^3 concrete. This value does not allow for the design of SCCs and is lower for concretes of the exposition class XF and XM if low cement contents are applied.

It can be concluded at present that particle packing in concrete mix design is limited to the grading of aggregates only. Recommendations for the optimum grading are based on the Fuller curve (Eq. (3.8)) which is not accounting for the smallest particle size D_{\min} present in the mix. The granulometric properties of the fines are not considered in concrete design codes. However, it is shown that the concrete properties of special concrete types, such as SCC, depend to a large extent on the granulometric properties of the fines (Hunger and Brouwers, 2009; Kordts, 2005; Reschke, 2000).

The ideas of particle packing models are not applied to the mix design of ordinary types of concrete like NWC or EMC. Here, a huge potential for optimization exists as these types of concrete form the largest part of the concrete production. Standard mix design concepts showed their robustness due to their application over many years. But it becomes obvious that the potential of concrete is not activated completely and that the performance of concrete in fresh and hardened state can be improved by an appropriate mix design concept that accounts for the granulometric properties of all materials.

4.2.3 New mix design concept

The main object of the new mix design concept consists in the proportioning of a performance based concrete mix based on particle packing theories. The positive effect of the modified Andreasen and Andersen equation (Eq. (3.9)) on the properties of self-compacting concrete was already shown by Brouwers and Radix (2005), and Hunger and Brouwers (2006). Also Schmidt et al. (2005) showed with their investigations that good results are obtained when the grading of the designed concrete mixes follows the grading curve described by the modified A&A equation. However, Schmidt et al. (2005) did not optimize the grading of their composed concrete mixes in consideration of the modified A&A equation. They compared the grading of the composed concrete mixes with the shape given by Eq. (3.9) using varying distribution moduli q . It appears that an aimed composition of the concrete mix considering the grading line given by the modified A&A equation results in concrete that meets required performance properties.

It was mentioned in the previous section that present design codes do not account for the granulometric properties of the fines and that only the grading of aggregates is considered in the mix design concept. The use of the modified A&A equation allows the mix design of concrete considering the entire grading of all solid ingredients. This fact is included in Eq. (3.9) by the maximum and minimum particle size D_{\max} and D_{\min} , respectively. The distribution modulus q

of Eq. (3.9) influences the ratio of coarse to fine particles. Higher values of the distribution modulus ($q > 0.5$) are leading to coarser mixes, whereas smaller values ($q < 0.25$) are resulting in concrete mixes that are rich in fine particles. The influence of the distribution modulus q on the grading curve of the composed aggregate mix is shown in Figure 4.2 for varying q and given D_{min} and D_{max} .

To change the ratio of coarse to fine particles in the composed aggregate is an important issue for the mix design. This allows for the composition of ideal graded concrete mixes for different types of concrete by changing one single parameter in the model only and enables the design of concrete mixes that fulfill different requirements on the workability due to their difference in the paste content. Figure 4.3 shows the influence of the distribution modulus q in Eq. (3.9) on the paste content and the ratio of coarse to fine particles.

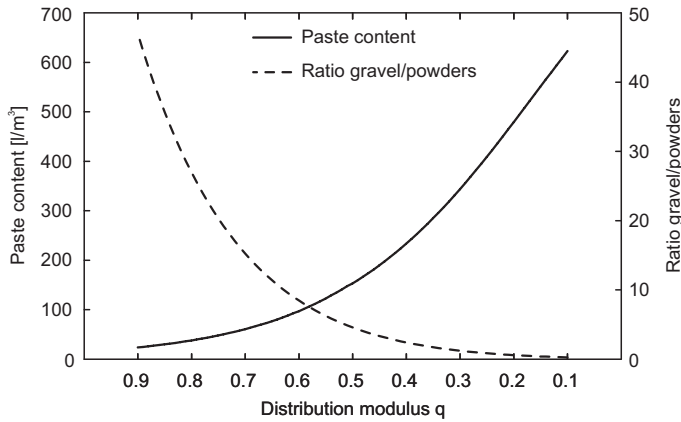


Figure 4.3: Influence of the distribution modulus q in the modified A&A equation (Eq. (3.9)) on the paste content per m^3 fresh concrete and the ratio of gravel ($4\text{ mm} < D < 16\text{ mm}$) to powders ($0.01\text{ }\mu\text{m} < D < 125\text{ }\mu\text{m}$); paste content for particles smaller than $125\text{ }\mu\text{m}$ considering a constant w/p ratio of 0.35, $D_{max} = 16\text{ mm}$, $D_{min} = 0.275\text{ }\mu\text{m}$.

For computing the paste content as well as the ratio of gravel to powders, the volumetric amount of particles smaller than $125\text{ }\mu\text{m}$ is used. The definition of *gravel*, *powder* and other constituents, as well as the associated particle sizes, are based on the definitions given in Figure 2.2. The different grading curves that have been used in Figure 4.3 are computed in the range between $0.01\text{ }\mu\text{m}$ (D_{min}) and 16 mm (D_{max}) using variant distribution moduli in steps of $\Delta q = 0.01$. The computed grading curves are resulting in similar lines as depicted in Figure 4.2. The computed paste contents are based on a constant water to powder ratio w/p of 0.35 that is aimed on the water content of standard EMC mixes. The w/p ratio characterizes the amount of water in the concrete mix based on the amount of powders and represents an important workability parameter. Usually, w/p ratios of 0.35 and lower are used for EMC and stiff concrete mixtures. Higher values are applied for plastic and flowable concretes. In this consideration, the influence of air is ignored.

In the analyzed range of the distribution modulus, from 0.1 to 0.9, both the paste content per m^3 fresh concrete and the ratio of gravel to powders varies in a wide range. The value of the paste content per m^3 fresh concrete ranges from $630 - 241/m^3$, while the ratio gravel to powders varies

between 0.3 and 47. The extreme values in the lower and upper area of $q = 0.1$ and $q = 0.9$, respectively, are not of interest for practical applications. Brouwers and Radix (2005) as well as Hunger and Brouwers (2006) recommend an optimum in regard to the workability of SCC for $0.22 \leq q \leq 0.25$. Schmidt et al. (2005) obtained good results with their experimental investigations if the grading of the designed concrete mixes showed good agreement with the modified A&A equation using a distribution moduli in the range around $q = 0.35$. The analysis of paste contents and corresponding w/p ratios of EMC mixes that are reported in literature (Bornemann, 2005; Stutech, 2005) resulted in an optimum range of $0.35 \leq q \leq 0.40$ for EMC having a maximum aggregates size of 16 mm. This range meets also the recommended percentage for particles smaller than $75 \mu\text{m}$ given by Nanni et al. (1996). According to Nanni et al. (1996), the percentage of aggregate passing the sieve No. 200 ($75 \mu\text{m}$) should be between 10% and 14% for RCC. This requirement is fulfilled for a distribution modulus of $q \geq 0.35$ and $D_{\text{max}} = 19 \text{ mm}$ which is typical for RCC (cp. Figure 4.3). The necessary paste content is not only influenced by the distribution modulus q , but also the maximum aggregate size of the raw materials influences the grading. This fact is also pointed out in Section 4.2.1. Figure 4.4 confirms this again and shows how the modified A&A equation is accounting for the maximum particle size in the mix.

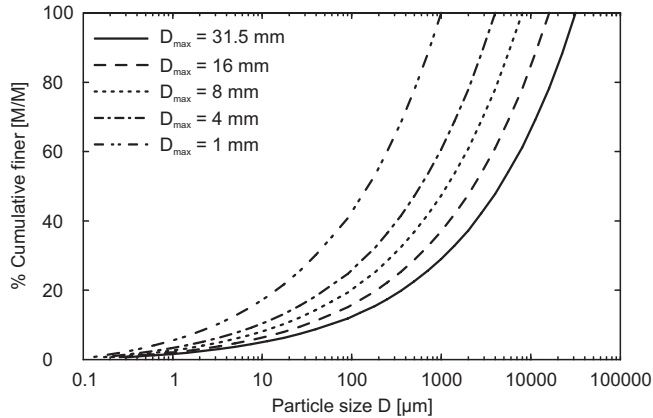


Figure 4.4: Influence of the maximum particle size D_{max} on the modified Andreasen and Andersen equation (Eq. (3.9)) using a constant distribution modulus of $q = 0.35$; $D_{\text{min}} = 0.12 \mu\text{m}$.

The requirements on particle packing in concrete mix design and the ideas of theories on particle packing, as addressed in Section 3.2, show that the grading curve of the composed concrete mix should follow a continuous distribution. Highest packing fractions of these continuous distributions are obtained when the size classes form a geometric progression (Brouwers, 2006). This geometric progression of the size classes is given by the modified A&A equation. However, a simple and easy to handle tool is necessary for composing a concrete mix that follows a given grading curve. Therefore, an algorithm was developed that allows for the composition of a concrete mix that follows the grading curve given by the modified A&A equation.

The developed algorithm considers the volumetric proportion of all ingredients present in the mix ($k = 1, 2, \dots, m$), including the non-solid ingredients air and water. The particle size D in Eq. (3.9) is given by the geometric mean D_i^{i+1} of the upper and lower sieve size of the respective

fraction obtained by particle size analysis as:

$$D_i^{i+1} = \sqrt{D_i D_{i+1}} \quad \text{for } i = 1, 2, \dots, n-1 \quad (4.1)$$

The sizes classes of the fractions vary in steps of $\sqrt{2}$ starting from 10 nm up to 125 mm and correspond to the size classes that are used for particle size analysis of the raw materials (see Figure 4.5). Consequently, 44 discrete sizes ($i = 1, 2, \dots, n+1$) are present and 43 fractions n are available for the classification of the $m-2$ solid ingredients. Taking this wide range of the PSD of the granular ingredients into account, the entire grading of all aggregates, binders, and filler materials is considered in the mix design.

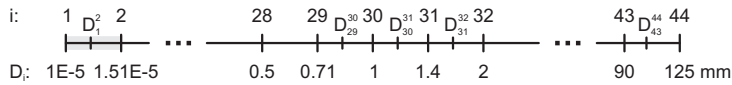


Figure 4.5: Sizes and definition of fractions used in the optimization algorithm.

It is noteworthy that in concretes with standard components, the finest particle present in the mix is around 300 nm, this is the finest cement, fly ash or filler size, a feature already observed by Plum (1950). The largest particle size is determined by the coarsest ingredient, which is the gravel fraction. Besides the characterization of the solid ingredients regarding their PSDs, some further material properties, such as specific density and specific surface area, are necessary for the optimization. The specific density is needed as the grading curve (cumulative finer fraction) of the target function is volume based, while the ingredients are dosed and analyzed (particle size analysis) on mass base. If the required material properties are known, the optimization problem is formulated and its solution gives the concrete mix proportioning.

4.3 Optimization algorithm

The solution of a mathematical optimization problem gives the optimum parameters for a complex system of elements. These elements contain data or describe processes or functions. Relations between the single elements have to exist that allow the mathematical description of the interactions between the single elements. The formulation of the optimization problem results in a target function whose parameters, or so-called variables, are giving the solution of the optimization problem. The solution of the target function can either be minimized or maximized. Different algorithms are available for solving the optimization problem. In principle, the formulation of an optimization problem requires three parts that have to be defined before. These parts are:

- Target function
- Variables
- Constraints

Figure 4.6 shows the principle of the considered optimization problems as an example for a composed concrete mix based on 4 solid ingredients ($m = 6$). Furthermore, the applied grading curve $P_{tar}(D_i)$ as well as the PSDs of the materials used and the resulting maximum and minimum particle size D_{max} and D_{min} are also depicted in Figure 4.6. The figure illustrates that by combining four ingredients only, which show a significant difference in their PSDs, a mix can be designed that closely follows the given grading curve (Eq. (3.9))

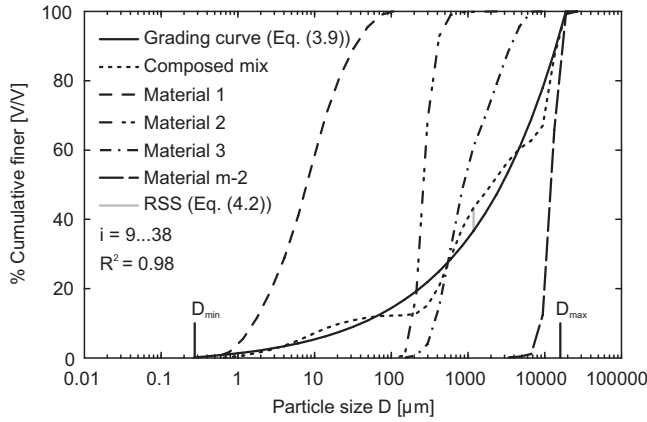


Figure 4.6: Concrete mix composed of 4 solid ingredients using the developed optimization algorithm; $D_{max} = 16 \text{ mm}$, $D_{min} = 0.275 \text{ } \mu\text{m}$, $q = 0.35$.

4.3.1 Target function

The target function represents the objective or goal of the optimization problem. This value can either be minimized or maximized. In the considered case, the deviation between the desired grading, given by the grading curve, and the grading of the composed mix shall be minimized and is resulting therefore in a curve fitting problem. Based on the given mathematical function of the grading curve $P_{tar}(D_i^{i+1})$, the best fit to a series of data points, depending on the grading of the aggregates used and their volumetric proportioning, will be obtained. The least squares technique is commonly used to solve a curve fitting problem. Thereby, the sum of the squares of the residuals RSS is minimized. Equation (4.2) expresses the least squares technique mathematically.

$$RSS := \sum_{i=1}^n e_i^2 = \sum_{i=1}^n (P_{mix}(D_i^{i+1}) - P_{tar}(D_i^{i+1}))^2 \rightarrow \min! \quad (4.2)$$

$$\text{with } P_{tar}(D_i^{i+1}) = \frac{(D_i^{i+1})^q - D_{min}^q}{D_{max}^q - D_{min}^q} \quad \forall D_i^{i+1} \in [D_{min}, D_{max}]$$

$$D_{min} = D_i \quad \text{for } P(D_{i-1}) = 0 \wedge P(D_i) > 0$$

$$D_{max} = D_i \quad \text{for } P(D_{i-1}) < 100 \wedge P(D_i) = 100$$

The quality of the curve fit is evaluated by the coefficient of determination R^2 as it gives a value for the correlation between the grading of the target line and the grading of the composed mix. The coefficient of variation is calculated as follows:

$$R^2 = 1 - \frac{\sum_{i=1}^n (P_{mix}(D_i^{i+1}) - P_{tar}(D_i^{i+1}))^2}{\sum_{i=1}^n (P_{mix}(D_i^{i+1}) - \bar{P}_{mix})^2} \quad \forall D_i^{i+1} \in [D_{min}, D_{max}] \quad (4.3)$$

with $\overline{P_{mix}} = \frac{1}{n} \sum_{i=1}^n P_{mix}(D_i^{i+1})$ as average of the entire distribution.

4.3.2 Variables

Variables are values that can be adjusted by the optimization algorithm to minimize or maximize the target function. These values are in the considered case representing the total amount of solids of the designed concrete mix V_{sol}^{tot} and the volumetric proportion $v_{sol,k}$ of each solid raw material. The total volume of solids V_{sol}^{tot} per m^3 concrete is given by:

$$V_{sol}^{tot} = \sum_{k=1}^{m-2} V_{sol,k} \quad (4.4)$$

and the volumetric proportion of each solid ingredient $v_{sol,k}$ is defined as:

$$v_{sol,k} = \frac{V_{sol,k}}{V_{sol}^{tot}} \quad \text{for } k = 1, 2, \dots, m-2. \quad (4.5)$$

The volumetric proportion $v_{sol,k}$ of each solid component influences the grading line (computed sieve residue) of the composed solid mix via:

$$Q_{mix}(D_i^{i+1}) = \frac{\sum_{k=1}^{m-2} \frac{v_{sol,k}}{\rho_{sol,k}^{spe}} Q_{sol,k}(D_i^{i+1})}{\sum_{i=1}^n \sum_{k=1}^{m-2} \frac{v_{sol,k}}{\rho_{sol,k}^{spe}} Q_{sol,k}(D_i^{i+1})} \quad (4.6)$$

with $Q_{sol,k}(D_i^{i+1})$ sieve residue of material k on sieve i
and $\rho_{sol,k}^{spe}$ as the specific density of material k .

The computed cumulative finer fraction for each size class D_i^{i+1} of the composed mix is given by:

$$P_{mix}(D_i^{i+1}) = P_{mix}(D_{i-1}^i) - Q_{mix}(D_i^{i+1}) \quad (4.7)$$

As mentioned before, the total volume of solids V_{sol}^{tot} per m^3 concrete can also be adjusted by the optimization algorithm. This value is not directly related to the target value as it is the case for the volumetric proportion of each solid ingredient $v_{sol,k}$. The total volume of solids V_{sol}^{tot} is influenced only by the constraints of the optimization algorithm.

4.3.3 Constraints

Constraints are restrictions to the variables and/or the target function and reflect practical limits or boundary conditions. These restrictions are expressed by equations or inequalities. The formulation of an optimization problem distinguishes between physical constraints and policy constraints. Physical constraints are determined by the physical nature of the optimization problem and result from the physical limits of the system, whereas policy constraints are determined by requirements of standards or particular demands on the designed concrete mix. In the lat-

ter case, the idea of a performance based mix design concept is realized. For the optimization problem that has to be formulated, the following physical constraints have to be considered:

Non-negativity constraint that takes into account that a negative volumetric proportion of each solid ingredient $v_{sol,k}$ as well as a negative total volume of solids V_{sol}^{tot} per m^3 concrete is not a valid solution and can be formulated as follows:

$$v_{sol,k} \geq 0 \quad \text{for } k = 1, 2, \dots, m-2 \quad (4.8)$$

Volumetric constraint which includes that the sum of the volumetric proportion $v_{sol,k}$ of the granular ingredients used in Eq. (4.6) cannot be higher than 1 and is expressed by:

$$\sum_{k=1}^{m-2} v_{sol,k} = 1 \quad (4.9)$$

Moreover, the total volume of all ingredients (including air and water) per m^3 fresh concrete, according to Eq. (4.10), cannot be higher or lower than $1 m^3$:

$$\begin{aligned} V_{con} &= V_{sol}^{tot} + V_{wat} + V_{adm} + V_{air} \\ &= V_{agg} + V_{cem} + V_{fil} + V_{wat} + V_{adm} + V_{air} = 1 m^3 \end{aligned} \quad (4.10)$$

Eq. (4.10) expresses the volumetric relation of the solid ingredients (aggregates V_{agg} , binders (cement) V_{cem} , fillers V_{fil} , and admixtures V_{adm}) as well as the water V_{wat} , and the air content V_{air} . The air content per m^3 fresh concrete is estimated a priori to be $0.04 m^3$ (4.0 V.-%). This value needs to be verified later as it is depending on the maximum packing fraction of all solids, the water content and the applied compaction efforts. Furthermore, Eq. (4.10) contains terms that can be described through further relations between the solid ingredients. These relations are influenced by policy constraints. As mentioned before, policy constraints represent requirements of standards or particular demands such as:

Water cement ratio w/c that is one of the oldest and most basic parameters used in concrete technology (Neville, 2006). The w/c ratio defines on mass base the ratio of water M_{wat} to cement M_{cem} and is computed as follows:

$$w/c = \frac{M_{wat}}{M_{cem}} = \frac{\rho_{wat} V_{wat}}{\rho_{cem}^{spe} V_{cem}} \quad (4.11)$$

Neville (2006) distinguishes between total w/c and effective w/c ratio, whereas the latter case corresponds to Eq. (4.11) and is accounting for the whole amount of water added to the mix. The effective w/c ratio considers only the saturated and surface dry condition of the aggregates without any free water on the surface of the aggregates. A further and more detailed explanation of the w/c ratio and its relevance for the properties of the hardened concrete is given by Neville (2006).

Water powder ratio w/p that is of greater interest for the workability of fresh concrete mixes. In particular, lean concrete mixes suffer from insufficient compaction when the w/c ratio of these mixes is maintained at the same level as used for conventional concrete. The reason for that is caused by the lower cement content of these lean concrete mixes and the reduced paste volume necessary for compaction.

Therefore, the fines lacking from low cement contents have to be replaced by fillers such as fly ash, or limestone powder. This increase in fine materials, necessary to fill the voids

between the coarser aggregates, requires a certain amount of water in order to obtain a paste that enables a sufficient compaction of the concrete mix. As a consequence of this, the w/c ratio increases. Hence, all fine particles of the designed concrete mix have to be considered if certain workability properties are required. In the considered case, the w/p ratio includes all particles in the mix having a particle size smaller than $125 \mu\text{m}$ and is calculated as follows:

$$w/p = \frac{M_{wat}}{\sum_{k=1}^{m-2} M_{sol,k}} = \frac{\rho_{wat} V_{wat}}{\sum_{k=1}^{m-2} \rho_{sol,k}^{spe} V_{sol,k} (D_i^{i+1})} \quad \text{for } D_i < 125 \mu\text{m} \quad (4.12)$$

The problem of increasing w/c ratios of lean concrete mixes and the universal validness of the w/c ratio is also addressed by Neville (2006) in his response to a letter to the editor. Neville (2006) states that the w/c ratio and the associated knowledge are not a universal law applying to any type of concrete as the w/c ratio applies to conventional concrete only. Consequently, both the w/c ratio and the w/p ratio can be chosen as a constraint of the optimization algorithm.

By choosing one of the two ratios explained before, the amount of water in the mix is determined and a relation with the volumetric constraint is made. This allows both the design of high-strength concrete mixes that are rich in cement and the composition of environmental friendly concrete mixes having low cement contents.

Binder ratio that allows for the composition of a concrete mix using two different binding materials. The ratio between the first binder $V_{cem,1}$ and the second binder $V_{cem,2}$ can be chosen without limitations. This can either be the use of an ordinary Portland cement in combination with a slag blended cement or the tailor-made composition of an individual blended slag cement by using Portland cement and ground granulated blast furnace slag as separate materials.

Most of the before mentioned constraints can be chosen in such a way that commonly used types of concrete as well as special types of concrete, e.g. eco-concretes or high-strength concretes, can be designed. It has to be noticed that an assessment of the optimization target and the constraints regarding their significance is not implemented in the optimization algorithm. Both criteria are treated equally. Therefore, a multitude of constraints that deviate from the standard rules applied to conventional concrete are resulting in mixes that have an optimized grading. This optimized grading considering the given boundary conditions can deviate from the best possible grading that can be obtained regardless limitations of the cement content or other restrictions.

4.3.4 Solution

The optimization problem can be formulated when all material properties and constraints are known. In order to simplify the formulation of the optimization problem, a so-called optimization algorithm was programmed in MICROSOFT EXCEL. The developed algorithm is making use of the solver tool embedded in MICROSOFT EXCEL and solves the optimization problem numerically. The solution for the variables of the optimization is obtained by an iterative method until the optimal volumetric proportion $v_{sol,k}$ of solids and the necessary total volume of solids V_{sol}^{tot} for producing 1 m^3 concrete are obtained.

The required material properties are provided by an external database that can be extended according to the user demands. Based on the solution of the optimization problem, a complete mix design including the necessary amounts of aggregates, binder, water, and air is provided to the user. Relevant parameters of the concrete mix such as binder content, water content based on the mass of dry solids, content of fines smaller $125 \mu\text{m}$ and $250 \mu\text{m}$, computed surface area and porosity are included in the suggested mix design. Furthermore, the deviation between the grading of the target line and the composed concrete mix is given. A concrete mix design including

the associated grading of the composed concrete as an exemplary solution of the optimization algorithm is given Appendix C.1 and Appendix C.2.

4.4 Experimental validation

Several concrete mixes have been designed and tested in the laboratory to validate the new mix design concept and to demonstrate the suitability of geometric packing for earth-moist concrete. First tests were also performed to investigate the influence of various target curves on the packing. For this purpose, EMC mixes have been designed, using the aforementioned optimization algorithm, and tested in fresh and hardened state.

The designed EMC mixes are solely based on cement and aggregates without the use of supplementary fillers. Plasticizers have been used for some mixes to study their effect on the filling behavior and the compaction behavior. Besides the tests carried out in the lab, some additional tests were carried out on concrete paving blocks produced on a laboratory paving block machine. The results of these tests will also be discussed in detail in this section.

4.4.1 Trial mixes

By means of the new mix design concept and the optimization algorithm discussed in the previous section, EMC mixes using different types of materials have been designed. Standard river aggregates (sand and gravel) and a slag blended cement type CEM III/B 42.5 N with low hydration heat release (LH) and high sulfate resistance (HS) were mainly used for the experiments. Furthermore, the before mentioned slag cement was blended with an ordinary Portland cement (CEM I 52.5 N) to fulfill the requirements of a paving block producer in higher strength properties after one day. The mix design of an EMC mix that is used for the production of concrete pipes was supplied by a commercial company. This mix (Blend 1) is used as reference mix and was optimized by means of the new mix design concept. The blended cement is composed of 35 % OPC and 65 % slag cement. The PSD of the materials used is given in Figure 4.7 and their material properties are listed in Appendix A.1.

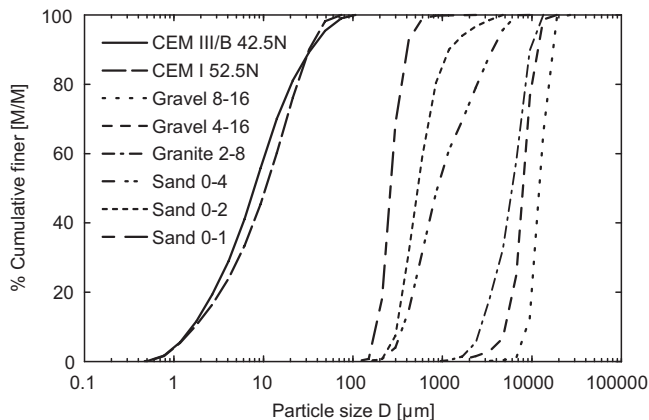


Figure 4.7: PSDs of aggregates and powders used (cumulative finer mass fraction).

The grading of the designed concrete mixes follows mainly the modified A&A curve (Eq. (3.9)) using varying distribution moduli q . Concrete mixes with distribution moduli q of 0.25, 0.30,

0.35, and 0.40 were designed and tested in fresh and hardened state. In cases where the modified A&A curve was not applied, the grading of the composed concrete mix follows the Fuller curve (Eq. (3.8)). Besides varying distribution moduli, different w/c ratios were also considered in the mix design.

For the modified A&A curve, a maximum particle size D_{max} of 16 mm and a minimum particle size D_{min} of 0.5 μm , based on the obtained data of the particle size analyses, were used. The maximum particle size D_{max} is determined by the coarsest aggregate used (gravel 4-16), whereas the minimum particle size D_{min} represents the smallest particle size in the mix (CEM III/B 42.5 N LH/HS). The PSD of the designed concrete mixes is given in Appendix D.1 and Appendix D.2 and further information on their mix design are given in Appendix D.3. The designed EMC mixes were mixed in a 35 l compulsory mixer for 5 min and tested for their fresh concrete properties immediately after mixing.

4.4.2 Fresh concrete tests

The fresh concrete properties of the mixes that have been designed using the optimization algorithm will be discussed in detail in this section. Different test methods are available for determining the properties of fresh concrete mixes. The most suitable test methods for EMC mixes are explained in Section 2.7. In the following, the fresh concrete is evaluated using the degree of compaction c_{DIN} as explained in Section 2.7.1. Furthermore, the density of the fresh concrete loosely and densely packed was computed. For doing so, the vessel of the air entrainment meter was used for determining the mass of the densely and loosely packed concrete and both values were used for calculating the packing fraction PF according to Eq. (3.1). The measurements of the tested trial mixes are depicted in Figure 4.8 considering the packing fraction PF^{den} of the densely packed concrete. The average values of the single measurements are given in Appendix E.9 and the measured void fraction according to Eq. (3.2) is compared in Table 4.2 for selected mixes with computed values using Eq. (3.10).

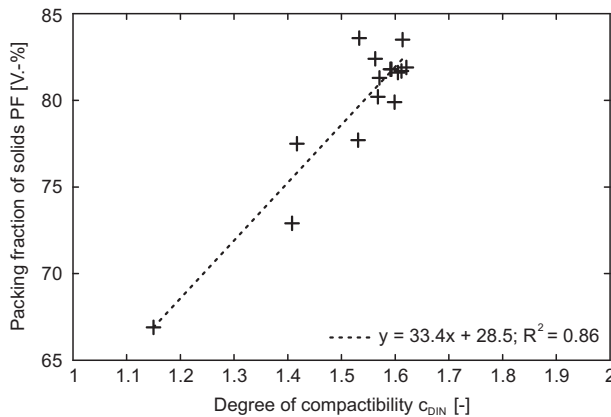


Figure 4.8: Measured packing fraction versus degree of compaction for tested EMC mixes.

The designed EMC mixes gave test values between 1.15 and 1.62 for the degree of compaction c_{DIN} . Most of the tested mixes exceed the upper limit of 1.46 as suggested by Bartos et al. (2002). The same fact is also reflected by the computed degree of compaction c_{com} . As both values, c_{DIN} and c_{com} , are in good agreement (cp. Figure 2.10), the explanation for this is given by the low

values of the loose packing fraction PF^{loo} . All designed EMC mixes that exceed the upper limit of the degree of compaction c_{DIN} showed rather low packing fractions when they are packed loosely. This is caused by the low water content of these EMC mixes that reduces the filling behavior of the fresh concrete. The void fraction of these mixes amounts up to 50%, whereas the degree of saturation S_w of the void fraction with water ranges from 15 - 20% (see Table E.9).

According to Rumpf (1975), a saturation of 20 - 30% characterizes the pendular state when liquid bridges are formed. The capillary forces, induced by the formation of liquid bridges, reach their maximum value within the pendular state and work as attractive forces between the smaller particles. This working mechanism prevents the wet EMC mixes from trickling like dry sand. Consequently, the packing fractions of the loosely packed EMC mixes are lower than the packing fractions of dry sand fractions listed in Table 3.1. This effect caused by the moisture content of the EMC mixes results in the large volume difference of the concrete in loose and dense state and causes, therefore, large values of the degree of compaction that exceed the limiting values.

The use of plasticizers in small amounts showed a beneficial effect on the filling behavior of the designed EMC mixes. The packing fraction PF^{loo} of these mixes could be increased and the degree of compaction is in the recommended range as suggested by Bartos et al. (2002). Furthermore, it is obvious from the data presented in Table E.9 that not only the filling behavior and the packing fraction PF^{loo} is improved but also the packing fraction PF^{den} is higher than without using plasticizers. However, the use of plasticizers showed a more pronounced effect on the packing fraction PF^{loo} than on the packing fraction PF^{den} as here only minor improvements have been achieved.

Table 4.2: Computed void fraction (Eq. (3.10)) and measured void fraction according to Eq. (3.2) of investigated trial mixes.

	Computed void fraction (Eq. (3.10))		Measured void fraction (Eq. (3.2))	
	φ_{com}^{loo} [%]	φ_{com}^{den} [%]	φ^{loo} [%]	φ^{den} [%]
Mix 4	25.6	6.6	49.5	18.1
Mix 5	25.6	6.6	50.0	18.2
Mix 9	25.6	6.6	38.4	16.3
Mix 10	26.2	7.0	47.7	17.6
Blend 2	24.3	5.7	48.1	16.5
Blend 3	24.3	5.7	40.0	16.0
Blend 4	24.3	5.7	38.3	15.3

The values depicted in Figure 4.8 show clearly the linear relation between the packing fraction PF^{den} and the degree of compaction c_{DIN} . This linear relation was expected as the degree of compaction is an indicator for the compaction behavior as explained in Section 2.7.1. Mixes that have low degree of compaction ($c_{DIN} < 1.40$) showed an insufficient compaction behavior caused by a suboptimal composition of the concrete ingredients. In this case, the resulting grading of the designed concrete mix showed a large deviation to the proposed target line (Eq. (3.9)) or the water content of these mixes was not adjusted to the optimum value necessary for sufficient compaction. Due to the linear relation between the packing fraction PF^{den} and the degree of compaction c_{DIN} , the packing fraction PF^{den} will be used in the following to relate the mechanical properties to packing of the fresh concrete mix.

4.4.3 Hardened concrete tests

The compressive strength f_c was determined on standard cubes of $150 \times 150 \times 150$ mm. In order to show the influence of improved and dense particle packing on the mechanical properties of concrete, the cubes used for determining the degree of compaction were used. The designed EMC mixes have been tested first for their degree of compaction as explained in Section 2.7.1. After this, the filling hopper and surplus material were removed and the cubes were smoothed using a trowel. Subsequently, the cubes were cured sealed during the first day, stripped from the mold after 24 hours, and cured for 27 days in a water basin according to the prescribed storing conditions given in the standard DIN-EN 12390-2.

After 28 days, the cubes were tested for their compressive strength f_c according to the requirements given by the standard DIN-EN 12390-3. The results of the compressive strength test are depicted in Figure 4.9 versus the packing fraction PF^{den} of the fresh concrete mix. Detailed values of the test, including statistical values, are given in Appendix E.10.

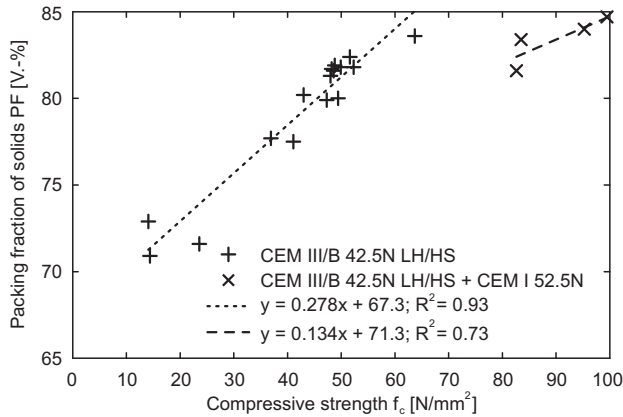


Figure 4.9: Measured packing fraction versus compressive strength for tested EMC mixes.

The values presented in Figure 4.9 show a linear relation between the packing fraction and the compressive strength of the hardened concrete. This holds for both mixes using only slag cement and mixes containing a blend of 65% slag cement and 35% Portland cement. The cement content used in the mixes that are purely based on slag cement ranges from 290 - 320 kg per m³ fresh concrete, whereas the cement content in the mixes using the blended cement was fixed to 325 kg per m³ fresh concrete.

The linear relation between packing fraction and compressive strength confirms the assumption that the mechanical properties of the hardened concrete can be improved by a dense granular structure having optimum particle packing. This fact is demonstrated by the experimental results of Mix 3 and Mix 10. The packing fraction of Mix 3 was determined with $PF^{den} = 77.7\%$. The aimed composition of the solid ingredients regarding their granulometric properties increased the packing fraction of Mix 10 to $PF^{den} = 82.4\%$. The optimization comprises in this case the grading of the composed concrete mix and the adjustment of the optimum water content. This first optimization increases not only the packing fraction of the fresh concrete, but also the compressive strength of the hardened concrete. The average compressive strength of Mix 3 amounts to $f_c = 36.9$ N/mm² and is improved to $f_c = 51.6$ N/mm² for Mix 10. Furthermore, it is worth-

while to mention that the cement content of Mix 10 amounts to 290 kg, whereas Mix 3 contains 310 kg per m³ fresh concrete.

The latter case shows that the compressive strength of the hardened concrete increases by using an optimized and dense packing and that cement can be used more efficiently. Due to an optimized particle packing it is possible to use less cement while obtaining the same performance of the concrete in hardened state or even to improve this performance. This fact can be addressed in a better way by a factor describing the cement efficiency. A parameter for considering the cement efficiency is also used by Su and Miao (2003) as well as Brouwers and Radix (2005) for the mix design of self-compacting concretes. This parameter x is computed according to Eq. (3.11) and gives the compressive strength provided by each kilogram of cement.

Considering the values given in Figure 4.9 and Table E.10, the cement efficiency factor could be increased for the slag cement mixes from 0.13 to 0.21 Nm³/kgmm². Due to the fact that the used Portland cement obtains a higher compressive strength than the used slag cement, it is possible to increase the cement efficiency factor of the mixes using the blended cement from 0.22 to 0.31 Nm³/kgmm².

The cement efficiency factor x_{cem} allows a performance based comparison of different types of concrete in terms of their actual capability of strength utilization per kg cement that is used. In case that different concrete mixes of the same strength class are compared, their ecological impact can be assessed. Mixes with a high cement efficiency factor x_{cem} are making use of less cement and show a better performance in the eco-balance.

The cement efficiency was not only improved by an optimized and denser particle packing but also the use of plasticizers showed a beneficial effect on the obtained packing fractions and the resulting compressive strength. Mix 7 and 9 show this fact exemplary. The packing fraction of Mix 7 amounts to $PF^{den} = 79.9\%$ without using a plasticizers and was increased to $PF^{den} = 83.7\%$ for mix 9 by the use of a plasticizers while keeping the w/p ratio constant. The higher packing fraction PF^{den} results in the considered case in a denser granular structure that improves the mechanical properties. Consequently, the average compressive strength f_c of Mix 7 is increased from 47 N/mm² to 64 N/mm² as determined for Mix 9.

Similar improvements have been obtained for the EMC mixes using the blended cement. Here, the packing density of the original mix (Blend 1) amounts to $PF^{den} = 81.6\%$ with a compressive strength of $f_c = 83\text{N/mm}^2$. Both values could be improved by an optimized particle size distribution and the use of a plasticizer to $PF^{den} = 84.7\%$ and $f_c = 100\text{N/mm}^2$ (Blend 4). It is worthwhile to mention that here also the cement content was reduced to a minimum content that is necessary to fill the remaining voids of the aggregate fraction. The high compressive strength values obtained by the EMC mixes using blended cement are not required for concrete mass products. This allows the replacement of cost intensive cement by cost-saving fillers such as fly ash, limestone powder or fine stone waste materials from the natural stone industry.

4.4.4 Discussion

The investigations and tests carried out on EMC showed that a general relation between particle packing and concrete properties in fresh and hardened state can be derived. Suitable models for particle packing help to improve the concrete properties by an aimed optimization of the grading of the composed concrete mix. In the considered case, the grading curve given by the modified A&A equation (Eq. (3.9)) was applied for the mix design of EMC mixes. This grading curve is not only suitable for the mix design of EMC mixes, but also other types of concrete, such as SCC or NWC, can be designed.

The major benefit of the modified A&A equation is given by the fact that the composed concrete mix follows an ideal grading curve that results in dense particle packing with a dense granular structure. Furthermore, the paste content is an important property of the composed concrete mix and is depending on the type of concrete and the required workability properties

thereof. This parameter is also considered by the modified A&A equation as a variation of the distribution modulus results both in variations of the paste content as well as the ratio of coarse to fine aggregates (cp. Section 4.2.3).

To investigate the effect of the distribution modulus q on the properties of EMC, concrete mixes with different distribution moduli q have been designed and tested on laboratory scale. Based on the data obtained from the concrete experiments, the relation between distribution modulus q and packing fraction PF^{den} is shown in Figure 4.10. The presented data clearly show that highest packing fractions have been achieved for a distribution modulus of $q = 0.35$. The same holds true for the compressive strength of hardened concrete. Here, mixes with a distribution modulus of $q = 0.35$ and high packing fractions achieved also higher compressive strength values than mixes with lower packing fractions caused by their lower distribution modulus or insufficient packing.

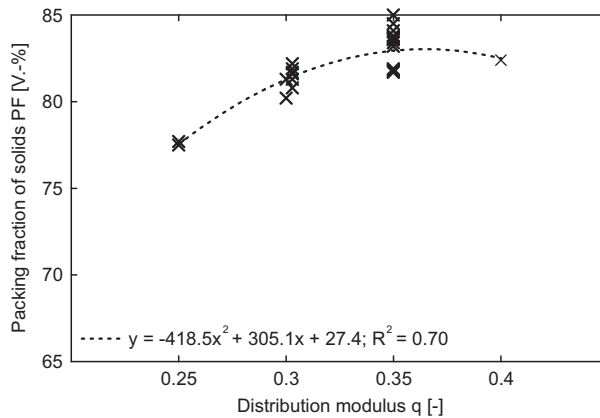


Figure 4.10: Influence of various distribution moduli q on the packing fraction.

Besides the use of appropriate distribution moduli for the composition of concrete aggregates, some further parameters are influencing the workability of the fresh concrete mix and will be partly influenced by the chosen distribution modulus. Based on the analysis of the experimental results, the following parameters are proposed for the design of workable EMC mixes:

- Distribution modulus q : 0.35 - 0.40
- Paste content: 225 - 250 dm^3
- w/p ratio: 0.30 - 0.35

The above mentioned characterization of EMC mixes is based on a maximum aggregate size of 16 mm and ignores the w/c ratio of the designed concrete. The classical definition of EMC, as used for example by Häring (2002), considers w/c ratios smaller than 0.40 as desirable for EMC. These low w/c ratios are achieved by traditional EMC mixes that are purely based on cement and characterized by low contents of filler materials. The compressive strength of these concretes is by far too high than actually necessary for concrete mass products like paving blocks so that the potential for cement replacement is given. The cement content of these mixes can be lowered by using inert or reactive filler materials. Part of the cement can be replaced by these materials to lower the compressive strength. Possible filler materials are industrial by-products, such as

fly ash, or fine stone waste materials generated in the natural stone industry. Decreasing cement contents and increasing amounts of filler materials, however, augments the difference between the w/c and the w/p ratio. Considering the workability of the concrete as a function of the w/p ratio, it is more appropriate for the concrete mix design to take the w/p ratio into account than the w/c ratio.

According to Powers and Brownyard (1947) as well as Locher (1976), an increase in the w/c ratio is resulting in higher capillary porosity. Caused by the remaining water content, capillary pores are formed and filled with hydration products in a progressed hydration state. As a result of increasing w/c ratios, also the capillary porosity of the cement stone is increasing, which makes the cement stone weak. Therefore, increasing w/c ratios result in decreasing compressive strength. This is not completely confirmed by the conducted experiments as a possible reduction in the compressive strength of the cement stone is compensated by a beneficial influence of an optimized and denser granular structure on the compressive strength.

It becomes clear that the absolute water content of the EMC mix is more relevant than the w/c . Nevertheless, the use of low w/c ratios is still important for the durability properties of the concrete as the capillary pores are influencing the impermeability as well as the durability of the hardened concrete. Therefore, a minimum of capillary pores is aimed at for a concrete that is considered as durable (Stark and Wicht, 2001). This fact should also be considered for the mix design of EMC and low w/c ratios should be therefore aimed on. Adding mixing water to the concrete is not the answer for decreased workability due to higher content of fine material.

The application of high contents of fine materials (e.g. stone waste materials) seems to be indeed hindering for this purpose as the water demand of the mix and therewith the w/c ratio is increasing with increasing amount of fine materials. Here, the use of plasticizers showed a positive effect. Due to the use of plasticizers, the workability of EMC mixes is improved for mixes containing high amounts of fine materials and low w/c ratios. Packing fractions between 84% and 85% have been achieved in the lab by using a paste content of 246 dm³ per m³ concrete with a w/p ratio of 0.33. These mixes resulted in 28 days compressive strength values between 95 and 100 N/mm². These high compressive strength values can be lowered by the use of filler materials. The application of alternative materials in EMC is discussed in detail in Chapter 5.

4.5 Conclusions

Based on the investigations presented in this chapter, the following conclusions can be drawn:

1. Particle packing influences the properties of concrete in fresh and hardened state. The workability of the fresh concrete is improved by an optimized grading of the composed concrete mix that follows a continuous grading curve for geometric packing. Higher packing fraction due to improved workability of the fresh concrete resulted in higher compressive strength of the hardened concrete.
2. Cement is used in a more efficient way when the grading of the composed concrete mix is optimized. The cement content of an EMC mix used for the production of concrete pipes was successfully lowered. The compressive strength of the concrete is not affected as long as the cement reduction is influencing the grading of the concrete mix in a negative way.
3. Higher compressive strength values are achieved for concrete mixes that have a dense granular structure. This allows for the partial replacement of cement by fine fillers.
4. The classical definition of EMC based on the w/c ratio mixes becomes questionable as the w/c ratio does not allow for the proper adjustment of the water content of EMC mixes that are low in their cement content due to the use of fine fillers. In this respect, the w/p ratio appears to be a more useful property.
5. The use of a plasticizer showed a positive effect on the workability of EMC mixes and helped to reduce the water content of mixes that make use of alternative fillers.

Utilization of alternative materials¹

5.1 Introduction

The production of sustainable concrete mixes requires a twofold approach in the design process. This twofold design approach is realized by i) the application of an appropriate mix design concept that allows for an integral consideration of the material properties in the concrete mix design and ii) the use of alternative materials that are characterized by their low environmental impact and that differ from classical raw materials with high CO₂ footprint. The beneficial influence of an integral mix design concept that considers the material properties of the raw materials in the mix design process is presented in Chapter 4. The cement content of EMC mixes is lowered by applying the ideas of optimized particle packing to concrete mix design and are, therefore, implemented in the new design concept. In this chapter, the application of different types of alternative materials and their influence on the concrete properties is discussed to facilitate the design of sustainable concrete mixes that are suitable for the production of concrete mass products.

In this respect, the term alternative materials refers to materials that differ from standard concrete ingredients like gravel, sand, and fillers. These standard ingredients are mainly produced for concrete production and referred to as primary raw materials. Alternative materials are generated by industrial processes where they are considered to be a waste material or industrial by-product. Many by-products, such as fly ash, blast-furnace slag or gypsum formed by flue gas desulfurization, are turned already into valuable products for building materials and are therefore considered as secondary raw materials or mineral admixtures.

The application of mineral admixtures is a commonly used practice for cement replacement in concrete technology. According to Mindess et al. (2003), these materials can be divided into i) pozzolanic materials, ii) cementitious materials, and iii) non-reactive or inert materials. The first two categories cover reactive materials that can be applied to interact chemically with the hydrating Portland cement. Fly ashes with their pozzolanic activity are routinely used in many types of concrete and their application and quality is regulated by standards (EN 206-1, EN 450-1, ASTM C311/C618, CSA A23.5, etc.). The utilization of blast furnace slags, classified as cementitious materials, is also commonly used practice in concrete technology. Here, blast furnace slags are primarily applied in blended cements. The application of slag blended cements and their requirements are also determined by standards (EN 206-1, EN 197, ASTM C595/C989, CSA A362, etc.).

Requirements on non-reactive filler materials are also specified by standards. These materials have either to fulfill the requirements on concrete aggregates (EN 12620, ASTM C 33, etc.) or their application is limited by design codes for concrete mixes regarding their maximum content (EN 206-1, CSA A23.1). These non-reactive fillers are intentionally produced for concrete production and considered as primary raw materials, but suitable materials are also generated in other industrial fields like mining or the natural stone industry. Here, high amounts of fine stone waste materials are generated during the production of dimensional stones by cutting or polishing processes. The production of broken aggregates for concrete or asphalt production also generates fine stone waste materials during the production process. Fines are generated by

¹Parts of this chapter were published elsewhere (Hüsken and Brouwers, 2008, 2009a).

the crushing of natural rock, the washing of aggregates, or collected as filter residue. The granulometric properties of these fines and their superior quality caused by the highly engineered production process turn these fines to a suitable material for replacing primary raw materials like cement or limestone powder.

Suitable alternative materials are not only produced as by-product of industrial processes, but also the recycling of construction materials attracts more and more attention with respect to the design of sustainable concrete. The demolition of existing buildings or structures generates a large amount of suitable materials that can be used for concrete production. The utilization of recycled concrete aggregates (RCA) in concrete production is a practiced concept for sustainable concrete. Up to 20% of natural aggregates can be replaced by crushed concrete aggregates > 4 mm without any negative effect on the concrete properties (Vázquez and Gonçalves, 2005). Larger amounts than 20% or the use of masonry rubble influence the mechanical properties and the durability of the produced concrete in a negative way. Here, the quality of the recycled material and the separation of the source material is important to guarantee constant material properties (Müller, 2003a). In this context, fractions < 4 mm are not used due to their high content of fines and the negative effects of sands generated from masonry rubble or RCA on the concrete properties.

The negative effects of RCA containing masonry rubble as reported by Poon and Chan (2006) originate from the low compressive strength of the crushed clay bricks and their high water absorption caused by the high open porosity of masonry rubble. These detrimental material properties lower the compressive strength of the produced concrete and its durability significantly. However, the fine fraction of RCA can have a beneficial influence on the hydration of the cement paste if the material is applied in low quantities. This beneficial effect is caused by the mineral composition of the fines and their related chemical reactivity. This chemical reactivity of the fines results from i) unhydrated cement particles in concretes having w/c ratios below 0.38 (Bentz and Conway, 2001), or ii) pozzolanic activity of the fines from masonry rubble utilized by fine grinding (Müller, 2003b). The utilization of the chemical reactivity of the fines opens new applications for heterogenous mixtures of recycled concrete fines (RCF) containing unhydrated cement and pozzolanic fines for cement replacement.

In the following, possible fields for the application of secondary raw materials generated during the production of broken aggregates, such as fine stone waste material, and the use of recycled concrete aggregates (RCA) and recycled concrete fines (RCF) are discussed in detail. The contribution of these alternative materials for producing sustainable concrete is evaluated. Furthermore, conclusions regarding the incorporation of alternative materials in the concrete mix design are drawn.

5.2 Stone waste materials

Stone powders, such as ground limestone, are used for the production of different types of concrete as filler material. Most of the energy of the production process of these materials is consumed by the grinding of the raw materials. Here, stone waste powders generated during the production of broken aggregates appear to be an appropriate replacement for inert fillers and cement as well. Therefore, the Premix 0-4, as characterized in Section 2.5.1, is primarily used in the following for the design of EMC mixes as cement replacement. The use of inert filler materials in EMC mixes is rather uncommon. However, positive effects on the packing of EMC mixes containing limestone powder have been reported by Bornemann (2005). Hence, the effectiveness of Premix 0-4 as filler material is also considered in the mix design as the material shows a wide grading combined with a substantial amount of fines smaller than 125 μm . Classical EMC mixes use low contents of fines and their workability properties are adjusted by the cement content as well as the amount of fine sand in the mix. This classical approach in the mix design of EMC results in low w/c ratios and high compressive strength values. Such high cement contents and compressive strength are not necessary for the production of concrete mass products that require

actually low mechanical resistance.

It was demonstrated in Section 4.4.3 that cement efficiency is enhanced when the grading of the composed EMC mix is optimized. This results in i) a reduction of the cement content as less cement is needed for obtaining the same compressive strength or ii) higher compressive strength values for identical cement contents. However, reducing the cement content in the designed concrete shows, at a certain extent, also a negative effect on the grading of the composed concrete mix as the necessary amount of fines is below the required limit for optimum grading. For this reason, the use of inert or reactive fines is required for the aimed optimization of EMC mixes regarding cement reduction. In this context, EMC mixes with varying cement contents were designed and first tested on mortar level. The designed mixes were further assessed by full scale concrete tests and the production of concrete paving blocks on a laboratory paving block machine using EMC mixes with high cement efficiency.

5.2.1 Mix design

Based on the results of the material characterization, particularly with respect to particle size distribution, four different EMC mixes were designed following the ideas of the new mix design concept as outlined in Chapter 4. The designed mixes are based on river gravel 8-16, broken granite 2-8, and premixed sand (Premix 0-4), containing both fine aggregate fraction and inert fines, in combination with varying cement contents. The PSDs of the applied materials are depicted in Figure 5.1 and it can be seen that the Premix 0-4 has a fines content (particles smaller than 125 μm) of about 11%. Further information on the Premix are given in Section 2.5.1. The paste content as well as the applied distribution modulus q were chosen according to the suggested parameters outlined in Section 4.4.4 for the design of EMC mixes. Considering a distribution modulus of $q = 0.35$ and a w/p ratio of 0.35, the necessary cement content amounts to 235 kg per m^3 concrete to follow the given target line (Eq. (3.9)) with lowest deviation.

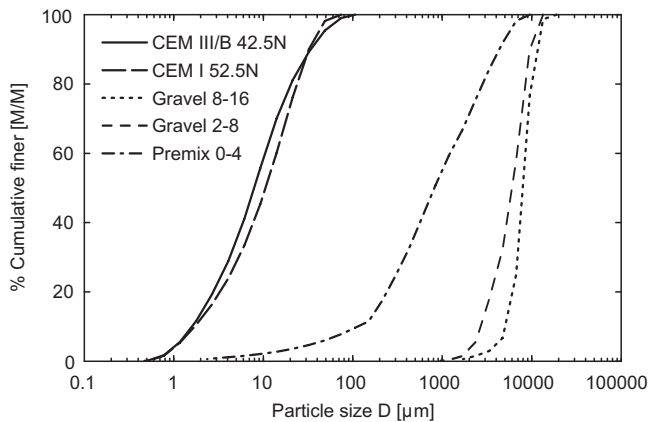


Figure 5.1: PSDs of the deployed materials used for the design of EMC mixes containing stone waste powders.

The cement content of the designed EMC mixes varies between 275 kg and 175 kg per m^3 concrete. A blend of 65% slag cement (CEM III/B 42.5 N LH/HS) and 35% Portland cement (CEM I 52.5 N) was used for mix C275, whereas 30% slag cement and 60% OPC were used for the blended cement of the mixes C250, C200, and C175 (Table 5.1). The volume difference caused

by the lower cement contents is compensated by higher contents of Premix 0-4 and coarse aggregate fraction. A possible influence on the packing and the PSDs of the designed EMC mixes due to slight variations in the mix proportioning, mainly caused by the difference in the cement contents, is considered to be negligible.

Owing to the high content of inert fines combined with low cement contents, the water content of the designed EMC mixes was adjusted by the w/p ratio. The w/p ratio of the mixes C275, C250, and C200 amounts to 0.33 and was increased to 0.35 for mix C175. These low w/p ratios resulted in w/c ratios between 0.47 and 0.62, which correspond to the low cement contents of the mixes. The resulting w/c ratios are higher than reported by Häring (2002). However, the use of a plasticizer was necessary to match the high packing fractions that are obtained on industrial scale. These high packing fractions of EMC mixes cannot be obtained with available compaction efforts under laboratory conditions without the use of plasticizers. The detailed mix proportioning of the designed EMC mixes are listed in Table 5.1 and the relevant mix parameters are depicted in Table 5.2.

Table 5.1: Mix proportioning of designed EMC mixes containing stone waste materials.

	C275		C250		C200		C175	
	[dm ³]	[kg]	[dm ³]	[kg]	[dm ³]	[kg]	[dm ³]	[kg]
CEM III/B 42.5 N	60.7	179.7	59.1	175.0	47.3	140.0	41.4	122.5
CEM I 52.5 N	31.1	95.3	24.5	75.0	19.6	60.0	17.1	52.5
Premix 0-4	370.8	982.0	390.6	1034.5	430.6	1140.3	446.7	1182.9
Granite 2-8	142.7	378.3	130.9	346.8	107.0	283.6	95.1	252.0
Gravel 8-16	216.8	574.5	223.3	591.8	236.4	626.6	241.1	638.8
Water	127.9	127.9	121.6	121.6	109.1	109.1	108.7	108.7
Air [‡]	48.2	—	48.1	—	48.3	—	48.3	—
Plasticizer	1.8	2.0	1.9	2.1	1.7	1.9	1.6	1.8
Total	1000.0	2339.7	1000.0	2346.8	1000.0	2361.5	1000.0	2359.2

[‡] estimated air content

Table 5.2: Characteristics of the designed EMC mixes containing stone waste materials.

	C275	C250	C200	C175
Distribution modulus q	0.35	0.35	0.35	0.35
w/c ratio	0.47	0.49	0.55	0.62
w/p ratio [#]	0.30	0.33	0.33	0.35
Fines [#] [kg/m ³]	389.5	368.5	330.6	310.5
Paste [#] [l/m ³]	253.3	249.9	225.3	218.4
Plasticizer dosage [‡] [M.-%]	0.73	0.84	0.95	1.03
Plasticizer dosage [#] [M.-%]	0.51	0.57	0.57	0.58

[#] based on fines smaller than 125 μm

[‡] based on cement content

The designed EMC mixes were tested first on mortar scale as mortars permit a quick and handy evaluation of preliminary mix designs. For conducting the tests on mortar scale, all ingredients smaller than 4 mm of the designed EMC mixes given in Table 5.1 have been used.

5.2.2 Mortar tests

The influence of varying cement contents on the mechanical properties of the designed EMC mixes listed in Table 5.1 was assessed first on mortar scale. It is assumed that variations in the cement content show a larger influence on mortar scale than on real concrete scale as the strength of the concrete is mainly influenced by the paste properties, and mortars are characterized by a high paste content. Therefore, the mortars of the designed EMC mixes were submitted to compressive as well as flexural strength. For testing the compressive strength, cubes of $50 \times 50 \times 50$ mm have been produced and tested after 3, 7 and 28 days. The development of the compressive strength is depicted in Figure 5.2 and the corresponding values are listed in Appendix E.3.

The compressive strength after 28 days of the mortar samples having a cement content of 275 kg and 250 kg is not influenced by the cement content of the designed mixes. Here, the mortar containing 250 kg cement achieves the same compressive strength after 28 days as the mortar that is based on 275 kg cement. The optimum cement content for lowest deviation between grading curve and grading of the composed EMC mix amounts to 235 kg per m^3 concrete. This optimum cement content results from the granulometric properties of the applied materials and the computed grading curve using Eq. (3.9) with a distribution modulus of $q = 0.35$ in the considered case.

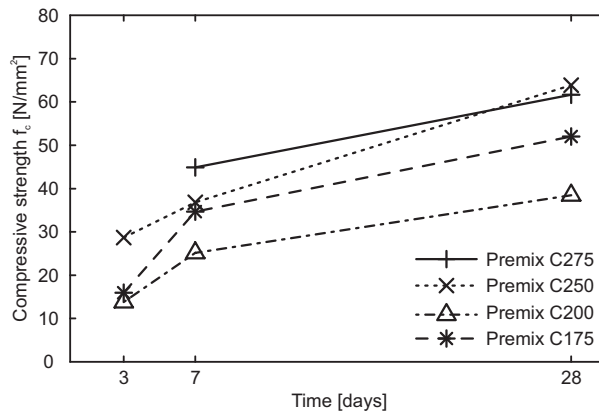


Figure 5.2: Compressive strength of tested mortar samples containing fine stone waste materials as cement replacement.

It appears that a reduction in the cement content is not influencing the compressive strength of the tested mortar samples significantly when the original cement content is already higher than actually needed for obtaining optimum packing. In this case, the actual surplus amount of cement acts as filling instead of a binding material. Reducing the cement content to a level that is below the required amount, necessary for optimum packing, shows a strong effect on the compressive strength. This further reduction in the cement content is influencing the packing fraction of the granular mix in a negative way and also the load bearing behavior of the granular structure

expressed by the compressive strength. This is indicated by the low compressive strength of mix C275.

Considering the mix proportioning of the designed mixes listed in Table 5.1, the w/p ratio is constant for the mixes C275, C250 and C200. The constant w/p ratio of these mixes resulted in comparable workability and similar compaction behavior (on this point, see also the mix characteristics listed in Table 5.1). However, the w/p ratio was increased from 0.33 to 0.35 for mix C175. This slight increase in the water content improved the workability properties of the mortar and resulted in a denser granular structure of the hardened mortar. Hence, the mortar that is based on a cement content of 175 kg achieved higher compressive strength than the mortar of mix C200. The presented results illustrate that cement can be used in a more efficient way when the packing of the granular materials is optimized. The dense granular structure, as a result of optimized particle packing, confirms again the assumptions presented in Section 3.3.2 on the positive influence of optimized particle packing on the concrete properties.

For determining the flexural strength, prisms of $40 \times 40 \times 160$ mm have been produced and tested after 3, 7 and 28 days. The development of the flexural strength is depicted in Figure 5.3 and the corresponding values are given in Appendix E.6.

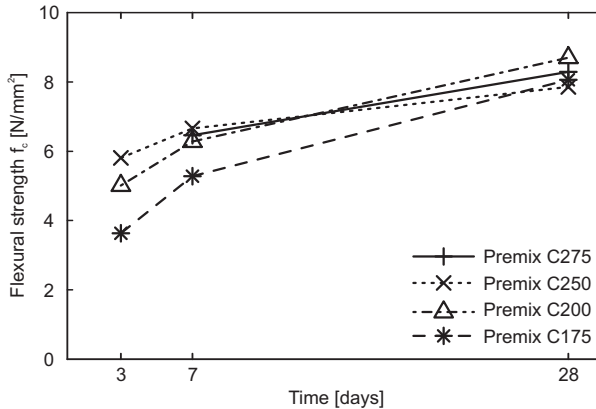


Figure 5.3: Flexural strength of tested mortar samples.

Significant variations in the development of the flexural strength with respect to the mortar composition are noticed up to 7 days. To illustrate the effect of cement reduction on the flexural strength after 28 days is hardly possible as the variation of the single measurements of one series is larger than the difference of the mean values of the tested mixes. Moreover, the Premix 0-4 and the granite 2-8 are broken materials with rough, textured surfaces. According to Mindess et al. (2003), this rough surface texture shows a positive effect on the mechanical bonding between paste and aggregates as the surface area available for bonding increases. This improved bonding results in higher flexural strength even for mixes having low cement contents and hampers therefore significant conclusions. The flexural strength is more crucial for products like concrete paving blocks that are made from EMC than the compressive strength. Furthermore, most of the tested mortar samples showed clearly split aggregates at the fracture surface of samples submitted to flexural strength. This fact is also confirmed by the split sample as depicted in Figure 5.4. All tested series using Premix 0-4 showed flexural strength values in the range between 7.9 N/mm^2 and 8.1 N/mm^2 after 28 days.

5.2.3 Concrete tests

Based on the results of the mortar tests, two of the designed EMC mixes listed in Table 5.1 were selected for further tests on concrete scale. Mix C275 was selected because of its mix characteristics that are comparable to the designed EMC mixes presented in Section 4.4.1. Consequently, mix C275 was tested on laboratory scale for its packing fraction PF according to Eq. (3.1) and submitted to compressive as well as splitting tensile strength. Mix C250 was selected for the production of concrete paving blocks using a laboratory paving block machine (Schauer & Haerberle, Laborpresse 917). Both mixes were tested on concrete scale including their coarse aggregate fractions according to the mix proportioning given in Table 5.1. The use of a plasticizing admixture was in this case not necessary as higher compaction efforts were obtained on the laboratory paving block machine.

The fresh and hardened concrete properties of mix C275 are presented in Table 5.3 and show a good agreement with the test results presented in Section 4.4.2 and 4.4.3, respectively, for EMC mixes containing a blend of slag cement and ordinary Portland cement. Mix C275 shows a packing fraction PF^{den} of 81.6%, which is in the same range as obtained for mix Blend 1 discussed in Section 4.4.1 (cp. Table E.9). This was expected as the mix characteristics, such as paste content and applied w/p ratio, are similar for both mixes and illustrate that the packing was not affected by the replacement of cement with stone waste powders.

Table 5.3: Test results of the designed EMC mix C275 (average values).

Measure	C275
Packing fraction PF [V.-%]	81.6
28 days Compressive strength f_c [N/mm ²]	56.2
Cement efficiency x_{cem} [N m ³ /kg mm ²]	0.204
28 days Splitting tensile strength $f_{ct,sp}$ [N/mm ²]	3.8

One of the main conclusions of Chapter 4 states that higher compressive strength is achieved when the packing of the aggregates is optimized. This increase in the cement efficiency allows for the partly replacement of cement to obtain mechanical strength as required for the aimed application. The cement content of mix C275 was reduced by 25% in comparison to the mix Blend 1 (cp. Table D.3). The reduction of the cement content resulted in lower compressive strength of the hardened concrete. The original compressive strength of mix Blend 1 amounts to 82.6 N/mm² and is considered to be excessive for the production of concrete paving blocks. Due to the lower cement content, the compressive strength of mix C275 amounts to 56.2 N/mm². In the same way, the splitting tensile strength of mix C275 is lower and amounts to 3.8 N/mm² instead of 4.9 N/mm² as determined for mix Blend 1.

According to Schießl and Müller (1997), the limit of the average compressive strength of concrete paving blocks amounts to 60 N/mm² as given by DIN 18501-1. This requirement on the compressive strength was used in the past as criterion for the production of concrete paving blocks suitable for the paving of traffic areas. The acceptance specification on the compressive strength was replaced by the introduction of the European standard EN 1338 in 2003 where the splitting tensile strength is used as criterion of the mechanical strength of concrete paving blocks.

Figure 5.4 shows as example the fracture surface obtained by the splitting tensile test of mix C275. The texture of the fracture surface shows clearly ruptured coarse aggregates. The rupture of coarse aggregates is a typical fracture mechanism of concretes with compressive strength higher than 50 N/mm² that are submitted to splitting tensile strength (König et al., 2008). Here,

the strength of the bond between coarse aggregates and hardened cement paste is larger than the tensile strength of the aggregates. This fact indicates that the compressive strength is sufficient in the considered case.

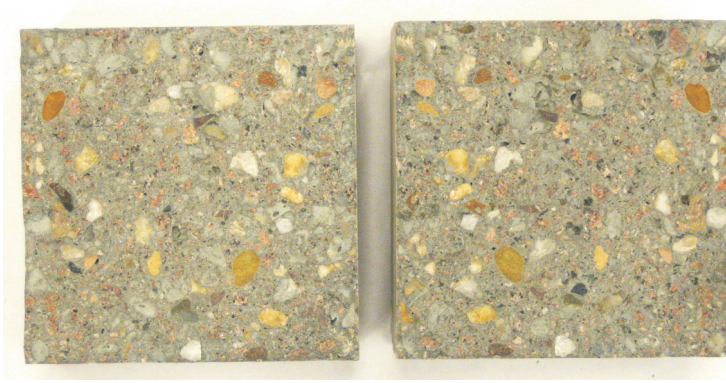


Figure 5.4: Example of the fracture surface of the splitting tensile test of mix C275.

Concrete paving blocks having a dimension of $200 \times 200 \times 80$ mm have been produced on a laboratory paving block machine to show the applicability of the Premix 0-4 for the production of concrete mass products. Mix C250 was used for the small scale production of concrete paving blocks as the compressive strength of this mix is comparable to mix C275, but contains less cement. The produced paving blocks were stored in plastic bags during the first day, and subsequently cured for 27 days under water. After 28 days, samples of $100 \times 200 \times 80$ mm were cut and tested for splitting tensile strength according to the EN 1338. The splitting tensile strength T of the tested samples follows from the height H and reads:

$$T = 0.637 \times k \times \frac{F_{max}}{a_{spl}H} \quad (5.1)$$

$$\text{with } k = \begin{cases} 1.3 - 30(0.18 - H/1000)^2 & \text{for } 40 \text{ mm} \leq H \leq 180 \text{ mm} \\ 1.3 & \text{for } H > 180 \text{ mm} \end{cases}$$

Furthermore, the breaking load F_{max} of the paving block has to be related to the length a_{spl} of the splitting area, the so-called length-related breaking load L_{spl} , via:

$$L_{spl} = \frac{F_{max}}{a_{spl}} \quad (5.2)$$

Besides the splitting tensile strength, the produced paving blocks have been tested for their water absorption as well as open porosity. The water absorption of the samples was determined according to the requirements described in EN 1338 on oven dry samples at the age of 28 days. First, the samples were stored at 105°C until constant mass in dry state was reached and subsequently submerged in water until the mass gain was constant. The water absorption calculates from Eq. (2.4) considering the mass M_{wet} of the partially saturated sample and the mass M_{dry} of

the oven dry sample. The water adsorption of two tested samples of the produced paving blocks is depicted over time in Figure 5.5 and the mean value is listed in Table 5.4 in comparison with the limit given by EN 1338. The open porosity φ_{open} of the produced concrete paving blocks is calculated according to Eq. (2.3) on samples at the age of 28 days. The measurement was carried out according to the procedure described in Section 2.2.2. The mean value of the open porosity φ_{open} is given in Table 5.4.

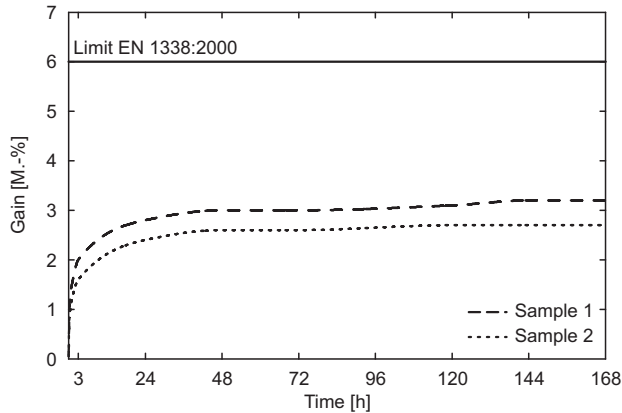


Figure 5.5: Water absorption of the produced paving blocks over time.

Table 5.4: Test results of the produced paving blocks and comparison with limits of the European standard EN 1338.

	Tensile splitting strength T	Breaking load L_{spl}	Water absorp- tion ψ_m	Density ρ_{con} (oven dry)	Open porosity φ_{open}
	[N/mm ²]	[N/mm]	[M.-%]	[g/cm ³]	[Vol.-%]
Average	6.4	839	3.0	2.48	7.5
Lowest single value	6.4	832	-	-	-
Standard deviation	0.06	6.77	-	-	-
COV	0.9	0.8	-	-	-
Limit EN 1338	Characteristic strength ≥ 3.6 ; lowest single value ≥ 2.9	≥ 250	not required for class A; avg. ≤ 6 for class B	not required	not required

The tested paving blocks fulfill the requirements on the splitting tensile strength as well as length-related breaking load as given by EN 1338. The average tensile splitting strength amounts to 6.4 N/mm^2 and is about two times higher than the required limit of 3.6 N/mm^2 . In the same way, the length-related breaking load exceeds the required limit by a factor of more than three

and offers the possibility for further cement reduction. The water absorption of the tested paving blocks is also in line with the requirements given by EN 1338 and indicates that the mix can be classified as durable since the water absorption is an indicator for the durability of the tested concrete blocks.

5.3 Recycled concrete fines

The successful application of inert fines in the form of stone waste materials as cement replacement was demonstrated in the previous section. Fine stone waste materials have been applied on laboratory scale for the production of concrete paving blocks that fulfill the requirements given by EN-1338. However, the applied stone waste material is considered to be an inert filler that replaces primary raw materials such as cement and limestone powder. As mentioned before, the application of mineral admixtures for cement replacement comprises also the use of materials that show cementitious or pozzolanic properties. In this respect, the use of recycled concrete fines (RCF) allows for the activation of unhydrated cement particles that are contained in the hardened cement paste of the old concrete.

Pozzolanic reactions of recycled materials can be activated by the fines of masonry rubble and can be enhanced to a further extent by the fine grading of masonry rubble to cement grain size. This processing is also discussed by Müller (2003b) for the production of reactive powders generated from masonry rubble. Within this approach, the pozzolanic reaction allows for the inclusion of additional constituents in the hydration process. These additional constituents are not contained in the cement and compensate therefore the theoretical dilution of the cement that is caused by the addition of RCF (Müller, 2003b). A further consideration for the application of RCF is given by Wassing (2002). Following this approach, small particles of the hardened cement paste of old concrete act as crystal nucleus for new phases that are formed during the early hydration period. It is also discussed by Wassing (2002) that the large specific surface area of RCF favors the dissolution of constituents of the old cement paste by the mixing water of the fresh concrete. This dissolution process can change the chemical conditions in the fresh concrete and can therefore also influence the hydration process and the strength development.

The generation of *pure* concrete rubble is quite difficult to realize when classical buildings and structures are demolished and can therefore only be obtained for materials that are generated from the demolishing of pure concrete structures such as concrete bridges, detachable precast concrete elements, etc. A mix of concrete and masonry rubble containing clay bricks, mineral bound bricks, mortar, and plaster is quite typical for recycled materials that are generated from demolished buildings. This mix of recycled materials contains fines both originating from the hardened cement paste as well as the masonry rubble that is partly contained in the building rubble and difficult to separate from the concrete. Two different powders that represent a mix of recycled materials have been selected for mortar tests on laboratory scale. The characteristics of the powders, RCF1 and RCF2, as well as their generation are explained in detail in Section 2.4. In the following section, the influence of the selected recycled concrete fines (RCF) on the development of the compressive strength is discussed.

5.3.1 Composition of tested mortars

The mix proportioning of the tested mortars follows the requirements given by the European standard EN 196-1 to account for constant test conditions. In this respect, the applied powders (cement, RCF, and quartz flour) have been selected in that way that the materials show comparable PSDs to minimize the effect of variations in the grading of the fines and resulting effects on the compressive strength. The PSDs of the applied materials are depicted in Figure 5.6.

Following the specifications given by EN 196-1, the strength development of the applied ordinary Portland cement with high early strength (CEM I 32.5 R) was determined. The strength properties of the applied OPC form the reference for further tests on cement replacement using RCF. For this purpose, part of the cement was replaced by mass by 10% and 20% of the recycled

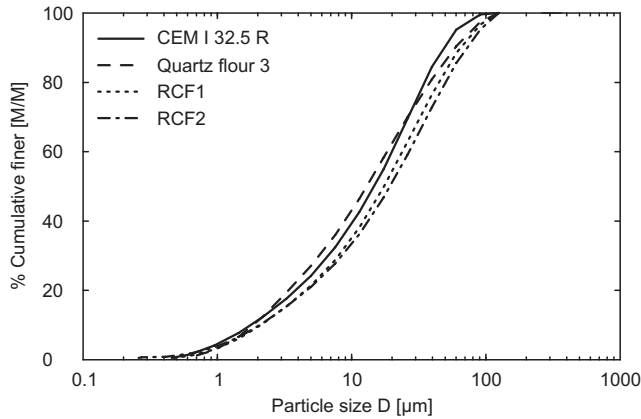


Figure 5.6: PSD of recycled concrete fines (RCF), quartz flour and cement used for mortar tests on cement replacement by recycled concrete fines.

concrete fines RCF1 and RCF2, respectively. To investigate the influence of both RCF on the development of the compressive strength, both materials, RCF1 and RCF2, have been substituted by an inert filler material (quartz flour 3) with similar PSD and comparable specific surface area to the applied cement (see Figure 5.6 and Appendix A.1). The mix proportioning of the tested mortars is given in detail in Table 5.5.

Table 5.5: Mix proportioning of tested mortars used for cement replacement by recycled concrete fines (RCF) and quartz flour.

Material	EN 196-1	10% RCF	20% RCF	10% Quartz	20% Quartz
	[g]	[g]	[g]	[g]	[g]
Norm sand	1350	1350	1350	1350	1350
CEM I 32.5 R	450	405	360	405	360
RCF	–	45	90	–	–
Quartz flour 3	–	–	–	45	90
Water	225	225	225	225	225

5.3.2 Mortar tests

Fresh mortar properties

The consistence of the fresh mortars was determined using the flow table test according to EN 1015-3. The data depicted in Figure 5.7 show a clear decrease in the consistence of the fresh mortars in dependence on the RCF content. The spread diameter after 15 strokes is reduced by 18% for both mortars containing RCF with a replacement ratio of 20% by mass. This decreased workability of the fresh mortars is related to the water absorption of the RCF as the powders were added in dry state. Similar observations are reported by Kerkhoff and Siebel (2002) for

crushed sand that was generated from recycled concrete aggregates and by Wassing (2002) for the application of recycled concrete fines.

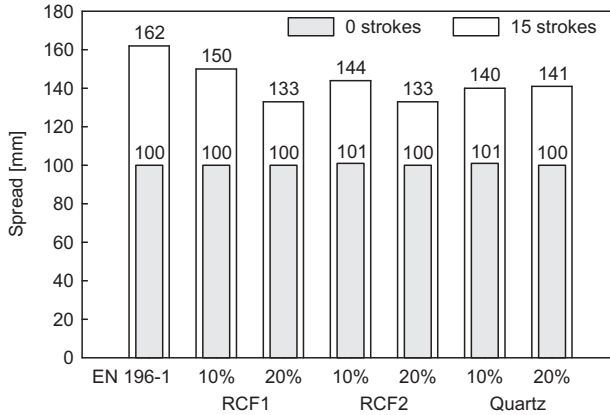


Figure 5.7: Consistency of fresh mortars containing recycled concrete fines (RCF) and quartz flour as cement replacement.

The processing of the RCF shows only an evident effect on the workability of the fresh mortars for a replacement ratio of 10% by mass. Here, the mortar containing fines extracted from the reprocessed material that was screened before the second crushing (RCF1) shows a better workability than the mortar containing fines extracted from the unscreened and crushed material (RCF2). This difference in the workability is also confirmed by the determined values of the water absorption as explained in Section 2.4.2. Here, the aggregate fraction 0.71-1.4 of the screened and reprocessed material RCA1 has a lower water content in saturated surface dry conditions than the unscreened and reprocessed material RCA2. The higher content of absorbed water in saturated surface dry condition leads to the conclusion that the higher porosity of the aggregate fraction of material RCA2 has also an effect on the sorption capacity of the fines of this material (RCF2) and decreases the workability of the fresh mortar. However, this trend is only valid for a replacement ratio of 10% by mass and does not hold for a replacement ratio of 20% by mass as the decrease in the workability is the same for both mortars at this higher replacement rate. A reduction of the spread diameter can also be noticed for both mortars containing quartz flour. In this case, the lower workability of the mortars is caused by the higher water demand of the quartz flour due to its higher specific surface area compared to the applied cement (see Appendix A.1). However, a direct relation between replacement ratio and spread diameter cannot be found in the considered case for the applied quartz flour.

Hardened mortar properties

Prisms having a dimension of $40 \times 40 \times 160$ mm were poured from the mortars listed in Table 5.5 and submitted to flexural and compressive strength after 3, 7 and 28 days. The prisms were covered with a plate of stainless steel and stored at 95% relative humidity during the first day, and subsequently cured under water until their test age. The results of the compressive strength test are discussed in the following only as the application of RCF showed a larger effect on the compressive than on the flexural strength of the tested samples. Detailed values of the compressive strength tests are given in Appendix E.4.

Figure 5.8a and Figure 5.8b illustrate the difference in the development of the compressive strength of the mortars containing RCF1 and RCF2 as cement replacement. Here, the mortars that contain RCF2 show generally the lowest strength after 28 days, whereas the strength of the RCF1 samples is comparable to samples made with quartz flour.

Based on the 28 days compressive strength values, it can be stated that both RCF and quartz flour reduced the compressive strength of the produced mortars depending on their replacement ratio and processing method. However, the compressive strength was reduced to the same extent for RCF1 and the applied quartz flour. Here, a replacement ratio of 10% by mass reduced the compressive strength by only 6% and resulted in a compressive strength of 47.4 N/mm² after 28 days for the material RCF1. This value is still sufficient to fulfill the specifications of the strength class 32.5 as required by the characteristic strength values of EN 197-1. In principle, the same classification is also possible for a replacement ratio of 20% by mass using material RCF1 with a compressive strength of 40.2 N/mm² after 28 days.

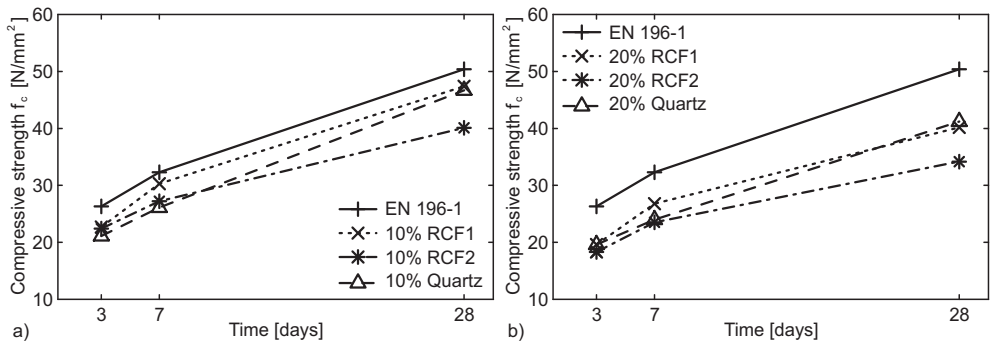


Figure 5.8: Compressive strength of tested mortar samples containing recycled concrete fines (RCF): a) comparison of the reference mortar (EN 196-1) and 10% cement replacement, and b) comparison of the reference mortar (EN 196-1) and 20% cement replacement.

The material RCF2 reduced the compressive strength after 28 days to a larger extent than the material RCF1. Consequently, the compressive strength of the produced mortars is below the values that were obtained for the comparable mortars containing quartz flour as cement replacement. However, this applies only for the compressive strength after 28 days and cannot be related to strength after 3 and 7 days. Here, the mortars containing RCF2 showed a similar mechanical performance as the mortars made with quartz flour. The large difference in the compressive strength after 28 days of mortars containing RCF and quartz flour cannot be explained by variations of the measurements and require a further analysis on microstructural level. Furthermore, the hardening time of 28 days proved to be insufficient to show pozzolanic effects on the compressive strength of the hardened mortars. However, it is questionable if the strengthening effect of the pozzolanic reaction can be verified by compressive strength tests after 91 days if the observed strength difference between 7 days and 28 days values is induced by constituents that have a deleterious effect on the hydration process. These deleterious effects have to be considered for RCF2 as the material was not screened before the second crushing.

Another interesting phenomenon can be observed for the compressive strength after 3 and 7 days. Here, the strength of the samples containing 10% RCF1 is higher than the strength of samples made with the same quantity of quartz flour (see Figure 5.8a). This fact indicates the

before mentioned influence of RCF on the early hydration process and the strength development. However, a clear explanation of the higher early strength values, due to possible dissolution processes or crystal nucleus enhancing the formation of new hydration phases as discussed by Wassing (2002), is not possible if only the values of the compressive strength are considered. These conclusions need further investigations on the development of the microstructure during the early hydration period. More detailed information on the influence of RCF on the microstructural development can be obtained by analyzing the pore water composition and determination of the phase composition of the hardened cement paste.

5.4 Recycled concrete aggregates

As mentioned before, the application of RCA containing masonry rubble in large quantities shows negative effects on the concrete properties. Therefore, many standards restrict the amount of masonry rubble in RCA used for concrete production (e.g. DIN 4226-100). However, the detrimental properties of masonry rubble that are known to affect the durability of concrete can turn into a valuable feature for special types of concrete if the material is used in low amounts. In this context, the high water absorption of crushed bricks and crushed recycled concrete sands has a beneficial effect when the material is considered as internal water source for shrinkage prevention. This aspect is addressed in the following section and the possible application in concrete mass products is illustrated. First, some general aspects related to the occurrence of shrinkage phenomena in concrete are discussed.

5.4.1 General aspects on the shrinkage of concrete

The hydration and hardening process of concrete is accompanied by volume changes. These volume changes are caused by chemical reactions, loss of water, changes in temperature, and applied external stresses (Mindess et al., 2003). In this respect, the volume change due to chemical reactions and the loss of water in the early age of the hardening concrete is the most critical one for standard concrete elements. This volume reduction is also referred to as shrinkage. Cracks and eigenstresses are caused as a result of the volume change and restraints of the concrete. These restraints can be of internal (e.g. reinforcement bars) or external nature (e.g. other concrete elements). The formed cracks allow deleterious substances, like chloride ions, to penetrate the concrete and the attack of reinforcement bars. Shrinkage cracks usually occur in the early age of the concrete as the increasing tensile stresses are not compensated by the concrete strength. Despite the formation of cracks, shrinkage can also cause the loss of initial stress in prestressed concrete elements.

Shrinkage is not only induced by chemical reactions or the loss of water, but also the heat release during the hydration process forms a source for volume changes in massive concrete elements. In general, shrinkage that is caused by a volume reduction resulting from chemical reactions or the loss of water can be subdivided into four categories:

Chemical shrinkage, or also referred to as hardening shrinkage, is induced by the volume difference between the unhydrated cement and water, and the volume of the hydration products. With proceeding hydration, the volume of the paste decreases as the volume of the reaction products is smaller than the total volume of the unhydrated cement and water at the initial situation. Chemical shrinkage is an intrinsic property of the hydration process and is often used as a method to evaluate the degree of cement hydration (Chen, 2007).

Plastic shrinkage is caused by the loss of water from the fresh concrete as a result of evaporation of water or suction of water from the concrete by formwork materials. According to Mindess et al. (2003), the evaporating water forms a complex series of menisci and is resulting in a negative capillary pressure that is causing the volume of the paste to contract. As the evaporation of water occurs only near to the surface of the concrete, differential volume changes are caused and the concrete starts to crack. This fact is also the reason

why plastic shrinkage occurs on horizontal surfaces of pavements and slabs where rapid evaporation is possible. Plastic shrinkage is a problem that is most prevalent for dry and windy conditions and can be prevented by appropriate curing conditions such as sealing and wetting.

Drying shrinkage is a phenomenon that occurs as a consequence of the loss of water from the hardened material. Drying shrinkage that is related to the first drying is irreversible, whereas later drying shrinkage can be compensated by rewetting and subsequent volume expansion (Mindess et al., 2003). Since the loss of water is the driving force of drying shrinkage, concrete elements having a large surface area, such as pavements and slabs, are affected. The placement of contraction joints in pavements and slabs prevents the formation of irregular, randomly distributed cracks due to drying shrinkage.

Autogenous shrinkage can be considered as a special case of chemical shrinkage that is induced by self-desiccation during the hydration process and the volume change of the hydration products (Kovler and Jensen, 2007), which are both not caused by external influences, such as loss or ingress of substances. In general, autogenous shrinkage is a phenomenon that occurs in concretes with low w/c ratios such as high-strength concrete (HSC) and ultra-high performance concrete (UHPC). In these types of concrete with a w/c ratio lower than 0.4, water is consumed during the proceeding hydration and a dense microstructure is obtained. However, the dense microstructure and the dense granular structure of HSC and UHPC due to optimized particle packing prevent the penetration of water from externally ponded surfaces. Hence, self-desiccation within the concrete occurs. If the remaining pores are not filled with water or hydration products, capillary forces are generated due to the formation of a complex series of menisci in the adsorption layer of the pore water. These capillary forces contract the solid walls of the pores and induce a volume reduction of the solid matrix (Chen, 2007). Since the aggregates in the concrete have a restraining function, micro-cracks are formed as a result of the self-desiccation. The addition of mineral admixtures with high fineness (e.g. silica fume) increases the autogenous shrinkage of concrete in the same way as the use of fine slags. In the latter case, shrinkage is caused by the large amount of CSH formed in the products and the refined pore structure (Chen, 2007).

In view of the aforementioned mechanisms, effective ways for lowering the shrinkage are given by reducing the chemical shrinkage (less cement will cause less chemical shrinkage), changes of the pore structure of the paste, decreasing the surface tension of the pore solution (Chen, 2007), or providing additional water for hydration. Conventional curing procedures, such as sealing by plastic sheeting or wetting by water ponding, water spraying or wet burlap, prevent or reduce the negative effects of plastic or drying shrinkage in standard concrete. However, the dense structure of HSC and UHPC limits the beneficial effect of conventional curing procedures to small cross sections or surface near areas. In view of these limitations, different strategies have been developed to mitigate the effect of autogenous shrinkage. The ideas for preventing autogenous shrinkage are mainly based on i) shrinkage compensating cements and admixtures, or ii) internal curing of the cement matrix.

The working principle of shrinkage compensating cements and admixtures is based on the idea to counteract the negative volume change of the shrinkage process by chemical reactions that exhibit expansive potential (Chen, 2007; Chen and Brouwers, 2009). The expansive potential is mainly activated by the formation of considerable quantities of ettringite during the first week of hydration (Mindess et al., 2003). These type of expansive agents are also referred to as 'ettringite-based' expansive cements. Different aluminate compounds are used to generate ettringite. Another type of expansive agents uses the formation of metal hydroxides and is therefore called 'hydroxide-based' expansive agents. According to Chen (2007), the reaction of quick lime and periclase shows expanding potential and can also be used to compensate autogenous

shrinkage in a beneficial way.

5.4.2 Mode of action of internal curing agents

The internal curing of HSC or UHPC having low w/c ratios is based on i) internal water curing when the curing agent is intended to delay or prevent the loss of water during the hydration process and/or ii) internal sealing when the curing agent performs as an internal water source. Internal water curing is preferable, since internal sealing is unable to prevent self-desiccation (Kovler and Jensen, 2007). Different types of materials can be used as internal water supply to overcome the effect of self-desiccation. Suitable materials that can introduce additional water to the cement matrix are:

Super-absorbent polymers (SAP) that absorb huge amounts of water during concrete mixing. The water is loosely bond by the SAP due to secondary chemical bonds. This loose binding allows that the water is released during the hydration process to prevent self-desiccation. According to (Kovler and Jensen, 2007), the theoretical maximum water absorption of SAP is around 5000 times their own mass and depends to a large extent on the absorbed liquid. Therefore, commercially available products show an absorbency around 20 g/g for cement paste pore fluid.

Since the concept of internal curing using SAP is analogous to air entrainment used for frost protection of concrete, it is also referred to as 'water entrainment' (Kovler and Jensen, 2007). Due to the fact that water is absorbed during the mixing process, additional mixing water has to be added. Mechtcherine et al. (2006) mentioned that the application of SAP shows a beneficial aspect on the autogenous shrinkage but the drying shrinkage increased. Furthermore, it is reported by Mechtcherine et al. (2006) that the strength of mixes containing SAP decreases as a result of the entrained pores that were initially filled with water. The introduction of these additional macro pores is in contrast to design concept of HSC and UHPC that is based on a dense microstructure due to optimized particle packing.

Light-weight aggregates having a high open porosity and added to the concrete in pre-saturated conditions. The theory behind this method consists in the idea that with proceeding hydration the extra water will be drawn from the 'larger' pores of the light-weight aggregates into the much smaller pores of the cement paste (Kovler and Jensen, 2007). This process diminishes the self-desiccation of the concrete and has also an effect on the hydration of the cement paste. Weber and Reinhardt (1997) observed that the mechanical properties of HSC containing pre-saturated light-weight aggregates improved. This effect is explained by Weber and Reinhardt (1997) by a decrease in the porosity of the cement paste. The lower porosity of the cement paste results in a more compact structure that explains the higher strength.

Recycled concrete aggregates that are characterized by their high water absorption. The working principle of RCA is analogous to pre-saturated light-weight aggregates. Maruyama and Sato (2005) illustrate that autogenous shrinkage at early ages is reduced in concrete containing RCA. Furthermore, lower shrinkage induced stresses in the reinforcement bars of concrete beams are reported by Maruyama and Sato (2005). These lower stresses are caused by a lower Young's modulus and the larger creep strain of concrete containing RCA.

The application of pre-saturated aggregates for internal water curing depends on a number of influencing factors. The main influence on the efficiency of the curing process is determined by the pore size distribution of the aggregates. As mentioned before, the water moves only from a coarse to a finer pore structure and may not migrate readily into the surrounding cement paste if the pore structure is too small (Zhutovsky et al., 2002). Kovler and Jensen (2007) mention a pore size of 100 nm to be the lower limit for effective water transport within the matrix.

Besides the pore size distribution, the spacing between the aggregates is influencing the availability of the internal curing water. The distance between the pre-saturated aggregates should not be too large so that water contained in the pre-saturated aggregates can access the surrounding cement paste in reasonable time (Zhutovsky et al., 2002). This means for practical applications that the grain size of the pre-saturated aggregates should not exceed a certain size to minimize the spacing between the aggregates. Furthermore, smaller aggregates fractions are denser distributed over the cement matrix than coarser ones of the same volume. This effect was also considered by the mix design of the mortars used for the shrinkage tests explained in the following. Here, recycled concrete aggregates of the fraction 0.71-1.4 are used for replacing parts of the original sand fraction in the designed HSC.

However, the pore size distribution in coarser aggregates seems to be more favorable for internal curing than their negative effect on the spacing ratio (Zhutovsky et al., 2002). In the case of light-weight aggregates, the diffusivity of the water to the surrounding cement paste is favored by the larger pores of the coarser aggregates.

5.4.3 Composition of tested mortars

The mix design of the used reference mix for conducting the shrinkage tests aims on a HSC that is favorable for autogenous shrinkage with high shrinkage values. For this purpose, the mix design tool as discussed in Chapter 4 is used for the design of a HSC. The designed reference mix is composed of an ordinary Portland cement (CEM I 52.5 N), fly ash, micro silica, and sand 0-4. A mix with a high content of fines (cement, fly ash, and micro silica) combined with a low w/p ratio of 0.24 was aimed to favor the conditions of autogenous shrinkage. The w/c ratio of the mix was kept below 0.4 to facilitate the self-desiccation of the paste. The maximum grain size of the reference mix was limited to 4 mm to obtain high strength and to minimize negative effects of bigger aggregates on the compressive strength.

The designed reference mix is based on the ideas of optimized particle packing as explained in Chapter 3. These ideas imply the composition of an continuously graded granular mix with optimized PSD ranging from the micro to the macro range. Table 5.6 gives the mix proportioning of the designed reference mix and its mix characteristics is listed in Table 5.7.

Table 5.6: Mix design of mortars used for shrinkage tests (dosage for 1 m³ concrete).

Material	Reference mix		10% RCA1 [‡]		20% RCA1 [‡]	
	[dm ³]	[kg]	[dm ³]	[kg]	[dm ³]	[kg]
CEM I 52.5 N	163.2	500.0	163.2	500.0	163.2	500.0
Fly ash	74.2	164.2	74.2	164.2	74.2	164.2
Micro silica	37.4	87.2	37.4	87.2	37.4	87.2
Sand 0-4	499.0	1318.4	449.1	1186.5	399.2	1054.7
RCA 0.71-1.4	—	—	49.9	131.8	99.8	263.6
Water	180.0	180.0	180.0	180.0	180.0	180.0
Air [‡]	30.0	—	30.0	—	30.0	—
Plasticizer	16.2	17.8	16.2	17.8	16.2	17.8
Total	1000.0	2267.5	1000.0	2267.5	1000.0	2267.5

[‡] based on oven dry condition (OD)

[‡] estimated air content

Table 5.7: Characteristics of the designed HSC mixes containing recycled aggregates.

	Reference mix	10% RCA1 [‡]	20% RCA1 [‡]
Distribution modulus q	0.22	0.22	0.22
Effective w/c ratio	0.36	0.36	0.36
Total w/c ratio	0.36		
w/p ratio [#]	0.24	0.24	0.24
Fines [#] [kg/m ³]	752.6	752.6	752.6
Paste [#] [l/m ³]	455.2	455.2	455.2
Plasticizer dosage [‡] [M.-%]	3.7	3.7	3.7
Plasticizer dosage [#] [M.-%]	2.4	2.4	2.4

[‡] based on pre-saturated aggregates

[#] based on fines smaller than 125 μm

[‡] based on cement content

A part of the original sand fraction was replaced by RCA1 of the fraction 0.71-1.4 as described in Section 2.4 to investigate the effect of internal curing on the autogenous shrinkage of the reference mix. The sand replacement rates amount to 10% and 20% (cp. Table 5.6). The RCA have been applied in different conditions regarding their moisture content. These conditions form the basis for the further analysis of the shrinkage measurements and are as follows:

Oven dry (OD): stored at 105 °C until constant mass, without additional mixing water.

Saturated surface dry (SSD): pre-saturated for 24 hours considering a moisture content of 4.9 M.-% of the RCA fraction as reported in Section 2.4.2.

Oven dry with additional mixing water (ODW): stored at 105 °C until constant mass, additional mixing water was added considering the water absorption given in Section 2.4.2.

5.4.4 Mortar tests

Besides the shrinkage tests that are discussed in Section 5.4.5, the designed mixes have been tested in fresh and hardened state to determine their properties. As the mixes are composed of materials with maximum aggregate size of 4 mm, the mixes were tested on mortar scale.

Fresh mortar properties

The fresh mortar properties were determined by means of the spread flow test using the Hagermann cone as described in EN 1015-3. The data depicted in Figure 5.9 show that with increasing RCA content the workability of the mixtures decreases. This fact holds both for oven dry condition (OD) and saturated surface dry condition (SSD). The lowest spread flow was obtained for the mortar containing 20% by mass of oven dry RCA. Here, parts of the mixing water are absorbed by the oven dry aggregates and the water is therefore not available to act as a lubricating layer around the particles. This negative effect on the workability is inhibited when the RCA is added in saturated surface dry conditions or additional mixing water is added to the mix in order to compensate the water absorption of the RCA.

Although the aggregates have been added in saturated surface dry conditions, the workability of the produced mortars was affected and the spread flow of the tested mortars decreased with increasing RCA content (cp. Figure 5.9). In this case, the compensation of the water absorption by additional mixing water showed a better effect on the workability of the produced mortars than using saturated surface dry aggregates. However, the mortar containing 20% by mass of oven dry RCA and additional mixing water shows a lower workability than the tested reference

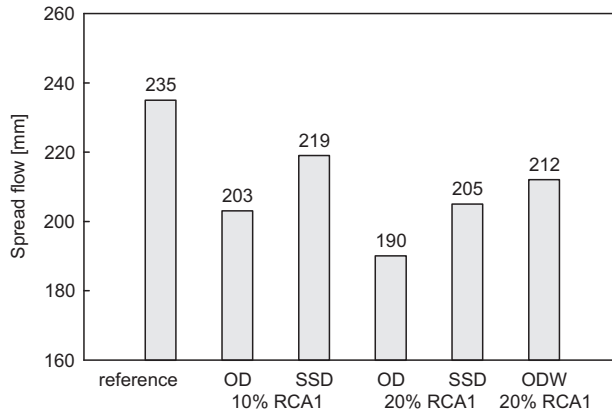


Figure 5.9: Spread flow values of designed reference mix and mortars containing recycled concrete aggregates (RCA) in varying quantities and conditions.

mix. It is assumed that the PSD of the designed mortar is influenced in a negative way by the RCA replacement. Here, replacing 20% by mass of the original sand fraction by RCA has a noticeable effect on the PSD of the designed mortar which also effects the workability of the produced mortars.

Mechanical properties

The mechanical properties of the designed mixes were evaluated by means of compressive and flexural strength. Cubes of $50 \times 50 \times 50$ mm have been produced and submitted to compressive strength. Furthermore, prisms of the dimension $40 \times 40 \times 160$ mm have been produced and submitted to flexural and compressive strength. The samples containing RCA have been produced with aggregates in saturated surface dry condition (SSD). All samples have been stored at 95% relative humidity for the first day and subsequently cured underwater until their test age (3, 7, and 28 days) was reached. Figure 5.10a depicts the strength development determined on cubes having a side length of 50 mm.

The values of the 28 days compressive strength show clearly that with increasing RCA content the strength decreases (see Figure 5.10a). This negative effect of RCA on the compressive strength of concrete is also reported by Maruyama and Sato (2005) and is likewise known for the application of light-weight aggregates in high-strength concrete. A reduction of the compressive strength of about 10% at the age of 7 days is reported by Bentur et al. (2001) for concrete in which 25% of the normal aggregates was replaced by light-weight aggregates. In the considered case, the compressive strength at the age of 28 days was reduced by 10% for the mix with 20% sand replacement by RCA and is in good agreement with the data given by Bentur et al. (2001).

The results of the compressive strength tests that were carried out on cross sections of 40×40 mm, obtained from the previously performed bending tests, show a similar trend in the strength development than the results obtained on cubes with a side length of 50 mm (see Figure 5.10a). Here, the compressive strength was reduced by 7% for the mix containing 20% RCA, whereas the mix containing 10% RCA showed slightly higher compressive strength than the reference mix. Detailed values of the performed compressive strength tests can be found in Appendix E.5.

The flexural strength of the tested samples was also affected by adding RCA to the mix. A

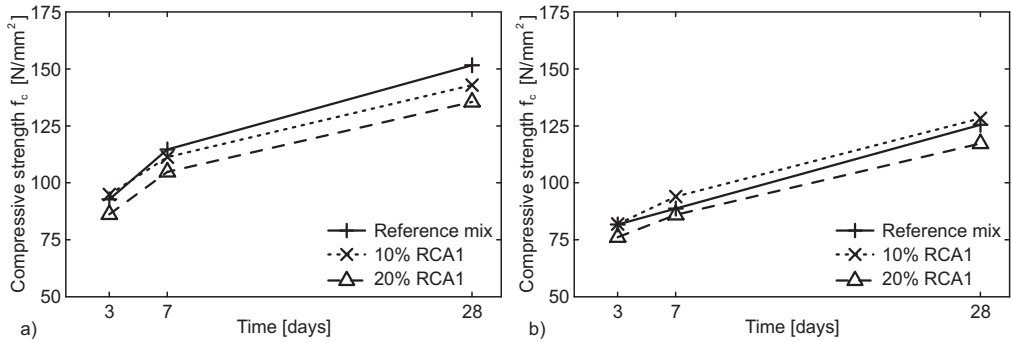


Figure 5.10: Compressive strength of tested mortar samples containing recycled concrete aggregates (RCA): a) values determined on cubes of $50 \times 50 \times 50$ mm, and b) values determined on cross sections of 40×40 mm that were obtained from the previously performed bending tests).

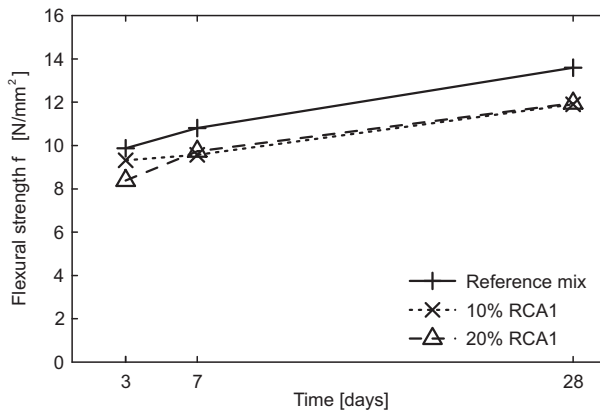


Figure 5.11: Flexural strength of tested mortar samples containing recycled concrete aggregates (RCA) for internal curing.

dependence on the replacement rate of RCA is not noticeable as the flexural strength is reduced by about 14% for both mixes containing 10% and 20% RCA, respectively. Detailed values of the performed flexural strength tests are given in Appendix E.7.

5.4.5 Shrinkage tests

The shrinkage measurements were performed on prisms with a dimension of $40 \times 40 \times 160$ mm according to the specifications given in DIN 52450. Measuring taps Type 1 have been inserted into the molds before casting the samples. The cast samples have been stored in a humid cabinet at 95% relative humidity and 21 °C for 17 hours. After hardening in the humid cabinet, the samples were stripped from the mold and the specimens used for determining autogenous shrinkage

were immediately wrapped to minimize their moisture loss. Aluminum adhesive tape and PE-foil were used to wrap the samples as depicted in Figure 5.12. Subsequently, the first shrinkage measurements were conducted directly after stripping the samples from the mold and before the samples were submitted to their final storage conditions. This first measurement reflects the zero point for all curing conditions.

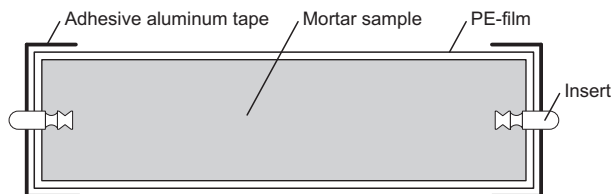


Figure 5.12: Schematic illustration of wrapped specimen used for autogenous shrinkage test.

The sealed samples were stored at 21 °C in the lab, whereas the samples used for determining the sum of autogenous and drying shrinkage were stored in a climate chamber at 45% relative humidity and 21 °C over a saturated solution of potassium carbonate (K_2CO_3) as prescribed by DIN 52450. Additionally, unsealed samples were cured underwater at 20 °C to determine the effect of possible moisture expansion. The moisture loss of the unsealed samples stored in the climate chamber was recorded by weighing the samples parallel to the performed shrinkage measurements. Similarly, the mass of the sealed samples was recorded to verify that no water loss is caused by a possible leakage of the sealing. The first shrinkage measurement was conducted 17 hours after adding the mixing water and was followed by the second measurement that took place 24 hours after adding the mixing water. Further shrinkage measurements were performed over a period of 28 days every 24 hours. Detailed values of the shrinkage measurements are given in Appendix E.8 for measurements after 1, 7, and 28 days. The results of the shrinkage measurements show the typical behavior for autogenous shrinkage, drying shrinkage, and moisture expansion. Depending on the moisture condition of the RCA, differences in the shrinkage behavior can be observed.

Oven dry condition (OD)

The autogenous shrinkage of the designed reference mortar was reduced only slightly by the applied RCA in oven dry condition (see Figure 5.13). However, other relevant phenomena related to the application of RCA became obvious. The values of the autogenous shrinkage measured for samples containing RCA (OD) are higher in the beginning of the measurements (period up to 14 days) than the values measured for the reference mortar.

A contrary behavior was observed at the end of the shrinkage measurements after 28 days. Here, samples containing RCA show less autogenous shrinkage than the reference mortar – although the autogenous shrinkage was not reduced to a noteworthy extent. The difference in the autogenous shrinkage behavior of the RCA and reference mortars is related to the water absorption of the oven dry aggregates. This water absorption of the aggregates reduces the mixing water and favors the self-desiccation of the cement paste.

The application of RCA influences not only the autogenous shrinkage, but also the total shrinkage (sum of autogenous shrinkage and drying shrinkage) as well as moisture expansion are effected. The total shrinkage increased by about 8% for RCA samples with a replacement ratio of 20% by mass. The RCA samples that were stored underwater showed a higher water expansion than the samples of the reference mortars.

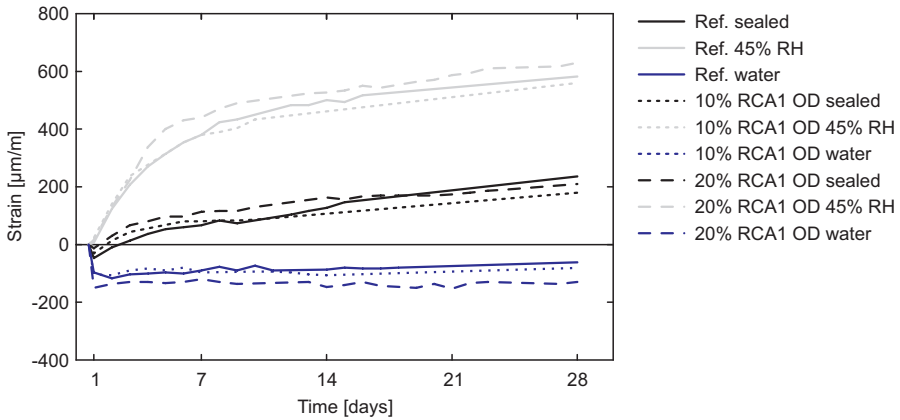


Figure 5.13: Results of shrinkage measurements on the designed reference mortar and mortars containing recycled concrete aggregates (RCA) in oven dry condition (OD).

Saturated surface dry condition (SSD)

Similar to the results obtained for RCA in oven dry condition, the autogenous shrinkage was not reduced significantly by the RCA in saturated surface dry condition as depicted in Figure 5.14, and the higher autogenous shrinkage due to water absorption in the beginning was avoided by the pre-saturation of the RCA.

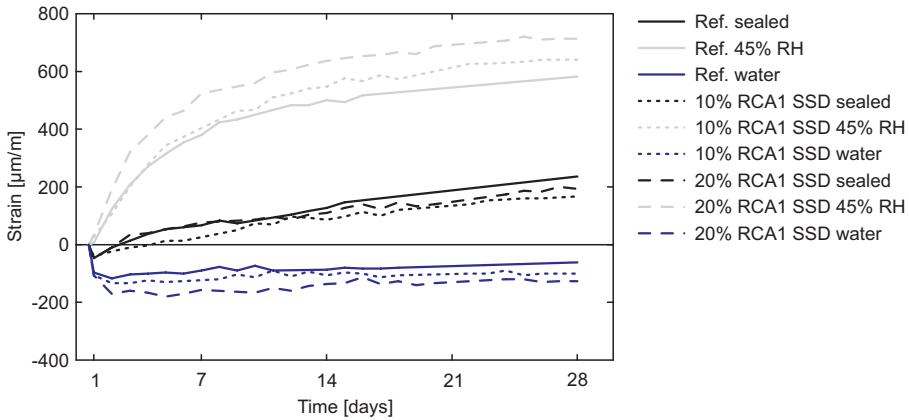


Figure 5.14: Results of shrinkage measurements on the designed reference mortar and mortars containing pre-saturated recycled concrete aggregates (RCA) in saturated surface dry condition (SSD).

However, the pre-saturation of the RCA increased the total shrinkage to a remarkable extent

(see Figure 5.14 and Figure 5.15). The difference is linear and amounts to about 10% for a replacement ratio of 10% by mass and to 22% for a replacement ratio of 20% by mass. This difference of the total shrinkage of RCA samples and reference mortar is lower than reported by Kerkhoff and Siebel (2002). According to the data given by Kerkhoff and Siebel (2002), the total shrinkage increased between 75% and 125% for the use of crushed recycled concrete sands. The higher total shrinkage of the RCA samples is caused by two different factors.

First, RCA have a lower Young's modulus than natural aggregates and show therefore a lower resistance against volume changes of the cement paste (Kerkhoff and Siebel, 2002; Maruyama and Sato, 2005). Secondly, the cement paste that is contained in the RCF fraction is exposed to drying shrinkage as well. The pre-saturation of the RCA causes an expansion of the dry aggregates as consequence of the rewetting. The swelling due to rewetting is referred by Mindess et al. (2003) as reversible part of the drying shrinkage and contributes to the total shrinkage of the samples containing RCA. These two factors, lower Young's modulus and swelling due to rewetting, double the influence of pre-saturated RCA on the total shrinkage. The moisture expansion of the samples containing RCA in saturated surface dry condition is at the same level as obtained for oven dry RCA.

Oven dry condition with additional mixing water (ODW)

The use of RCA in combination with additional mixing water for compensating the water absorption of the aggregates resulted in a better workability of the mortars, but showed no remarkable effects on the autogenous shrinkage of the produced samples. Compared to RCA added in oven dry condition, the higher autogenous shrinkage values in the beginning were avoided by adding extra mixing water, but the autogenous shrinkage after 28 days is at the same level as obtained for RCA in saturated surface dry condition. The same facts holds for drying shrinkage and moisture expansion.

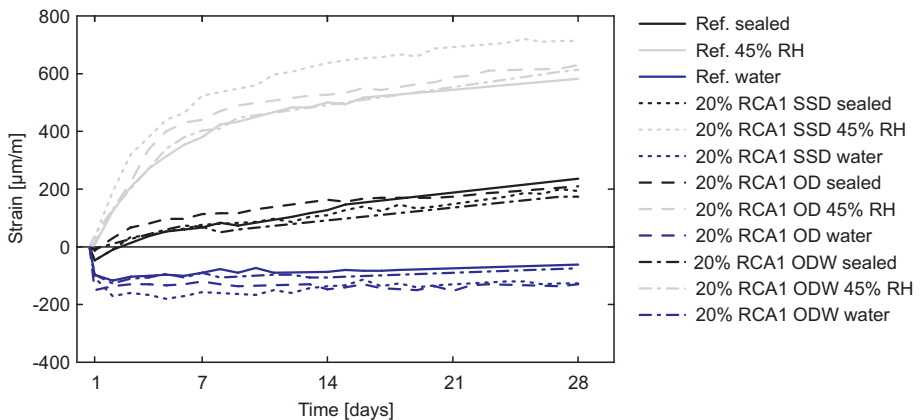


Figure 5.15: Results of shrinkage measurements on the designed reference mortar and mortars containing recycled concrete aggregates (RCA) with a replacement ratio of 20% by mass and varying moisture conditions.

5.5 Conclusions

The application of alternative materials in concrete mixes suitable for the production of concrete mass products is presented in this chapter. Based on the experimental investigations and the obtained results, the following conclusions can be drawn:

1. The application of stone waste materials in EMC mixes offers possibilities for the replacement of reactive or non-reactive primary raw materials. In the considered case, a premixed and unwashed aggregate, called Premix 0-4, was successfully applied in EMC suitable for the production of concrete paving blocks.
2. The high content of fines smaller than 125 μm present in Premix 0-4 (percentage of particles smaller than 125 μm amounts to 11% by mass, see Figure 2.4) allows for a reduction in the cement content. Applying Premix 0-4, the cement content was reduced without negative effects on the PSD of the designed concrete mix since a suitable filler material was provided.
3. Concrete paving blocks with a cement content of 250 kg per m^3 have been produced and tested according to the requirements specified by EN 1338. The produced paving blocks fulfill the limiting values given by EN 1338 on mechanical strength and water absorption.
4. Recycled concrete fines (RCF) have been applied in mortar systems as cement replacement to reduce the environmental load. The mechanical properties and the workability of the produced mortars containing RCF were reduced depending on the replacement rate and processing method of the recycled material.
5. RCF with a low content of masonry rubble reduced the compressive strength and the workability of the produced mortars to a lower extent than RCF with a high content of masonry rubble at the same replacement ratio.
6. The compressive strength of mortars containing RCF with a low content of masonry rubble was reduced to the same extent as for mortars with an inert filler material (quartz flour) in comparable quantities.
7. The pozzolanic properties of RCF having a higher content of masonry rubble could not be activated till the test age at 28 days. A longer hardening period is required to account for the pozzolanic effect of the masonry fines as the pozzolanic reaction proceeds slowly and noticeable effects on the compressive strength become obvious not until 28 days. However, the mortars with a higher fines content of masonry rubble obtained after 28 days lower compressive strength than the comparable mortars with quartz flour.
8. The application of RCF with a low content of masonry rubble showed a beneficial effect on the strength development during the early hydration period. The compressive strength after 3 and 7 days for mortars with RCF having a low content of masonry rubble was higher than for mortar using quartz flour as cement replacement.
9. Recycled aggregates (RCA) have been applied in high-strength mortars to reduce the effect of autogenous shrinkage by internal curing. The retained water of the pre-saturated RCA was not sufficient to prevent autogenous shrinkage, but it reduced its magnitude slightly.
10. The total shrinkage of samples with pre-saturated RCA was higher than the total shrinkage of the produced reference mortar. This demonstrates that the drying shrinkage of concrete containing RCA is higher due to the swelling of RCA during the rewetting process. This swelling of the aggregates is a reversible process that contributes to the total drying shrinkage when the hardened concrete loses water again.
11. The compressive strength of the produced mortars containing RCA was reduced to same extent as reported in literature for the application of light-weight aggregates (Bentur et al., 2001).

Early-age behavior of earth-moist concrete¹

6.1 Introduction

The so-called green-strength of earth-moist concrete in the early age is caused by the internal friction of the fresh concrete and the formation of interparticle forces between the fine particles. The formed interparticle forces are characterized by their different working mechanisms and influence the properties of the dry or wet concrete mix in different ways. The prevailing forces are electrostatic forces, van der Waals forces, and capillary forces due to the formation of liquid bridges. An overview on the magnitude of the particular forces on spherical particles in dependence of the particle diameter is given in Figure 6.1. From this it follows that the influence of the interparticle forces is strongly depending on the mode of action and the particle size as with increasing particle diameter the weight of the particles preponderate the effect of interparticle forces. This effect is caused by the fact that the weight of the particles increases by the third power of the particle diameter, whereas the interparticle forces show a linear dependency on the particle diameter in most cases (Israelachvili, 1991). Therefore, the influence of interparticle forces is solely predominant for spherical particles having a diameter smaller than 100 μm .

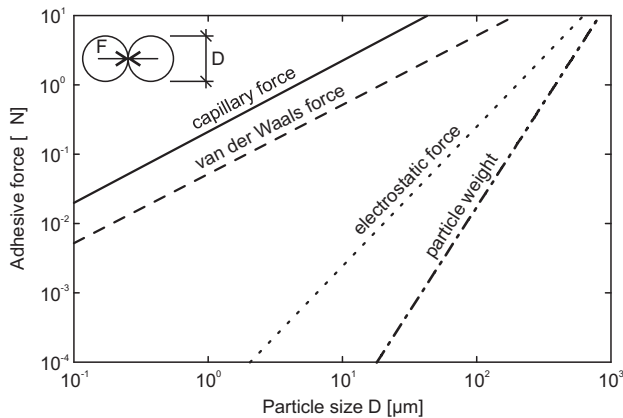


Figure 6.1: Interparticle forces of spherical particles and particle weight in dependence of the particle diameter.

Besides the particle diameter, the distance between the particles effects the strength of the interparticle forces as shown in Figure 6.2. However, the distance between particles cannot become

¹Parts of this chapter were published elsewhere (Hüsken and Brouwers, 2009b).

zero as the Born repulsion causes a minimal particle distance. The minimal distance is given by Krupp (1967) to be 4 \AA for colloidal particles in vacuum and is depicted in Figure 6.2 as well.

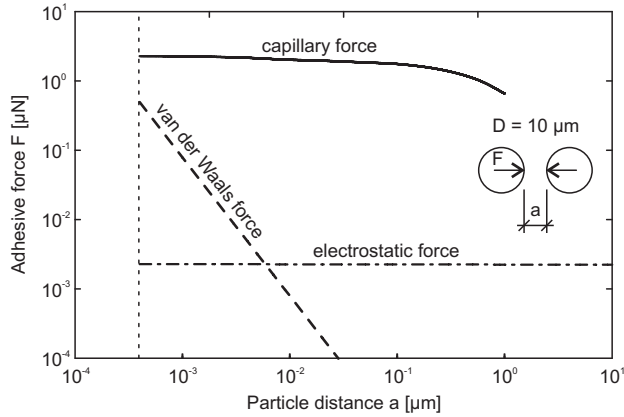


Figure 6.2: Interparticle forces of spherical particles in dependence of the particle distance.

In this chapter, the basic mechanism of interparticle forces are discussed and their influence on the early-age behavior of EMC, especially on the compaction behavior and the green-strength, is addressed. Here, the significant influence of adhesive forces due to the formation of liquid bridges is pointed out and discussed in detail. Influencing factors, such as particle size, particle size distribution, surface tension of the wetting liquid, and degree of saturation, are discussed in detail.

6.2 Interparticle forces

The effect of interparticle forces between dry particles is of minor interest for the green-strength of EMC as the order of magnitude of these forces is much lower than for forces caused by the formation of liquid bridges. However, the formation of interparticle forces between dry particles, especially for powders having a high fineness, cause the tendency of fine powders to agglomerate. These agglomerates affect the mixing behavior and inhibit a heterogeneous and complete dispersion of the fines within the concrete mix, which is resulting in an inefficient use of the possible potential of the fines and the water tied up in the formed agglomerates. Although the contribution of interparticle forces to the green-strength of EMC is negligible, the basic principles behind these forces are important for the right application of modern concrete admixtures to avoid the formation of agglomerates.

6.2.1 Electrostatic forces

Fine particles are usually not charged as they appear to be neutral. However, an electrostatic charge of the particles can be caused by an electron transfer due to particle collisions during milling processes or can be induced by particle friction. The generated electrostatic charge of the particles can either result in adhesive or repelling forces depending on the particle charge. Although electrostatic forces are considered to be long-range forces, they do not show such a strong effect on surrounding particles as the van der Waals forces whose order of magnitude is much higher (see Figure 6.1). Therefore, electrostatic forces cannot be considered to show a remarkable effect on the green-strength of EMC in its early age.

The resulting adhesive electrostatic forces due to opposing charges of fine particles, regardless the fact if cement particles or other fine particles of mineral origin are involved, cause the behavior of the fine particle to flocculate when water is added. The formed agglomerates contain a considerable amount of water both within the agglomerates and on the surface. This amount of water is not available for further lubrication of the fine particles and the workability is reduced by an increase of the viscosity of the paste. The electrostatic force between two spherical isolators can be computed according to Stieß (2008) as follows:

$$F_{ele} = \frac{\pi \psi^2 D^2}{4 \epsilon_0 \epsilon_r \left(1 + \frac{a}{D}\right)} \quad (6.1)$$

For illustrating the influence of the particle diameter D as well as the particle distance a in Figure 6.1 and Figure 6.2, respectively, the relative static permittivity ϵ_r amounts to 1 (vacuum), the electric surface charge density ψ is approximated to be $100 \text{ e}/\mu\text{m}^2$ and ϵ_0 represents the electric constant.

6.2.2 Van der Waals forces

Van der Waals forces are of crucial importance in the field of particle technology as they are constantly acting forces. The effect of the van der Waals forces on small particles preponderates the effect of the particle weight by far so that a number of undesired effects, such as agglomeration, are caused. Van der Waals forces are also considered to be long-range forces although their range is smaller than that of electrostatic forces (cp. Figure 6.2).

There are two methods of calculating the van der Waals forces between small particles (Krupp, 1967). The microscopic approach of Hamaker (1937) considers the resulting energy of interactions between individual atoms and molecules. This approach assumes that the interactions are additive and not affecting each other. The macroscopic and physically more satisfactory approach of Lifshitz (1956) is based on the optical and electrical properties of the interacting macroscopic particles. Krupp (1967) gives an equation for calculating the van der Waals force between two spherical particles based on the microscopic theory of Hamaker (1937) and the van der Waals pressure according to the theory of Lifshitz (1956). This equation allows calculating the van der Waals force between two spheres in dependence of particle diameter D and particle distance a as follows:

$$F_{vdW} = \frac{\hbar\omega}{32\pi a^2} D \quad (6.2)$$

where $\hbar\omega$ is the Lifshitz-van der Waals constant that depends on the material involved and is assumed to be 5 eV in the considered case.

6.3 Liquid bridges

The formation of liquid bridges between fine particles is causing the cohesive character of EMC in its early age. The resulting interparticle force of the formed liquid bridge is one of the strongest adhesive forces between fine particles (cp. Figure 6.1). Due to the fact that water is required to form a liquid bridge and the fixed amount of water contained in the liquid bridge, the resulting adhesive force cannot be considered to be a long-range force or constantly working. Compared to other interparticle forces, such as van der Waals force or electrostatic force, more parameters are influencing the formation of liquid bridges and their interaction is more complex. In the following section, the formation of liquid bridges and the influencing factors will be discussed.

6.3.1 Surface tension

The surface tension is also referred to as interfacial tension as its formation is strongly coupled to the existence of a phase interface (Schubert, 1982). The phase interface can emerge between two immiscible liquids, or between a liquid and a gas. The phase interface between solids and liquids, and solids and gases is only considered theoretically in the literature, as a confirmation of the resulting interfacial tension by measurements is not possible.

The formation of the surface tension is explained by Schubert (1982) using the thermodynamically based model of Gibbs. The surface tension is explained in the following using a mechanical interpretation on a liquid-gas interface. According to this explanation, various intermolecular forces attract the molecules inside the liquid. These attracting forces are equally distributed in every direction so that they are balanced inside the liquid. At the phase interface, an inward force which is caused by the inner molecules of the liquid and which is not balanced attracts the molecules by attracting forces of the neighboring gaseous phase. Therefore, all molecules at the phase interface are subject to an inward force which is only compensated by the liquid's resistance to compression. Consequently, the liquid aims to obtain a steady state of lowest energy and a minimal surface having a curved shape is formed.

The formed surface of the liquid resembles an elastic membrane in which the surface tension acts parallel to phase interface. Owing to the fact that the surface tension is caused by the interparticle forces acting in all directions of the liquid surface, the surface tension cannot be considered to be a vector quantity. Likewise, the surface tension cannot be determined by a direct measurement within the surface of the liquid and can therefore only be measured by its various effects. The surface tension γ at the phase interface between phase A and B has the dimension of force per unit length.

6.3.2 Admixtures and their influence on the surface tension

Chemical admixtures are a powerful tool of modern concrete technology to control the concrete properties in a specific way. Numerous developments, such as pumpable concrete and self-leveling or self-compacting concrete, have only been become possible due to the development of chemical admixtures during the past 20 years. According to Mindess et al. (2003), three main categories of admixtures can be distinguished:

Air-entraining agents that primarily improve the resistance of concrete to freezing and thawing by an improved pore size distribution.

Set-controlling admixtures to control the setting behavior, such as retarders or accelerators.

Plasticizing admixtures on the basis of water-soluble polymers for improving the flow behavior of flowing concrete or to reduce the water demand.

The application of water-reducing admixtures or so-called plasticizers to EMC is of special interest as the workability and the therewith connected compaction behavior can be improved significantly. The use of air-entraining agents or set-controlling admixtures is usually not necessary as the pore size distribution of traditionally designed EMC mixes is uniformly distributed after production (Häring, 2002).

The dispersing effect of plasticizers is based on electrostatic repulsion and steric repulsion. The electrostatic repulsion is caused by the negative charge of the acid groups of the plasticizer polymers (Mindess et al., 2003). The plasticizer molecules are adsorbed onto the solid-water interface of the fine particles. Consequently, the particles' surfaces are negatively charged and an electrostatic repulsion is caused by the uniform charge. According to Spiratos et al. (2003), the effect of electrostatic repulsion preponderates for sulfonate-type plasticizers. With increasing molecular mass the effect of steric repulsion becomes more dominant. The long side chains of polycarboxylates, or so-called superplasticizers (SP), contribute to the effect of steric repulsion

of these bulky molecules adsorbed onto the surface of the fine particles. The latter mechanism is believed to be the major working mechanism of polycarboxylates and to be more effective than the electrostatic repulsion caused by these molecules (Spiratos et al., 2003).

Besides the effect of repulsive interactions, plasticizers influence also the surface tension of the wetting liquid. Figure 6.3 depicts the results of own measurements on the influence of plasticizers on the surface tension of water. Two different types of plasticizers are used for the measurements. These are a polycarboxylate-based superplasticizer (SP1) and a standard plasticizer recommend for EMC (SP 2). The measurements have been performed on a Krüss K11 tensiometer using the plate method.

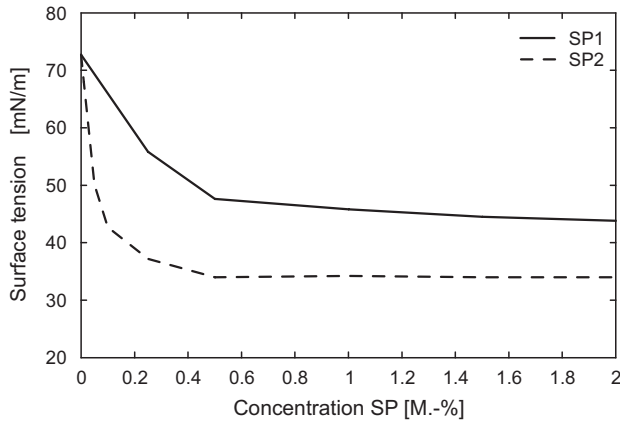


Figure 6.3: Influence of the concentration of superplasticizer on the surface tension of water.

Both plasticizers show a saturation point of about 0.5 M.-% with a corresponding surface tension γ of 44 mN/m and 34 mN/m, respectively. The influence of the surface tension on the early-age behavior of EMC, especially on the green-strength, will be focused on in Section 6.4.3.

6.3.3 Capillary pressure

As illustrated in Section 6.3.1, an inward force acts on the molecules at the phase interface, which causes the formation of the surface tension. Due to the inward force, the liquid forms a minimal surface of lowest energy. The formation of such a minimal surface without the limitation by solid or other liquid phases is only possible by obtaining a spherical shape. The curved shape of the liquid and its surface tension at the surface of the liquid is raising the pressure inside the liquid. The resulting pressure difference across the phase interface between phase A and B is described by the capillary pressure Δp and is given according to Schubert (1982) by the Young-Laplace equation as follows:

$$\Delta p = p_A - p_B = \gamma \left(\frac{1}{R_1} + \frac{1}{R_2} \right) \quad (6.3)$$

with R_1 and R_2 as principal radii of curvature. It arises from Eq. (6.3) that the capillary pressure is increasing with decreasing particle diameters. The capillary pressure within a capillary system is subject to the same basic principle that applies for two-phase systems. However, the influence of

the contact angle θ between liquid and solid phase has to be considered for capillary systems, as here a three-phase system exists. Contact angles smaller than 90° are resulting in a positive value of the capillary pressure. This positive pressure is resulting in the so-called capillary attraction as a result of the outward force of the liquid within the capillary. The capillary pressure is obtaining negative values for contact angles larger than 90° . Here, an inward force is formed in the liquid, which is resulting in capillary repulsion.

The capillary pressure within a capillary tube can be calculated for small capillary diameter ($2R$) when the liquid's meniscus is assumed to be spherical (Schubert, 1982). In this case, the equation of the capillary pressure reads:

$$\Delta p = \frac{2\gamma}{R} \cos \theta \quad (6.4)$$

Eq. (6.4) also reflects that the absolute value of the capillary pressure is increasing with decreasing capillary diameter which is important for the formation of liquid bridges and the draining behavior of granular materials.

6.3.4 Formation of liquid bridges

The liquid volume between two particles of a granular material in the non-saturated state is referred to as liquid bridge. The formation of liquid bridges is of vital importance for the early-age behavior of EMC and is strongly related to the inclusion of water within the void fraction of granular materials. Here, the void fraction ϕ and the degree of water saturation S_w of the voids are essential.

According to Rumpf (1975), the liquid volume within the void fraction is composed of capillary liquid, liquid of the liquid bridge, surface bound liquid, and inner particle liquid. The existence of the particular liquid volumes is depending on the degree of saturation S_w . The surface bound liquid can be found in all wettable granular solids that are in contact with air of normal relative humidity. The degree of saturation for this state is almost zero, as the liquid does not occupy the capillary space. The inner particle liquid contained in the open pore system of the granular particles is also not reducing the void fraction within the granular structure. Here, solely the formation of liquid bridges is reducing the air content within the void fraction. The liquid volume captured by the formation of liquid bridges between the particles is referred to as liquid of the liquid bridge. The total volume of liquid that fills up the void fraction completely is called capillary liquid ($S_w = 100\%$).

Furthermore, the formation of liquid bridges between particles can be classified in dependence on the liquid volume. Here, it is essential to distinguish between the formation of liquid bridges and their expansion until the void fraction is completely filled by the liquid. The beginning formation of liquid bridges in the pendular state can be described according to Halsey and Levine (1998) by three regimes as a function of the added liquid volume V_{liq} . In Figure 6.4 the three regimes are illustrated schematically and their influence on the capillary force F_{cap} is depicted.

Asperity regime for low water contents, where liquid bridges are formed by the accumulation of liquid around asperities at which two adjacent particles are in contact. According to Halsey and Levine (1998), this process continues until the lateral extent of the liquid-filled region exceeds the lateral dimension of the asperity. This determines the maximum volume of the liquid in the contact area V_1 for this regime. At that time, the capillary force is only influenced by the formation of liquid bridges around asperities at the contact points of two particles.

Roughness regime of larger liquid volumes than V_1 , where the liquid bridge expands laterally around the asperity in a region that is still small enough that the macroscopic curvature

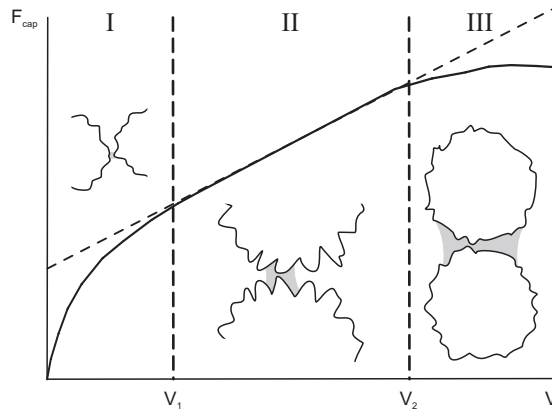


Figure 6.4: Behavior of the wetting liquid between two rough spherical particles. I asperity regime, II roughness regime, III spherical regime (Halsey and Levine, 1998).

of the particle has no influence on the liquid bridge. However, the volume of the liquid bridge exceeds the volume around a single asperity as the liquid bridge expands laterally. During this regime, the increase of the capillary force is proportional to the volume of the added liquid.

Spherical regime, where the liquid bridge is influenced by the macroscopic curvature of the particle as the lateral extent of the liquid in the contact area of two particles exceeds the lateral dimension of one or more asperities. A further increase of the liquid volume is now not resulting in an increase of the capillary force that reaches a constant value.

During the pendular state, liquid bridges are formed and expanding laterally, whereas the liquid bridges are not connected. The degree of saturation S_w at that state depends on the porosity of the granular structure. Rumpf (1975) mentions saturation values between 0.2 and 0.3 for a porosity of about 0.4 of packed equal spheres. The pendular state is followed by the funicular state where the void fraction is partly saturated but also liquid bridges are still existing. If the granular structure is largely saturated by the liquid, the capillary state is reached where liquid bridges and resulting capillary forces are not existing anymore. The degree of saturation S_w for the capillary state amounts to 0.8 for equal spheres having a porosity of about 0.4 (Rumpf, 1975).

6.3.5 Capillary forces

The term capillary force is used in the following for the denomination of the adhesive force between two particles resulting from the formation of a liquid bridge. According to Rumpf (1975), two mechanisms are contributing to the formation of capillary forces. The meniscus of the liquid bridge between the particles causes the formation of forces acting parallel to the surface of the liquid. The resultant force involves an attraction of the particles connected by the liquid bridge. This attractive force can either be increased or decreased by the rate of the capillary pressure. As explained in Section 6.3.3, the capillary pressure in the liquid bridge can be calculated using Eq. (6.3). A lower pressure in the liquid bridge p_A than outside the bridge p_B is defined as positive capillary pressure. In this case, the positive capillary pressure contributes to the attractive force. However, a negative capillary pressure is reducing the attractive force between the particles.

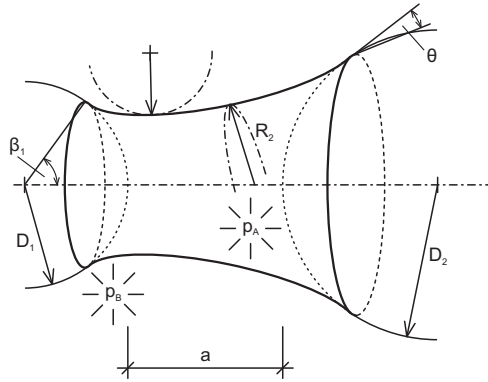


Figure 6.5: Liquid bridge between two spherical particles with different size (Schubert, 1982).

Figure 6.5 shows a liquid bridge between two spherical particles and the associated geometric constraints. The liquid bridge between two spheres is determined by the surface tension γ , the sphere diameters D_1 and D_2 , the central angle β , the contact angle θ , and the particle distance a . Hence, the dimensionless parameters of the normalized adhesive force, normalized capillary pressure and normalized liquid volume in the liquid bridge can be formed according to Rumpf (1975); Schubert (1982). The function of the normalized adhesive force ($F_{adh}/(\gamma \cdot D)$) arises from the geometric constraints to be:

$$F_{adh}/(\gamma \cdot D) = f(t, \theta, a/D) \quad (6.5)$$

Substituting the geometric constraints in Eq. (6.3) and considering a local coordinate system of the liquid bridge results in an ordinary differential equation of the second order. This equation can be transformed to a linear differential equation of the first order for the special case of equal spheres. The results of the numerical solution are given by Schubert (1982) in terms of diagrams for the normalized adhesive force, normalized capillary pressure and normalized liquid volume in the bridge.

Some geometric constraints have to be considered for the formation of a liquid bridge between two equal spheres as schematically depicted in Figure 6.5. These geometric constraints are as follows:

- From the assumption that the liquid bridge is formed between two equal spheres it follows that $D_1 = D_2$
- The distance a between the two spheres amounts to zero due to the formation of the attractive capillary force so that ratio a/D is zero
- According to Schubert (1982), the contact angle θ amounts to zero for a complete wetting of the particles by the surface bound liquid as mentioned in Section 6.3.4

For the before mentioned constraints, an estimation of the normalized adhesive force is given by Rumpf (1975):

$$F_{adh}/(\gamma \cdot D) \approx \pi - \beta \quad (6.6)$$

The central angle β of the liquid bridge in Eq. (6.6) amounts to 5.24 mrad. This value is given by Schubert (1982) for the minimal liquid volume in the bridge which is resulting in the highest adhesive force between the two spheres. Hence, the adhesive force between the two spheres can be estimated as:

$$F_{adh} \approx \pi \cdot \gamma \cdot D \quad (6.7)$$

According to Eq. 6.7, the adhesive force between two spheres are increasing with increasing particle diameter. However, this effect is preponderated by an increase in the particle weight as already mentioned in Section 6.1 and illustrated in Figure 6.1. Furthermore, it has to be noticed at this point that exemplary calculations are only possible for ideal spherical particles. An accurate calculation of the capillary pressure is very difficult as the menisci formed between two arbitrary particles are not regularly shaped due to the irregular particle shape and the existing surface roughness.

6.4 The early-age behavior of earth-moist concrete

The green-strength of EMC in the early-age gives this type of stiff concrete a special feature that allows for direct stripping of the produced concrete products and short process times as the unhardened product can be transported to a place with defined curing conditions. However, the handling of the unhardened product requires a minimum strength of the fresh concrete so that the product keeps its original shape during transportation and storage without undesired deformations. In the case of concrete sewage pipes, insufficient strength of the unhardened product can even result in a total collapse of the product during transportation in the early age. To minimize the number of deficient products, insights on the green-strength and related influencing factors, such as granulometric properties of the mix, influence of chemical admixtures, and water content, are required. Therefore, the influence of the aforementioned factors on the green-strength of EMC is investigated and discussed in detail in this section.

6.4.1 Experimental procedure

The early-age behavior of EMC is mainly influenced by the properties of the fines (Bornemann, 2005; Schmidt, 1999). In this respect, the compaction behavior and the green-strength of EMC are governed by the granulometric properties as well as the water demand of the fines. Hence, the influence of the fines on the green-strength was investigated in the first instance and two different fines were selected for the experimental work. The selected fines are a quartz flour (quartz flour 2) and a fly ash with similar PSD. The PSDs of the selected fines are depicted in Figure 6.6 and further information are given in Appendix A.1. The quartz flour was chosen, as it is an inert powder that does not react with water, but has similar granulometric properties as cement (PSD and angular particle shape). That way, the influence of proceeding hydration on the early-age behavior is prevented. The selected fly ash is characterized by a similar PSD as determined for the quartz flour, but having particles with a more spherical shape. Furthermore, the selected fly ash is considered to be inert when mixed with water. Besides the influence of the granulometric properties of the fines, the effect of chemical admixtures on the early-age behavior of EMC was investigated. A polycarboxylate-based superplasticizer (SP1), introduced in Section 6.3.1, was selected for the further investigations on the influence of chemical admixtures and was applied in combination with the selected fines.

The experimental investigations carried out on the fines were extended to EMC mixes having a maximum particle size of 8 mm. The tested EMC mixes were designed by means of the optimization algorithm as discussed in Section 4.3. Two different distribution moduli of $q = 0.25$ (Quartz 1, Fly ash 1) and $q = 0.40$ (Quartz 2, Fly ash 2) were selected to compose two different EMC mixes that are characterized by a high and a low content of fines, respectively. The selected quartz flour as well as the fly ash were used as fines in the designed EMC mixes in order to en-

sure comparable conditions and to relate the results obtained on EMC mixes to the fundamental properties of the fines. For the design of the tested EMC mixes, a river sand 0-2 and a river gravel 2-8 were selected and used to compose the aggregate fraction. The PSDs of the sand 0-2 and the gravel 2-8 are included in Figure 6.6 and their physical properties are given in Appendix A.1.

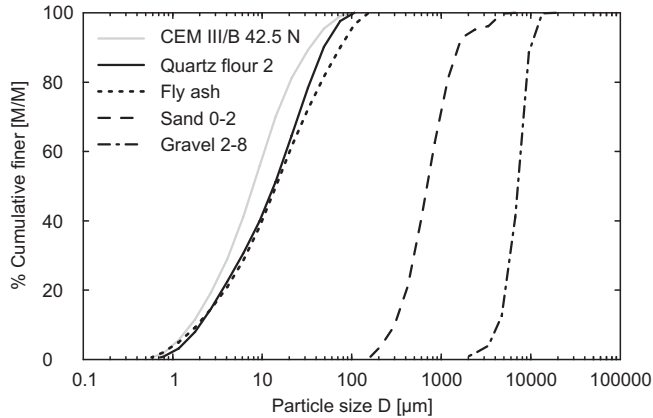


Figure 6.6: PSDs of the selected materials used for the experimental investigations on the early-age behavior of EMC.

The tested mixes were designed in such a way that comparable conditions regarding the content of fines for equal distribution moduli q were achieved. The mix designs presented in Table 6.1 are based on a water content of about 3.0 M.-% till 3.25 M.-% and the air content was estimated a priori to be 3%. Further details on the mix characteristics are given in Table 6.2 and the PSDs of the designed mixes are depicted in Figure 6.7.

Table 6.1: Mix proportioning of the designed mixes used for the experimental investigations on the early-age behavior of EMC.

Material	Quartz 1		Quartz 2		Fly ash 1		Fly ash 2	
	[dm ³]	[kg]	[dm ³]	[kg]	[dm ³]	[kg]	[dm ³]	[kg]
Quartz flour 2	196.4	520.5	109.6	290.4	—	—	—	—
Fly ash	—	—	—	—	216.0	477.6	107.3	237.2
Sand 0-2	375.6	995.3	343.2	909.5	358.3	949.5	352.3	933.7
Gravel 2-8	318.6	844.3	438.0	1160.6	319.4	846.5	439.4	1164.3
Water	79.4	79.4	79.2	79.2	76.3	76.3	71.0	71.0
Air [‡]	30.0	—	30.0	—	30.0	—	30.0	—
Total	1000.0	2439.5	1000.0	2439.7	1000.0	2349.9	1000.0	2406.2

[‡] estimated air content

Table 6.2: Mix characteristics of the designed mixes used for the experimental investigations on the early-age behavior of EMC.

	Quartz 1	Quartz 2	Fly ash 1	Fly ash 2
Distribution modulus q	0.25	0.40	0.25	0.40
w/p ratio [‡]	0.15	0.27	0.16	0.30
Fines [‡] [kg/m ³]	520.5	290.4	477.6	237.2
Paste [‡] [l/m ³]	275.8	188.8	292.3	178.3

[‡] based on fines smaller than 125 μm and considering a water content as given in Table 6.1

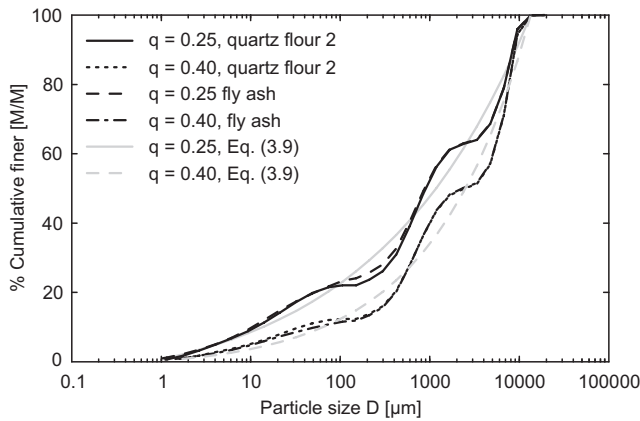


Figure 6.7: PSD of the designed mixes used for the experimental investigations on the early-age behavior of EMC; $D_{max} = 11.2 \text{ mm}$, $D_{min} = 0.63 \text{ }\mu\text{m}$

The selected fines, quartz flour and fly ash, were mixed with water and tested for their compaction behavior and green-strength to study the influence of varying water contents. The compaction behavior was tested using the IC-test as introduced in Section 2.7.4. Samples having a diameter of 100 mm and a height of about 100 mm were produced. Possible differences in the height of the samples due to improved compaction behavior and higher packing fractions were compensated by an increased sample mass so that a constant height for all samples was obtained. All samples were compacted using the working parameters as given in Section 2.7.4 and a maximum amount of 100 working cycles. The samples produced by the IC-test were subsequently tested for their green-strength and submitted to compressive strength. The compressive strength test was conducted displacement-controlled with a crosshead speed of 1 mm/min.

The designed mixes listed in Table 6.1 were tested the same way for their compaction behavior and green-strength. Water contents during the test were varied in small steps until the slurry point of the samples was reached within the last 10 working cycles. This so-called slurry point is characterized by slurry, usually paste, that drains from the sample during the test caused by high water contents and a complete saturation of the void fraction. Usually, if the slurry point is reached, it is not possible anymore to increase the packing fraction of the sample to a further

extent. Therefore, no more water was added to the samples and the test was finished. The results obtained by the IC-test and tests on the green-strength will be discussed in the following sections

6.4.2 Fines

The influence of the selected fines on the compaction behavior was investigated using the IC-test with the corresponding parameters as mentioned in the previous section. The obtained results are depicted in Figure 6.8 for varying water contents. Detailed values of the performed tests are given in Appendix E.11.

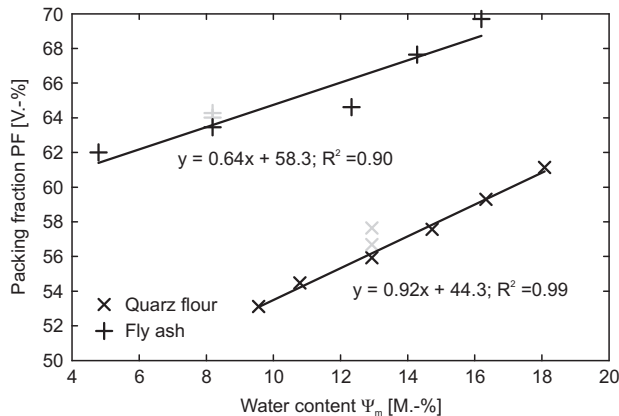


Figure 6.8: Packing fractions of the tested fines for varying water contents ψ_m (mass-based, Eq. (2.4)). The shaded values represent comparable measurements with SP1 having a content of 0.25 M.-% and 1.0 M.-%, respectively.

It is evident from the data depicted in Figure 6.8 that both fines differ in their compaction behavior to a large extent. The fly ash achieves higher packing fractions for comparable water contents than the quartz flour and less water is required to reach the aforementioned slurry point that is characterized by a complete saturation of the void fraction. This fact can be explained by the difference in the particle shape of the fines. The selected fly ash is mainly composed of spherical particles compared to the more angular particles of the quartz flour. Hunger (2010) reports a shape factor ξ of 1.09 for the applied fly ash, whereas a value of about 1.4 has to be considered for the quartz flour. The shape factor ξ expresses the ratio of an effective surface area of a particle to the surface area of an ideal sphere with equal volume (Hunger, 2010). According to this definition, a lower value of ξ corresponds to a more spherical particle shape, which results in a value of 1.0 for spheres.

The more spherical shape of the fly ash particles has a beneficial effect on the compaction behavior and the final packing fractions that were obtained (cp. Figure 6.8). In contrast to this, the angular shape of the quartz flour increases the internal friction of the mix and lower values of the packing fraction are obtained for the same compaction efforts and water contents. However, the higher internal friction of the angular particles of the quartz flour influences the green-strength of the tested samples in a positive way (cp. Figure 6.9a and Figure 6.9b). Here, higher green-strength was measured for the tested quartz flour than for the fly ash samples. This demonstrates that the internal friction of the mix has a larger influence on the green-strength than the packing fraction or the water content of the mix. The maximum green-strength that was obtained near the

slurry point amounts to 0.173 N/mm^2 for the quartz flour having a water content of 18.2 M.-%. The corresponding value of the tested fly ash amounts to 0.121 N/mm^2 for a water content of 16.2 M.-%.

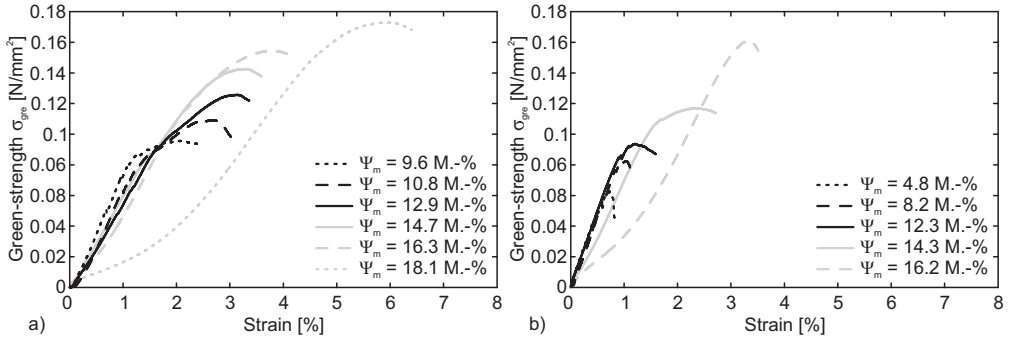


Figure 6.9: Stress-strain curves of tested fines for varying water contents Ψ_m (mass-based, Eq. (2.4)): a) quartz flour, and b) fly ash.

Moreover, information on the deformation behavior of the tested samples can be derived from the graphs depicted in Figure 6.9a and Figure 6.9b. Here, the higher internal friction of the quartz flour samples results not only in higher green-strength, but has also an effect on the deformation behavior near the maximum load. In this range, larger plastic deformations were measured for the quartz flour than determined for the tested fly ash. The fly ash samples showed a rapid decrease in their green-strength when the maximum load was reached and which was not observed for the quartz flour. Larger plastic deformations in the range of the maximum load were measured for the tested fly ash samples only for higher water contents.

A further interesting fact was observed for the deformation behavior of the samples near the so-called slurry point. At this point, the remaining void fraction of the samples is almost saturated with water and the degree of saturation amounts to values larger than 0.9 (cp. Appendix E.11). According to the definitions of Rumpf (1975) as well as Halsey and Levine (1998) discussed in Section 6.3.4, the capillary forces should decrease at this point as liquid bridges are not existing anymore or reach at least a constant value (cp. Figure 6.4). However, this was not the case as highest green-strength values were measured at this point and indicates again that the internal friction, as a result of high packing fractions, dominates the green-strength.

6.4.3 Chemical admixtures

Besides the effect of the granulometric properties of the fines, the influence of chemical admixtures on the green-strength was investigated. For this purpose, the compaction behavior and the green-strength of the fines were determined for fixed water contents, but varying SP1 concentrations. The water content was fixed to be 12.9 M.-% for the quartz flour and 8.2 M.-% for the fly ash. The investigated SP concentrations of the mixing water amount to 0.25 M.-% and 1.0 M.-%, respectively. The compaction behavior of the samples was investigated by means of the IC-test in two different ways. In the first instance, the samples were compacted to the same packing fractions as obtained by the tests without addition of SP1 and the required working cycles as well as the green-strength were determined. Next, the samples were compacted using the same compaction efforts as applied for the tests without addition of SP1 (100 working cy-

cles) and the influence on the compaction behavior and the green-strength was determined. The shaded values depicted in Figure 6.8 show the packing fractions that were obtained for different SP concentrations and detailed values are given in Appendix E.12 as well as Table 6.3.

Table 6.3: Test results of the IC-test for the investigated SP concentrations.

	Quartz flour			Fly ash		
	no SP	0.25% SP	1.0% SP	no SP	0.25% SP	1.0% SP
Working cycles [‡]	100	71	41	100	83	62
Packing fraction [‡] [V.-%]	55.9	56.7	57.6	63.5	64.0	64.3

[‡] amount of working cycles required to obtain the same packing fraction as determined without SP addition

[‡] packing fraction after 100 working cycles

The test results of the IC-test listed in Table 6.3 demonstrate that the compaction behavior is improved when a plasticizing admixture is used and that this effect is depending on the SP concentration. In both cases, quartz flour and fly ash, less working cycles were required to obtain equal packing fractions as determined for the tests without adding SP. The same holds for the packing fractions that were obtained for equal compaction efforts. Here, the packing fractions after 100 working cycles increased with increasing SP contents.

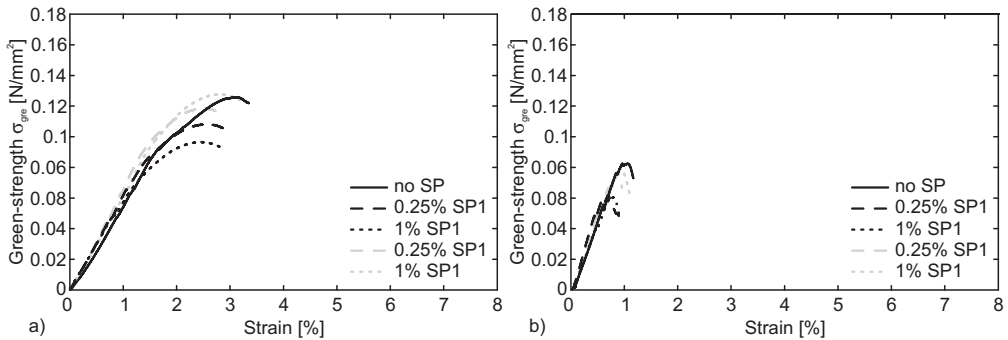


Figure 6.10: Stress-strain curves for constant water contents ψ_m (mass-based, Eq. (2.4)) and varying SP contents: a) quartz flour, $\psi_m = 12.9$ M.-%, and b) fly ash, $\psi_m = 8.2$ M.-%. The shaded graphs show the Stress-strain curves that were obtained for the samples after 100 working cycles.

However, the applied SP influenced not only the compaction behavior of the tested samples, but showed also an effect on the green-strength as illustrated in Figure 6.10a and Figure 6.10b. The green-strength of the samples that were compacted to the same packing fractions as obtained without SP addition decreased with increasing SP content. This fact demonstrates that the green-strength is also influenced by the surface tension of the wetting liquid and that with increasing SP content the surface tension decreases. Considering Eq. 6.7, a lower surface tension results

in lower adhesive force between the fine particles and decreases therefore the green-strength (cp. Figure 6.3 and 6.10a as well as Figure 6.10b). The negative effect caused by the lower surface tension of the wetting liquid is compensated when equal compaction efforts are applied. In this case, the packing fractions after 100 working cycles increased and similar values of the green-strength were obtained as illustrated by the shaded graphs in Figure 6.10a and Figure 6.10b.

6.4.4 Grading

As a next step, the experimental investigations on the influence of the fines on the compaction behavior and the green-strength were extended to continuously graded mixes. For that purpose, the four different mixes with varying distribution moduli q were used. The mix design of the granular mixes is discussed in Section 6.4.1 and their compositions are given in Table 6.1. The designed mixes were tested for their compaction behavior as well as their green-strength. The results of the IC-test are depicted in Figure 6.11a and Figure 6.11b. Detailed values of the performed tests are given in Appendix E.13.

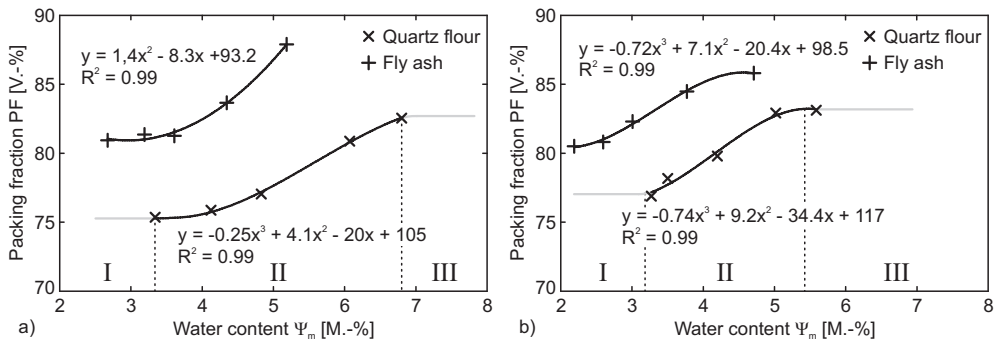


Figure 6.11: Packing fractions of the tested mixes for varying water contents ψ_m (mass-based, Eq. (2.4)) and suggested compaction regimes (I dry state, II moist state, III wet state): a) $q = 0.25$, and b) $q = 0.40$.

The data depicted in Figure 6.11a and Figure 6.11b confirm the assumption on the beneficial effect of spherical particles on the compaction behavior also for continuously graded granular mixes. This fact was already demonstrated in Section 6.4.2 and applies for both investigated distribution moduli of $q = 0.25$ and $q = 0.40$. Furthermore, it reveals from the depicted data that a lower distribution modulus q results in better compaction behavior and higher packing fractions. This effect is more evident for the applied fly ash than the quartz flour. Here, the higher content of spherical particles increased the packing fraction of the fly ash mixes to a remarkable extent. The maximum packing fraction of the tested fly ash mixes increased from 85.8% to 87.9% when a distribution modulus of $q = 0.25$ was used instead of $q = 0.40$. Furthermore, an insight into the sensitivity of the designed mixes on changes in their water content is provided by the data depicted in Figure 6.11a and Figure 6.11b and will be discussed in the following by means of the designed quartz flour mixes.

As illustrated in Figure 6.11a, the graph that was obtained by the IC-test for varying water contents of the quartz flour differs from the compaction curve of the classical Proctor test as depicted in Figure 2.11b. The Proctor test gives a value for the optimum water content at which highest dry density of the sample is obtained. This point of optimum water content for highest

packing fraction was not obtained by the IC-test. Here, the compaction behavior can be divided into three regimes as illustrated in Figure 6.11a and which are:

Dry state that is assumed by the shaded horizontal line in sector I of Figure 6.11a. In this state, variations in the water content of the mix show no or only minor effects on the packing fractions. The water content of the mix is too low to form water layers around the particles that have a lubricating effect and that improve the compaction behavior. Therefore, the packing fractions in this state are equal to the dry conditions or only slightly higher.

Moist state that is represented by the black solid line in sector II of Figure 6.11a. The lubricating effect of the particles grows in this state and the packing fractions increase with increasing water contents. This state determines the optimum range for the practical application of EMC mixes in production.

Wet state that is assumed by the shaded horizontal line in sector III of Figure 6.11a and that is determined by the slurry point of the sample. In this state, a further increase in the water content is not resulting in higher packing fractions as the granular mix obtained the highest possible densification and minimum void fraction. A further increase in the water content shows no positive effect on the packing fractions and excessive water drains from the sample as the remaining void fraction is saturated with water. At this point, the degree of saturation S_w is larger than 90% (see Appendix E.13).

The range of the moist state determines the aforementioned sensitivity of the designed mixes on changes in the water content. The width of sector II is depending on the content of fines and increases with decreasing distribution modulus q (cp. Figure 6.11a and 6.11b). Consequently, mixes with a lower distribution modulus q are less sensitive on small changes in the water content due to their higher amount of fines and their compaction behavior and green-strength is less affected.

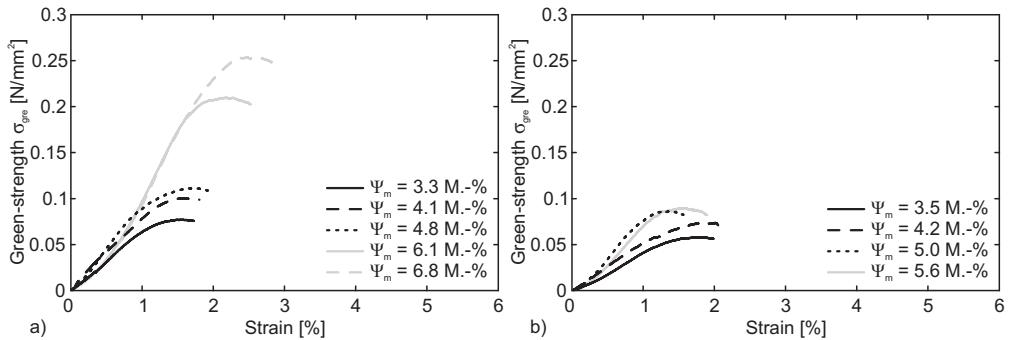


Figure 6.12: Stress-strain curves for varying water contents ψ_m (mass-based, Eq. (2.4)) of the tested mixes containing quartz flour: a) $q = 0.25$, and b) $q = 0.40$.

Variations of the distribution modulus q are not having an impact only on the compaction behavior of the designed mixes, but also the green-strength was influenced. As illustrated by the data depicted in Figure 6.12a and Figure 6.12b, the green-strength of the mixes containing quartz flour was decreasing with increasing distribution modulus q . Similar observations are reported by Bornemann (2005), which are explained by the higher cohesive character of mixes with a high

paste content. Furthermore, the higher content of fines improves the compaction behavior of the mixes and more contact points of particles in the micro range exist. Similar observations were made for the mixes containing fly ash. The results of the measurements on the green-strength of the mixes containing fly ash are depicted in Figure 6.13a and Figure 6.13b.

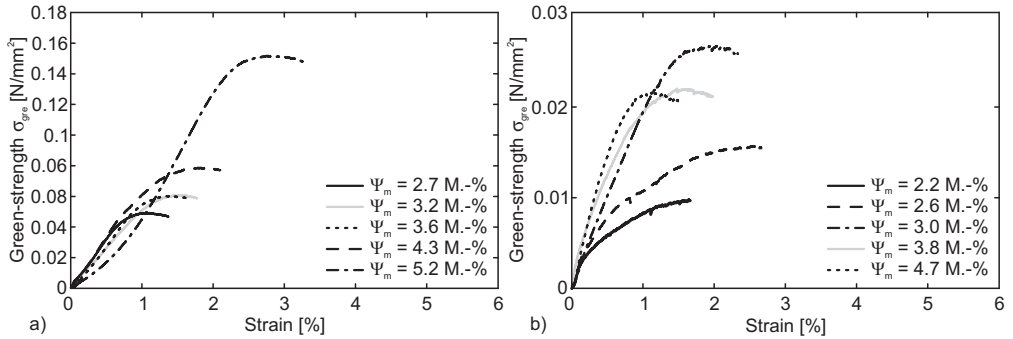


Figure 6.13: Stress-strain curves for varying water contents Ψ_m (mass-based, Eq. (2.4)) of the tested mixes containing fly ash: a) $q = 0.25$, and b) $q = 0.40$.

Although the spherical shape of the fly ash improved the compaction behavior of the tested samples and was resulting in higher packing fractions, the green-strength of these samples is lower than that of samples containing quartz flour. This fact is related to the lower internal friction of the fly ash mixes and was already addressed in Section 6.4.2.

6.4.5 Discussion

The influencing factors on the early-age behavior of earth-moist concrete were investigated and have been discussed in this section. The experimental results reveal that the granulometric properties of the fines influence the compaction behavior and the green-strength of EMC in the early age to a large extent. Considering the compaction behavior, spherical particles increase the packing fraction of EMC mixes, but reduce their green-strength as the internal friction of the mix is reduced due to less grain interlocking. In this respect, angular particles, such as the applied quartz flour, show a beneficial effect on the green-strength. Furthermore, it was demonstrated that the internal friction of the granular mix has a larger impact on the green-strength of EMC than the formation of capillary forces caused by liquid bridges that are formed between the fines. The internal friction of the mix is depending on the particle shape of the fines and the obtained packing fraction, which is depending on the water content of the mix. However, higher green-strength was obtained for mixes of angular particles although their packing fraction was lower than that of mixes with spherical particles.

The application of a plasticizing admixture improved the compaction behavior, but reduced also the green-strength for similar packing fractions. This negative effect of plasticizing admixtures on the green-strength is related to their influence on the surface tension. As shown in Section 6.3.2, the surface tension of the wetting liquid decreases with increasing SP content and results in lower adhesive forces between the fine particles. This decrease in the green-strength was compensated when the samples were compacted using the same compaction efforts than applied for samples without SP addition. In this case, the application of the plasticizing admixture increased the packing fraction, which was resulting in higher internal friction of the sample and

comparable green-strength as obtained for samples without SP addition.

The compaction behavior and the green-strength of continuously graded mixes following the modified Andreasen and Andersen equation (Eq. 3.9) is improved when low distribution moduli q are applied. Lower values of q result in mixes with higher content of fines. This higher content of fines improves the compaction behavior of the mix as the friction between the coarser aggregates is reduced. In this way higher packing fractions are obtained that result in higher internal friction and improved green-strength. In this respect, spherical particles increased the packing fractions of the mix to a larger extent than angular particles, but reduced the green-strength due to less grain interlocking between the fines.

6.5 New mix design concept and compaction behavior

The relevance of an tailored composition of the concrete ingredients considering their granulometric properties and the beneficial influence of improved and denser particle packing on the mechanical properties of EMC were illustrated in Section 4.4. In this respect, several EMC mixes were developed and tested in fresh and hardened state in order to validate the new mix design concept introduced in Section 4.2.3. At the start of this research, the validation of the fresh concrete properties of the designed EMC mixes was limited to simple workability tests, such as the degree of compaction test. The simple layout of the degree of compaction test, as discussed in Section 2.7.1, allows only for evaluating the compaction behavior of concretes with low workability in terms of volume changes before and after compaction. Conclusions regarding the compaction efforts and the compaction behavior of the fresh concrete over time cannot be drawn by the degree of compaction test in its standard form. In this respect, more detailed information on the compaction behavior are obtained by the IC-test as demonstrated in the previous section.

The IC-test became available in the final stage of this research and was used, therefore, for the optimization of an EMC mix used by a company for the production of concrete paving blocks. The optimization of the EMC mix presented in this section concerns the beneficial effect of improved particle packing on both fresh and hardened concrete properties by means of the mix design algorithm discussed in Section 4.3. Furthermore, insights obtained on the early-age behavior of EMC as discussed in the previous section were considered. Considering these aspects, the application of the IC-test for the aimed optimization of EMC is demonstrated and the advantage of the test method for the evaluation of EMC mixes on laboratory scale is shown.

6.5.1 Mix design

Insights obtained from the experimental work discussed in Section 4.4 form the basis for the optimization of an EMC mix that is used for the production of concrete paving blocks. Information on the mix proportioning of the applied EMC mix as well as necessary raw materials were provided by the paving block producer. Based on the available information and material properties, the original mix was tested on laboratory scale and compared with the results of the modified mixes. The following modifications on the original mix were made by three optimization steps:

Optimization 1 is characterized by an optimization of the aggregates grading of the original EMC mix. This first optimization step uses the granulometric properties of the raw materials to compose a solid mix that follows the given grading line (modified A&A equation (Eq. (3.9)) with lowest deviation. The boundary conditions for the grading line have been chosen in such a way that the optimized mix shows similar characteristics as the original mix (cp. Table 6.5). In this respect, the cement content was only slightly reduced to allow for a comparison with the compressive strength of the original mix and to illustrate the effect of improved particle packing.

Optimization 2 was made under the aspect of cement reduction and has therefore a lower cement content. The reduced content of fines was compensated by a higher fly ash content.

The amount of fly ash used in this mix was even increased to a further extent to obtain a higher fines content than in the original mix.

Optimization 3 is oriented on a cement content similar to the one of the original mix but now combined with a higher fines content. Therefore, the amount of fly ash was increased and the grading of the solid mix was optimized according to Eq. (3.9).

All three optimizations were made using the algorithm discussed in Section 4.3 and the grading of the composed mixes follows the grading line of the modified A&A equation (Eq. (3.9)). A constant w/p ratio of 0.30 was used to produce a paste with similar workability and to ensure constant test conditions. The influence of varying water contents on the compaction behavior was investigated on the original mix. These tests were further extended by investigations on the effect of plasticizing admixtures on the workability of the original mix. Therefore, a plasticizing admixture was added to the original mix. Further information on the mix proportioning of the original mix and the three modifications thereof are given in Table 6.4. The mix characteristics are given in Table 6.5 and their PSDs are depicted in Figure 6.14.

Table 6.4: Mix proportioning of the commercial EMC mix and the optimized EMC mixes using the new mix design concept.

Material	Original mix		Optimization 1		Optimization 2		Optimization 3	
	[dm ³]	[kg]	[dm ³]	[kg]	[dm ³]	[kg]	[dm ³]	[kg]
CEM I 52.5N	85.4	261.6	81.6	250.0	75.1	230.0	81.6	250.0
Fly Ash	51.6	114.0	54.6	120.6	88.4	195.5	94.3	208.5
Fijnzand	303.4	804.1	307.1	813.8	484.4	1283.6	464.2	1230.1
Betonzand	217.8	577.1	204.7	542.6	–	–	–	–
Gravel 2-8	154.6	405.1	164.8	431.8	173.4	454.3	171.3	448.9
Water	112.2	112.2	112.2	112.2	128.7	128.7	138.6	138.6
Air [‡]	75.0	–	75.0	–	50.0	–	50.0	–
Total	1000.0	2274.2	1000.0	2271.0	1000.0	2292.2	1000.0	2276.1

[‡] estimated air content

Table 6.5: Characteristics of the tested EMC mixes listed in Table 6.4.

	Original mix	Optimization 1	Optimization 2	Optimization 3
Distribution modulus q	–	0.35	0.30	0.30
w/c ratio	0.43	0.45	0.56	0.55
w/p ratio [‡]	0.30	0.30	0.30	0.30
Fines [‡] [kg/m ³]	379.1	374.1	429.1	461.9
Paste [‡] [l/m ³]	250.4	249.6	293.5	315.8

[‡] based on fines smaller than 125 μm

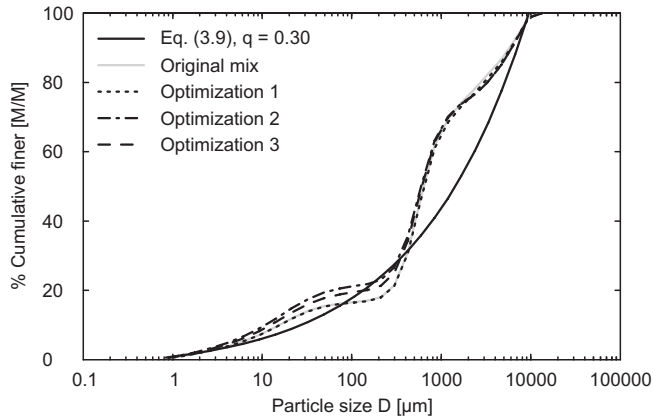


Figure 6.14: PSDs of the commercial EMC mix and the optimized EMC mixes using the new mix design concept; $D_{max} = 8 \text{ mm}$, $D_{min} = \mu\text{m}$.

6.5.2 Fresh and hardened concrete tests

The EMC mixes listed in Table 6.4 were tested for their compaction behavior using the IC-test with the corresponding parameters as given in Section 2.7.4. Detailed values of the test results are given in Appendix E.14. The 28-days compressive strength was determined on the cylindrical samples produced by the IC-test. Therefore, the samples were cured in a humid cabinet at 95% relative humidity and 21 °C for one day. After hardening in the humid cabinet, the samples were stored underwater until their test age was reached.

Fresh concrete properties

The results of the IC-test obtained for the three modifications that were made and the original company mix are depicted in Figure 6.15 for the packing fraction versus working cycles. In Table 6.6, the computed void fraction (Eq. (3.10)) and measured void fraction according to Eq. (3.2) are compared. The shear stresses measured by the IC-tester are plotted in Figure 6.16 versus the working cycles.

The mix of the first optimization step showed a similar compaction behavior over time as the original mix and its final packing fraction is with 77.8% only slightly lower than the value of the original mix which resulted in a packing fraction of 78.2% after 150 cycles. The two mixes with a higher content of fines than the original mix obtained higher packing fractions. Here, the mix of the second optimization step obtained a packing fraction of 81.8%, which was further increased to 83.2% by the third optimization step. However, not only the final packing fraction is higher, but also the initial packing fraction of the mixes Optimization 1 and Optimization 2 is higher than obtained for the original mix. In this case, the higher paste content of the mixes had a beneficial effect on the compaction behavior and the final packing fraction. In this case, the computed void fraction is lower than predicted by the theoretical model according to Eq. (3.10) for the loose packing of dry particles.

Considering the data depicted in Figure 6.15, it becomes obvious that steady values were obtained after about 100 working cycles and that further compaction efforts did not increase the packing fraction of the mixes Optimization 1 and Optimization 2 anymore. Here, a further increase in the packing fraction requires the addition of finer particles to the mix. The finer

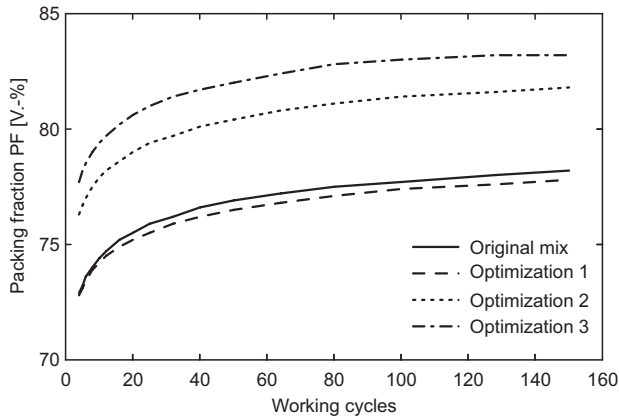


Figure 6.15: Influence of the grading on the compaction behavior.

particles will fill the remaining void fraction in the micro range and which is governed in the present case by the smallest particle size of cement and fly ash.

Table 6.6: Computed void fraction (Eq. (3.10)) using $\phi_1^{loo} = 0.52$, $\beta^{loo} = 0.16$, $\phi_1^{den} = 0.46$, $\beta^{den} = 0.39$, and measured void fraction according to Eq. (3.2) of the tested EMC mixes.

	Computed void fraction (Eq. (3.10))		Measured void fraction (Eq. (3.2))
	ϕ_{com}^{loo} [%]	ϕ_{com}^{den} [%]	ϕ^{den} [%]
Original mix	–	–	20.3
Optimization 1	25.7	6.7	22.2
Optimization 2	25.7	6.7	18.2
Optimization 3	25.7	6.7	16.8

The diagram of the shear stress differs only slightly from Figure 6.15. Here, the final shear stress after 150 working cycles is related to the achieved packing fractions and higher shear stresses were recorded for samples with higher packing fractions. However, it becomes obvious that at the beginning of the compaction process lower shear stresses were measured for the mix of the first optimization step, whereas the development of shear stresses in the mix of the second optimization step is similar to the original mix. Here, a difference between the second optimization step and the original mix is only noticeable at the end of the compaction process. The highest shear stresses were obtained by the mix of the third optimization step, which also obtained the highest packing fraction.

As mentioned in the previous section, the w/p ratio was kept constant to ensure that the produced paste shows similar workability properties. It is known that not only the paste content is influencing the workability of EMC, but also the water content is of vital importance for the compaction behavior of the fresh concrete (Bornemann, 2005; Juvas, 1996). Therefore, the effect

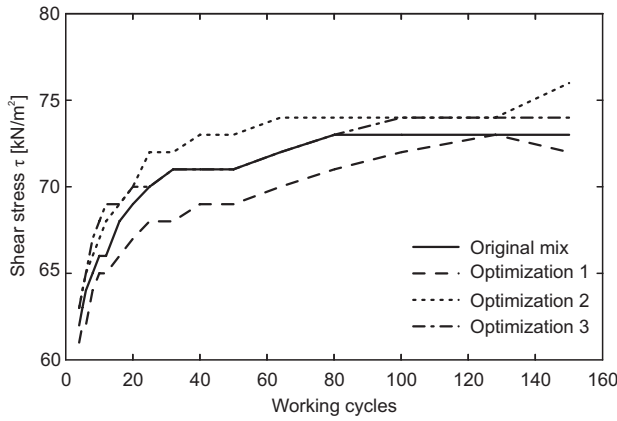


Figure 6.16: Influence of the grading on the shear stress during compaction.

of the water content on the compaction behavior was investigated on the original company mix. The obtained packing fractions after 150 working cycles are depicted in Figure 6.17 for varying water contents. The highest packing fraction was achieved for a water content of about 6 M.-%, which results in a total water content of 127 liters per m³ concrete and corresponds to a w/p ratio of 0.33.

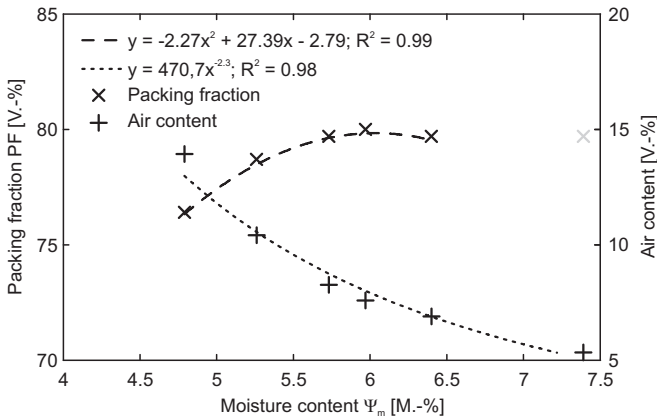


Figure 6.17: Influence of the water content (mass-based, Eq. (2.4)) on the maximum packing fraction of the original company mix and the calculated air contents.

A further increase of the water content is not resulting in higher packing fractions of the dry solids. Here, a similar behavior as discussed in Section 6.4.4 was observed. Water contents that exceed the optimum range as depicted in Figure 6.11 a are not increasing the packing fraction of the solids and a stable value is obtained. This fact is demonstrated by the shaded value depicted

in Figure 6.17 and which corresponds to a water content of about 7.4 M.-%. At this high water content, the test was stopped before 150 working cycles were reached as with increasing packing fraction cement slurry was pressed out of the sample.

It becomes evident from the data depicted in Figure 6.18 that variations of the water content influence also the shear stresses in the sample during compaction. The highest shear stresses were measured for the sample with the highest packing fraction and demonstrates again that highest packing fractions result in high shear stresses within the sample. Lower shear stresses were measured for samples with a water content higher than the optimum value. Here, the excessive water acts like an additional lubricant that is decreasing the shear stresses formed at the beginning of the compaction. This lubricating effect was increasing with higher water contents and excessive water was pressed out of the sample when the degree of saturation of the remaining void fraction approached 100%. The air content of the compacted samples was continuously decreasing with increasing water content until the saturation point of the remaining void fraction was approached (cp. Figure 6.17).

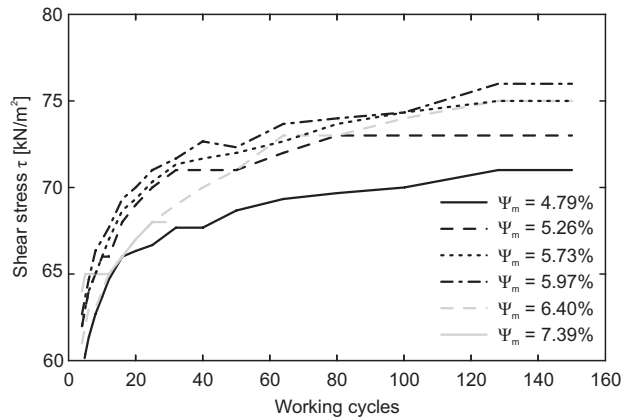


Figure 6.18: Influence of the water content on the shear stresses during compaction of the original company mix.

Next, the influence of chemical admixtures on the compaction behavior was investigated as the use of admixtures with a plasticizing effect is a common practice for other types of concrete like conventional or self-compacting concrete. These admixtures help to reduce the water content of the concrete mix or can increase the workability and therewith the compaction behavior of the fresh concrete mix. Figure 6.19 shows the beneficial effect of a superplasticizer (SP1) on the compaction behavior of the original mix. A slight increase of the SP content helps to increase the final density of the compacted sample to a remarkable extent while the water content is constant. However, the beneficial effect of the applied SP is decreasing over time. The decrease of the plasticizer's effectiveness over time is depicted in Figure 6.20.

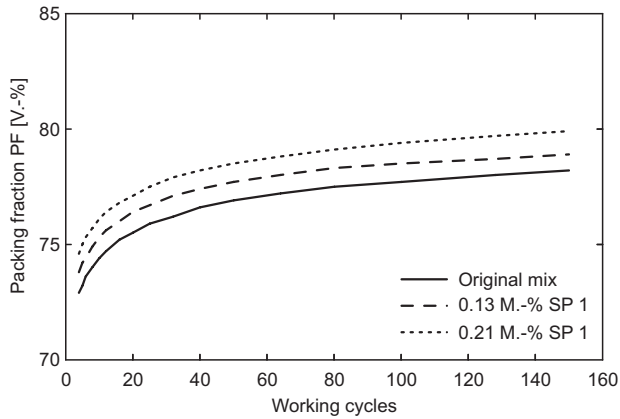


Figure 6.19: Influence of the plasticizer content on the compaction behavior of the original company mix. The content of the applied plasticizer is based on the mass of the fines smaller than 125 μm .

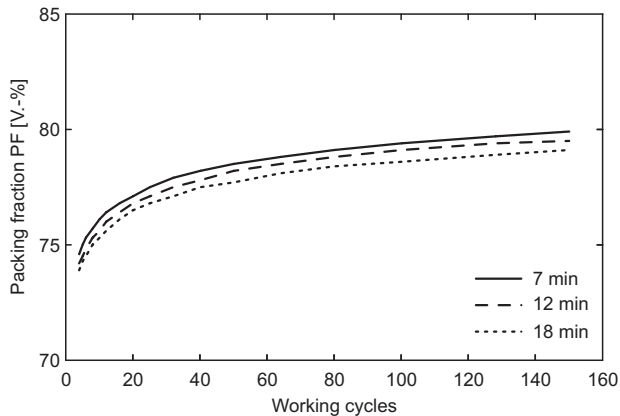


Figure 6.20: Time dependency of the plasticizer's effectiveness on the compaction behavior of the original company mix using a SP content of 2.4%.

Hardened concrete properties

The compressive strength of the tested samples was determined using the cylindrical samples of the IC-test. The produced cylinders have a diameter of 100 mm and a height of 110 mm. The produced samples were ground before they were submitted to compressive strength to obtain a constant height of 100 mm, resulting in a diameter to height ratio of unity, and to ensure that the surfaces for introducing the load are parallel. The test results of the compressive strength test are listed in Table 6.7.

Table 6.7: 28-days compressive strength of samples obtained by the IC-test.

Mix	ψ_m	PF	f_c
	[M.-%]	[%]	[N/mm ²]
Original mix [‡]	4.79	76.4	8.3
	5.26	78.2	17.4
	5.73	79.7	18.2
	5.97	80.0	22.3
	6.40	79.7	25.8
Optimization 1	5.20	77.8	38.5
Optimization 2	5.95	81.8	29.0
Optimization 3	6.48	83.2	41.6

[‡] The water content of the company mix amounts to 5.26 M.-%

The test results confirm again that improved particle packing results in higher packing fractions of the solids and in improved mechanical properties, such as higher compressive strength. The compressive strength of the EMC mix that is used by a paving block producer for the production of concrete paving blocks amounts to 17.4 N/mm² after 28 days and was increased by optimizing the grading of the solids to a value of 41.6 N/mm². Higher compressive strength was also obtained when packing fractions increased due to changes of the water content. Here, the compressive strength of the original mix was increased to 25.8 N/mm² without modifications on the grading of the mix nor the cement content.

6.5.3 Discussion

The influence of improved particle packing on the compaction behavior of an EMC mix used for the production of concrete paving blocks was investigated. The grading of the company mix was optimized and the optimum water content of the original EMC mix was determined to obtain highest packing fractions of the solids. Tests using the IC-test as described in Section 2.7.4 were carried out to investigate the compaction behavior and the influence of modifications that were made on the original EMC mix.

The aimed optimization of the solids grading based on the ideas of the new mix design concept discussed in Section 4.2.3 resulted in higher packing fractions of the solids and improved mechanical properties. In the first instance, the grading of the aggregates was optimized only without considering the grading of the fines (Optimization 1). This first optimization step was not resulting in higher packing fractions, but decreased the shear stresses that are formed during compaction. As a consequence of the lower shear stresses, lower forces are required for compacting the sample, and shorter production times can be expected. The optimization of the solids grading was not resulting in higher packing fractions as the granulometric properties of the fines were not considered and the remaining void fraction of the aggregates was not ideally filled. However, the optimized grading of the aggregates was resulting in higher compressive strength due to an improved granular structure of the aggregates. Consequently, the compressive strength increased from 17.4 N/mm² to 38.5 N/mm², which corresponds to an increase of more than 200%.

Considering the granulometric properties of the fines, it was possible to increase the packing fraction of the solids to a further extent. The increased packing fraction of mix Optimization 1

and Optimization 2 led to a further increase of the compressive strength as the content of fines was increased to follow the given grading with lowest deviation. Fly ash was used to increase the fines content and consequently the beneficial effect of the spherical particles on the compaction behavior has to be considered in both cases as well. Furthermore, the pozzolanic properties of the applied fly ash influence the compressive strength of the hardened concrete. Here, a notably effect of the pozzolanic reaction on the compressive strength is expected. As already addressed in Section 4.4.4 as well as Section 5.2.3, the increased compressive strength allows for cement reduction as cement was replaced by a suitable filler material. This fact was confirmed again by the second optimization step. Here, the cement content was reduced and fly ash was used in this case as cement substitute and filler material.

The tests carried out with the IC-tester demonstrated that higher packing fractions are associated with higher internal shear stresses. The shear compaction of the sample and the resulting movement of the coarser particles against each other cause the increase in shear stresses. At higher densifications, the moving of the particles is hindered and increases therefore the internal friction. In this respect, the higher paste content of the mixes Optimization 2 and Optimization 3 was not causing a reduction of the internal friction due to less grain-to-grain contacts of the coarse particles as stated by Ritchie (1962) and Schmidt (1999).

The aforementioned effect of higher packing fractions on the shear stresses was also confirmed by tests of the original EMC mix using varying water contents. Here, the shear stresses increased with increasing packing fractions of the solids until the optimum water content was reached. Higher water contents than defined by the optimum value were not resulting in higher packing fractions but reduced the packing fraction of the solids only slightly. Up to a certain water content, the remaining void fraction was filled with water and the air content of the samples was reduced as long as the saturation of the void fraction is below 100%. Once the void fraction was saturated, excessive water was pressed out of the sample. These high water contents reduced also the stability of the produced samples as the consistency of the concrete at this high water contents was comparable to normal strength, normal weight concrete with high plastic consistency and low workability. In view of improved workability and higher packing fractions of the solids, the use of a plasticizing admixture reduces the stability of the concrete less than water did. Finally, it was confirmed that the IC-test provides a suitable method for testing EMC mixes on laboratory scale. The automation of the measuring procedure allows for identifying the influence of small changes in the mix design on the compaction behavior. In the considered case, it was possible to identify the effects on the packing fraction of the solids caused by improved grading, changes in the water content, the use of a plasticizing admixtures, and the time dependence of plasticizing the admixture.

Based on the experimental results of the investigations on the early-age behavior of EMC presented in Section 6.4 as well as Section 6.5, the following design parameters are proposed:

- Distribution modulus q : 0.25 - 0.30
- Paste content: 275 - 295 dm³
- w/p ratio: 0.25 - 0.30

These parameters recommended for the design of EMC mixes with good compaction behavior and high-green strength consider a maximum aggregates size of 8 mm and differ, therefore, from the values given in Section 4.4.4.

6.6 Conclusions

Based on the theoretical and experimental investigations on the early-age behavior of earth-moist concrete presented in this chapter, the following conclusions can be derived:

1. The IC-test provides a suitable test method to characterize the compaction behavior of EMC mixes and to identify changes in the compaction behavior in a precise way. The

IC-test was used to investigate the influencing factors on the early age-behavior of EMC mixes, effects of optimized grading on the compaction behavior of EMC mixes, and to compare the early-age behavior of different mix designs. Furthermore, the IC-test allows for adjusting the water content of the mix as well as the amount of chemical admixtures to obtain highest packing fractions of the solids.

2. The early-age behavior of EMC is influenced mainly by the granulometric properties of the fines. In this respect, the particle shape has the main impact on both compaction behavior and green-strength.
3. It was demonstrated that spherical particles achieve higher packing fractions than angular particles having the same PSD. Contrary to this, higher green-strength was achieved with angular particles although their packing fractions were lower than obtained for comparable tests with spherical particles.
4. The green-strength of EMC is a result of internal friction and adhesive forces between the particles, which are generated as a result of formed liquid bridges. It was demonstrated that the internal friction has a larger impact on the green-strength than the formation of liquid bridges. Furthermore, the particle shape and the packing fraction of the mix govern the internal friction of EMC, whereas the particle shape has a larger influence than the packing fraction. Considering a constant particle shape, higher packing fractions are increasing the internal friction of the mix.
5. Higher packing fractions of the solids increase the internal resistance of EMC mixes at higher densification rates and show, therefore, a restraining effect on coarser particles that are moving against each other. Consequently, shear stresses increase at higher packing fractions and higher compaction efforts are required to compact the sample to a further extent.
6. The influence of improved particle packing on both fresh and hardened concrete properties was demonstrated. In this respect, the compaction behavior of EMC mixes was improved by optimized grading of the aggregate fraction. The packing of the aggregates was optimized and the denser granular structure resulted in higher compressive strength of the hardened concrete.
7. Higher packing fractions were obtained when the entire grading of the mix was optimized using the modified Andreasen and Andersen equation (Eq. 3.9). In this respect, lower values of the distribution modulus q resulted in mixes with higher contents of fines and better compaction behavior. Consequently, the void fraction of the granular structure was reduced to a further extent and the strength in fresh and hardened state was increased substantially.
8. The application of a plasticizing admixture improved the compaction behavior and resulted in higher packing fractions for comparable compaction efforts. However, the green-strength was reduced for comparable packing fractions as obtained for mixes without addition of a plasticizing admixture. This negative effect on the green-strength was compensated by the higher packing fractions that were obtained due to the application of a plasticizing admixture.

Introduction to photocatalysis¹

7.1 Introduction

The focus on photocatalytic materials and their manifold application in different types of products is increasing since the middle of the 1990s. Varying products such as self-cleaning glasses and tiles, anti-fogging glasses, blended cements for the application in fair faced concrete, photocatalytic active concrete paving blocks and roofing tiles, and special tile grouts against molds have been introduced to the market of building materials. Although these products are aiming on different types of applications, they are based on the same mode of action. Their underlying working principle is the photocatalytic reaction of oxides of semiconducting materials under the exposition of electromagnetic radiation of all wavelengths, whether visible or not.

It should be mentioned that the term photocatalysis is discussed manifold in the literature regarding its inappropriate use. Although this term is widely used in the literature and more or less established for the light induced catalytic reaction, it actually refers to a reaction where light is used as a catalyst. However, this is not the case as a semiconductor material is acting as catalyst and light is one of the reactants that is consumed by the chemical process. This catalytic reaction is defined by Mills and Le Hunte (1997) as 'acceleration of a photo-reaction by the presence of a catalyst'.

Titanium dioxide (TiO₂) in the anatase modification is preferably used as photocatalyst due to its optoelectronic properties, non-toxic behavior, chemical stability and high efficiency. Other oxides of semiconducting materials such as zinc oxide (ZnO), tin dioxide (SnO₂) or salts of semiconducting materials such as zinc sulfide (ZnS) or cadmium sulfide (CdS) can also serve as photocatalyst (Mills and Le Hunte, 1997). Recent developments in this field are aiming on new types of photocatalytic materials that offer a wider range regarding their characteristic wavelength or shift the characteristic wavelength of the photocatalyst to the visible light. A modification of the optoelectronic properties of the photocatalyst can be achieved by the introduction of impurities into the crystal structure of the semiconductor oxide. This process is referred to as doping.

In this chapter, an overview on the working principle of photocatalytic materials and their application to building materials is provided. Furthermore, a test methods for evaluating the efficiency of photocatalytic concrete products is presented and compared with standards. Recommendations and requirements given by the discussed standards are used for the development of an own test setup for the assessment of air-purifying characteristics of photocatalytic concrete products.

7.2 Working mechanism of photocatalysts

7.2.1 A brief history

The photocatalytic reaction of TiO₂ is known since the beginning of the 20th century. The fading of paint containing titanium white was reported by Keidel (1929) and Wagner (1929). In this respect, Wagner (1929) mentioned the term catalysis associated with titanium white. In paints, TiO₂ is used as a coloring pigment and its belonging photocatalytic behavior is known to cause

¹Parts of this chapter were published elsewhere (Hunger et al., 2008a,b; Hüsken et al., 2008, 2009a,b).

durability problems when the paint is exposed to sunlight or other UV sources. The photocatalytic reaction of the TiO_2 pigments is decomposing the organic binder contained in the paint. The decomposition of the binder is resulting in a reduced brilliance of the original paint as the white TiO_2 pigments appear at the surface that seems to be covered by a fine thin powder layer. This effect is referred to as chalking due to its characteristic appearance.

However, the extensive research on photocatalytic materials was initiated many years later by the photoelectrochemical cell for water splitting which was developed by Fujishima and Honda (1972). After discovering the so-called Honda-Fujishima effect, a lot of research was conducted on photocatalytic reactions as the demand on artificial systems for converting solar energy to chemical or electrical energy was high. According to Mills and Le Hunte (1997), the use of TiO_2 as semiconductor for the production of solar cells is considered as less than ideal. This is caused by the low solar conversion efficiency of only 1% combined with a low proportioning of UV light in the solar spectrum of less than 5%. For that reason, more attention was paid to the photosensitized reduction, oxidation or cleavage of water. The possible water cleavage without the use of any sacrificial electron donors and acceptors is critically discussed by Mills and Le Hunte (1997) and therefore considered to be working in an inefficient and not serviceable mode. However, there is no doubt about the working mechanism of the photosensitized reduction and oxidation potential of water by means of sacrificial electron donors and acceptors, respectively, as reported by Mills and Le Hunte (1997).

The photosensitized reduction and oxidation potential of aqueous solutions containing TiO_2 photocatalyst was the starting point for several research activities on the decomposition of organic and inorganic pollutants. Kawai and Sakata (1981) reported the successful decomposition of several organic compounds like synthetic polymers, solvents and proteins. It was first presumed that the reaction is limited to non aromatic compounds as shown, for example, by Pruden and Ollis (1982). These concerns were disproved later by other researchers. Barbeni et al. (1984) demonstrated the successful photocatalytic degradation of 4-Chlorophenol, a chlorinated aromatic compound, over TiO_2 . Due to the decomposing capabilities, the research on TiO_2 focused to a main extent on the treatment of wastewater, primarily generated by pharmaceutical or coloration processes. Not only the degradation of organic compounds was part of the early research but also the kinetics of the reaction and their modeling (Matthews, 1988). In this respect, the Langmuir-Hinshelwood kinetics are widely used for the modeling of the photocatalytic degradation process. The Langmuir-Hinshelwood model and its application to photocatalytic concrete products is addressed in the next chapter.

Besides the degradation of aqueous organic compounds, also gaseous organic and inorganic compounds can be decomposed by TiO_2 . Mills and Le Hunte (1997) mention that the degradation efficiency of gaseous organic compounds over TiO_2 is more than tenfold greater than for the same organic compound dissolved in aqueous solution. One of the first applications of TiO_2 to gaseous pollutants was the degradation of 2-Methylbutan shown by Djeghri and Teichner (1980). Later, Peral and Ollis (1992) gave an overview on the degradation of further relevant air contaminants. A comprehensive explanation of the degradation of gaseous organic compounds is given in Section 7.2.3.

However, the research on the photocatalytic reaction and its pertaining qualities was not only limited to scientific applications. Also the industry became aware of the beneficial effects of the photocatalytic reaction and their application to practical problems. Especially the building material industry spent many efforts on the development of new building materials and new types of products. The first applications are based on the photocatalytic degradation of organic compounds and therefore related to the abatement of gaseous contaminants and odors by photocatalytic materials applied on a honeycomb carrier material (Suzuki, 1993). The laboratory investigations as well as practical feasibility tests on an air-purification unit were conducted by Suzuki (1993) for Toyota Central R&D Laboratories. The deodorizing effect was also applied to tiles coated with a thin film of photocatalytic material. These investigations on tiles were

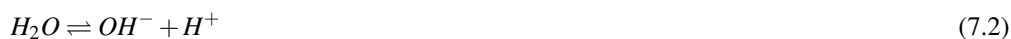
conducted by Watanabe et al. (1993) for the R&D division of TOTO Ltd. Japan.

A further application of the photocatalytic reaction is reported by Murata et al. (1998) and was applied for the first time on industrial scale by Mitsubishi Materials Laboratory in 1997. In this respect, the photocatalytic oxidation (PCO) is used for the oxidation of nitrogen oxides (NO_x) by oxygen (O_2) to nitrate (NO_3^-). The application of TiO_2 in concrete paving blocks is patented (Murata et al., 1997) and was guided by parallel developments in Europe on the application of TiO_2 in paving tiles carried out by Italcementi S.p.A. However, the research carried out by Italcementi S.p.A. was not only resulting in a patent for paving tiles comprising an hydraulic binder and a photocatalyst (Cassar and Pepe, 1997), but resulted also in an hydraulic binder with self-cleaning properties, named TX Active®, to maintain the aesthetic characteristics of applied concrete, mainly based on white cement (Cassar et al., 2003). A comparison of both relevant patents is given in Appendix F.

7.2.2 Photocatalytic principle

Titanium dioxide is one of the oxides of titanium and appears in remarkable extent in nature - the ninth most abundant element in the Earth's crust. In solid state, TiO_2 appears in three different crystalline modifications namely: rutile (tetragonal unit cell), anatase (tetragonal unit cell) and brookite (orthorhombic unit cell). The most common crystalline modification of TiO_2 is the rutile modification. This modification is the only stable modification of TiO_2 at high temperatures. The rutile modification shows almost no photocatalytic properties and is used as a coloring pigment due to its a high refractive index and inert feature. The brookite modification is of minor technical interest due to its properties and rare occurrence in nature. Brookite shows, similar to rutile, no remarkable photocatalytic activity. In contrast to the before mentioned crystalline modifications rutile and brookite, the anatase modification shows photocatalytic properties of practical and technical use. Besides the application as photocatalyst, the mineral is also used as white pigment.

The optoelectronic properties of the anatase modification turn this material to the photocatalyst with highest efficiency regarding the photocatalytic reaction. On the one hand, the semiconductor band gap E_g of 3.2 eV is wide, and, on the other hand, the oxidizing potential of the valence band is with 3.1 eV (at pH = 0) also relatively high. The photocatalytic reaction is induced by the transfer of electrons from the valence band to the conduction band by photons in the UV-A range (see Figure 7.1). The UV-A absorption creates electron holes which are responsible for the formation of radicals and charged species such as OH^\bullet , $\text{O}_2^{\bullet-}$, HO_2^\bullet and follows from:



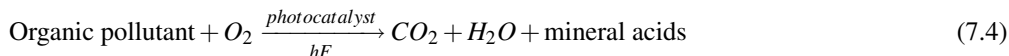
The generated radicals and charged species at the surface of the photocatalyst have a strong oxidizing potential and can therefore decompose organic and inorganic pollutants in gaseous or aqueous form. This comprises also the decomposition of cancer cells, bacteria and viruses (Mills and Le Hunte, 1997). According to Herrmann et al. (2007), the most reactive species are OH^\bullet radicals that are the second best oxidizing species after fluorine. The further reactions are being subject to the heterogeneous photocatalysis and characterized by the adsorption of the precursor and the desorption of the reaction products.

For generating hydroxyl radicals, the presence of water at the surface of the photocatalyst is necessary (cp. Eqs. (7.2)) and determines one of the major influencing factors of the degradation of gaseous pollutants. Therefore, a certain amount of water molecules, supplied by water vapor, is required to start the degradation process. The electromagnetic radiation is expressed by the product of the Planck constant h and the frequency F (Herrmann et al., 2007). In the following,

the intensity of the electromagnetic radiation is accounted for by the UV-A irradiance E , influencing the efficiency of the photocatalytic reaction. Since the oxidation of organic or inorganic compounds proceed at, or close to, the surface of the photocatalyst, a large number of surface contacts is desirable. This is achieved by photocatalysts with high specific surface area.

7.2.3 Degradation of organic compounds

The degradation of organic compounds by means of the photosensitized reaction of a semiconductor, such as TiO_2 , forms the broadest field of application. The decomposition of organic materials was reported for the first time by Kawai and Sakata (1981) and Pruden and Ollis (1982) and forms the basis for indoor air-purification by means of decomposing odors or volatile organic compounds (VOCs²). In addition, the treatment of waste water generated by the pharmaceutical industry or contaminated with synthetic dyes from the textile industry is a further application of the photoinduced degradation. More than 200 organic compounds are reported by Mills and Le Hunte (1997) that can be decomposed using a photocatalyst. In this respect, the photocatalytic degradation of organic compounds is also referred to as semiconductor-sensitized photo-mineralization of organic substrates by oxygen (Mills and Le Hunte, 1997). The underlying chemical reaction can be described by Eq. (7.4) for aqueous solutions or gaseous substances.



Based on Eq. (7.4), the principle of the photoinduced reaction is illustrated in Figure 7.1 and shows the complexity of this reaction in the aqueous phase. The basic principle, as depicted in Figure 7.1, can also be applied for the decomposition of organic substances in the gas phase. According to Mills and Le Hunte (1997), the decomposition of organic compounds in the gaseous phase is more efficient than those found for the same substance dissolved in aqueous solution.

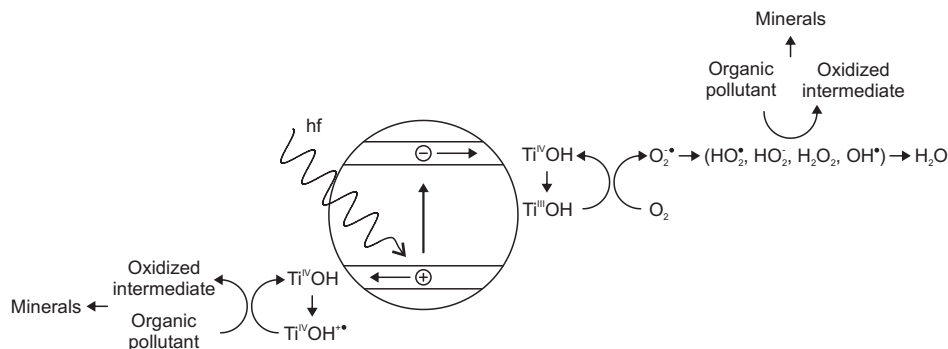


Figure 7.1: General reactions for the decomposition of organic compounds in aqueous solution (Mills and Le Hunte, 1997).

As obvious from Figure 7.1, the formation of relatively stable intermediates is possible and shows

²In this context, volatile organic compounds (VOCs) mean all organic compounds arising from human activities, other than methane, which are capable of producing photochemical oxidants by reactions with nitrogen oxides in the presence of sunlight (Directive 2001/81/EC, 2001).

a weak point of the photoinduced degradation of odors and VOCs. This negative effect is reported, amongst others, by Peral and Ollis (1992) which showed that the efficiency of the system decreases if a relatively stable intermediate is formed and oxidized at lower rates than the initial substance. This process can lead to a complete deactivation of the photocatalyst or a desorption of the intermediate products can occur in periods with no illumination. Furthermore, the generation of intermediates that show a higher toxic potential than the original compound is possible under certain boundary conditions and has to be avoided.

However, the photoinduced degradation of odors and VOCs shows a great potential for air-purification in indoor climate or the treatment of exhaust gases from industrial plants. Several products are already available for the decomposition of organic pollutants in air or water. Besides the decomposition of organic compounds, some inorganic substances can be oxidized by the PCO, which will be explained in the following.

7.2.4 Degradation of inorganic compounds

The photocatalytic oxidation of inorganic compounds is a promising approach for the degradation of nitrogen oxides (NO_x) that are emitted in large quantities in metropolitan areas with high traffic loads. Besides the degradation of NO_x , other inorganic and toxic substances such as sulfur oxide (SO_x), bromate (BrO_3^-), etc. are decomposed to less harmful substances. It is also reported by Mills and Le Hunte (1997) that CO_2 can be reduced by a semiconductor photocatalyst. However, the yield of the reduction of CO_2 is very low and the photocatalyst has to undergo an intensive pre-treatment. In this respect, the degradation of non-metal oxides, such as NO_x , shows the highest conversion rate and will be discussed in the following.

As mentioned in Section 7.2.2, hydroxyl radicals (OH^\bullet) are formed on the surface of the photocatalyst. The generated radicals are involved in the oxidation of NO that can be described as two-stage reaction on the surface of the photocatalyst:



The first step of the degradation of NO_x is characterized by the oxidation of NO to NO_2 which is a key precursor of the so-called denitrogenization (De NO_x -process). The generated NO_2 is an intermediate product that is oxidized by a further reaction to nitrate ions (NO_3^-). The formed NO_3^- ions agglomerate on the active surface of the photocatalyst and result in the deactivation of the photocatalyst over time. This deactivation of the photocatalyst can be reversed by removing the reaction products from the active sites. A simple flushing with water is sufficient to remove the generated NO_3^- ions from the surface as weak nitric acid. The effect of such a washing cycle on the degradation performance is depicted in Figure 7.2 for a concrete paving block having air-purifying properties.

After removing the reaction products, the performance of the photocatalyst is fully recovered and the NO_x removal performance reaches the original value. The removal of reaction products from the active sites of the photocatalyst is realized under practical conditions by a rainfall of average intensity and has been proven to be sufficient (Murata et al., 1999). This allows the application of the PCO in products that are used for paving of traffic areas such a parking lots, sidewalks, etc. The NO_3^- ions contained in the rain water collected from areas covered with air-purifying products can be recycled by modern sewage plants.

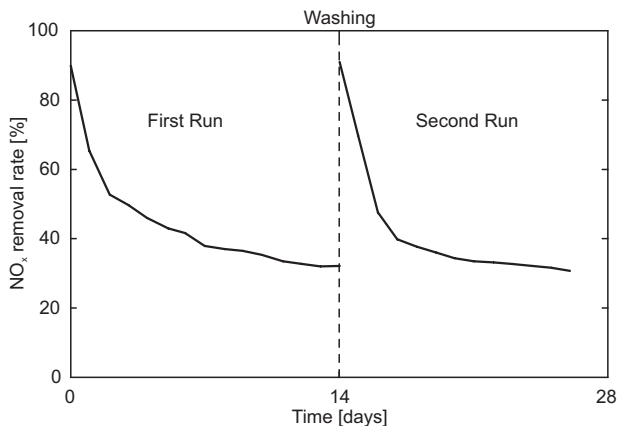


Figure 7.2: Recovery of NO_x degradation performance after removal of reaction products by a washing cycle (Mitsubishi, 2005).

7.2.5 Degradation of microorganisms

Besides the photocatalytic degradation of a wide range of organic and inorganic compounds, microorganisms, such as viruses, bacteria, algae, and molds, are decomposed by means of UV-A light in the presence of TiO₂. Examples for the sensitizing effect of TiO₂ particles on the 'photo-killing' of bacteria are given by Mills and Le Hunte (1997) for *Lactobacillus acidophilus*, *Saccharomyces cerevisiae*, and *Escherichia coli*. The photo-killing of bacteria is induced by the decomposition of intracellular CoA due to photocatalytic oxidation. Although the kinetics of this photo-disinfection are generally slow, products with self-disinfecting surfaces are manufactured. These products are available on the market as TiO₂-coated ceramic tiles.

Another aspect with more relevance for the practical application of TiO₂ in concrete paving blocks results from the ability of TiO₂ particles to inhibit the growth of filamentous algae. The decomposing effect of TiO₂ coated glass beads on green algae *Cladophora* is reported by Peller et al. (2007) which also postulated a mechanism of the photocatalytic degradation of *Cladophora*. According to this mechanism, the protective cell structures (cell wall, cell membrane, and organelle membrane) are affected by the high oxidative potential of the formed hydroxyl radicals (see Section 7.2.2). The protective cell structures undergo radical induced changes prior the chlorophyll is decomposed. This degradation of the chlorophyll leads to a dysfunction in the metabolism which results in the die-off of the entire cell.

The inhibited growth of green algae on surfaces containing photocatalytic materials is also verified by own experiments. Figure 7.3 shows concrete paving blocks that were exposed at a location with humid conditions and low direct sunlight. At this location, the staining of an already existing paving is a typical problem that is caused by algae growth. After a short period of time, the reference sample (sample ① in Figure 7.3) was covered with green algae on its lateral side as well as on its top side. Green algae were also growing on the lateral side of the concrete paving block containing TiO₂. Here, the lateral side was covered with algae up to the level of the core mix which is not containing photocatalytic active TiO₂. The remaining lateral side of the functional top-layer as well as the top side of the paving block are not covered by any green algae as here the photocatalytic material prevents the fouling by algae. This exposition of concrete paving blocks at a location that is actually not suitable for the degradation of NO_x due

to its high humidity and low natural light showed another potential of photocatalytic products regarding the prevention of undesirable staining due to algae growth.



Figure 7.3: Staining of concrete paving blocks caused by algae growth: a) untreated sample, b) paving of standard paving blocks, and c) paving block containing TiO_2 in the functional top layer.

7.2.6 Super-hydrophilicity

The history of the research on the photocatalysis of TiO_2 comprises numerous fundamental results with potential for practical applications. However, only few of these developments have been realized by successful industrial applications so far. One of these widely used characteristics is related to the latest finding in the field of TiO_2 photocatalysis, the so-called super-hydrophilicity. The highly hydrophilic behavior of surfaces coated with TiO_2 was reported for the first time by Wang et al. (1997) and is actually referred to as amphiphilic behavior as the TiO_2 coated surface shows hydrophilic and oleophilic areas. In the considered case, the contact angle of water droplets on the substrate surface decreases to almost zero and a uniform water layer is formed. This thin water layer can flow under pollutants that adhere to the surface and allows that the pollutants are easily flushed from the surface. The same mechanism prevents also the fogging of glasses or mirrors coated with photocatalytic materials.

A model for the hydrophilic behavior of TiO_2 coated surfaces is proposed by Wang et al. (1997). According to this model, the photoinduced hydrophilic surface is not distributed uniformly on microscopic level, but shows hydrophilic domains. Within these hydrophilic domains, oxygen vacancies at bridging sites are formed that result in the conversion of relevant $\text{Ti}^{\text{IV}+}$ sites to $\text{Ti}^{\text{III}+}$ sites which are favorable for dissociative water adsorption (cp. Figure 7.1). Wang et al. (1997) presume that these defects influence the affinity to chemisorbed water of their surrounding sites, forming hydrophilic domains, whereas the remaining surface is oleophilic. The hydrophilic and oleophilic domains are distinguishable on microscopic level, but become amphiphilic on macroscopic level. Furthermore, the dimension of a liquid droplet is substantially larger than the hydrophilic and oleophilic domains which results in a bridging of several domains by one droplet and the instantaneous spread on such a surface. Since concrete is a porous system that absorbs water near its surface and the fact that the surface roughness of standard concrete is much higher compared to the micro-roughness of glass, it is assumed that the hydrophilic behavior of photocatalytic surfaces and their potential regarding removal of pollutants is not of interest for concrete surfaces. A free-flowing behavior of the water is not assured by the high surface

roughness of concrete. This means that water indeed flows under the pollutants that adhere onto the surface, but the free-flowing of the water and the subsequent removal of the pollutants is inhibited by the high surface roughness of the concrete surface. The free-flowing of the water is required to remove the pollutants completely from the surface and is not the case for concrete surfaces that are oriented with a small angle to the horizontal direction. Furthermore, TiO_2 particles are homogeneously distributed and embedded in the cement matrix of the concrete and are, therefore, not available as constant TiO_2 layer as obtained by the production of self-cleaning glasses.

7.3 Tests for evaluating the efficiency of photocatalysts

The air-purifying properties of products containing photocatalytic materials can be evaluated by different test methods. One of the most common methods for testing the performance of these products is based on the degradation of NO and/or NO_2 under defined conditions in a plug flow reactor. This method forms the basis for national and international standards on the evaluation of photocatalytic products having air-purifying properties. Although these standards aim on constant and repeatable measurements, their boundary conditions differ and hamper therefore a comparison of products tested according to different standards. A comparison of the boundary conditions is given in Table 7.1 for the international standard ISO 22197-1:2007 and the Italian standard UNI 11247:2007. Further differences in sample preparation, execution of measurements as well as their evaluation are addressed in the following.

Table 7.1: Comparison of standards applicable for determining air-purifying properties of products containing photocatalyst.

Condition	ISO 22197-1:2007	UNI 11247:2007	This research
Pollutant gas	NO	NO_x	NO
Supply concentration [ppm]	1.0	0.55 [‡]	1.0
Light source	UV-A	UV-A	UV-A
Irradiance E [W/m^2]	10.0	20.0	10.0
Flow rate \dot{V} [l/s]	3.0	5.0	3.0
Relative humidity RH [%]	50	50	50
Sample surface	49.5×99.5 mm	65 cm^2	100×200 mm
Exposition time [min]	300	variable [‡]	30
Evaluation	n_{NO} [μmol]	A_F [m/h]	η_{NO} [%]

[‡] Composed of 0.4 ppm NO and 0.15 ppm NO_2

[‡] Test lasts until a constant NO_x degradation is reached for at least ten minutes

7.3.1 ISO 22197-1:2007

The international standard ISO 22197-1:2007 is the approved version of the drafted standard of ISO TC 206/SC N. The drafted version of this standard is oriented on the withdrawn Japanese standard JIS TR Z 0018 that was replaced by JIS R 1701-1:2004. The main specifications of the standards ISO 22197-1:2007 are given in Table 7.1 and were adopted from the drafted version without significant modifications.

Besides the specifications given in Table 7.1, further requirements on the preparation of the sample and the test procedure are given. The sample is illuminated by UV-A light with an irradiance of $10 \text{ W}/\text{m}^2$ or higher for 5 h in order to decompose residual organic matter on the

samples surface prior the NO removal test. This process is followed by immersing the sample in deionized water for 2 h and the subsequent drying of the sample at 110 °C until constant mass is reached. The pretreatment of the samples is followed by the NO removal test. For conducting the measurement, the sample is placed in the reactor leaving a slit of 5 mm between the sample surface and the covering glass pane. The test gas is introduced in the sealed reactor according to the specifications given in Table 7.1 and the NO and NO₂ concentrations are recorded for the first 30 min without photo-irradiation. The pollutant concentration has to exceed 90% of the initial concentration after 30 min under dark conditions in order to proceed with the measurement. If the initial concentration is reached again, the test continues for 5 h and the sample is exposed to UV-A radiation within that time. The photo-irradiation of the sample is stopped after 5 h and the sample is exposed to the zero-calibration gas for further 30 min under dark conditions. The amount of NO removed by the tested sample is calculated by:

$$n_{NO} = (f/22.4) \int (\phi_{NO,in} - \phi_{NO,out}) dt \quad (7.7)$$

with

f	converted air-flow rate at standard state (0 °C, 101.3 kPa, dry gas) [l/min]
$\phi_{NO,in}$	NO volume fraction at the reactor inlet [μl/l]
$\phi_{NO,out}$	NO volume fraction at the reactor outlet [μl/l]

In a similar way to Eq. (7.7), the NO_x adsorption of the sample as well as the amount of formed NO₂ is calculated by integrating the relevant data over time. After the NO removal test is finished, the sample is immersed in purified water for an elution test. This elution test is conducted twice and each immersion cycle lasts for 1 h. The pH-value as well as the concentration of NO₃⁻ ions and NO₂⁻ ions in the two eluates is determined by liquid chromatography.

The data of a round-robin test performed by four laboratories are given in the appendix of ISO 22197-1:2007 and show a good repeatability and reproducibility of the NO removal test conducted according to the ISO standard.

7.3.2 UNI 11247:2007

The principle of NO degradation measurements in a plug flow reactor is also used by the Italian standard UNI 11247:2007 for the evaluation of air-purifying products. However, this standard differs to a large extent from the specifications given by ISO 22197-1:2007 (cp. Table 7.1). The main difference is caused by the pollutant gas, which is in this case a mixture of NO and NO₂ resulting in a lower total NO_x concentration than required by ISO 22197-1:2007. Besides the pollutant gas and its concentration, the specifications of the volumetric flow rate and the UV-A irradiance are higher than given in the ISO standard. Furthermore, the geometry of the plug flow reactor described by UNI 11247:2007 differs to a large extent from the ISO standard and is resulting therefore in turbulent flow conditions. A round vessel having a total volume of 3 liters and made of borosilicate glass is used as reactor. The sample is fixed 1 cm beneath the inlet of the pollutant gas in the middle of the reactor. The inlet and outlet of the pollutant gas are placed in the center of the side walls. The removal of inorganic or organic pollutants by means of an appropriate pretreatment of the sample prior the measurement is not required by the Italian standard.

Despite the differences in the specifications given by UNI 11247:2007 and ISO 22197-1:2007 and variations in the geometry of the reactor, the measurement on the pollutant degradation performance follows the same principle. According to the Italian standard, the initial concentration of the pollutant gas has to be adjusted to a stable concentration before the gas is entering the re-

actor. Therefore, a bypass of the reactor is used to ensure constant concentrations at the inlet and outlet of the reactor and to avoid premature pollution of the sample. The pollutant gas concentration has to be recorded for at least 10 min to ensure a stable inlet concentration. The adjustment of the initial pollutant concentration is followed by measurements conveying the controlled pollutant gas over the sample surface under dark conditions. A time range for this exposition under dark conditions, as for example given by the ISO standard, is not defined by the Italian standard. Solely, the pollutant concentration has to remain constant 10 min with an maximum error of 5%. After a constant pollutant concentration under dark conditions is achieved, the sample is exposed to UV-A light. This photo-irradiation lasts until a constant degradation level is obtained. The criterion for this is, again, defined by a constant concentration measured over a period of 10 min with an maximum error of 5%. A subsequent flushing of the reactor with a zero-calibration gas is not required. Furthermore, requirements on elution tests for determining the concentration of NO_3^- ions and NO_2^- ions are not given. The degradation performance of the tested sample is solely evaluated by the photocatalytic activity of the NO_x reduction for varying time intervals and follows from:

$$A_F = \frac{\dot{V} (C_{g,dark} - C_{g,light})}{C_{g,dark} S} I \quad (7.8)$$

with:

$C_{g,dark}$	NO_x , NO_2 and NO outlet concentrations under dark conditions [$\mu\text{g}/\text{m}^3$]
$C_{g,light}$	NO_x , NO_2 and NO outlet concentrations under photo-irradiation [$\mu\text{g}/\text{m}^3$]
S	Surface area of the sample exposed to NO degradation [m^2]
I	Non-dimensional intensity of the luminous flux
\dot{V}	Flow rate [m^3/h]

The non-dimensional intensity of the luminous flux introduced in Eq. (7.8) reflects the ratio of the intensity of the solar light at noon on an average day in July to the experimentally measured intensity I' . Assuming the intensity of the solar light to be $1000 \text{ W}/\text{m}^2$ in the entire spectrum, the non-dimensional intensity of the luminous flux follows from:

$$I = \frac{1000}{I'} \quad (7.9)$$

Statistical data that reflect the repeatability and reproducibility of the test method are not given by the Italian standard.

7.4 Development of an experimental setup

Constant and appropriate test conditions are required for conducting comparable and repeatable measurements. In addition to this, a reliable measuring procedure is necessary that provides an effective and product-independent evaluation of the relevant product characteristics. For that purpose, an experimental setup for measuring the NO degradation performance of photocatalytic concrete products was developed in collaboration with Hunger (2010). The developed test setup will be explained in detail in the following paragraph.

Up to the time the research on photocatalytic concrete products was started, no common or standardized measuring protocol or test setup was available. Consequently, a setup for measuring the NO degradation performance of photocatalytic concrete products was designed. The developed test setup as well as the suggested measuring protocol use the UV-A induced degradation

of NO as explained in Section 7.2.4. Furthermore, recommendations obtained from literature and the draft ISO TC 206/SC N provide a basis for the development of the test setup and the associated measuring protocol. The draft standard holds for advanced technical ceramics but it satisfies also the needs for measurements on photocatalytic concrete specimens. The recommendations given by the standard were largely followed and scaled according to the demands for measurements of photocatalytic concrete products. In addition, several technical improvements on the setup, obtained by measurements during the development phase, are implemented in the final design of the setup that is schematically depicted in Figure 7.4.

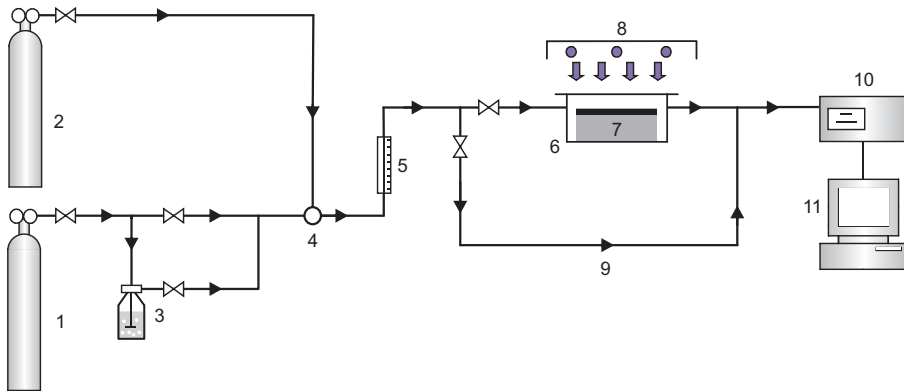


Figure 7.4: Schematic diagram of the test setup: 1) Synthetic air, 2) NO source, 3) Gas washing bottle, 4) Temperature and relative humidity sensor, 5) Flow controller, 6) Reactor cell, 7) Paving block, 8) Light source, 9) Bypass, 10) NO_x analyzer, 11) Computer (Hüsken et al., 2009a).

7.4.1 Reactor

The reactor forms the core of the experimental setup and was designed to allow a planar sample of the size 100 x 200 mm to be embedded and considers the size of standard concrete paving blocks. A schematic illustration of the reactor cell is given in Figure 7.5. The reactor is made from material that shows high UV-A resistance and that is non-absorbing to the applied pollutant gas. The reactor is tightly closed on top with a glass plate made from borosilicate glass that allows the UV-A radiation to pass through. The samples are fixed in the reactor that way that the resulting slit between the glass pane and the parallel surface of the sample can be adjusted in its height. The slit height H_{slit} can be varied between 2 mm and 10 mm. Unless not mentioned otherwise, a slit height of 3 mm is used for the tests described in the following.

The active sample area, available for the photocatalytic reaction, is deviating from the ISO draft and was enlarged from 49.5 mm in width and 99.5 mm in length to $B = 100 \text{ mm} \pm 0.5 \text{ mm}$ and $L = 200 \text{ mm} \pm 0.5 \text{ mm}$ considering similar tolerance. It is ensured by means of profiles and seals that the sample gas can only pass the reactor through the slit between the surface of the sample and the glass pane in longitudinal direction. All structural parts inside the box are designed to enable laminar flow conditions of the gas along the sample surface and to prevent turbulences.

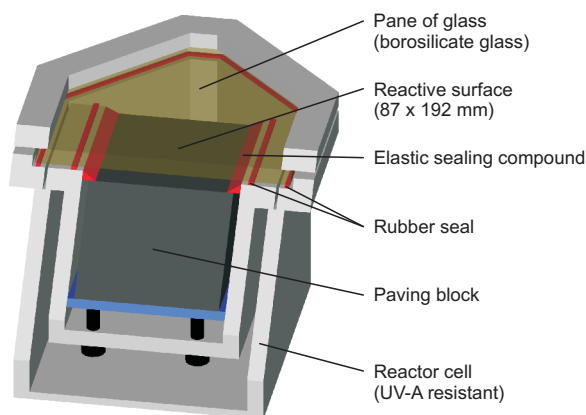


Figure 7.5: Schematic diagram of the reactor cell (Hüsken et al., 2009a).

7.4.2 Light source

The market of photocatalysts offers a number of varying powders that are available as doped and undoped TiO_2 . The use of undoped TiO_2 requires the application of UV-A light as the cut-off wavelength of conventional TiO_2 is around 380 nm and can be shifted to 535 nm for carbon doped TiO_2 (Blöß and Elfenthal, 2007). Therefore, the spectrum of the light source has to be adjusted according to the cut-off wavelength of the applied powder. This fact was considered by the development of the setup which allows for a swift replacement of the light source. Two separate light sources with different peaks in their emitted spectrum were selected. These are i) a UV-A light source (Figure 7.6a) for tests on undoped TiO_2 in the anatase modification and ii) a light source using standard fluorescent lamps (Figure 7.6b) for doped TiO_2 having a broader activation spectrum that covers also the visible light spectrum. An easy replacement of the light source is enabled by the setup.

The applied light source for measurements using UV-A radiation is composed of three fluorescent tubes of 25 W each, emitting UV-A radiation ranging from 300 - 400 nm with maximum intensity at about 345 nm. Due to the narrow range in the wavelength and the low heat release of the fluorescent tubes, an additional filter was not necessary. The standard fluorescent tubes of 18 W each emit cool day light in the range from 420 - 650 nm with three prominent peaks at 460 nm, 560 nm and 600 nm. The standard fluorescent tubes are standardized in their length and can therefore easily be replaced by other fluorescent tubes for indoor illumination having a different color spectrum. Warming of the reactor and the embedded sample by the light source is prevented by the spatial separation of the light source and the reactor. Furthermore, the fluorescent tubes are cooled by means of fans to prevent the heating of the light source.

All fluorescent tubes can be adjusted in their irradiance with a dimming electronic ballast that allows for an adjustment of the irradiance according to the required test conditions. The irradiance is adjusted to 10 W/m^2 at the sample surface in the case of UV-A fluorescent tubes by means of a calibrated UV-A radiometer. For adjusting the standard fluorescent tubes, two different types of sensors are available. The available sensors of the instrument measure either i) the irradiance for blue-green light ranging from 400 - 480 nm (VIS-BG) or ii) the illuminance of the incident light according to the day sensitivity curve of the human eye in the range of 440 - 650 nm (VIS-L). The sensors are equipped with an integrated diffusor for the cosine correction

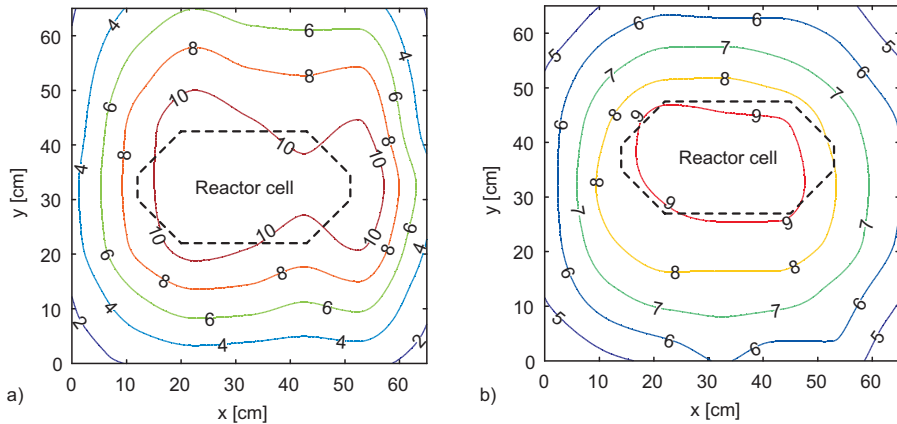


Figure 7.6: Light distribution of the applied light sources: a) UV-A source, and b) standard fluorescent tubes.

as necessary in the case of non-perpendicular irradiation. A lead time of about 15 minutes has to be considered for all fluorescent tubes until a stable radiation is achieved.

7.4.3 Testing gas supply

The evaluation of the air-purifying properties of photocatalytic concrete products is based on the degradation of nitric oxide (NO). Therefore, NO was chosen as model pollutant for conducting the experiments. As required by the draft ISO TC 206/SC N, the concentration $C_{g,in}$ of NO at the inlet of the reactor has to be 1 ppm. The model pollutant is provided in gas cylinders with a concentration of 50 ppm and is stabilized in nitrogen N_2 . In order to obtain the required concentration of 1 ppm, the model pollutant is mixed with a transport fluid. As transport fluid, synthetic air being composed of 20.5 V.-% of oxygen O_2 and 79.5 V.-% of nitrogen N_2 is deployed. Since both gases, pollutant and transport fluid, are provided in gas cylinders under high pressure, they have to pass a pressure reducing valve before entering the system. Here, the pressure is reduced to 0.3 bar and both gases, pollutant and transport fluid, are fed to the system via an adjustable flow controller. The concentration of the pollutant gas is adjusted to 1 ppm using a high precision valve that is placed in the NO line before the two gas flows are combined (see Figure 7.4). While adjusting the NO concentration to the desired value, the reactor can be bridged by a bypass in the system in order to avoid a premature pollution of the samples surface due to NO adsorption. The NO concentration is monitored during the adjustment of the system by a NO_x analyzer connected to the outlet of the gas supply unit.

Parallel to the NO line, the transport fluid is split in two flows and partly conveyed through a gas-washing bottle, filled with demineralized water, in order to adjust the relative humidity of the pollutant gas to 50%. The remaining second line of the transport fluid is not modified and controlled only by a metering valve. Before joined with the NO line, the dry and humidified line of the transport fluid are combined (see Figure 7.4). The gas, mixed and humidified as described before, enters the reactor via the inlet and is conveyed along the illuminated photocatalytic surface of the sample. The gas leaves the reactor at the opposite outlet and is transported to a flue or outside the lab with the help of an exhaust air duct. The NO_x analyzer samples the reacted test gas from the exhaust line. The installation of check valves in the exhaust line prevents the NO_x analyzer from sucking leak air.

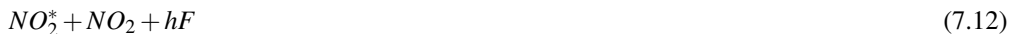
The volume flow \dot{V} of the pollutant gas is adjusted by means of an adjustable flow controller to 31/min. This volumetric flow corresponds to a flow velocity u_{air} of 0.17 m/s along the sample surface considering the geometric dimensions of the cross section, $B = 100$ mm and $H_{sli} = 3$ mm. The corresponding Reynolds number of the flow reads:

$$Re = \frac{u_{air} D_h \rho_{air}}{\mu_{air}} = \frac{2u_{air} H_{sli} \rho_{air}}{\mu_{air}} = \frac{2\dot{V}}{B v_{air}} \quad (7.10)$$

D_h is the hydraulic diameter of the considered cross section, defined as four times the cross-sectional area divided by the perimeter. It is assumed in the considered case that $B \gg H$ so that $D_h = 2H_{sli}$. Substituting $\dot{V} = 31/\text{min}$, $B = 100$ mm and $v_{air} = 1.54 \times 10^{-5}$ m²/s (1 bar, 20 °C) yields $Re \approx 65$. This low Reynolds number implies a laminar flow within the slit of the reactor. A fully developed parabolic velocity profile is developed at $L_d = 0.1ReH$ (Burmeister, 1993). For the given parameters of the slit, the critical length calculates to $L_d \approx 20$ mm. That means that only the first 10% of the slit are influenced by entrance effects and that a fully developed laminar flow profile appears during the remaining 90% of the reactor length.

7.4.4 Analyzer

The concentration of the pollutant gas is analyzed using a chemiluminescent NO_x analyzer as described in ISO 7996:1985. The chemiluminescence is based on the emission of non-thermal light ranging from 560 - 1250 nm. Light of a defined spectrum is emitted when NO₂^{*} in its excited state transforms to the de-excitation state (operation manual Horiba (2006)). This reaction occurs when NO/NO₂ reacts with ozone O₃. During this reaction, the NO is partly oxidized by O₃ to become NO₂. As mentioned before, part of the generated NO exists in an excited state and radiates light when it transforms to the ground state.



This reaction proceeds rapidly and only NO is involved in the reaction kinetics. For that reason, the NO_x analyzer separates the sample gas in two apart lines. In line one, NO₂ is reduced to NO by the NO_x converter and used for determining the NO_x concentration of the sample gas. The remaining second line deploys the sample gas for the direct measurement of the NO concentration. The required O₃ for the oxidation process is supplied by the ozone generator using dried ambient air.

O₃ is conveyed to the reaction chamber where also the sample gases are fed in alternating sequence by solenoid-controlled valves. The O₃ reacts in the reaction chamber with the sample gasses and the emitted light is detected by a photodiode with upstream optical filters. The output signal of the photodiode is proportional to the NO concentration. Evaluation electronics enables the output of the concentration of NO, NO₂ and NO_x as continuous signal that can be recorded over the measuring period. The gas sampling rate of the deploys NO_x analyzer amounts to 0.81/min and its detection limit is given with 0.5 ppb.

7.5 Measurements

For the sake of repeatability and accuracy, a defined measuring procedure using constant experimental conditions is necessary. By means of defined process conditions, photocatalytic concrete products can either be characterized with respect to their specific photocatalytic behavior or a comparison of different products is possible when all samples are tested under equal test conditions. Therefore, a measuring procedure was established that is based on the experience obtained

by several measurements carried out during the development phase of the test setup and recommendations of the proposed ISO standard ISO TC 206/SC N.

7.5.1 Measuring protocol

The basic scheme of a measurement is illustrated in Figure 7.7. The suggested measuring procedure distinguishes between a bridged and non-bridged flow (see Figure 7.4). The bypass of the reactor cell allows for a shorter and straightforward adjustment of the volumetric flow, pollutant concentration, and relative humidity. Once a stable pollutant concentration has been achieved, the bypass is closed and the pollutant gas flows through the reactor along the sample surface. Closing the bypass and introducing the pollutant gas to the reactor reduces the concentration $C_{NO,out}$ of the pollutant gas at the outlet of the reactor since the air containing no NO within the reactor has to be driven out and adsorption of NO will take place at the sample surface. After a short period of time, the surface of the sample is saturated and the NO outlet concentration $C_{NO,out}$ equals again to the inlet concentration $C_{NO,in}$. The measurement of varying samples having different surface texture showed that the area and amplitude of this adsorption curve in the beginning is strongly influenced by the surface texture of the sample. For standard flow conditions ($\dot{V} = 3\text{ l/min}$, $C_{NO,in} = 1.0\text{ ppm}$), a period of five minutes is considered to be adequate for obtaining the primary inlet concentration $C_{g,in}$ again. After the outlet concentration has reached 1.0 ppm again, the sample is exposed to UV-A light for the case of undoped TiO_2 . Tests of samples containing doped TiO_2 are performed with visible or UV-A light. The application of a combined light source emitting both visible and UV-A light is also possible but was not conducted in this research.

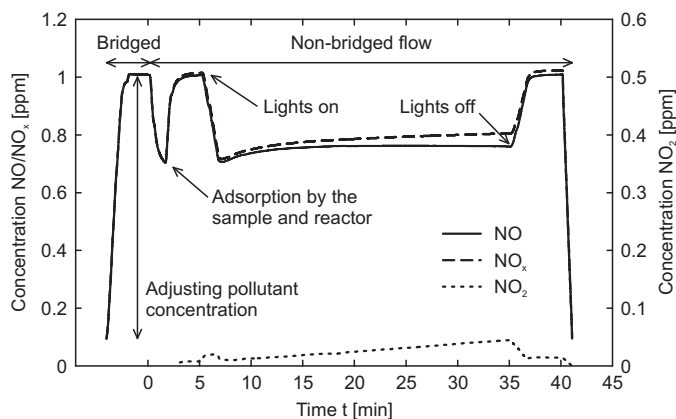


Figure 7.7: Sequence of a standard measurement (Hüsken et al., 2009a).

The exposition to an appropriate light source leads to an immediate decrease in the NO outlet concentration. This process of active degradation of the model pollutant is conducted for 30 minutes. At the end, the light source is switched off and the NO outlet concentration has to return to the original inlet concentration again. Here, a period of five minutes also proved to be sufficient, as the degradation of NO is not stopped immediately after switching off the light source. The reason for delayed degradation is explained by the inertia of the system. As a matter of principle, no conversion can take place after removing the light source. However, already formed hydroxyl radicals and other charged species can still start an oxidation of NO or NO_2

molecules. This process lasts till the hydroxyl radicals and other charged species are consumed completely. For this reason, the terminal degradation of NO and NO₂ without light exposure is not further assessed.

As far as not mentioned otherwise, the experimental parameters of the setup are oriented on the requirements given by the proposed ISO standard ISO TC 206/SC N and the measurements are conducted according to the measuring protocol described in this section. The following parameters are used for conducting the measurements:

- Pollutant concentration $C_{NO,in}$: 1.0 ppm
- Flow rate \dot{V} : 3.01/min
- UV-A irradiance E : 10 W/m²
- Relative humidity RH : 50%

It is agreed to apply a pollutant concentration of 1 ppm to the sample as recommended in the standard ISO 22197-1:2007. It is known that a pollutant concentration of 1 ppm is not representing the conditions at locations with high traffic loads. Here, hourly mean values ranges from 0.25 - 0.35 ppm during the rush-hour times. Temporary values up to 0.8 ppm can only be considered as peak value at locations with high traffic loads.

7.5.2 Analysis of the measurements

All samples have been tested according to the protocol described in the previous section. The further analysis of the obtained data is conducted following a three stage analysis. For this purpose, the course of the NO conversion is assessed for a time range of five minutes equally distributed over the period of active degradation. Figure 7.8 illustrates this procedure for the degradation of NO of an arbitrary sample. The NO removal rate η_{NO} in the assessed time range is calculated by the ratio of inlet concentration $C_{NO,in}$ to outlet concentration $C_{NO,out}$ as follows:

$$\eta_{NO} = 100 - \frac{C_{NO,in}}{C_{NO,out}} \times 100 \quad (7.13)$$

The NO concentration at the inlet and the outlet of the reactor as used in Eq. (7.13) is calculated by integrating the associated, descriptive function in the limits of time by using the trapezoid rule:

$$C_{NO} = \sum_{i=1}^n \frac{t_{i+1} - t_i}{2} (C_{NO,i} + C_{NO,i+1}) \quad \forall t_i \in [t_{beg}, t_{beg} + 5 \text{ min}] \quad (7.14)$$

This approach is assumed to be sufficiently precise, given the fact that the interval $[t_i, t_{i+1}]$ only lasts for 5 sec. In the same way, the NO₂ removal rate η_{NO_2} is computed. Furthermore, the yield η_{NO_x} of the NO_x degradation is calculated considering the conversion of NO and NO₂ as follows:

$$\eta_{NO_x} = 100 - \frac{C_{NO,out} + C_{NO_2,out}}{C_{NO,in} + C_{NO_2,in}} \times 100 \quad (7.15)$$

The first time interval for the beginning conversion $C_{NO,out,beg}$ starts immediately after the sample is exposed to UV-A or visible light for the first time and lasts for 5 minutes. Using this approach, the slope of the starting conversion up to the maximum degradation rate in the beginning is included and therefore characterizing this value. In other words, the progress of the degradation up to the maximum conversion is included and evaluated.

The second time frame represents the conversion after half of the total time of light exposure

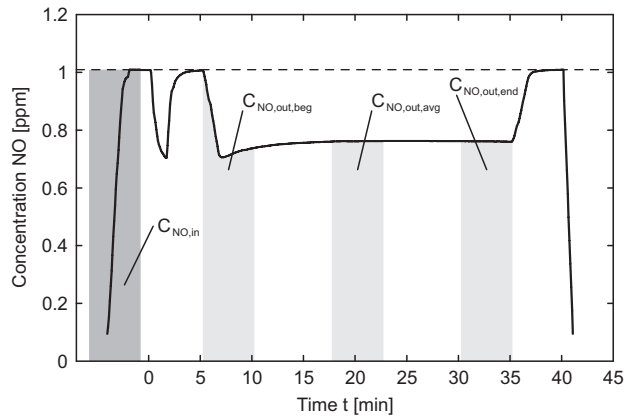


Figure 7.8: Basic scheme of data analysis.

when the degradation of NO has reached a constant value. This conversion is referred to as average conversion $C_{NO,out,avg}$. The average conversion is given by the chronological middle of the active light exposition ± 2.5 minutes.

For the last time interval, the conversion at the end of the measurement $C_{NO,out,end}$ is calculated. For that purpose, the last 5 minutes prior to the power-down of the light source are considered in order to avoid the influence of the delayed decrease of the conversion after the obvious inflection point. The conversion at the end of the measurement considers the agglomeration of reaction products at the active sites of the photocatalyst and determines the lowest value and is therefore used for the characterization of the NO degradation performance.

7.6 Influencing parameters

The performance of the photocatalytic reaction is governed by physicochemical parameters and their interaction. Changes of the physicochemical parameters have a strong influence on the reaction kinetics and the degradation of NO. In the following, an experimental survey of the influencing factors irradiance, relative humidity, pollutant concentration and flow rate is given. The influence of the before mentioned parameters on the photocatalytic reaction is investigated using a photocatalytic concrete paving block that showed sufficient degradation efficiency under standard test conditions. The sample was carefully cleaned after each measuring cycle and dried at 105°C for 24 hours. As not mentioned otherwise, the remaining process conditions of the conducted measurements are based on the suggestions given in Section 7.5 and kept constant at 50% relative humidity RH , 31/min flow rate \dot{V} , 1 ppm pollutant concentration $C_{NO,in}$ and 10 W/m^2 irradiance E .

7.6.1 Irradiance

The influence of the UV-A irradiance on the photocatalytic reaction of TiO_2 has been studied extensively in the literature (Herrmann et al., 2007; Lim et al., 2000; Obee and Brown, 1995; Ollis et al., 1991; Peral and Ollis, 1992). As mentioned in Section 7.2, the photocatalytic reaction is caused by the optoelectronic properties of TiO_2 in the anatase modification. According to the given explanation of the photocatalytic process, the UV-A light shows the most suitable range regarding the wavelength λ to start the PCO of undoped TiO_2 .

However, not only the wavelength of the light shows an impact on the system's efficiency,

but also the intensity of the electromagnetic radiation or so-called irradiance E influences the reaction kinetics to a large extent. This increase of the photocatalytic activity for increasing irradiance is divided by Herrmann et al. (2007) into two regimes: i) for $E \leq 250 \text{ W/m}^2$ the degradation increases proportional to E and ii) for $E > 250 \text{ W/m}^2$ the photocatalytic activity increases with the square root of E . These two regimes are also reported by Lim et al. (2000). In contrast to Herrmann et al. (2007), Lim et al. (2000) give a deviant value for the transition from first-order regime (linear behavior) to half-order regime (non-linear behavior) that ranges from $10 - 20 \text{ W/m}^2$. This value for the transition from linear to non-linear behavior is defined by Obee and Brown (1995) as one sun equivalent.

The cause for the transition from linear to non-linear behavior is explained by Jacoby et al. (1995) by the fact that the first-order regime is dominated by the consumption of electron-hole pairs as they are consumed more rapidly by the chemical reactions than by recombination. The photoefficiency³ in the linear regime is therefore nearly constant and not influenced by the irradiance E , whereas the recombination of holes and electrons is dominant for the half-order regime and leads to a decrease in the photoefficiency with increasing irradiance. The linear behavior for values of low irradiance, as described in the literature, could not be verified by own measurements. Figure 7.9 depicts the experimental results of NO and NO₂ degradation in dependence on the irradiance E . Detailed values of the conducted measurement are listed in Appendix G.1.

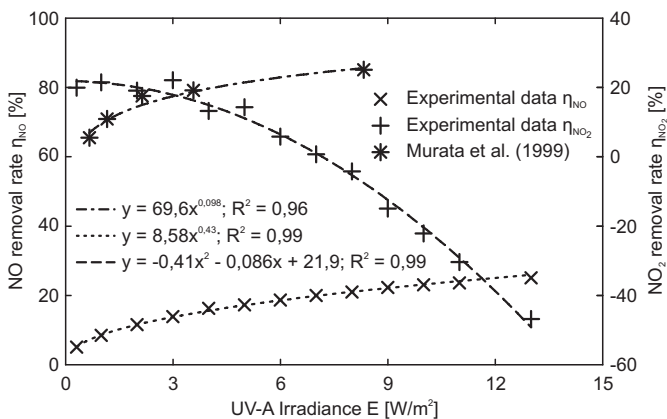


Figure 7.9: Influence of the UV-A irradiance on the NO and NO₂ degradation.

The NO removal rate depicted in Figure 7.9 show a similar trend as the data reported by Murata et al. (1999) for comparable measurements conducted on concrete paving blocks. The dependence of the NO removal rate on the irradiance E can be described by a power-law function of the type:

$$\eta_{NO} = \alpha_1 E^{\alpha_2} \quad (7.16)$$

³In this respect, photoefficiency is defined as the ratio of the number of converted molecules to the number of photons of sufficient energy (Jacoby et al., 1995).

A linear behavior can only be observed for values above 5 W/m^2 and is not confirmed by the experimental data for values lower than 5 W/m^2 . Furthermore, the data depicted in Figure 7.9 illustrate that the NO_2 removal rate η_{NO_2} is decreasing with increasing conversion of NO molecules in the considered case. This increase in the NO_2 concentration indicates that NO molecules are not completely degraded to NO_3^- ions and that desorption of stable intermediates occurs when higher removal rates are obtained. This fact was already addressed in Section 7.2.3 for the decomposition of organic compounds. However, the total NO_x degradation of the system, expressed by the yield η_{NO_x} , is still positive due to the low NO_2 concentration that was measured at the outlet of the reactor.

The configuration of the applied UV-A light source limits the irradiance on the sample's surface to 15 W/m^2 . This maximum irradiance is confirmed by own measurements conducted on a cloudy day in the Netherlands where values in the range of $7 - 16 \text{ W/m}^2$ were measured. Standard test conditions as described in Section 7.5.1 have been applied for the outdoor measurement, whereby solely the solar radiation was varying over time. The results of the outdoor measurement are depicted in Figure 7.10 and confirm the effectiveness of the PCO of NO at average solar irradiation.

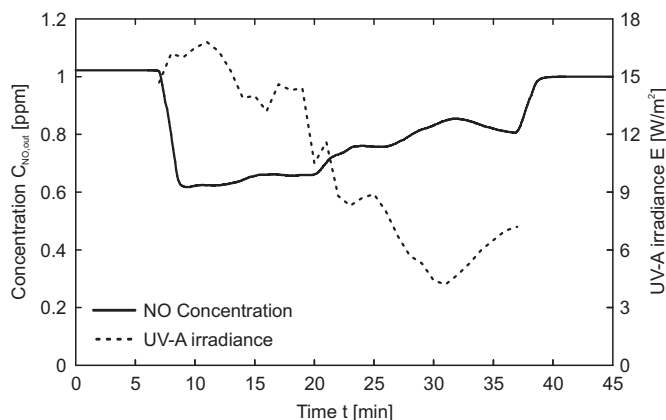


Figure 7.10: NO concentration versus present UV-A irradiance for an outdoor measurement.

The results of the conducted outdoor measurement show clearly the response of the system on variations in the irradiance. The delayed response of the system regarding NO degradation is caused by the inertia of the system and the time necessary for analyzing the test gas. Nevertheless, the NO removal rate η_{NO} amounts to about 40% for an irradiance of 16 W/m^2 and demonstrates that the functional capability of the photocatalytic reaction is ensured even for cloudy weather conditions with low UV-A irradiance. It is reported in the literature that the mean UV-A irradiance of a cloudless summer midday amounts to about 35 W/m^2 for Central Europe (Blöß and Elfenthal, 2007; Mills and Le Hunte, 1997), which enhances the efficiency of the PCO to a further extent.

7.6.2 Relative humidity

Besides variations in the UV-A irradiance, changes of the relative humidity have a major influence on the photocatalytic degradation of NO and can be caused in practice by changing weather conditions. According to Beeldens (2007), the conversion rate of the degradation process is reduced by increasing relative humidity of the test gas. This is a consequence of the hydrophilic effect at the surface of the photocatalyst which prevails over the oxidizing potential. This is line with findings reported by Hashimoto (2007) for the application of super-hydrophilic materials for the production of self-cleaning glasses or anti-fogging glasses and mirrors. The dependence of the NO removal rate η_{NO} on the relative humidity RH is depicted in Figure 7.11. In this context, values lower than 10% RH are not considered since water is essential for the formation of hydroxyl radicals (see Eq. (7.2)).

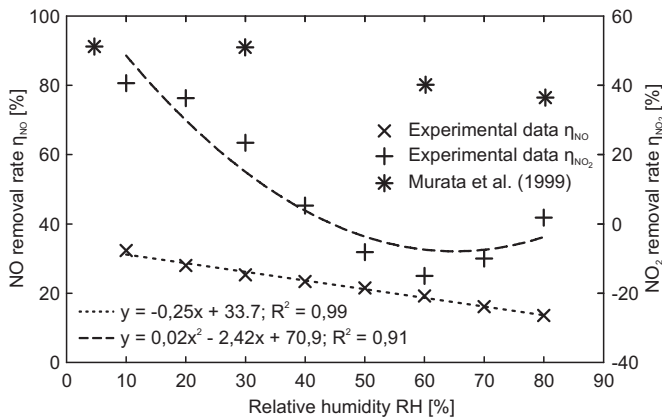


Figure 7.11: Influence of the relative humidity on the NO and NO₂ degradation.

It is evident from the experimental data that with increasing relative humidity the NO degradation decreases linearly, whereas the NO₂ removal rate shows a non-linear behavior. However, the values listed in Appendix G.3 demonstrate that for low relative humidity values NO₂ was degraded and that with increasing relative humidity less NO₂ was decomposed until the original NO₂ inlet concentration was obtained at a relative humidity of about 45%. Higher relative humidity than 45% was resulting in higher NO₂ outlet concentration than measured at the beginning, which indicates that NO₂ was generated due to an insufficient NO degradation.

Decreasing NO conversion for relative humidity higher than 50% is reported by Murata et al. (1999) for similar measurements conducted on concrete paving blocks. However, these findings are not in line with data reported by Devahasdin et al. (2003) who report increasing conversion rates up to 50% RH and a steady state behavior up to 75% RH . A possible explanation for the difference in the NO degradation performance is given by the higher pollutant gas concentration of 40 ppm NO used by Devahasdin et al. (2003) and the higher catalyst loading of about 1.0 mg/cm². The corresponding values of the own experiments amount to 1.0 ppm pollutant concentration and a catalyst loading⁴ of about 0.3 mg/cm². The higher NO concentration re-

⁴The catalyst loading is given by Devahasdin et al. (2003) for a brush coated sample, whereas the TiO₂ is mixed in bulk in the mortar layer of the own samples. The TiO₂ content of the produced mortars amounts to 30 mg/cm³ which

sults, according to Devahasdin et al. (2003), in a higher probability for the NO molecules to be absorbed at the active sites of the catalyst.

Besides the controversial discussion on the effect of water vapor on the photocatalytic reaction, it can be stated that water molecules compete with the reactants for active sites on the photocatalyst surface (Beeldens, 2007; Devahasdin et al., 2003; Zhao and Yang, 2003), which prevents the pollutant molecules to be adsorbed onto the catalysts surface and further reactions are, therefore, hampered or blocked.

7.6.3 Pollutant concentration

The pollutant concentration effects the NO degradation to a large extent and is an important factor for the comparison of degradation performance of photocatalytic concrete products. Figure 7.12 shows the influence of varying NO inlet concentrations on the NO removal rate. Increasing inlet concentrations of the pollutant result in lower removal rates, whereas lower pollutant concentrations are performance enhancing. Furthermore, variations of the pollutant concentration in the lower range result in remarkable higher changes of the NO conversion than changes in the range of higher concentrations. This fact indicates that the PCO is limited by an equilibrium. This is in line with observations reported by Herrmann et al. (2007) and Devahasdin et al. (2003).

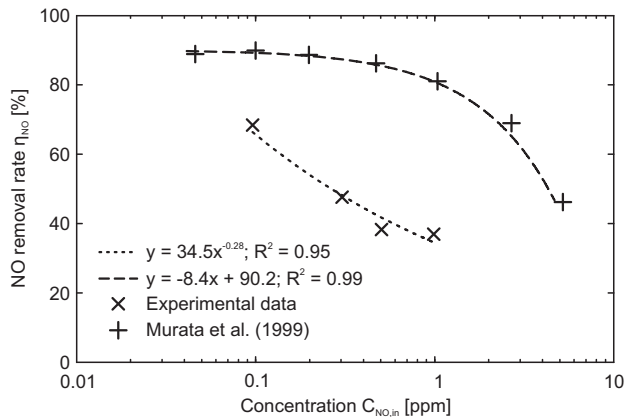


Figure 7.12: Influence of the pollutant concentration on the NO degradation.

7.6.4 Flow rate

The residence time of a pollutant molecule within the system influences, as well as the pollutant concentration, the number of available molecules with possible contacts to the active sites of the photocatalyst. The retention time of a pollutant molecule in the system is directly related to the flow rate \dot{V} of the pollutant gas. Figure 7.13 shows the experimental results for varying flow rates and their influence on the NO degradation.

High flow rates reduce the residence time of the pollutant molecules on the active sites of the photocatalyst. Furthermore, the number of pollutant molecules per time unit increases with

corresponds to a catalyst loading of 0.3 mg/cm^2 assuming a thickness of $100 \text{ }\mu\text{m}$ of the active layer that is involved in the photocatalytic reaction. The catalyst loading is even lower if the thickness of the active layer becomes smaller than $100 \text{ }\mu\text{m}$.

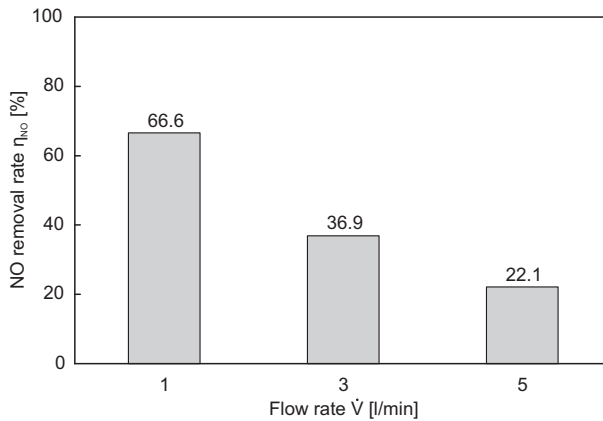


Figure 7.13: Influence of the flow rate on the NO degradation.

higher flow rates while the number of possible contacts at the active sites of the photocatalyst is limited by the equilibrium. Hence, the degradation rate is subsequently reduced, whereas lower flow rates enhance the degradation rate by a longer residence time of the model pollutant within the system. Various flow rates can be realized under laboratory conditions, which result in unequal conditions that are not suitable for comparative tests and, therefore, constant test conditions as suggested in Section 7.5.1 are required. The residence time of the pollutant molecules at the active surface of the concrete paving blocks varies also under outdoor conditions extensively as wind speed and wind direction are not constant under practical conditions. In this respect, the wind speed shows more relevance on the residence time than the wind direction and needs to be considered for an appropriate modeling of the NO degradation process.

7.6.5 TiO₂ related properties

Besides varying process conditions, the influence of product related parameters such as type of TiO₂, fineness, content, and application technique influence the efficiency of the PCO. Hence, the effects of parameters that are related to the applied photocatalyst and its application technique have been investigated and will be discussed in this section.

Mortars containing 3%, 5% and 10% TiO₂ have been produced to investigate the influence of the fineness and the TiO₂ content on the NO degradation performance. The mix design of the composed mortars is given in Table 7.2. In addition, the application technique of the photocatalysts as dry powder or as water based suspension was investigated by experiments under laboratory conditions. The dry powder was added to the mix with the binder, whereas the suspension was added with the mixing water. The TiO₂ content of the mixes using the photocatalyst in suspension form was adjusted by the dosage of the suspension and equals to the comparable mixes that are based on dry powders. The TiO₂ suspensions were produced under laboratory conditions by high-speed stirring and parallel ultrasound treatment.

The TiO₂ content of the produced mortars is related to the binder content which is chosen to be equal for all tested powders. Samples having a dimension of 100 × 200 × 20 mm have been produced and prepared after hardening for the tests on NO degradation. The bottom side of the hardened slabs was sandblasted in order to remove a covering cement layer from the TiO₂ particles and to roughen this side. The top side of the cast slabs was ground to smoothen this surface. The produced and pretreated slabs were tested according to the measuring protocol

Table 7.2: Mix proportioning of tested mortars using TiO₂ A-E (see Table 2.5).

Material	3% TiO ₂	5% TiO ₂	10% TiO ₂
	[kg/m ³]	[kg/m ³]	[kg/m ³]
CEM I 52.5 N	600.0	600.0	600.0
Sand 0-2	1300.0	1300.0	1300.0
TiO ₂	18.0	30.0	60.0
Water	250.0	250.0	250.0
Total	2168.0	2180.0	2210

described in Section 7.5.1.

The obtained NO removal rates for samples containing 3% TiO₂ added in suspension form are shown in Figure 7.14. The experimental data show a clear dependence on the fineness of the applied TiO₂ (cp. Figure 7.14 and Table 2.5). This is in line with the expectations caused by the higher specific surface area of e.g. TiO₂ C, which is about 30% higher than the surface area of TiO₂ B.

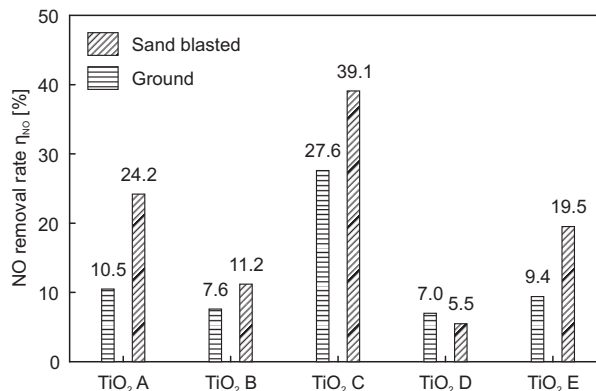


Figure 7.14: Influence of the powder type on the NO degradation of mortar samples containing 3% TiO₂.

The performance of the NO degradation increased for the doped TiO₂ E. This modified powder uses UV-A radiation as well as parts of the visible light spectrum for activating the photocatalyst (see Figure 7.15). Although the contribution in the visible light spectrum (measuring range of the VIS-L sensor 500–640 nm) is marginal, the UV-A radiation is used more efficiently in the higher UV-A range ($\lambda < 380$ nm) and the lower range of the visible light spectrum ($\lambda < 500$ nm) as the photocatalytic activity is enhanced in this range and increases the overall performance of TiO₂ E (Blöß and Elfenthal, 2007).

The efficiency of the PCO is not only influenced by the fineness of the powder or the type of photocatalyst, but shows also a dependence on the powder content. The NO removal rates

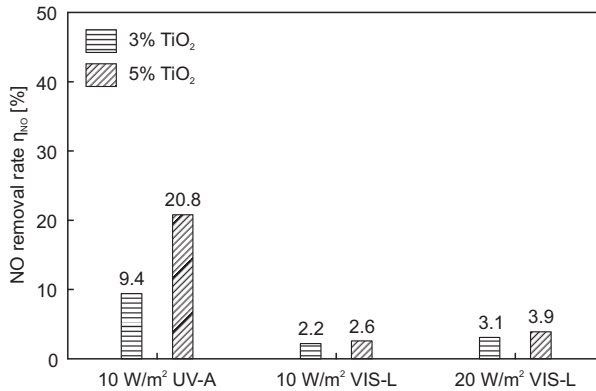


Figure 7.15: Influence of the light spectrum on the NO degradation of a sample containing TiO₂ E (carbon doped).

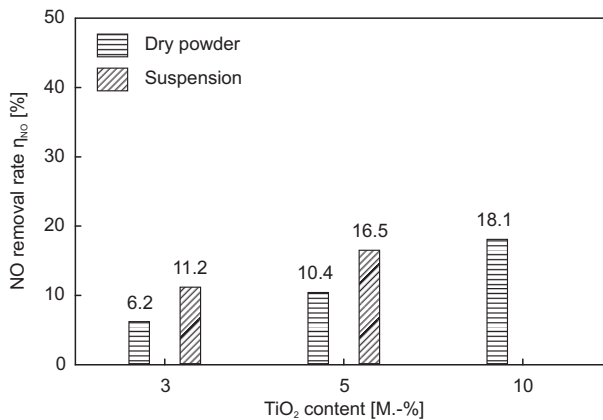


Figure 7.16: Influence of the application technique and TiO₂ content on the NO degradation.

for varying powder contents are depicted in Figure 7.15 and Figure 7.16. Both figures clearly show that with increasing powder content the NO degradation also increases. Furthermore, it is obvious from Figure 7.16 that higher removal rates are obtained when the powder is applied as suspension. The advantage of a better distribution of the powder is illustrated by the higher removal rates of the slabs containing 3% and 5% TiO₂ in suspension form. Hence, the application of the powder as suspension added to the mixing water allows for a better and more homogeneous distribution of the photocatalyst.

7.7 Conclusions

In the present chapter, the principles of the photocatalytic reaction of TiO_2 were addressed and the influence of variations of physicochemical parameters on the photocatalytic oxidation of NO were investigated. Based on the findings reported in the literature and new experimental results, the following conclusions can be drawn:

1. The principles of the photocatalytic oxidation of organic and inorganic compounds provides a suitable method for the degradation of NO_x and was proven to work effectively under laboratory conditions. The application of photocatalytic materials in concrete mass products like paving blocks or paving slabs provides a sustainable solution for air purification in metropolitan and urban areas where the exceeding of limiting values poses a serious problem during the rush hour.
2. The formation of charged species with a strong oxidizing potential is not only beneficial for the degradation of inorganic air pollutants, but can also prevent the soiling of concrete products by algae growth. Moreover, the original appearance of buildings is preserved.
3. A test setup was developed to determine the NO degradation performance of concrete products containing photocatalytic materials. The developed test setup allows, in combination with the suggested measuring protocol, for comparative measurements on photocatalytic concrete products using constant boundary conditions.
4. The NO degradation performance of the analyzed samples is influenced by a number of physicochemical parameters which have to be considered for an appropriate evaluation of the air purifying properties of photocatalytic concrete products. The importance of constant test conditions is also reflected by the international standard ISO 22197:2007 and the Italian standard UNI 11247:2007. However, both standards demand a different sample preparation and conduction of the measurements.
5. With respect to the number of influencing parameters and their major influence on the measurement results it is advisable to agree a common test procedure using equal boundary conditions. Based on these findings as well as specifications in the literature and standards, a suitable test procedure for the evaluation of concrete paving blocks is suggested.
6. The UV-A irradiance shows a major influence on the NO degradation performance of photocatalytic concrete products. Increasing UV-A irradiance is resulting in higher NO removal rates as the number of electron holes increases. The formed electron holes are important for further reaction that occur on the catalysts surface.
7. Although water is needed for the PCO, increasing relative humidity shows a negative effect on the NO degradation performance of photocatalytic concrete products as water molecules and pollutant molecules compete for the same active sites on the catalyst surface. In the same way, the degradation of NO_2 was affected and additional NO_2 was generated under certain boundary conditions, which indicates an interaction of NO and NO_2 in the degradation process.
8. The pollutant concentration as well as the flow rate of the pollutant gas determines the number of contacts of the pollutant molecules with the active sites of the photocatalyst. Higher pollutant concentrations result in lower NO removal rates as the total number of pollutant molecules in the system is increasing, whereas the number of active sites of the photocatalyst remains constant. The same principle applies for increasing flow rates. Here, higher flow rates result in lower NO removal rates.
9. The dosage of the TiO_2 and its fineness is influencing the number of active sites available on the product surface. Higher concentrations of the catalyst result in higher NO removal rates as the number of active sites increases. The same fact holds for powders with higher fineness. Furthermore, it became obvious that the fineness of the powder has a larger influence on the NO degradation performance than the catalyst dosage.

10. The application technique of the TiO_2 has a great influence on the NO degradation performance. The experimental results illustrate that higher NO removal rates are obtained when the powder is added as water based suspension. The application technique becomes more important for powders with a high fineness. Here, a better and more homogeneous distribution of the powders is obtained when the photocatalyst is applied as suspension and not as dry powder. The appropriate production of the suspension by means of high energy mixing and ultrasound treatment improves the stability of the produced suspension and prevents the formation of agglomerates.

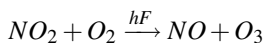
Application of photocatalysis to concrete products and its modeling ¹

8.1 Introduction

The emission of air pollutants is one of the major problems in metropolitan and urban areas and more efforts towards innovative solutions for improved air quality will be made in the coming years by the public authorities. In Europe, these efforts are related to reduced limiting values given by the European Council Directive 1999/30/EC, on the one hand, and increasing traffic rates on the other. Despite the intensifying installation of systems for emission control and reduction, air pollution, and in particular the pollution by NO and NO₂, will remain a serious issue in the near future. NO and NO₂ are mainly generated as by-product of combustion processes when nitrogen (N₂) contained in the air is oxidized. The highest NO concentrations can be found at the outlet of a chimney or exhaust pipes of diesel powered passenger cars and freight vehicles. Here, exhaust fumes are emitted that contain more than 90% NO which is rapidly oxidized in the atmosphere to more harmful NO₂ (HLUG, 2009). Part of the NO₂ contained in the atmosphere is oxidized by further reactions to nitrate (NO₃⁻) or removed from the atmosphere due to adsorption by fine particles. The literature gives a residence time for NO₂ in the atmosphere of 2 - 5 days. Pure NO is hardly removed from the atmosphere by rain. The main contribution to acid rain results therefore from the formation of NO₃⁻ in the atmosphere.

The damaging effect of NO₂ results from its strong oxidizing and corroding potential. The harmful influence of higher NO_x concentrations, especially NO₂, to health and environment is known and manifold documented (HLUG, 2009). The longer exposition to high concentrations of NO₂ causes chronic obstructive pulmonary disease and a higher sensibility against respiratory infections. Moreover, NO₂ has also a negative impact on plants as here the upper cell layers of the leaves are damaged. The damage to forests is in many cases related to the emission of NO_x and its contribution to acid rain. Acid rain damages not only the environment, but has also a harmful impact on buildings as it is affecting metals and mineral based building materials.

The formation and degradation of tropospheric ozone (O₃) is also influenced by NO_x emissions. Two opposing chemical reactions occur depending on the sun intensity and the presence of organic species in the atmosphere. The formation of tropospheric O₃ according to Eq. (8.1) is strongly coupled on the presence of partly oxidized organic species or peroxide radicals. These species react with the NO to form NO₂ that undergoes a further reaction under the presence of sunlight to form O₃.



¹Parts of this chapter were published elsewhere (Hunger et al., 2008a,b, 2010; Hüsken et al., 2008, 2009a,b).

Simultaneously, NO is also involved in the degradation of O₃:



The formation of O₃ (Eq. (8.1)) and its degradation (Eq. (8.2)) result in a closed cycle with constant O₃ concentration, which depends only on the intensity of the sunlight and the presence of radicals. However, different O₃ concentrations in urban and rural areas are observed during summer time. This fact results from the faster O₃ degradation in urban areas due to the enhancing effect of emitted NO, whereas in rural areas less NO and more VOCs, e.g. terpene from trees, are emitted that contribute to the O₃ formation and its delayed degradation in these areas.

The NO_x concentration in urban areas is strongly influenced by the emitted pollutants of the local traffic during the rush hours (cp. Figure 8.1). The local traffic is by far the major source for the emission of NO_x in urban areas. Other sources, such as industry and heating systems, have a minor influence on the local NO_x concentration as they contribute to the constant urban background pollution.

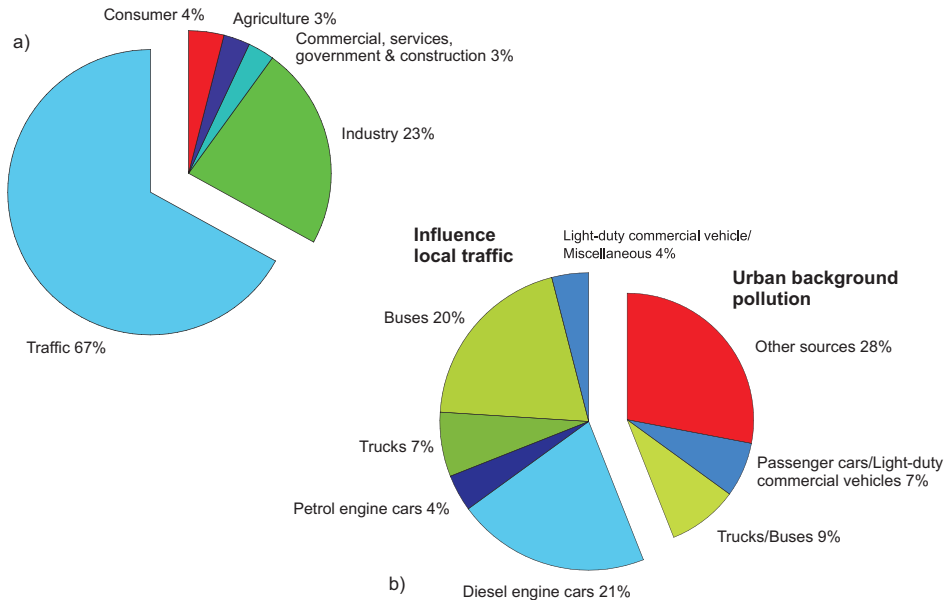


Figure 8.1: Sources of NO₂ emission: a) total emissions for the Netherlands, and b) contributory factors at a monitoring site located in central Stuttgart “Stuttgart-Mitte” (Lahl and Lambrecht, 2008).

Different attempts are given in the literature for the reduction of NO_x emissions. An active reduction of NO_x emissions is obtained by filters for industrial stacks (denitrogenation - DeNO_x plants) or active filter systems for ventilation outlets of tunnels. These methods are effective in reducing the urban background concentration but show no effect on the high NO_x concentrations in areas with high traffic loads. Here, an effective reduction of the peak values is obtained by the photochemical conversion of NO_x to low dosed nitrates and is suggested, among others, by

Matsuda et al. (2001); Murata et al. (1999) and Zhang et al. (2001).

A variety of products containing TiO_2 for the photochemical conversion of NO_x are already available on the European market and their working mechanism under laboratory conditions is proven as demonstrated in the previous section. In the following, the test results of a selection of existing and newly developed concrete products with air-purifying properties, tested under constant laboratory conditions, are compared regarding their NO_x removal efficiency. This comparative study is extended by the development of own top-layer mixes for the production of air-purifying concrete paving blocks used in a demonstration project in the Dutch city of Hengelo. In addition to the comparative study, a model for the degradation of NO is proposed on basis of the Langmuir-Hinshelwood kinetics, which can serve as input for computational fluid dynamic simulations of urban areas.

8.2 Comparative study on concrete paving blocks

A comparative assessment of different products regarding their efficiency was not carried out in the past. There is no doubt about the working mechanisms of the photocatalytic reaction under laboratory conditions, but there are still open questions regarding the efficiency of different products and their usefulness for practical applications. The comparison of different products is rather difficult as different test procedures are used by the manufacturers (cp. Section 7.3). These test procedures differ in their execution and their underlying test conditions. A comparison of different products based on data given by the literature or company information is therefore questionable. Hence, a representative profile of economically available products of the European market was selected and tested in the laboratory under equal test conditions.

8.2.1 Patent situation

The application of TiO_2 for the production of concrete paving blocks is patent-protected for the European market. Two different patents are of interest for the development and production of photocatalytic concrete products in this field. The use of TiO_2 in concrete paving blocks is patented by Murata et al. (1997) for Mitsubishi Materials Corporation. Furthermore, a patent is held by Cassar and Pepe (1997) for Italcementi S.p.A. on the use of TiO_2 in a premixed binder for the production of concrete paving blocks and concrete paving tiles. These two patents claim the main conditions for the production of photocatalytic concrete products applicable for the paving of traffic areas.

The patent held by Mitsubishi Materials Corporation is based on the early developments in the field of air-purifying pavements reported by Murata et al. (1998) and comprises the application of TiO_2 in the functional surface layer of a double-layer paving block having enhanced NO_x degradation capability. The patent describes explicitly the decomposition of NO_x by TiO_2 and sunlight – specifically UV light. The thickness, porosity as well as the surface texture of the surface layer is claimed by the patent. Furthermore, the patent claims the concentration of TiO_2 , the additional use of appropriate aggregates having high NO_x adsorption properties, and the application of light transmitting aggregates.

The claims in the patent of Italcementi S.p.A. cover in a broader range the application of suitable photocatalytic particles, most preferably TiO_2 , in concrete paving tiles capable of oxidizing polluting substances present in the environment. Actually, the patent is not claiming the degradation of NO_x or other pollutants, but is rather describing the oxidation of polluting substances present in the environment to maintain the brilliance and color quantity of the product after installation. The patent describes further the application of the photocatalytic material in mass with respect to the amount of cement or binder used. Moreover, the patent claims the composition of a dry premix containing a hydraulic binder and a TiO_2 based photocatalyst capable of oxidizing organic and inorganic pollutants to maintain the original brilliance and color quantity. For a better understanding, a tabular comparison of both patents is given in Appendix F.

8.2.2 Characteristics of the tested samples

Regarding the current market situation, a variety of cement-based products containing TiO_2 are available on the European market for horizontal and vertical applications. The field of photocatalytic concrete products ranges from concrete paving blocks and paving tiles to noise barriers and cementitious asphalt slurry seals. Even concrete roofing tiles containing TiO_2 are produced. These products show varying amounts of TiO_2 , having preferably the active anatase structure, but also the application of blends of titanium dioxide having anatase and rutile structure is comprised in the patents. Most of the photocatalytic concrete products are promoted regarding their photocatalytic capabilities under laboratory conditions.

Different concrete products containing TiO_2 were selected for the comparative assessment of the air-purifying properties. Most of the received samples are concrete paving blocks produced according to the regulations of the before mentioned patents. In addition, a sample of a product usually used for asphalt sealing was tested as this product also shows air-purifying properties. It is assumed that the European market of photocatalytic concrete paving products is sufficiently covered by this survey. In Table 8.1, the denomination and description of the tested samples is given.

Table 8.1: Denomination and origin of tested concrete samples.

Denomination	Samples	Sample type	Origin
D1.1 - D1.2	2	Paving block	Taken from uncovered outside storage
D2.1 - D2.2	2	Paving block	Taken from outside testing area
D3.1 - D3.3	3	Paving block	Samples withdrawn from production
D4.1 - D4.3	3	Asphalt slurry seal	Thin slab of cast pure slurry
D5.1	1	Paving block	Samples withdrawn from production

Samples of the series D1, D2, D3 and D5 are paving blocks received from different producers. The tested paving blocks are produced in double-layer technique having an economically priced core mix and a high-quality top-layer mix containing the photocatalyst and satisfying all esthetic requirements. The samples of the series D1 and D2 were stored outside for almost one year (D1) and almost two years (D2), whereas the samples from series D3 and D5 were taken directly from the production.

The material used for the samples of series D4 represents a slurry that is used to fill the open cavity of asphalt roads and is therefore not considered as material for sett paving. It is a cementitious suspension consisting of cement, water, TiO_2 , a fine sand fraction, and other admixtures. This slurry is mixed on-site and deployed on asphalt pavements to fill the open voids connected to the surface. After the application of the slurry, a thin cement layer covers the asphalt pavement. This layer is removed within a short period of time depending on the traffic load and other parameters. The polishing effect of the wheel loads removes the hardened material in layers. The matrix of the asphalt appears again and at a certain point of use, the asphalt matrix bears all loads and the removal rate of the cement layer slows down to marginal magnitudes. Hence, only a certain percentage of the total surface can be considered to be covered by the photocatalytic material and to be an active surface. This situation should preferably be the starting point for comparative measurements. However, the slurry producer provided thin slabs, cast purely from this material. For this reason, the whole surface is considered to be active. Furthermore, the surface structure of the cast slabs shows distinct differences in its surface texture and roughness. As the samples are made of a slurry consisting of fine ingredients only, the top side is plain and smooth, whereas the backside shows a certain roughness. The rougher backside

is assumed to represent the outside situation best and was therefore tested with respect to its NO_x degradation performance.

8.2.3 Mineralogical composition

The chemical composition of the tested concrete paving blocks was determined by means of XRF analysis to compute the TiO₂ content of the samples. This procedure was necessary as information on the TiO₂ content of the samples were not provided by paving block producers. Therefore, a reference mortar was produced with known TiO₂ content and analyzed by XRF to allow for a backward calculation of the TiO₂ content of the analyzed samples. The mortar of the analyzed reference samples was produced according to the mix proportioning given in Section 7.2 for mortars having TiO₂ of 10% per kg binder. Two different photocatalysts, TiO₂ B and TiO₂ C as given in Table 2.5, were applied for the reference samples to investigate the accuracy of the XRF analysis and a possible influence of the powder type on the results of the XRF analysis. This way, it was possible to calculate the unknown TiO₂. The calculated TiO₂ contents of the tested samples are listed in Table 8.2 and detailed values are given in Appendix A.3.

Table 8.2: TiO₂ content of tested concrete paving blocks and reference mixes (Pöllmann, 2007).

	D1	D5	Ref1 [‡]	Ref2a [‡]
TiO ₂ (XRF) [%]	1.16	0.91	2.40	2.43
TiO ₂ [kg/m ³]	29.0	22.8	60.0	60.0
TiO ₂ [#] [M.-%]	–	–	2.71	2.71

[‡] containing TiO₂ B

[‡] containing TiO₂ C

[#] based on the total mass inclusive mixing water

The data obtained by the XRF analysis show that both photocatalysts, TiO₂ B and TiO₂ C, result in almost equal TiO₂ contents for the reference samples with known and fixed TiO₂ content. This fact confirms the suitability of the test method for the backward calculation of the unknown TiO₂ content of the tested paving blocks. The calculated TiO₂ contents of the tested samples, D1 and D5, are also presented in Table 8.2. It is assumed that the calculated values reflect the content of TiO₂ in the anatase modification as other crystalline modifications of TiO₂ cannot be distinguished by XRF analysis. Furthermore, a characterization of the tested samples regarding their TiO₂ percentage by mass of the binder is not possible as data on the total binder content of the top-layer mixes were not provided by the paving block producers.

8.2.4 Experimental results and discussion

Prior the measurements, the samples were brushed and rinsed with tap water in order to remove pollutants that adhere to the surface. After the cleaning, the samples were dried at 105 °C until constant mass was reached. The pretreated samples were tested at 21 °C according to the measuring protocol described in Section 7.5.1 and further analyzed following the three stage analysis explained in Section 7.5.2. The data of the considered intervals are listed in Table 8.3 and the NO degradation performance of selected samples is depicted in Figure 8.2.

The obtained data show a wide spectrum of NO degradation. Samples of the series D2 achieved the by far highest NO removal rates of about 40% and show therewith the highest air-purifying potential. These results are followed by samples of the series D4 with a NO removal rate of about 33%. Here, it has to be noticed that for later application of this slurry seal the active surface is reduced by the percentage of the asphalt matrix. The samples of the series D4 represent

Table 8.3: NO removal rates of tested samples.

Sample	NO removal rate [%]			Sample	NO removal rate [%]		
	$\eta_{NO,beg}$	$\eta_{NO,avg}$	$\eta_{NO,end}$		$\eta_{NO,beg}$	$\eta_{NO,avg}$	$\eta_{NO,end}$
D1-1	14.2	15.9	15.9	D3-3	5.2	6.6	6.7
D1-2	7.0	8.3	8.2	D4-1 (coarse)	31.0	34.0	32.2
D2-1	41.1	44.6	42.4	D4-1 (fine)	2.1	2.8	2.7
D2-2	37.6	41.3	38.7	D4-2 (coarse)	32.4	33.5	30.9
D3-1	5.0	6.6	6.6	D4-3 (coarse)	32.3	37.7	36.4
D3-2	5.2	6.6	6.5	D5-1	2.5	4.0	4.1

therefore a situation which is not comparable with the surface condition of the later application. A sample of cut asphalt being in service already for some time is therefore necessary for a direct comparison with the concrete paving blocks. A notably lower NO removal rate was obtained by the samples of the series D1 that showed an average NO removal rate of about 12%. This series showed also the largest deviation within the measured data. The lowest NO degradation was obtained by samples of the series D3 with a NO removal rate of about 6% and samples of the series D5 with about 4%. Considering these low NO removal rates, it is questionable if the increased production expenses and the likely higher market price are justified by the low air-purifying performance of these paving blocks.

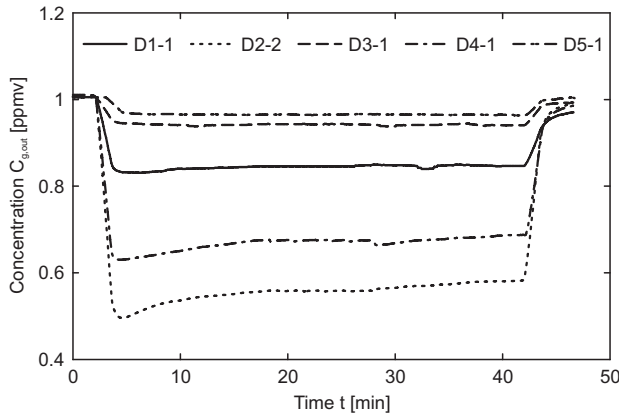


Figure 8.2: Degradation of nitric oxide over time for the tested concrete samples.

As mentioned before, a relation was found between the progress of the NO degradation in the beginning with its maximum NO removal rate and the decline of NO degradation during the measurement (see Figure 8.2). It was noticed for all samples that with higher maximum NO removal rates in the beginning, the initial conversion progresses faster and that the decline over time becomes more apparent. The observed decline of the NO degradation maintained a constant level in all cases.

8.3 Development of new top-layer mixes

The experimental results on the influence of varying types of TiO₂ discussed in Section 7.6.5 and the insights of the comparative study presented in the previous section form the basis for the development of new top-layer mixes for the production of concrete paving having air-purifying properties. The NO degradation performance of the developed mortars was tested both on samples produced in the laboratory and concrete paving blocks manufactured on industrial scale.

8.3.1 Composed mixtures

The development of new top-layer mixes was influenced by the application of different pigment types, as colored concrete paving blocks are used to fulfill the enhanced aesthetic and architectural requirements in inner-city areas. The application of pigments helps to integrate a concrete paving within an already existing architectural situation or offers the possibility to put emphasis on the paving. This meets the public perceptions regarding aesthetic quality of public places but also causes problems when photocatalytic materials with high fineness are applied. Problems mainly result from the increased water demand when further particles with high fineness are added.

The influence of red pigments on the NO degradation performance was first studied on laboratory scale using one of the mortars discussed in Section 7.6.5 and having a TiO₂ content of 3% (Reference). The water content of the reference mortar was reduced in comparison to the original mix proportioning given in Table 7.2 and two different pigments were added to the mix. In addition to this, two further mixes, Pig3 and Pig4, with higher TiO₂ content and available materials from a paving block producer were designed. Besides the higher TiO₂ content, these mixes are characterized by higher pigment contents in order to compensate the desaturating effect of the white TiO₂ on the color of the pigments. The detailed mix proportioning of the designed mortars is given in Table 8.4.

Table 8.4: Mortar composition of tested top-layer mixes.

Material	Reference	Pig1	Pig2	Pig3	Pig4/Pav1
	[kg/m ³]	[kg/m ³]	[kg/m ³]	[kg/m ³]	[kg/m ³]
CEM I 52.5N	600.0	600.0	600.0	–	–
CEM III/A 42.5	–	–	–	450.0	450.0
TiO ₂ A [‡]	18.0	18.0	18.0	22.5	45.0
Pigment 1	–	12.0	–	22.5	22.5
Pigment 2	–	–	12.0	–	–
Sand 0-2	1300.0	1300.0	1300.0	–	–
Sand 0-4	–	–	–	1657.8	1620.6
Water	220.0	220.0	220.0	174.8	183.2
Total	2138.0	2150.0	2150.0	2327.6	2321.3

[‡] TiO₂ was added as water based suspension

Slabs having a dimension of 100 × 200 × 20 mm were produced under laboratory conditions from the composed mortars given in Table 8.4. In addition, concrete paving blocks (Pav1) were produced in two-layer technique on industrial scale using mix Pig4 as top-layer mix as well as two mix designs suggested by the paving block producer (Pav2/Pav3, and Pav 4). Further information on the mix proportioning of these two mixes were not provided by the company. Therefore,

these samples were analyzed regarding their chemical composition and compared with a known reference sample to allow a backward calculation of the TiO_2 content of the analyzed samples.

8.3.2 Mineralogical composition

As mentioned in the previous section, information on the TiO_2 content of the two mixes designed by the paving block producer were not provided. However, a reasonable analysis of the NO degradation performance requires further information on the type as well as the content of TiO_2 used. In this respect, it was illustrated in Section 8.2.3 that the analysis of the chemical composition by means of XRF is a suitable method to determine the TiO_2 content. For this purpose, two samples with known TiO_2 content, Pav1 and Ref2b, and three samples with unknown TiO_2 content from the paving block producer were analyzed. These three samples comprise two samples with identical mix proportioning but different production dates to investigate the quality of the produced paving blocks over time (Pav2, Pav3) and a further sample with a mix proportioning differing from the first two samples (Pav4). The results of the XRF analysis as well as the calculated TiO_2 contents of the unknown samples are given in Table 8.5 and detailed values of the chemical composition can be found in Appendix A.3.

Table 8.5: TiO_2 content of produced concrete paving blocks and reference mix (Pöllmann, 2009).

	Pav1	Pav2	Pav3	Pav4	Ref2b [‡]
TiO_2 (XRF) [%]	1.88	5.91	5.43	0.59	2.94
cal. TiO_2 [‡] [kg/m^3]	42.0	132.1	121.3	13.2	–
TiO_2 [‡] [M.-%]	1.94	–	–	–	2.71

[‡] calculated based on the average of the last XRF analysis (Ref2b) and values given in Table 8.2

[‡] based on the total mass inclusive mixing water

The results of the backward calculation presented in Table 8.5 are based on the averaged TiO_2 content of the reference sample Ref2 which amounts to 2.69%. Both measurements of the reference sample, Ref2a (Table 8.2) as well as Ref2b, show a low deviation in the determined TiO_2 content. The same fact holds also for other mineral oxides as illustrated in Appendix A.3. Considering the averaged TiO_2 content of the reference sample Ref2, the TiO_2 content of the sample Pav1 was determined to be $42.0 \text{ kg}/\text{m}^3$ and is in good agreement with the mix proportioning given in Table 8.4. Similar TiO_2 contents were determined for the two samples with identical mix proportioning, but different production dates. The deviation of the two measurements is, compared to the amount of TiO_2 on the overall mass of the concrete, rather small and can be related to the heterogenous distribution of the TiO_2 within the top-layer and which is addressed in detail in the following section. The TiO_2 content of the sample Pav4 amounts to one tenth of the amount that was used for the other two samples and represents the lowest TiO_2 content in this series. It is known that same type of TiO_2 was used by the paving block producer for the production of the samples Pav1, Pav2, Pav3, and Pav4 to allow for a comparative assessment of the NO degradation performance.

8.3.3 Experimental results and discussion

The measuring protocol presented in Section 7.5.1 forms the basis for testing the NO degradation performance of the designed mixes presented in Table 8.4 and further tests performed on concrete paving blocks produced on industrial scale.

The results of the NO degradation of the samples produced in the lab are depicted in Figure

8.3 and detailed values of the measurements are given in Appendix G.6. The direct comparison reveals that the NO degradation was not affected by the added pigments. The application of pigments increased even slightly the NO degradation performance of mixes with same TiO₂ content (Pig1, Pig2). A similar effect was also obtained for mixes with a higher content of TiO₂ and pigments. Here, the NO degradation performance increased with increasing TiO₂ content and was not affected by the applied pigments.

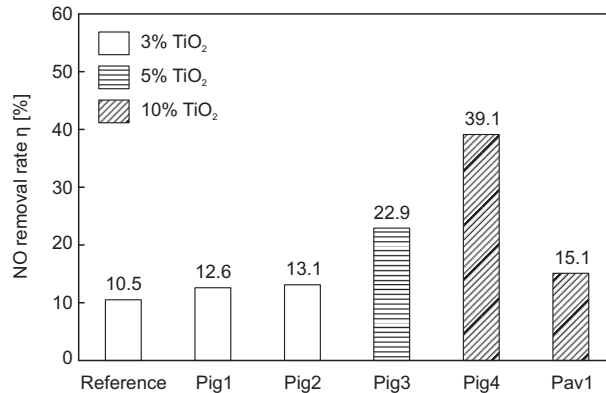


Figure 8.3: Influence of red pigments on the NO removal rate: no pigment (Reference); 2% pigment type 1 (Pig1); 2% pigment type 2 (Pig2); 5% pigment type 1 (Pig3, Pig4, Pav1).

However, another important issue is evident from the data depicted in Figure 8.3. The degradation performance of the paving blocks produced on industrial scale differs to a large extent from the experimental results. This sizable difference is mainly caused by different application techniques of the powders. The TiO₂ was added as water based suspension and the mortars were mixed in a compulsory mixer over a period of 5 minutes to allow for a homogeneous distribution of the fines in the case of samples produced on laboratory scale. It was not possible to follow this procedure on industrial scale, as there the TiO₂ was added as dry powder to the mix. The application of TiO₂ as dry powder was resulting, as already discussed in Section 7.6.5, in an inhomogeneous distribution of the TiO₂ and the formation of agglomerates in the top-layer. Figure 8.4 shows agglomerated TiO₂ that was observed on the surface of one of the produced concrete paving blocks and illustrates the importance of an appropriate dispersion of the fine TiO₂ particles.

The formation of TiO₂ agglomerates was avoided in the later tests by modifications in the concrete mixing and the use of plasticizing admixtures in such a way that an attractive surface quality was still achieved. The use plasticizing admixtures helps also to improve the workability of the top-layer mixes as the content of particles with high fineness (TiO₂ and red pigments) increases in the case of colored concrete paving blocks and which leads to a significantly reduced workability. Consequently, agglomerates of fine particles, preferably TiO₂, are formed in case the water content is maintained or plasticizers are not used.

The NO degradation performance of the produced paving blocks is depicted in Figure 8.5 and compared with results obtained by the comparative study discussed in Section 8.2. Considering the data depicted in Figure 8.5 and the corresponding TiO₂ contents listed in Table 8.2 and Table 8.5, the effect of the TiO₂ content and type on the NO degradation performance is demonstrated



Figure 8.4: Agglomerates of TiO_2 formed on the surface of a concrete paving block.

again. In this respect, the samples of the series D5 featured with 4.1% the lowest NO removal rate having a TiO_2 content of 22.8 kg/m^3 . It was possible to double this low NO removal rate while reducing the amount of TiO_2 used in the mix. The sample of the series Pav4 yield a NO removal rate of 8.6% and having with 13.2 kg/m^3 the lowest TiO_2 content. The highest NO removal rate was obtained by samples of the series Pav4 which also contain the highest amount of TiO_2 . Here, a degradation rate of 46.5% was obtained with a TiO_2 content that is ten times higher than that of the sample Pav4. The NO degradation performance of the paving blocks produced with the self developed top-layer mortar (Pav1) averages to 15.1% which is one-third of the value obtained by the samples of the series Pav2. However, it has to be noticed that the TiO_2 content of the samples of the series Pav1 is also one-third of the amount that was used for series Pav2.

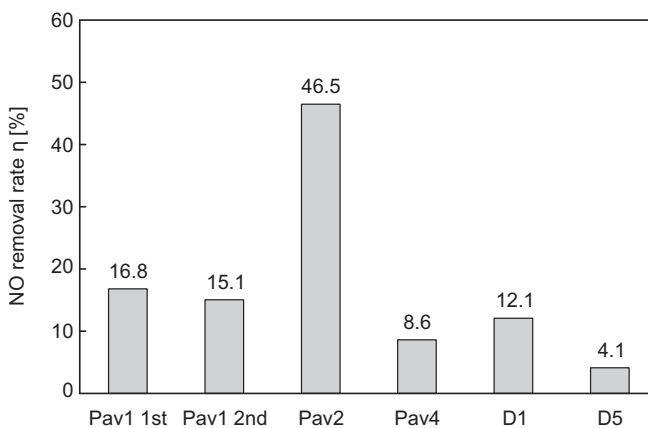


Figure 8.5: NO removal rates of paving blocks produced on industrial scale.

The recovery of the NO degradation performance was confirmed by a second measuring run which was conducted on four paving blocks of the series Pav1. For this purpose, the selected paving blocks were brushed and rinsed with tap water to remove reaction products from the active surface. After the manual cleaning process, the samples were dried and their NO removal rate was determined again. The values of the first and second measuring run are listed in Table 8.6 and show a low deviation between both measuring cycles. The NO removal rate of the second measurement of the samples Pav1-5 and Pav1-6 deviates only to a minor extent from the first run and confirms the findings depicted in Figure 7.2.

Table 8.6: NO degradation of tested samples for repeated measurements using equal test conditions.

Sample	First run		Second run	
	η_{NO}	η_{NO_x}	η_{NO}	η_{NO_x}
Pav1-1	15.4	14.3	10.9	10.7
Pav1-2	15.5	13.7	13.6	12.4
Pav1-5	19.5	15.5	19.3	14.3
Pav1-6	16.8	13.6	16.5	14.2
Average	16.8	14.3	15.1	12.9

8.4 Modeling

The successful application of air-purifying paving under practical conditions requires both fundamental knowledge on the working principle of the photocatalytic reaction as well as the modeling of the degradation process. Based on the numerous measurements that were conducted in this research project, the NO degradation process needs to be described by an appropriate model. The degradation of NO follows in the considered case the mechanisms of heterogeneous catalysis. A commonly used model in that field is given by the Langmuir-Hinshelwood mechanism for surface catalysis. The Langmuir-Hinshelwood model is widely used for the characterization of the PCO (Devahasdin et al., 2003; Jacoby et al., 1995; Peral and Ollis, 1992; Wang et al., 2007; Yamazaki et al., 1999; Zhao and Yang, 2003) and contains relevant parameters of the degradation process, such as pollutant concentration and volumetric flow.

8.4.1 Theoretical model

As mentioned in Section 7.2.2, the degradation of NO is subject to the principles of heterogeneous photocatalysis. According to Yamazaki et al. (1999), a heterogeneous catalytic reaction comprises the following processes: 1) mass transfer of the reactants (pollutants) to the catalyst surface, 2) adsorption of the reactants on the catalyst surface, 3) photochemical reaction on the active sites of the catalyst, 4) desorption of reaction products from the catalyst surface, and 5) mass transfer of the reaction products from the surface. These consecutive steps involve both the mass transfer of the pollutant gas from the bulk to the active surface of the concrete paving block and the subsequent conversion of NO on the active sites of the catalyst. Under these circumstances, one of the two processes may be the rate-limiting step in the reaction mechanism (Denbigh and Turner, 1965).

In the considered case, it was already demonstrated by Yamazaki et al. (1999) as well as Hunger et al. (2010) that the external mass transfer is not the rate-determining step and that a plug flow reactor model can be used to describe the chemical reactions. The model of a tubular

plug flow reactor considers an unmixed flow with constant velocity profile (Schmidt, 1998). The reactor in the present case does not obtain such a constant velocity profile, but the fluid is considered to be unmixed due to the laminar flow conditions as explained in Section 7.4.3. In this case, the resulting error in the plug-flow approximation is assumed to be only a few percent (Schmidt, 1998). The differential mass balance for a single gaseous species in a tubular plug flow reactor follows according to Schmidt (1998) from:

$$u_{air} \frac{dC_g}{dx} = \kappa r \quad (8.3)$$

The stoichiometric coefficient κ in Eq. (8.3) amounts to -1 as the considered specie (NO) is consumed during reaction. Furthermore, the reaction rate r is expressed according to Schmidt (1998) for the Langmuir-Hinshelwood kinetics by:

$$r = \frac{kK_d C_g}{1 + K_d C_g} \quad (8.4)$$

with k as reaction rate constant ($\text{mg}/\text{m}^3\text{s}$), K_d as the adsorption equilibrium constant (m^3/mg) and C_g as the NO concentration (mg NO per m^3 air) in the inlet gas. The NO mass balance now reads:

$$u_{air} \frac{dC_g}{dx} = -r_{NO} = -\frac{kK_d C_g}{1 + K_d C_g} \quad (8.5)$$

Assuming that $C_g = C_{g,in}$ and considering the reactor geometry, integration of Eq. (8.5) yields:

$$\frac{1}{k} + \frac{1}{kK_d} \frac{\ln \frac{C_{g,in}}{C_{g,out}}}{(C_{g,in} - C_{g,out})} = \frac{L}{u_{air}(C_{g,in} - C_{g,out})} = \frac{V_{Reactor}}{\dot{V}(C_{g,in} - C_{g,out})} \quad (8.6)$$

with $V_{Reactor} = LBH_{sli}$ and $\dot{V} = u_{air}BH_{sli}$, and again, $C_{g,out} = C_g(x = L)$. The reaction rate constant k as well as the adsorption equilibrium constant K_d are determined from the measured kinematic data using a curve-fitting routine which is explained in the following section. It has to be noticed that Eq. (8.5) is only valid for a single component under steady state conditions. Therefore, the pollutant gas concentration $C_{g,in}$ is given by the initial pollutant gas concentration $C_{NO,in}$, whereas $C_{g,out}$ is expressed by the NO outlet concentration $C_{NO,out,end}$ (cp. Figure 7.8).

8.4.2 Experimental validation of the model

As mentioned in the previous section, the reaction rate constant k and the adsorption equilibrium constant K_d are determined by a curve-fitting routine. In Figure 8.6, $V_{Reactor}/\dot{V}(C_{g,in} - C_{g,out})$ obtained by measurements using sample D2-2 is set out versus $\ln(C_{g,in}/C_{g,out})/(C_{g,in} - C_{g,out})$ and a regression line was fit to the data that were obtained for varying flow rates and inlet concentrations. The intersection of the regression line with the ordinate corresponds to $1/k$ so that $k = 0.42 \text{ mg}/\text{m}^3\text{s}$ and the slope corresponds to $1/kK_d$ so that $K_d = 2.00 \text{ m}^3/\text{mg}$. The corresponding kinematic data of the measurement are given in Appendix G.8. By means of the obtained values, the reaction rate constant and the adsorption equilibrium constant of different products can be compared.

Further relevant data on the NO degradation of concrete paving blocks were found in Mitsubishi (2005) and are given in Appendix G.9. Here, the concrete paving block type NOXER was exposed to varying NO concentrations. As not mentioned otherwise by the data presented in

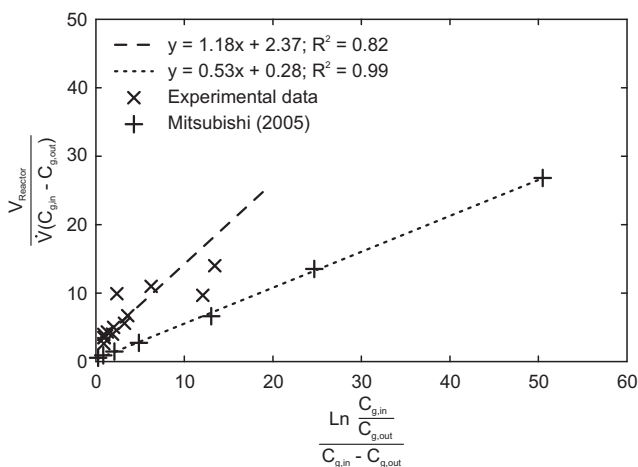


Figure 8.6: Regression analysis of experimental data of NO degradation measurements using sample D2-2 discussed in Section 8.2.2 and data given by Mitsubishi (2005).

Mitsubishi (2005), the boundary conditions were assumed to be the same as discussed in Section 7.5.1. Considering the background information on the conducted measurements, the Langmuir-Hinshelwood model was applied on the data presented in Mitsubishi (2005) and a linear fit was performed. The additional data of Mitsubishi (2005) depicted in Figure 8.6 are in good agreement with the model. A reaction rate constant k of $3.54 \text{ mg/m}^3\text{s}$ and an adsorption equilibrium constant K_d of $0.538 \text{ m}^3/\text{mg}$ were determined for the extracted data. Compared with own experiments, the reaction rate constant is notably higher and was already expected considering the higher NO removal rates that were obtained at comparable boundary conditions (cp. results Table G.8 and Table G.9). It is assumed that the different reaction rate constants are related to different amounts and types of photocatalyst used. However, further information on the TiO_2 content and type are not given in Mitsubishi (2005). A similar deviation exists also for the adsorption equilibrium constant, which can be explained by differences in the surface texture of the samples.

It is obvious from the comparison with similar data extracted from Mitsubishi (2005) that the respective constants vary as expected, but values in the same order of magnitude are obtained. This fact is also confirmed by the data reported by Wang et al. (2007) for the NO degradation performance of woven glass fabrics. Here, a reaction rate constant of $6.84 \text{ mg/m}^3\text{s}$ and an adsorption equilibrium constant of $1.13 \text{ m}^3/\text{mg}$ were obtained by Wang et al. (2007) for NO inlet concentrations ranging from 40 - 80 ppm.

8.4.3 Influencing factors

As demonstrated in Section 7.6, the degradation of NO and therewith the performance of the photocatalytic reaction is governed by physicochemical as well as product related parameters, namely k and K_D . A general model for the reaction kinetics was derived in Section 8.4.1 considering the reactor dimension, volumetric flow rate, and pollutant concentration. The derived model was validated in Section 8.4.2 by own experimental data as well as data extracted from the literature. However, the physicochemical parameters with influence on the NO degradation performance, as discussed in Section 7.6, comprise also two further parameters, namely the UV-A irradiance and the concentration of water expressed by the relative humidity. Therefore, the

proposed model will be extended to allow for a comprehensive modeling of the NO degradation under laboratory conditions.

Irradiance

The influence of the UV-A irradiance on the NO degradation performance is discussed in detail in Section 7.6.1. Based on the previous findings, it is assumed that the UV-A irradiance only has an influence on the reaction rate constant k as with increasing UV-A irradiance the amount of electron holes increases and also the amount of radicals and charged species that can decompose the molecules of the pollutant gas. This assumption is also confirmed theoretically by the definition of the adsorption equilibrium constant given by Schmidt (1998). According to this definition, the adsorption equilibrium constant K_d expresses the ratio of adsorption and desorption of the pollutant molecule and follows from:

$$K_d = \frac{k_{d,ads}}{k_{d,des}} \quad (8.7)$$

with $k_{d,ads}$ and $k_{d,des}$ as adsorption and desorption rate constant, respectively. In order to confirm this hypothesis also experimentally, an analysis similar to the measurements described in Section 8.4.2 was carried out. For this purpose, the NO degradation was measured for NO inlet concentrations of 0.1, 0.3, 0.5, 0.7, and 1.0 ppm at a flow rate of 31/min for varying UV-A irradiance ranging from 1 - 11 W/m² in steps of 1 W/m² which was resulting in a set of 55 measurements (11 × 5 matrix). The obtained data are depicted in Figure 8.7 and extended with data from Figure 7.9 (shaded values) that were determined using the sample D2-2 as introduced in Section 8.2.2. A curve fit using Eq. (7.16) was made to the measured data. Detailed values of the single measurements and the parameters of the curve fit are given in Appendix G.10.

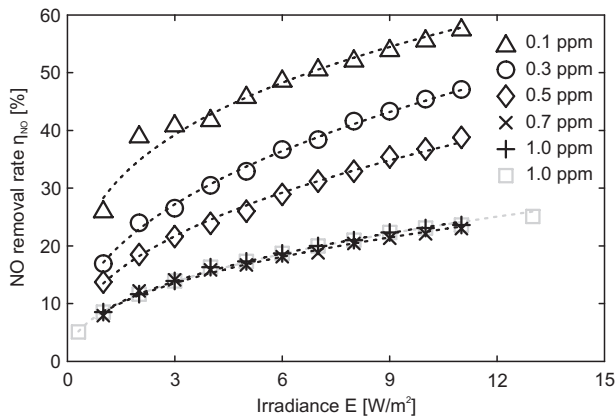


Figure 8.7: Influence of the UV-A irradiance on the NO removal rate for varying NO inlet concentrations (shaded values refer to data depicted in Figure 7.9). The data were obtained using the sample D2-2 as introduced in Section 8.2.2.

The data of the performed curve fit show that a constant factor of 0.42 was derived for the fit parameter α_2 used in Eq. (7.16), which is, despite for the measurements using a NO inlet

concentration of 0.1 ppm, not depending on the NO inlet concentration. However, a similar value for α_2 is obtained for the measuring set using a NO inlet concentration of 0.1 ppm if the first three values for low UV-A irradiance are not considered. Besides the constant value obtained for α_2 , another interesting fact becomes obvious from the data of the performed curve fit. The values determined for the fit parameter α_1 used in Eq. (7.16) show a clear dependence on the NO inlet concentration. Here, higher values with a large dependence on the inlet concentration were derived for lower NO inlet concentrations, whereas factors with lower dependence on the NO inlet concentration were determined for higher NO concentrations. This is in line with the observations discussed in Section 7.6.3.

A linear fit, similar to the one presented in Figure 8.6, was performed to the data for each set of measurements with constant UV-A irradiance. That way, the reaction rate constants and the adsorption equilibrium constants for varying UV-A irradiance were determined. The data of the linear fit and the resulting values of k and K_d are listed in Appendix G.12. Figure 8.8 shows the influence of the UV-A irradiance on the reaction rate constant k and the adsorption equilibrium constant K_d . Based on these data and the kinetic model proposed by Imoberdorf et al. (2005), a mathematical expression for the influence of the UV-A irradiance on the reaction rate constant k can be derived:

$$k = \alpha_3 \left(-1 + \sqrt{1 + \alpha_4 E} \right) \tag{8.8}$$

with α_3 and α_4 being factors to be fitted from the experiments. Eq. (8.8) considers the linear and nonlinear behavior of the degradation process for varying UV-A irradiance, which was already explained in Section 7.6.1. Furthermore, the expression for the reaction rate constant becomes zero when UV-A radiation is absent ($E = 0$). A good agreement with the experimental results was obtained by fitting the corresponding parameter in Eq. (8.8) to the experimental data, yielding $\alpha_3 = 0.03 \text{ mg/m}^3\text{s}$, and $\alpha_4 = 9.1 \text{ m}^2/\text{W}$.

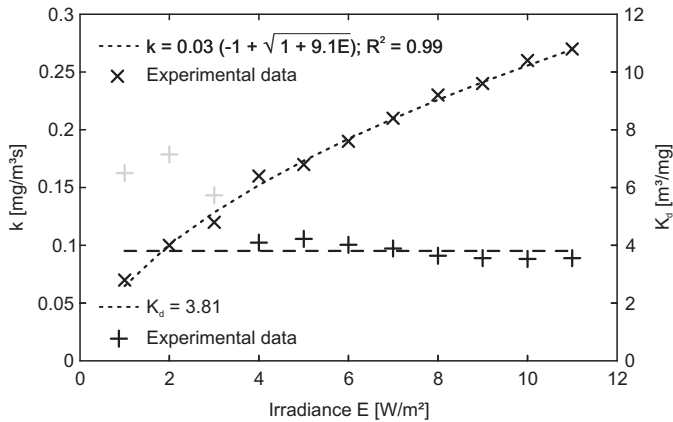


Figure 8.8: Influence of the UV-A irradiance E on the reaction rate constant k and the adsorption equilibrium constant K_d .

It was already assumed before that changes in the UV-A irradiance are not influencing the mass

transfer from the bulk to the active surface of the catalyst. This assumption is confirmed by the data depicted in Figure 8.8. Ignoring the first three values for the lowest UV-A irradiances, the adsorption equilibrium constant K_d amounts to $3.81 \text{ m}^3/\text{mg}$ in the considered case. The shaded values in Figure 8.8 are considered as outlying measurements due to very low irradiance levels where the light source might not operate under stable conditions.

Considering the influence of the UV-A irradiance on the NO degradation, the equation of the reaction rate, as expressed by Eq. (8.4), is modified and follows now from:

$$r_{NO} = \frac{K_d C_{NO}}{1 + K_d C_{NO}} \alpha_3 \left(-1 + \sqrt{1 + \alpha_4 E} \right) \quad (8.9)$$

Relative humidity

The influence of the relative humidity on the NO degradation performance was discussed in detail in Section 7.6.2 and it was demonstrated that the hydrophilic effect on the active surface is gaining over the oxidizing potential for higher values of the relative humidity. Consequently, water molecules and pollutant molecules compete for the same active sites on the catalyst surface. This effect results in lower NO removal rates for increasing relative humidity as illustrated in Section 7.6.2. The influence of the relative humidity on the reaction rate constant k and the adsorption equilibrium constant K_d was investigated by similar measurements as described before, but now conducted for varying levels of the relative humidity. For this purpose, the NO degradation was measured for varying relative humidity at different NO inlet concentrations. The relative humidity was varied in steps of 10% ranging from 10 - 70% resulting in a 7×5 measurement matrix. The dependence of the NO removal rate is depicted in Figure 8.9 for varying NO inlet concentrations.

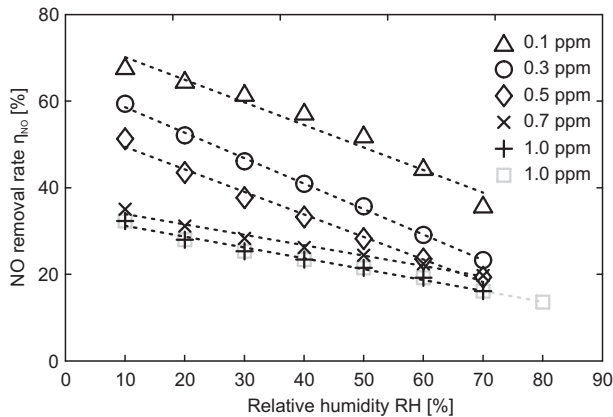


Figure 8.9: Influence of the relative humidity on the NO removal rate for varying NO inlet concentrations.

As already illustrated in Section 7.6.2, the NO removal rate shows a linear dependence on the relative humidity and is decreasing with increasing moisture content of the pollutant gas. Despite the linear behavior, a further interesting aspect becomes obvious from the data and the fitted lines depicted in Figure 7.6.2. Lower NO inlet concentrations, considering values of 0.5 ppm and

lower in this case, are characterized by the same slope of the lines that were fitted to the experimental data and result therefore in parallel lines which only differ by their ordinate intercept. The same fact holds also for concentrations above 0.5 ppm, but here the fitted lines show a lower decrease for increasing relative humidity. This fact leads to the assumption that with higher NO inlet concentrations a change in the reaction kinetics occur. In the next step, the data of the single measurements were analyzed again by further linear fits to determine the corresponding values of k and K_d for every data set of constant relative humidity. The dependence of the reaction rate constant k and the adsorption equilibrium constant K_d on the relative humidity are depicted in Figure 8.10 and the data of the linear fits are given in Appendix G.13.

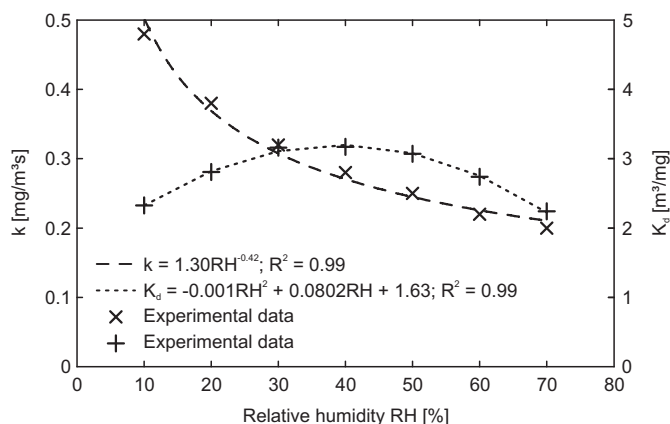


Figure 8.10: Influence of the relative humidity RH on the reaction rate constant k and the adsorption equilibrium constant K_d .

The data depicted in Figure 8.10 show that for relative humidity lower than 40% the adsorption equilibrium constant increases with increasing relative humidity and reaches a maximum value at about 40%. A further increase in the relative humidity leads to a decrease in adsorption equilibrium constant. A clear phenomenological expression for this behavior was not found in the literature. However, it is noteworthy that the corresponding relative humidity value at the observed maximum adsorption equilibrium is consistent with the observed deflection point of the NO₂ degradation outlined in Section 7.6.2. At this relative humidity, the NO₂ outlet and inlet concentration become equal. Furthermore, it was demonstrated in Section 7.6.2 that NO and water molecules compete for the same active sites onto the catalyst's surface. This competitive reaction results in lower NO degradation rates as less NO molecules are adsorbed onto the active sites. Considering the definition of the adsorption equilibrium constant K_d given in Eq. (8.7), the adsorption equilibrium constant must decrease with increasing relative humidity. As this is not the case for increasing relative humidity values lower than 40%, a more complex interaction of NO, NO₂ and water molecules must be assumed that decreases the desorption rate constant $k_{d,des}$ in Eq. 8.7 to a larger extent than the adsorption rate constant $k_{d,ads}$. It is assumed that NO, NO₂ and water molecules compete for the same active sites onto the catalyst's surface and that this reaction is dominated by the water molecules. In the considered case, the dependency of the

adsorption equilibrium constant K_d on the relative humidity is described by a quadratic function:

$$K_d = \alpha_5 RH^2 + \alpha_6 RH + \alpha_7 \quad (8.10)$$

The parameters α_5 , α_6 , and α_7 were fitted to the experimental data and amount to -0.001, 0.0802 and 1.63 m³/mg, respectively.

As mentioned before, the adsorption of the pollutant molecules onto the catalyst's surface is of major importance for the overall degradation performance. The previous discussion on the experimental results of varying relative humidity learned that the adsorption equilibrium constant K_d is influenced by changes in the relative humidity and that complex interactions between NO, NO₂ and water molecules arise. It is assumed that both adsorption rate constant $k_{d,ads}$ and desorption rate constant $k_{d,des}$ are affected by varying relative humidity. Consequently, the residence time of the pollutant molecules onto the active sites of the catalyst is also influenced and changes in the reaction rate constant k are assumed. This assumption is reflected by the decreasing reaction rate constant k for increasing relative humidity. Considering the experimental data presented in Figure 8.10, the influence of the relative humidity on the reaction rate constant k is expressed by a power law function that reads:

$$k = \alpha_8 RH^{\alpha_9} \quad (8.11)$$

Again, the corresponding parameters in Eq. 8.11 were fitted to the experimental data, yielding $\alpha_8 = 1.30 \text{ mg/m}^3\text{s}$, and $\alpha_9 = 0.42$. The assumed behavior is in good agreement with the experimental data. The experimental data determined for varying irradiance and relative humidity show a good agreement in their common points at 10 W/m² irradiance and 50% relative humidity (cp. Appendix G.12 and Appendix G.13) and were combined, therefore, to express the influence on both constants k and K_d . The combined influence of varying irradiance and relative humidity is depicted in Figure 8.11a for the reaction rate constant k and in Figure 8.11b for the adsorption equilibrium constant K_d .

Based on Eq. (8.8) and Eq. (8.11), the overall reaction rate constant k can be expressed as a function of irradiance and relative humidity which reads:

$$k = \alpha'_3 \left(-1 + \sqrt{1 + \alpha'_4 E} \right) \alpha'_8 RH^{\alpha'_9} \quad (8.12)$$

In the same way, the adsorption equilibrium constant K_d can be expressed in dependence of the varying boundary conditions. Here, the constant value of the adsorption equilibrium constant results in a function for K_d that depends only on the relative humidity and which follows, similar to Eq. (8.10), from:

$$K_d = \alpha'_5 RH^2 + \alpha'_6 RH + \alpha'_7 \quad (8.13)$$

Considering the data of the performed measurements on varying irradiance and relative humidity, the parameters in Eq. (8.12) and Eq. (8.13) were determined by linear regression analysis and the obtained values are listed in Table 8.7. The corresponding graphs of Eq. (8.12) and Eq. (8.13) are depicted in Figure 8.11 and were extended with lines showing the performed measurements for varying irradiance and relative humidity (bold lines).

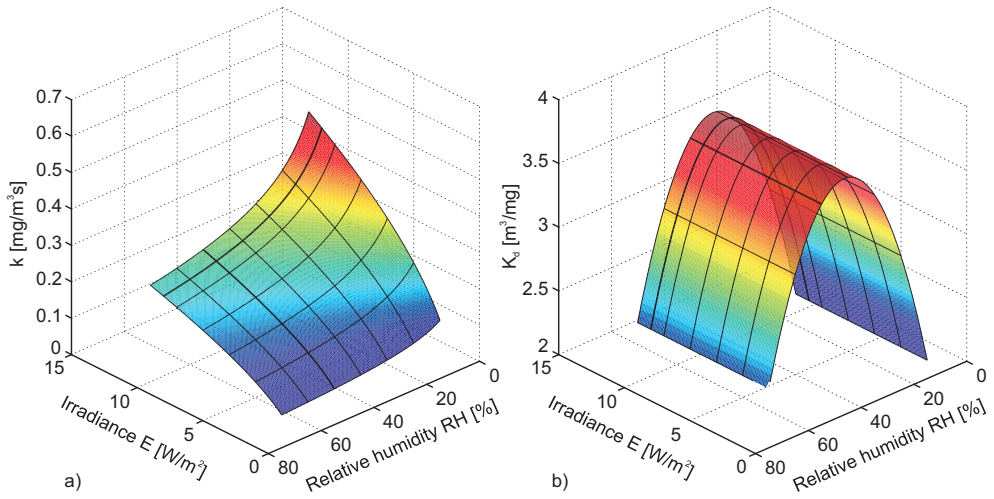


Figure 8.11: Combined influence of varying irradiance and relative humidity: a) reaction rate constant, and b) adsorption equilibrium constant.

Table 8.7: Fit parameter determined by linear regression analysis.

Parameter	Value	Parameter	Value
α'_3 [mg/m ³ s]	0.1090	α'_7 [m ³ /mg]	0.7907
α'_4 [m ² /W]	10.1771	α'_8 [mg/m ³ s]	1.2801
α'_5 [m ³ /mg]	-0.0017	α'_9 [-]	-0.4141
α'_6 [m ³ /mg]	0.1429		

Applying Eq. (8.12) and Eq. (8.13) to Eq. (8.4), the reaction rate r_{NO} can be rewritten and follows now from:

$$r_{NO} = \frac{\alpha'_3(-1 + \sqrt{1 + \alpha'_4 E})\alpha'_8 RH^{\alpha'_9}(\alpha'_5 RH^2 + \alpha'_6 RH + \alpha'_7)C_{NO}}{1 + (\alpha'_5 RH^2 + \alpha'_6 RH + \alpha'_7)C_{NO}} \quad (8.14)$$

According to Ballari et al. (2010), the coupled NO mass balance (Eq. (8.5)) can be solved by a discretization of the differential equation (Euler's Method) as follows:

$$C_{NO}(x_{i+1}) = - \frac{\alpha'_3(-1 + \sqrt{1 + \alpha'_4 E})\alpha'_8 RH^{\alpha'_9}(\alpha'_5 RH^2 + \alpha'_6 RH + \alpha'_7)C_{NO}(x_i)}{1 + (\alpha'_5 RH^2 + \alpha'_6 RH + \alpha'_7)C_{NO}(x_i)} + \frac{x_{i+1} - x_i}{u_{air}} C_{NO}(x_i) \quad (8.15)$$

Eq. (8.15) allows for the numerical evaluation of the coupled mass balance considering the NO inlet concentration at $x_i = 0$ and to calculate $C_{NO,out}$ at the outlet of the reactor at $x_i = L$. Using this method, the NO concentration at the reactor outlet was calculated and compared with the experimental values. In Figure 8.12, the experimental results of 90 measurements conducted for varying irradiance and relative humidity are plotted against the model predictions and illustrate that the applied model is capable to predict the NO degradation performance of the analyzed paving block. The variation of boundary conditions such as irradiance, relative humidity, and velocity of the pollutant gas at the photocatalytic surface are considered in the model and allow for a proper prediction of the NO degradation behavior. Required constants of the model have to be determined by a set of appropriate measurements under varying boundary conditions.

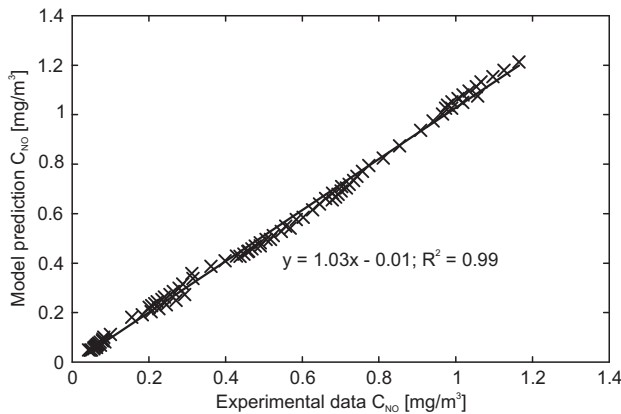


Figure 8.12: Comparison of experimental results and model predictions.

8.4.4 Discussion

The modeling of the NO degradation process demonstrated that the applied Langmuir-Hinshelwood model can be used to predict the performance of a photocatalytic system under varying boundary conditions, and that good agreement between experimental results and model predictions was obtained. However, the thorough analysis of the experiments revealed that the NO degradation is governed by complex interactions between NO, NO₂ and water molecules. These interactions of the involved molecules influence the degradation performance of the photocatalytic system to a large extent. In the present case, variations of the boundary conditions, such as irradiance and relative humidity, were described by mathematical expressions of the reaction rate constant k (Eq. (8.12)) and the adsorption equilibrium constant K_d (Eq. (8.13)) and were used to rewrite the equation of the reaction rate as given by Eq. (8.4). This approach is suitable as in the present case the applied model considers only the degradation of NO without consideration of intermediate products or competitive reactions that can occur onto the surface of the catalyst and simplifies also the application of the model for steady boundary conditions.

A more suitable approach for the modeling of the NO_x degradation under practical conditions using computational fluid dynamics is obtained when the interaction of the involved species is considered by adequate terms in the equation of the reaction rate. For this purpose, an extended equation of the reaction rate is used by Ballari et al. (2010). This extended equation considers the interaction between pollutant gas (NO) and formed intermediate products (NO₂) by sep-

arate reaction rate constants (k_{NO} , k_{NO_2}) as well as intrinsic adsorption equilibrium constants (K_{NO} , K_{NO_2}). Furthermore, this extended model considers the influence of the relative humidity on the degradation performance by introducing the water vapor as additional reactant that is competing for the free active sites onto the catalyst surface. Consequently, an adsorption equilibrium constant K_{H_2O} is also assigned to the concentration of water molecules in the system.

The applied models, as used in this research as well as the extended version of Ballari et al. (2010), are both capable to predict the NO degradation performance of photocatalytic concrete products and were validated by experimental results. In this respect, the applied model of this research is more suitable for a simplified prediction of the NO degradation performance under steady boundary conditions, whereas the extended model of Ballari et al. (2010) gives more information on the formation of intermediate products and their influence on the degradation performance under varying boundary conditions. These information of the extended model allow the application in computational fluid dynamics for modeling the effect of photocatalytic concrete products on the air quality in inner-city areas.

8.5 Conclusions

In the present chapter, the degradation performance of photocatalytic concrete products was investigated on a laboratory scale. For this purpose, a selection of concrete products containing TiO_2 was selected from the European market and tested regarding their degradation performance under constant laboratory conditions. Moreover, new top-layer mixes were developed and compared with the NO degradation performance of the available products. In addition to the qualitative measurements on the NO degradation performance, a model is proposed that allows for predicting the NO degradation performance considering the influence of boundary conditions, such as irradiance, relative humidity, and velocity of the pollutant gas.

Based on the experimental and theoretical investigations, the following conclusions can be drawn:

1. The European market provides a variety of concrete products containing photocatalytic materials for both vertical and horizontal applications. It was found that the efficiency of these products regarding NO degradation is directly related to the TiO_2 content, and varies to a large extent. Products with an average NO removal rate of about 40% were tested under optimum laboratory conditions, whereas other products showed almost no or only insignificant NO removal rates.
2. The application of red pigments in combination with TiO_2 has no explicit influence on the NO degradation performance of concrete paving blocks. Top-layer mixes containing TiO_2 and red pigments were designed and samples thereof were produced on both laboratory scale and industrial level. The produced samples were evaluated regarding their NO degradation performance and the experimental results are not differing from the measurements conducted on paving blocks that contain no pigments.
3. The transformation of new top-layer mixes from the development on laboratory scale to the industrial production demonstrated again the importance of a good dispersion of the photocatalytic powders. The high fineness of the applied powders and pigments was increasing the water demand of the produced mortars and is favoring the formation of agglomerates. A good dispersion of the photocatalytic powder was obtained on lab scale by the application of a water based suspension. The formation of agglomerates and a negative effect of the high fineness of both photocatalytic powders and pigments was avoided on industrial scale by the use of plasticizing admixtures.
4. The reaction kinetics of the NO degradation process under constant UV-A irradiance and relative humidity were successfully modeled using the Langmuir-Hinshelwood model. This model describes the reaction kinetics of a heterogenous photocatalytic reaction. The predictions of the proposed model are in good agreement with both experimental data de-

rived from own experiments and data found in the literature.

5. It was demonstrated that the UV-A irradiance influences the reaction kinetics of the NO degradation process. The proposed Langmuir-Hinshelwood model showed that only the reaction rate is influenced by changes of the UV-A irradiance and that the adsorption of NO is not governed by the radiation intensity.
6. The experimental data showed that both the reaction rate of the NO degradation and the adsorption of NO are influenced by changes of the relative humidity. In this respect, the reaction rate is decreasing with increasing relative humidity, whereas the adsorption equilibrium constant obtains a maximum value at 40%. This behavior of the adsorption equilibrium constant for varying relative humidity indicates a more complex interaction between NO, NO₂ and water molecules.

Conclusions and recommendations

In this thesis, multifunctional design aspects are combined for the design of sustainable concrete mixes that are applicable for the production of concrete mass products. This production process is characterized by a large production volume and financial aspects, which drive most of the concrete related processes. In this respect, high production rates with low rejection rates and short process times are required by the industry. Concretes with stiff consistency, so-called earth-moist concrete (EMC), fulfill these requirements. The practical knowledge on these concrete mixes is governed by experience and variations that are adopted from production machines, and which limits the ability of this sector to innovative and sustainable solutions. One of these conservative design rules is given by the definition of EMC mixes and states that the w/c ratio of EMC mixes is in the range of 0.3 - 0.4 to fulfill workability and durability related requirements. As a consequence of this, the workability of EMC mixes is adjusted by their cement contents and results in the fact that cement is used as filler material. Considering the annual cement production and embodied energy involved in the cement production, this is a wrong solution in terms of sustainability and economy.

A solution to this problem is provided by the new mix design concept for EMC. This concept allows the performance-based design of EMC, but also other types of standard concrete, in consideration of optimized particle packing. By means of this concept, EMC mixes can be designed that contain less cement, having better workability and higher packing fractions, which results both in environmental and financial benefits. These combined benefits make the presented mix design a valuable tool for the performance-based design concept of sustainable concrete. In this respect, the use of cement in EMC for achieving specific properties of the fresh and hardened concrete should not be overemphasized. From this point of view, the application of additional filler materials in EMC mixes is of sustainable interest, but again, not favored by classical design concepts.

Besides the possible reduction of the environmental impact of concrete due to lower cement contents, the utilization of alternative materials in concrete allows for further improvements with financial and environmental benefits. Here, stone waste powders and recycled concrete aggregates and fines have been used as source for replacing primary raw materials. By means of these alternative materials, natural resources are preserved and the life cycle of concrete is closed. The research carried out in that field revealed that the properties of the applied fine stone waste materials are not affecting the mechanical resistance or the workability of the fresh concrete. Contrary to this, more problems were encountered when recycled concrete aggregates from masonry rubble were used. Here, impurities, such as metal, wood fiberboard and plastic, were found in the material and are not favorable for the use of recycled material in concrete production. Consequently, a better processing of the recycled material is required and more attention should be paid to separating material streams when buildings are demolished.

A passive contribution to the overall ecological balance of concrete is obtained when photocatalytic materials are applied. The photocatalytic reaction on the material's surface provides the possibility to degrade inorganic and organic pollutants that are deposited on the surface. This allows for the design of multifunctional concrete products that feature i) the degradation of air pollutants such as nitrogen oxides NO_x and ii) the prevention of surface soiling due to algae

growth or other soiling substances. The degradation of NO_x was studied extensively on laboratory scale and has proven to be highly efficient. Further insight on the practical application, optimization and modeling of the photocatalytic reaction were obtained in this thesis.

9.1 Conclusions

The main conclusions of the research are summarized in the following. Distinction with respect to the field of possible applications is made.

9.1.1 Mix design concept

Based on a profound characterization of the raw materials regarding their relevant material properties, a mix design concept for earth-moist concrete was developed. Insights obtained from classical and recent theories on particle packing have been included in the design algorithm. The review on current particle packing models and the numerical simulation of particle packing revealed that a reliable prediction of packing phenomena is still limited to special and ideal conditions. The reliability of most of the numerical models suffers from complex interactions between granulometric properties and interparticle forces. To overcome this problem, not only fundamental research on particle packing is needed, but also computational power. Furthermore, the size range of particles in multi-component mixes is limited as it depends on the available computational power. These limitations promote the application of a continuous geometric packing model for the mix design of EMC, as presented and used here.

Furthermore, the review on particle packing models illustrated that the entire size range of the concrete ingredients is of vital importance for the fresh and hardened concrete properties (Féret, 1892; Funk and Dinger, 1994; Plum, 1950) and should be considered in concrete mix design. However, limited characterization techniques of the past restricted an aimed composition of concrete mixes to fine and coarse aggregates. By means of modern techniques, such as laser diffraction analysis, the granulometric properties of the fines can also be determined and adequately considered in the current concrete mix design method. For this overall consideration of the grading of the raw materials, the modified equation of Andreasen and Andersen, suggested by Funk and Dinger (1994), was used in the algorithm. Practical requirements, such as cement content as well as w/c or w/p ratios, are considered in the mix design tool and allow for the composition of concrete mixes according to the demands of the industry of concrete mass products.

EMC mixes have been designed using the new mix design tool and tested under laboratory conditions. The results of the fresh and hardened concrete tests reveal that concrete mixes with lower cement content can be designed that fulfill practical demands in fresh and hardened state. The experimental validation of the optimization algorithm demonstrated that the cement content of mixes with optimized particle packing can be reduced up to 13% without negative effects on the mechanical resistance. This successful reduction in the cement content is one of the main objectives of this thesis and forms the core principle of sustainability in concrete mix design.

9.1.2 Application of stone waste materials

The reduction of cement contents requires also the utilization of suitable fine filler materials that need to be included in the entire grading of the composed concrete mix. By means of the new mix design concept, an appropriate tool for the incorporation of fine filler materials in concrete mixes is given. The developed design tool allows for the application of these filler materials in concrete considering the aspects of optimized particle packing. Ground rock powders, such as limestone powder, are usually used in concrete as inert filler materials. The production of these artificial filler materials requires energy for quarry processes and grinding. Although the embodied energy of these primary filler materials is lower than compared to cement, their replacement by suitable waste materials results in additional environmental benefits regarding energy savings and preservation of natural resources. A suitable waste material for replacing primary fillers was

found in fine stone waste materials generated by the production of crushed concrete aggregates from natural rock (granite).

In this research, fine stone waste materials have been applied in form of a premixed unwashed granite sand, the so-called Premix 0-4, which contains about 11% of fines smaller than 125 μm at a constant level. Using the Premix 0-4 and the new mix design concept, EMC mixes were designed that are suitable for the production of concrete paving blocks. The designed mixes were evaluated on laboratory scale and concrete paving blocks were produced on a laboratory paving block machine. The produced paving blocks fulfill the requirements given by EN 1338 on mechanical resistance (splitting tensile strength) and durability (water absorption).

The investigations on the application of fine stone materials in EMC revealed that the cement content of the designed mixes can be reduced up to 10% without a negative effect on the mechanical resistance. In this context, a reduction of the cement content of about 35% resulted in a decrease of the compressive strength of about 15%, but still sufficient for the aimed application.

9.1.3 Application of recycled aggregates

As outlined in the Introduction of this thesis, the reduction in the use of primary raw materials in concrete production is one of the main objectives of this research and the presented mix design concept. However, the use of concrete in our modern world is still a quite linear process and efficient material recycling of old concrete occurs only to a marginal extent. Most of the material is used as sub-base for roads and highways because landfill of concrete rubble is restricted in many European countries. This way, resources of natural aggregates are preserved and the aspects of sustainability are fulfilled by a low level application. The utilization of recycled concrete aggregates in concrete production will increase the application level of the material and closes the life cycle of concrete buildings and structures.

It was demonstrated in this thesis that both fine recycled aggregates and recycled concrete fines (RCF) can be used in concrete production without large detrimental effects on the mechanical properties in hardened state. In case of using RCF with low content of masonry rubble as cement replacement, the compressive strength after 28 days was reduced to the same extent as for systems with inert filler materials. However, the application of this recycled material showed a beneficial effect on the strength development during the early hydration period and increased the compressive strength after 3 and 7 days compared to the strength of systems with inert filler materials.

The application of fine recycled concrete aggregates did not yield the expected results, as it was not possible to use the material in a multifunctional way. The mechanical properties in hardened state were not affected to a larger extent than reported in the literature. However, the research in that field was also inspired by the idea to make use of the higher porosity of the material, which is actually known to have a deleterious effect on the properties of the hardened concrete, and to activate the potential of water absorption for internal curing of high-strength concretes to prevent autogenous shrinkage. The attempt of reducing autogenous shrinkage was confirmed by the experimental results, but the magnitude of the autogenous shrinkage was reduced less compared to other methods like super-absorbing polymers or pre-saturated light-weight aggregates.

The utilization of waste materials and recycled concrete for the replacement of primary raw materials is a further pillar of the presented mix design concept in respect to sustainability. This way, the cement content is not reduced primarily due to optimized particle packing, but the ideas of optimized particle packing form the basis for the incorporation of waste materials and recycled concrete in the mix design of EMC mixes.

9.1.4 Application of photocatalytic materials

The application of multifunctional concrete products for the paving of roads and parking lots is a promising approach to reduce environmental loads caused by NO_x emissions in areas with high traffic loads. The degradation of NO_x by means of photocatalytic oxidation (PCO) in the presence of TiO_2 provides the possibility for the effective degradation of air pollutants close to the source of emission by cars and other vehicles. In this respect, the application of photocatalytic materials in concrete mass products is a sustainable contribution to the air quality in inner-city areas.

A test setup was established to assess the air-purifying abilities of concrete products and to study the influence of varying boundary conditions on the PCO. By means of the test setup, a representative selection of air-purifying concrete products of the European market was assessed. The comparative study revealed that the air-purifying properties of the selected products differ to a large extent and that the NO_x degradation performance ranges from zero to reasonable performance. The obtained results justified the demand for conducting further research on the influencing parameters of the PCO. In this respect, the most influencing parameters of the PCO were studied and their effect on the NO_x degradation was quantified. Furthermore, the obtained data were used for the modeling of the reaction kinetics of the PCO by means of the Langmuir-Hinshelwood model. This model is widely used for heterogeneous catalytic reactions and showed good agreement with experimental data.

Based on the results of the comparative study and information on the influencing parameters, new top layer mixes were designed and tested in the lab. These new top-layer mixes proved to work efficiently and were suggested for the production of concrete paving blocks on industrial scale. The produced paving blocks were applied in an ongoing demonstration project in the Dutch city of Hengelo. The positive effect of the air-purifying properties of the designed concrete paving blocks on the air quality was proven by first measurements in the street in Hengelo and will be reported elsewhere.

The outside exposition of concrete paving containing photocatalytic material in their top-layer demonstrated an interesting side effect of the PCO. As the paving blocks were placed on a moist and shadowed location that favors soiling due to algae growth, the inhibited growth of green algae on a concrete surface containing a photocatalyst was studied. The outside exposition of the photocatalytic samples revealed that soiling due to algae growth is prevented and that concrete surfaces containing a photocatalyst keep their original appearance.

9.2 Recommendations and future work

The presented mix design concept and the related design approach are a valuable tool for the design of sustainable EMC mixes. The applicability to other types of concrete, such as high-strength concrete or normal strength, normal weight concrete, is also given and can easily be realized by the modification of a single parameter, the distribution modulus q of the applied grading curve (Eq. (3.9)). Within the scope of this research, aspects of sustainability were focused on by i) cement reduction, ii) utilization of secondary or waste materials for replacement of primary raw materials such as cement, fillers, and aggregates, and iii) addition of air-purifying ability. For this purpose, a selection of suitable alternative materials was incorporated in the concrete mix design and tested experimentally. Still, additional research is needed to put the sustainable design approach, presented in this thesis, into practice. Based on the research presented in this thesis, the following recommendations for further research are given:

1. Particle packing plays an important role when concrete ingredients are composed. The beneficial effect of improved particle packing was demonstrated in this thesis and an appropriate software tool for the mix design of EMC mixes was developed that needs the grading of the raw materials as input parameter. However, it became obvious during this research

that the particle packing as well as the fresh and hardened concrete properties are not only governed by the PSD of the composed mix, but also by the particle shape of the raw materials. In case of EMC, the particle shape of the fine and coarse aggregates is having a large influence on the green-strength of the fresh concrete and the packing behavior. The optimization algorithm and the underlying grading curve do not consider this influence of the particle shape and forms, therefore, the starting point for further research and the incorporation of supplementary granulometric properties, such as particle shape and surface roughness, in the optimization algorithm.

2. Few input parameters of the design tool, such as the paste content required for sufficient compaction behavior and high green-strength, have to be selected based on preliminary tests that are not related to the parameter of the applied grading function. In this respect, it is of interest to relate these parameters also to granulometric properties of the designed concrete mix and to incorporate their influence in the optimization algorithm.
3. Sustainable concrete mass products have to be durable. In this respect, it was shown that the designed EMC mixes have sufficient mechanical strength – one argument of the classical definition that was critically discussed in the Introduction. However, a performance-based design of concrete requires also a performance based evaluation in terms of durability. A number of indirect tests, such as capillary water absorption, open porosity and improved packing densities, indicated already the durability of the tested mixes. However, additional durability tests have to prove directly that the produced paving blocks fulfill the requirements on freeze-thaw resistance.
4. The application of photocatalytic materials in concrete paving blocks is a direct contribution to improved air-quality in metropolitan areas with high traffic loads. The efficiency of the PCO was demonstrated under laboratory conditions and first measurements from a demonstration project showed promising results. However, there is still a large potential for conducting further research to increase the efficiency of the photocatalytic reaction, e.g. by applying doped photocatalysts with a broader activation spectrum or porous systems to increase the active surface area.

List of Figures

1.1	Stress conditions at the Mohr-Coulomb failure criterion	5
1.2	World cement production and unit value per metric ton	7
1.3	Framework of the thesis	14
2.1	Comparison of cumulative finer and sieve residue	17
2.2	Size classes used for the denomination of granular materials and concrete ingredients	17
2.3	Impurities contained in the recycled material RCA1	21
2.4	PSD of the Premix 0-4 and variations in the grading determined by a monthly quality control conducted over a period of 11 months	24
2.5	PSD of the granite fines contained in the Premix 0-4 and variations in the grading thereof determined by a monthly quality control conducted over a period of 7 months	25
2.6	PSD of the granite fines of the analyzed filter cake and variations in the grading thereof determined by a monthly quality control conducted over a period of 13 months	26
2.7	Grading of selected fines and sands	27
2.8	SEM micrographs of analyzed powders showing their comparable particle shape	27
2.9	Square container used for determining the degree of compaction according to DIN-EN 12350-4	32
2.10	Relation between the degree of compactibility c_{DIN} and the computed degree of compaction c_{com}	32
2.11	Schematic illustration of the Proctor test and compaction curves for different compaction efforts	33
2.12	Schematic illustration of the CemTec test	35
2.13	Schematic illustration of the working principle of the IC-test	36
2.14	Packing fraction and shear rate versus time for two different EMC mixes	37
3.1	Schematic illustration of possible arrangements of monosized particles	41
3.2	Bimodal mix of monodispers particles	42
3.3	Relation between void fraction and size ratio in bimodal systems of broken solids	43
3.4	Schematic illustration of the influence of the size ratio s on the packing fraction PF of discrete bimodal mixtures in a unit cell.	44
3.5	Algorithm according to Westman and Hugil	45
3.6	Packing of a system consisting of three components	46
3.7	Comparison between the algorithm of Westman and Hugil and experimental results	51
3.8	Packing fraction for varying size ratios	52
3.9	Packing fraction and compressive strength of the tested mortar samples for varying size ratios	53

3.10	Computed PSDs for varying distribution modulus q	54
3.11	Packing fractions of designed aggregate mixes for varying distribution modulus in loose and dense state	55
3.12	Compressive strength of designed aggregate mixes for varying distribution modulus q	56
3.13	PSDs of materials used	57
3.14	Packing fractions PF of the original cements, quartz flour and blends thereof	58
3.15	Development of the compressive strength according to EN 196-1 for blends of OPC of different fineness.	59
3.16	Development of the compressive strength according to EN 196-1 for blends of slag cement and OPC of different fineness.	60
3.17	PSD of the designed mortar mixes and comparison with the grading of a mortar according to EN 196-1	61
3.18	Development of the compressive strength for blends of OPC having different fineness	62
3.19	Development of the compressive strength for blends of slag cement and OPC	63
4.1	Schematic composition of RCD, NWC and SCC	67
4.2	Grading curves for varying distribution moduli q of the modified A&A equation and grading curves A, B and C of the Dutch standard NEN 5950	69
4.3	Influence of the distribution modulus on the paste content and the ratio gravel to powders	71
4.4	Influence of the maximum particle size D_{max} on the modified Andreasen and Andersen equation	72
4.5	Sizes and definition of fractions used in the optimization algorithm	73
4.6	Composed concrete mix using the developed optimization algorithm	74
4.7	PSDs of aggregates and powders used (cumulative finer mass fraction)	78
4.8	Measured packing fraction versus degree of compaction for tested EMC	79
4.9	Measured packing fraction versus compressive strength for tested EMC mixes	81
4.10	Influence of various distribution moduli q on the packing fraction	83
5.1	PSDs of the deployed materials used for the design of EMC mixes containing stone waste powders	87
5.2	Compressive strength of tested mortar samples containing stone waste materials	89
5.3	Flexural strength of tested mortar samples	90
5.4	Example of the fracture surface of the splitting tensile test of mix C275	92
5.5	Water absorption of the produced paving blocks over time	93
5.6	PSD of recycled concrete fines (RCF), quartz flour and cement used for mortar tests on cement replacement by recycled concrete fines	95
5.7	Consistence of fresh mortars containing recycled concrete fines and quartz flour as cement replacement	96
5.8	Compressive strength of tested mortar samples containing recycled concrete fines	97
5.9	Spread flow values of designed reference mix and mortars containing recycled concrete aggregates in varying quantities and conditions	103
5.10	Compressive strength of tested mortar samples containing recycled concrete aggregates	104

5.11	Flexural strength of tested mortar samples containing recycled concrete aggregates for internal curing	104
5.12	Schematic illustration of wrapped specimen used for autogenous shrinkage test	105
5.13	Results of shrinkage measurements on the designed reference mortar and mortars containing recycled concrete aggregates in oven dry condition	106
5.14	Results of shrinkage measurements on the designed reference mortar and mortars containing pre-saturated recycled concrete aggregates in saturated surface dry condition	106
5.15	Results of shrinkage measurements on the designed reference mortar and mortars containing recycled concrete aggregates with a replacement ratio of 20% by mass and varying moisture conditions	107
6.1	Interparticle forces of spherical particles and particle weight in dependence of the particle diameter	109
6.2	Interparticle forces of spherical particles in dependence of the particle distance.	110
6.3	Influence of the concentration of superplasticizer on the surface tension of water	113
6.4	Behavior of the wetting liquid between two rough spherical particles	115
6.5	Liquid bridge between two spherical particles with different size	116
6.6	PSDs of the selected materials used for the experimental investigations on the early-age behavior of EMC	118
6.7	PSD of the designed mixes used for the experimental investigations on the early-age behavior of EMC	119
6.8	Packing fractions of the tested fines for varying water contents	120
6.9	Stress-strain curves of tested fines for varying water contents	121
6.10	Stress-strain curves for constant water contents and varying SP contents	122
6.11	Packing fractions of tested mixes for different distribution moduli q and varying water contents	123
6.12	Stress-strain curves for varying water contents and different distribution moduli of the tested mixes containing quartz flour	124
6.13	Stress-strain curves for varying water contents and different distribution moduli of the tested mixes containing fly ash	125
6.14	PSDs of a commercial EMC mix and the optimized EMC mixes using the new mix design concept	128
6.15	Influence of the grading on the compaction behavior	129
6.16	Influence of the grading on the shear stress during compaction	130
6.17	Influence of the water content on the maximum packing fraction and calculated air contents	130
6.18	Influence of the water content on the shear stresses during compaction	131
6.19	Influence of the plasticizer content on the compaction behavior	132
6.20	Time dependency of the plasticizer's effectiveness	132
7.1	General reactions for the decomposition of organic compounds in aqueous solution	140
7.2	Recovery of NO_x degradation performance after removal of reaction products by a washing cycle	142
7.3	Staining of concrete paving blocks caused by algae growth	143
7.4	Schematic diagram of the test setup	147
7.5	Schematic diagram of the reactor cell	148

7.6	Light distribution of the applied light sources	149
7.7	Sequence of a standard measurement	151
7.8	Basic scheme of data analysis	153
7.9	Influence of the UV-A irradiance on the NO and NO ₂ degradation	154
7.10	NO concentration versus present UV-A irradiance for an outdoor measurement	155
7.11	Influence of the relative humidity on the NO and NO ₂ degradation	156
7.12	Influence of the pollutant concentration on the degradation	157
7.13	Influence of the flow rate on the NO degradation	158
7.14	Influence of the powder type on the NO degradation	159
7.15	Influence of the light spectrum on the NO degradation of a sample containing carbon doped TiO ₂	160
7.16	Influence of the application technique and TiO ₂ content on the NO degradation	160
8.1	Sources for NO ₂ emission	164
8.2	Degradation of nitric oxide over time for the tested concrete samples	168
8.3	Influence of red pigments on the NO removal rate	171
8.4	Agglomerates of TiO ₂ formed on the surface of a concrete paving block	172
8.5	NO removal rates of paving blocks produced on industrial scale	172
8.6	Regression analysis of experimental data of NO degradation measurements	175
8.7	Influence of the UV-A irradiance on the NO removal rate for varying NO inlet concentrations	176
8.8	Influence of the UV-A irradiance on the reaction rate constant and the adsorption equilibrium constant	177
8.9	Influence of the relative humidity on the NO removal rate for varying NO inlet concentrations	178
8.10	Influence of the relative humidity on the reaction rate constant and the adsorption equilibrium constant	179
8.11	Combined influence of varying irradiance and relative humidity on reaction rate constant and adsorption equilibrium constant	181
8.12	Comparison of experimental results and model predictions	182

List of Tables

1.1	Overview of prefabricated concrete mass products and applied production techniques	2
1.2	Comparison of EMC mix characteristics	3
2.1	Major oxides of the recycled concrete fines (RCF) determined by XRF-analysis	22
2.2	Water absorption of recycled concrete aggregates of the fraction 0.71-1.4 determined according to EN 1097-6 in saturated surface dry condition	23
2.3	Granulometric properties of the analyzed stone waste materials	25
2.4	Technical specifications of the applied cements	29
2.5	Properties of applied photocatalytic materials	30
3.1	Material properties of size classes used	50
3.2	Mix proportioning of the tested concrete mixes on the influence of varying distribution modulus	55
3.3	Densities and packing fractions of fines for different densification	57
3.4	Mix proportioning of the blended cements	58
3.5	Mix proportioning of the designed mortars	61
4.1	Minimum amount of fine material as defined by NEN 5950	70
4.2	Computed void fraction and measured void fraction of the investigated trial mixes	80
5.1	Mix proportioning of designed EMC mixes containing stone waste materials . .	88
5.2	Characteristics of the designed EMC mixes containing stone waste materials . .	88
5.3	Test results of the designed EMC mix C275	91
5.4	Test results of the produced paving blocks and comparison with limits of the European standard EN 1338	93
5.5	Mix proportioning of tested mortars used for cement replacement by recycled concrete fines and quartz flour	95
5.6	Mix design of mortars used for shrinkage tests	101
5.7	Characteristics of the designed HSC mixes containing recycled aggregates . . .	102
6.1	Mix proportioning of the designed mixes used for the experimental investigations on the early-age behavior of EMC	118
6.2	Mix characteristics of the designed mixes used for the experimental investigations on the early-age behavior of EMC	119
6.3	Test results of the IC-test for the investigated SP concentrations	122
6.4	Mix proportioning of a commercial EMC mix and the optimized EMC mixes using the new mix design concept	127

6.5	Characteristics of the tested EMC mixes listed in Table 6.4	127
6.6	Computed void fraction and measured void fraction of the tested EMC mixes	129
6.7	28-days compressive strength of samples obtained by the IC-test	133
7.1	Comparison of standards applicable for determining air-purifying properties of products containing photocatalyst	144
7.2	Mix proportioning of tested mortars using different types of TiO ₂	159
8.1	Denomination and origin of tested concrete samples	166
8.2	TiO ₂ content of tested concrete paving blocks and reference mixes	167
8.3	NO removal rates of tested samples	168
8.4	Mortar composition of tested top-layer mixes	169
8.5	TiO ₂ content of produced concrete paving blocks and reference mix	170
8.6	NO degradation of tested samples for repeated measurements using equal test conditions	173
8.7	Fit parameter determined by linear regression analysis	181

Bibliography

- Abrams, D. A. (1922). Proportioning Concrete Mixtures, *Proceedings of the 18th Annual Convention of the American Concrete Institute*, Vol. 18, Detroit, Michigan, U.S., pp. 174–181.
- ACI (2002). Guide for Selecting Proportions for No-Slump Concrete, *ACI 211.3R-02*, American Concrete Institute, PO Box 9094, Farmington Hills, US.
- Aitcin, P.-C. (2000). Cements of yesterday and today: Concrete of tomorrow, *Cement and Concrete Research* **30**(9): 1349–1359.
- Alex, W. (2008). Krümelkunde: lecture notes on granular materials
<http://www.abklex.de/skripten/kruemel.pdf>.
- Andreasen, A. H. M. and Andersen, J. (1930). Ueber die Beziehungen zwischen Kornabstufungen und Zwischenraum in Produkten aus losen Körnern (mit einigen Experimenten), *Kolloid-Zeitschrift* **50**: 217–228 (in German).
- Ballari, M. M., Hunger, M., Hüsken, G. and Brouwers, H. J. H. (2010). Modelling and experimental study of the NO_x photocatalytic degradation employing concrete pavement with titanium dioxide, *Catalysis Today* **151**(1-2): 71–76.
- Barbeni, M., Pramauro, E., Pelizzetti, E., Borgarello, E., Grätzel, M. and Serpone, N. (1984). Photodegradation of 4-chlorophenol catalyzed by titanium dioxide particles, *Nouveau Journal de Chimie* **8**(8-9): 547–550.
- Bartos, P. J. M., Sonebi, M. and Tamimi, A. K. (2002). Workability and Rheology of Fresh Concrete: Compendium of Tests, *Report of RILEM TC 145-WSM*, RILEM, Bagnex, France.
- Beeldens, A. (2007). Air purification by road materials: results of the test project in antwerp, in P. Baglioni and L. Cassar (eds), *Proceedings International RILEM Symposium on Photocatalysis, Environment and Construction Materials, 8-9 October 2007, Florence, Italy*, RILEM Publications, Bagnex, France, pp. 187–194.
- Bentur, A., Igarashi, S. and Kovler, K. (2001). Prevention of autogenous shrinkage in high-strength concrete by internal curing using wet lightweight aggregates, *Cement and Concrete Research* **31**(11): 1587–1591.
- Bentz, D. P. and Conway, J. T. (2001). Computer modeling of the replacement of "coarse" cement particles by inert fillers in low w/c ratio concretes: Hydration and strength, *Cement and Concrete Research* **31**(3): 503–506.
- Bilgeri, P. (2006). Optimization of earth-moist concrete for industrial application using a laboratory paving block machine, Private communication.
- Blöß, S. P. and Elfenthal, L. (2007). Doped titanium dioxide as a photocatalyst for UV and visible light, in P. Baglioni and L. Cassar (eds), *Proceedings International RILEM Symposium on Photocatalysis, Environment and Construction Materials, 8-9 October 2007, Florence, Italy*, RILEM Publications, Bagnex, France, pp. 31–38.
- Borho, K., Polke, R., Wintermantel, K., Schubert, H. and Sommer, K. (1991). Produkteigenschaften und Verfahrenstechnik, *Chemie Ingenieur Technik* **63**(8): 792–808.
- Bornemann, R. (2005). *Untersuchung zur Modellierung des Frisch- und Festbetonverhaltens erdfuchter Betone*, PhD thesis, University of Kassel, Kassel, Germany (in German).

- Brouwers, H. J. H. (2006). Particle-size distribution and packing fraction of geometric random packings, *Physical Review* **74**(3): 031309:1–031309:14.
- Brouwers, H. J. H. and Radix, H. (2005). Self-compacting concrete: Theoretical and experimental study, *Cement and Concrete Research* **35**: 2116–2136.
- Burmeister, L. C. (1993). *Convective Heat Transfer*, John Wiley & Sons, New York, US.
- Calmon, J. L., Moratti, M., Moraes, S. and Cenci, D. (2005). Self-compacting concrete using marble and granite sawing wastes as filler, *Proceedings of the 2005 World Sustainable Building Conference, 27-29 September 2005, Tokyo, Japan*, pp. 4146 – 4153.
- Cassar, L. and Pepe, C. (1997). *Paving tile comprising an hydraulic binder and photocatalyst particles*, EP-patent 1 600 430 A1, Italcementi S.p.A., Italy.
- Cassar, L., Pepe, C., Tognon, G., Guerrini, G. L. and Amadelli, R. (2003). White cement for architectural concrete, possessing photocatalytic properties, *Proceedings of 11th International Congress on the Chemistry of Cement, 11-16 May 2003, Durban, South Africa*, pp. 2012–2022.
- CEMBUREAU (2010). Cement: Key Facts & Figures
<http://www.cembureau.be/about-cement/key-facts-figures>.
- Chen, W. (2007). *Hydration of slag cement: Theory, modeling and application*, PhD thesis, University of Twente, Enschede, The Netherlands.
- Chen, W. and Brouwers, H. J. H. (2009). Mineral shrinkage-compensating admixtures for concrete: Experiments and numerical simulation, *Cement and Concrete Research* (submitted).
- CIPEC (2001). Energy consumption benchmark guide: Cement clinker production, Natural Resources Canada, Office of Energy Efficiency, Ottawa, Canada
http://oee.nrcan.gc.ca/publications/industrial/BenchmCement_e.pdf.
- Craig, R. F. (1994). *Soil Mechanics*, 6th edn, Spoon Press, London, UK.
- De Goey, A. W. (1954). *Betonwaren*, 2nd edn, Bond van Fabrikanten van Betonwaren in Nederland, Amsterdam, The Netherlands (in Dutch).
- De Larrard, F. (1989). Ultrafine particles for the making of very high strength concretes, *Cement and Concrete Research* **19**(2): 161–172.
- De Larrard, F. and Sedran, T. (1994). Optimization of ultra-high-performance concrete by the use of a packing model, *Cement and Concrete Research* **24**(6): 997–1009.
- De Larrard, F. and Sedran, T. (2002). Mixture-proportioning of high-performance concrete, *Cement and Concrete Research* **32**(11): 1699–1704.
- Denbigh, K. G. and Turner, J. C. R. (1965). *Chemical reactor theory : An introduction*, 3rd edn, Cambridge University Press, Cambridge, UK.
- Devahasdin, S., Chiun, F., Li, K. and Chen, D. H. (2003). TiO₂ photocatalytic oxidation of nitric oxide: Transient behavior and reaction kinetics, *Journal of Photochemistry and Photobiology A: Chemistry* **156**(1-3): 161–170.
- Directive 2001/81/EC (2001). Directive of the European Parliament and of the Council on national emission ceilings for certain atmospheric pollutants, *Official Journal of the European Communities*: L 309/22–L 309/30.
- Djehghri, N. and Teichner, J. (1980). Heterogeneous Photocatalysis: The Photooxidation of 2-Methylbutane, *Journal of Catalysis* **62**(1): 99–106.
- Domone, P. L. (2007). A review of the hardened mechanical properties of self-compacting concrete, *Cement & Concrete Composites* **29**(1): 1–12.
- Fennis, S. A. A. M., Walraven, J. C. and den Uijl, J. A. (2009). The use of particle packing models to design ecological concrete, *Heron* **54**(2-3): 185–204.
- Féret, R. (1892). Sur la compactié des mortiers hydrdrauliques, *Ann. Ponts Chaussée, mémoires et*

- documents* 7(4): 5–164 (in French).
- Ferraris, C. F. (1996). Measurement of Rheological Properties of High Performance Concrete: Sate of the Art Report, *Report NISTIR 5869*, National Institute of Standards and Technology, Gaithersburg, U.S.
- Fujishima, A. and Honda, K. (1972). Electrochemical Photolysis of Water at a Semiconductor Electrode, *Nature* 238(5358): 37–38.
- Fuller, W. B. and Thompson, S. E. (1907). The laws of proportioning concrete, *Transactions of the American Society of Civil Engineers* 33: 222–298.
- Funk, J. E. and Dinger, D. R. (1994). *Predictive Process Control of Crowded Particulate Suspensions: Applied to Ceramic Manufacturing*, Kluwer Academic Press, Boston, US.
- Furnas, C. C. (1928). The Relations between Specific Volume, Voids, and Size Composition in Systems of Broken Solids of Mixed Sizes, *Report of Investigation, Serial No. 2894*, US Department of Commerce, Bureau of Mines.
- Furnas, C. C. (1931). Grading Aggregates: I – Mathematical Relations for Beds of Broken Solids of Maximum Density, *Industrial and Engineering Chemistry* 23(9): 1052–1058.
- Geisenhanslüke, C. (2008). *Einfluss der Granulometrie von Feinstoffen auf die Rheologie von Feinstoffleimen*, PhD thesis, University of Kassel, Kassel, Germany (in German).
- Halsey, T. C. and Levine, A. J. (1998). How Sandcastles Fall, *Physical Review Letters* 80(14): 3141–3144.
- Hamaker, H. C. (1937). The London-Van der Waals attraction between spherical particles, *Physica* 4(10): 1058–1072.
- Häring, C. (2000). Production of earth-moist directly unmolded test specimens, *BFT International: Concrete Plant + Precast Technology* 66(7): 100–102.
- Häring, C. (2002). Development of earth-moist, direct-stripping, mix designs, *BFT International: Concrete Plant + Precast Technology* 68(1): 69–71.
- Häring, C. (2003). *Gebrauchsanweisung für CemTec Probenfertiger Generation 8*, CemTec Beratung GmbH, Cham, Switzerland (in German).
- Hashimoto, K. (2007). TiO₂ photocatalysts towards novel building materials, in P. Baglioni and L. Cassar (eds), *Proceedings International RILEM Symposium on Photocatalysis, Environment and Construction Materials, 8-9 October 2007, Florence, Italy*, RILEM Publications SARL, Bagneux, France, pp. 3–8.
- Herrmann, J. M., Péruchon, L., Puzenat, E. and Guillard, C. (2007). Photocatalysis: From fundamentals to self-cleaning glass application, in P. Baglioni and L. Cassar (eds), *Proceedings International RILEM Symposium on Photocatalysis, Environment and Construction Materials, 8-9 October 2007, Florence, Italy*, RILEM Publications SARL, Bagneux, France, pp. 41–48.
- HLUG (2009). Hessisches Landesamt für Umwelt und Geologie - Nitrogen oxides (NO/NO₂) <http://www.hlug.de/medien/luft/komponenten/stickoxide/stickoxide.htm>.
- Ho, D. W. S., Sheinn, A. M. M., Ng, C. C. and Tam, C. T. (2002). The use of quarry dust for SCC applications, *Cement and Concrete Research* 32(4): 505–511.
- Horiba (2006). *Operations manual – ambient NO_x monitor APNA-370*, 3rd edn, published in September 2006.
- Hummel, A. (1959). *Das Beton-ABC : Ein Lehrbuch der Technik des Schwerbetons und des Leichtbetons*, Verlag von Wilhelm Ernst & Sohn, Berlin, Germany (in German).
- Hunger, M. (2010). *An integral design concept for ecological Self-Compacting Concrete*, PhD thesis, Eindhoven University of Technology, Eindhoven, The Netherlands.
- Hunger, M. and Brouwers, H. J. H. (2006). Development of Self-Compacting Eco-Concrete, in H. B. Fischer (ed.), *Proceedings 16th ibausil, International Conference on Building Materials*,

- F.A. Finger Institut für Baustoffkunde, Weimar, Germany, pp. 2:0189–2:0198.
- Hunger, M. and Brouwers, H. J. H. (2009). Flow analysis of water–powder mixtures: Application to specific surface area and shape factor, *Cement and Concrete Composites* **31**(1): 39–59.
- Hunger, M., Hüskén, G. and Brouwers, H. J. H. (2008a). Photocatalysis applied to concrete products – part 1: Principles and test procedure, *ZKG International* **61**(10): 77–85.
- Hunger, M., Hüskén, G. and Brouwers, H. J. H. (2008b). Photocatalysis applied to concrete products – part 2: Influencing factors and product performance, *ZKG International* **61**(10): 76–84.
- Hunger, M., Hüskén, G. and Brouwers, H. J. H. (2010). Photocatalytic degradation of air pollutants – From modeling to large scale application, *Cement and Concrete Research* **40**(2): 313–320.
- Hüskén, G. and Brouwers, H. J. H. (2008). A new mix design concept for earth-moist concrete: A theoretical and experimental study, *Cement and Concrete Research* **38**(10): 1246–1259.
- Hüskén, G. and Brouwers, H. J. H. (2009a). Development of eco earth-moist concrete, *Proceedings of the International Conference Excellence in Concrete Construction through Innovation, 9-10 September 2008, Kingston University, London, UK*, pp. 97–105.
- Hüskén, G. and Brouwers, H. J. H. (2009b). On the Early Age Behavior of Earth-Moist Concrete, in H. B. Fischer (ed.), *Proceedings 17th ibausil, International Conference on Building Materials*, pp. 2:0531–2:0536.
- Hüskén, G. and Brouwers, H. J. H. (2010). Eco-SCC: From Theory to Practical Application, *1st International Conference on Sustainable Construction Materials: Design, Performance and Application, 10-12 August 2010, Wuhan, China*, pp. 720–732.
- Hüskén, G., Hunger, M. and Brouwers, H. J. H. (2008). Comparative study on air-purifying concrete products, *BFT international: concrete plant + precast technology* **74**(4): 12–18.
- Hüskén, G., Hunger, M. and Brouwers, H. J. H. (2009a). Experimental study of photocatalytic concrete products for air purification, *Building and Environment* **44**(12): 2463–2474.
- Hüskén, G., Hunger, M. and Brouwers, H. J. H. (2009b). Photocatalytic concrete products – practical application and modeling, *BFT international: concrete plant + precast technology* **75**(12): 24–33.
- Imoberdorf, G. E., Irazoqui, H. A., Cassano, A. E. and Alfano, O. M. (2005). Photocatalytic Degradation of Tetrachloroethylene in Gas Phase on TiO₂ Films: A Kinetic Study, *Industrial & Engineering Chemistry* **44**(16): 6075–6085.
- Invelop (2005). *Intensive Compaction Tester: Operating Instructions*, Invelop Oy, Savonlinna, Finland.
- Israelachvili, J. N. (1991). *Intermolecular and Surface Forces*, Academic Press Ltd, London, UK.
- Jacoby, W. A., Blake, D. M., Noble, R. D. and Koval, C. A. (1995). Kinetics of the Oxidation of Trichloroethylene in Air via Heterogeneous Photocatalysis, *Journal of Catalysis* **157**(1): 87–96.
- Jones, M. R., Zhen, L. and Newlands, M. D. (2002). Comparison of particle packing models for proportioning concrete constituents for minimum void ratio, *Materials and Structures* **35**(5): 301–309.
- Juvas, K. J. (1996). Very dry precasting concretes, in P. J. M. Bartos, D. L. Marrs and D. J. Cleland (eds), *Production Methods and Workability of Concrete*, E & FN Spon, London, UK, pp. 153–168.
- Käppi, A. and Nordenswan, E. (2007). Workability of No-Slump Concrete, *Concrete International* **29**(3): 37–41.

- Katz, A. (2003). Properties of concrete made with recycled aggregate from partially hydrated old concrete, *Cement and Concrete Research* **33**(5): 703–711.
- Kawai, T. and Sakata, T. (1981). Photocatalytic hydrogen production from water by the decomposition of poly-vinylchloride, protein, algae, dead insects, and excrement, *Chemistry Letters* **10**(1): 81–84.
- Keidel, E. (1929). Die Beeinflussung der Lichtechtheit von Teerfarblacken durch Titanweiss, *Farben-Zeitung* **34**: 1242–1243 (in German).
- Keller, B. and Rutz, S. (2010). *Pinpoint: key facts and figures for sustainable buildings*, Birkhäuser, Basel, Switzerland.
- Kerkhoff, B. and Siebel, E. (2002). Einfluss von rezykliertem Zuschlag aus Betonbruch auf die Dauerhaftigkeit von Beton, *Deutsches Institut für Normung: Deutscher Ausschuss für Stahlbeton, Heft 514*, Deutscher Ausschuss für Stahlbeton, Berlin, Germany, pp. 3–36.
- Koehler, E. P. and Fowler, D. W. (2003). Summary of Concrete Workability Test Methods, *Report ICAR 105.1*, University of Texas at Austin, Austin, U.S.
- König, E., Tue, N. V. and Schenk, G. (2008). *Grundlagen des Stahlbetonbaus: Einführung in die Bemessung nach DIN 1045-1*, Vieweg + Teubner, Wiesbaden, Germany.
- Kordts, S. (2005). *Herstellung und Steuerung der Verarbeitbarkeitseigenschaften selbstverdichtender Betone*, PhD thesis, Technische Universität Berlin, Berlin, Germany (in German).
- Kosmatka, S. H., Kerkhoff, B., Panarese, W. C., MacLeod, N. F. and McGrath, R. J. (2002). *Design and Control of Concrete Mixtures*, 7th Canadian edn, Cement Association of Canada, Ottawa, Canada.
- Kou, S. C. and Poon, C. S. (2009). Properties of self-compacting concrete prepared with coarse and fine recycled concrete aggregates, *Cement & Concrete Composites* **31**(9): 622–627.
- Kovler, K. and Jensen, O. M. (2007). Internal curing of concrete: State-of-the-art report of RILEM technical committee 196-icc, *Report*, RILEM Publications SARL, Bagneux, France.
- Krikhaar, H. M. M. (2010). Betonpocket 2010, ENCI B.V., PO Box 3232, 5203 DE, 's Hertogenbosch, The Netherlands (in Dutch).
- Krupp, H. (1967). Particle Adhesion - Theory and Experiment, *Advances in Colloid and Interface Science* **1**(2): 111–239.
- Lahl, U. and Lambrecht, U. (2008). High NO₂ Levels: Ongoing Need for Action on Diesel Emissions, *Technical Congress 2008*, Verband der Automobilindustrie.
- Lifshitz, E. M. (1956). The theory of molecular attractive forces between solids, *Soviet Physics JETP letters* **2**: 73–83.
- Lim, T. H., Jeong, S. M., Kim, S. D. and Gyenis, J. (2000). Photocatalytic decomposition of NO by TiO₂ particles, *Journal of Photochemistry and Photobiology A: Chemistry* **134**(3): 209–217.
- Locher, F. W. (1976). Die Festigkeit des Zements, *Beton* **26**(8): 283–286 (in German).
- Marceau, M. L., Nisbet, M. A. and VanGeem, M. G. (2007). Life Cycle Inventory of Portland Cement Concrete, *Report*, Portland Cement Association, Skokie, U.S.
- Maruyama, I. and Sato, R. (2005). A trial of reducing autogenous shrinkage by recycled aggregate, in B. Persson, D. Bentz and L. Nilsson (eds), *Proceedings of the Fourth International Research Seminar on Self-Desiccation and its Importance in Concrete Technology, June 2005*, Gaithersburg, U.S., pp. 264–270.
- Matsuda, S., Hatanoa, H. and Tsutsumib, A. (2001). Ultrafine particle fluidization and its application to photocatalytic NO_x treatment, *Chemical Engineering Journal* **82**(1-3): 183–188.
- Mathews, R. W. (1988). Kinetics of photocatalytic oxidation of organic solutes over titanium dioxide, *Journal of Catalysis* **111**(2): 264–272.

- Mechtcherine, V., Dudziak, L. and Schulze, J. (2006). Internal curing by super absorbent polymers (SAP): Effects on material properties of self-compacting fibre-reinforced high performance concrete, in P. Jensen, O.M. Lura and K. Kovler (eds), *International RILEM Conference on Volume Changes of Hardening Concrete: Testing and Mitigation*, RILEM Publications SARL, Bagnaux, France, pp. 87–96.
- Mills, A. and Le Hunte, S. (1997). An overview of semiconductor photocatalysis, *Journal of Photochemistry and Photobiology A: Chemistry* **108**(1): 1–35.
- Mindess, S., Young, J. F. and Darwin, D. (2003). *Concrete*, 2nd edn, Prentice Hall, Upper Saddle River, U.S.
- Mitsubishi (2005). *Noxer – NO_x removing paving block*, Mitsubishi Materials Corporation.
- Mooney, M. (1951). The viscosity of a concentrated suspension of spherical particles, *Journal of Colloid Science* **6**(2): 162–170.
- Moosberg-Bustnes, H., Lagerblad, B. and Forsberg, E. (2004). The function of fillers in concrete, *Materials and Structures* **37**(2): 74–81.
- Müller, A. (2003a). Recycling of masonry rubble: Status and new utilization methods (Part 1), *Brick and Tile Industry International* **56**(6): 17–25.
- Müller, A. (2003b). Utilization of recycling construction materials from masonry rubble: Own developments (Part 3), *Brick and Tile Industry International* **56**(10): 2–10.
- Murata, Y., Kamitani, K., Tawara, H. and Takeuchi, K. (1998). Air purifying pavement: Development of photocatalytic concrete blocks for removal of NO_x, *Shigen to Sozai* **114**(5): 381–386.
- Murata, Y., Obata, H., Tawara, H. and Murata, K. (1997). *NO_x-cleaning paving block*, EP-patent 0 786 283 A1, Mitsubishi Materials Corporation, Tokyo, Japan.
- Murata, Y., Tawara, H., Obata, H. and Takeuchi, K. (1999). Air purifying pavement: Development of photocatalytic concrete blocks, *Journal of Advanced Oxidation Technologies* **4**(2): 227–230.
- Nanni, A., Ludwigg, D. and Shoenberger, J. (1996). Roller compacted concrete for highway pavements, *Concrete International* **18**(5): 33–38.
- Neville, A. (1997). Maintenance and Durability of Structures, *Concrete International* **19**(11): 52–56.
- Neville, A. (1999). How Useful is the Water-Cement Ratio?, *Concrete International* **21**(9): 69–70.
- Neville, A. (2006). *Concrete: Neville's insights and issues*, Thomas Telford Ltd, London, UK.
- Obee, T. N. and Brown, R. T. (1995). TiO₂ Photocatalysis for Indoor Air Applications: Effects of Humidity and Trace Contaminant Levels on the Oxidation Rates of Formaldehyde, Toluene, and 1,3-Butadiene, *Environmental Science and Technology* **29**(5): 1223–1231.
- Okamura, H. and Ouchi, M. (2003). Self-compacting concrete, *Journal of Advanced Concrete Technology* **1**(1): 5–15.
- Ollis, D. F., Pelizzetti, E. and Serpone, N. (1991). Photocatalyzed destruction of water contaminants, *Environmental Science and Technology* **25**(9): 1523–1529.
- Paakkinen, I. (1986). Intensive compaction tester device for testing the compactability of no-slump concrete, *Nordic Concrete Research Publication No. 5* pp. 109–116.
- Peikert, R. (1994). Dichteste Packungen von gleichen Kreisen in einem Quadrat, *Elemente der Mathematik* **49**: 16–26 (in German).
- Peller, J. R., Whitman, R. L., Griffith, S., Harris, P., Peller, C. and Scalzitti, J. (2007). TiO₂ as a photocatalyst for control of the aquatic invasive alga, cladophora, under natural and artificial light, *Journal of Photochemistry and Photobiology A: Chemistry* **186**(2-3): 212–217.
- Peral, J. and Ollis, D. F. (1992). Heterogeneous Photocatalytic Oxidation of Gas-Phase Organ-

- ics for Air Purification: Acetone, 1-Butanol, Butyraldehyde, Formaldehyde, and m-Xylene Oxidation, *Journal of Catalysis* **136**(2): 554–565.
- Plum, N. M. (1950). The predetermination of water requirement and optimum grading of concrete under various conditions, *Building Research Studies No. 3*, The Danish National Institute of Building Research, Copenhagen, Denmark.
- Pöllmann, H. (2007). Private communication.
- Pöllmann, H. (2009). Private communication.
- Poon, C. S. and Chan, D. (2006). Paving blocks made with recycled concrete aggregate and crushed clay brick, *Construction and Building Materials* **20**(8): 569–577.
- Powers, T. C. and Brownyard, T. L. (1947). Studies of the physical properties of hardened portland cement paste, *Bulletin 22*, Research Laboratories of the Portland Cement Association, Skokie, U.S.
- Pruden, A. L. and Ollis, D. F. (1982). Photoassisted Heterogeneous Catalysis: The Degradation of Trichloroethylene in Water, *Journal of Catalysis* **82**(2): 404–417.
- Reschke, T. (2000). *Der Einfluß der Granulometrie der Feinstoffe auf die Gefügeentwicklung und die Festigkeit von Beton*, PhD thesis, Bauhaus-Universität Weimar, Weimar, Germany (in German).
- Ritchie, A. G. B. (1962). The triaxial testing of fresh concrete, *Magazine of Concrete Research* **14**(40): 37–42.
- Rumpf, H. (1975). *Mechanische Verfahrenstechnik*, Carl Hanser Verlag, München, Germany (in German).
- Schießl, P. and Müller, C. (1997). Betonwaren mit Recyclingzuschlägen: Zwischenbericht f2550/2 (Kurzfassung), *Report*, Institut für Bauforschung, Rheinisch-Westfälische Technische Hochschule Aachen, Aachen, Germany (in German).
- Schmidt, L. D. (1998). *The Engineering of Chemical Reactions*, Oxford University Press, Oxford, UK.
- Schmidt, M. (1999). Erdfeuchte Betone - Anforderungen, Verarbeitbarkeit, Grünstandfestigkeit und Prüfverfahren, *BFT International: Concrete Plant + Precast Technology* **65**(11): 14–24.
- Schmidt, M., Bornemann, R. and Bilgeri, P. (2005). Entwicklung optimierter hüttensandhaltiger Zemente für den Einsatz in der Betonwarenindustrie, *Betonwerk International* **8**(3): 62–72 (in German).
- Schmidt, M. and Geisenhanslüke, C. (2005). Optimierung der Zusammensetzung des Feinstkorns von Ultra-Hochleistungs- und von selbstverdichtendem Beton, *beton* **55**(5): 224–235.
- Schubert, H. (1982). *Kapillarität in porösen Feststoffsystemen*, Springer Verlag, Berlin, Germany.
- Spiratos, N., Page, M., Mailvaganam, N., Malhotra, V. M. and Jolicoeur, C. (2003). *Superplasticizers for Concrete - Fundamentals, Technology and Practice*, AGMV Marquis, Quebec, Canada.
- Stark, J. and Wicht, B. (2001). *Dauerhaftigkeit von Beton: Der Baustoff als Werkstoff*, Birkhäuser, Basel, Switzerland (in German).
- Stiess, M. (2008). *Mechanische Verfahrenstechnik - Partikeltechnologie 1*, Springer Verlag, Berlin, Germany (in German).
- Stutech (2005). Aardvochtig beton, *Stutech report No. 22*, STUTECH - Studievereniging Beton-technologie, 's Hertogenbosch, The Netherlands (in Dutch).
- Su, N. and Miao, B. (2003). A new method for the mix design of medium strength flowing concrete with low cement content, *Cement and Concrete Composites* **25**(2): 215–222.
- Suzuki, K. (1993). Photocatalytic Air Purification on TiO₂ Coated Honeycomb Support, *in*

- D. F. Ollis and H. Al-Ekabi (eds), *Proceedings of the 1st International Conference on TiO₂ Photocatalytic Purification and Treatment of Water and Air, 8-13 November 1992, London, Ontario, Canada*, Elsevier Science Publishers, Amsterdam, The Netherlands, pp. 421–434.
- U.S. Geological Survey (2010). Cement Statistics
<http://minerals.usgs.gov/ds/2005/140/cement.pdf>.
- Vázquez, E. and Gonçalves, A. (2005). Recycled aggregate in concrete, *Use of Recycled Materials - Final Report of RILEM TC 198-URM*, RILEM Publications SARL, Bagneux, France, pp. 41–43.
- VDZ (2002). *Zement-Taschenbuch 2002*, Verein Deutscher Zementwerke e.V., Düsseldorf, Germany (in German).
- Vissers, L. J. L. (1997). Fly ash as binder in concrete, *Studies in Environmental Science* **71**: 279–288.
- Wagner, A. (1929). Titanweißkatalyse?, *Farben-Zeitung* **34**: 1243–1245 (in German).
- Walz, K. (1964). Kennzeichnung der Betonkonsistenz durch das Verdichtungsmass v , *Beton Herstellung Verwendung* **14**: 3–7.
- Wang, H., Wu, Z., Zhao, W. and Guan, B. (2007). Photocatalytic oxidation of nitrogen oxides using TiO₂ loading on woven glass fabric, *Chemosphere* **66**(1): 185–190.
- Wang, R., Hashimoto, K., Fujishima, A., Chikuni, M., Kojima, E., Kitamura, A., Shimohigoshi, M. and Watanabe, T. (1997). Light-induced amphiphilic surfaces, *Nature* **388**(6641): 431–432.
- Wassermann, R., Katz, A. and Bentur, A. (2009). Minimum cement content requirements: A must or a myth?, *Materials and Structures* **42**(7): 973–982.
- Wassing, W. (2002). Einfluß von Feinstoffen aus Betonbruch auf den Hydratationsfortschritt, *Deutsches Institut für Normung: Deutscher Ausschuss für Stahlbeton, Heft 514*, Deutscher Ausschuss für Stahlbeton, Berlin, Germany, pp. 37–72.
- Watanabe, T., Kitamura, A., Kojima, E., Nakayama, C., Hashimoto, K. and Fujishima, A. (1993). Photocatalytic Activity of TiO₂ Thin Film under Room Light, in D. F. Ollis and H. Al-Ekabi (eds), *Proceedings of the 1st International Conference on TiO₂ Photocatalytic Purification and Treatment of Water and Air, 8-13 November 1992, London, Ontario, Canada*, Elsevier Science Publishers, Amsterdam, The Netherlands, pp. 747–751.
- Weber, S. and Reinhardt, H. W. (1997). A new generation of high performance concrete: Concrete with autogenous curing, *Advanced Cement Based Materials* **6**(2): 59–68.
- Westman, A. and Hugill, H. (1930). The packing of particles, *Journal of the American Ceramic Society* **13**: 767–779.
- Worrell, E., Martin, N. and Price, L. (1999). Energy Efficiency and Carbon Dioxide Emissions Reduction Opportunities in the U.S. Iron and Steel Sector, *Report*, Energy Analysis Department, University of California, Berkeley, U.S.
- Yamazaki, S., Tanaka, S. and Tsukamoto, H. (1999). Kinetic studies of oxidation of ethylene over a TiO₂ photocatalyst, *Journal of Photochemistry and Photobiology A: Chemistry* **121**(1): 55–61.
- Zhang, J., Ayusawa, T., Minagawa, M., Kinugawa, K., Yamashita, H., Matsuoka, M. and Anpo, M. (2001). Investigations of TiO₂ Photocatalysts for the Decomposition of NO in the Flow System: The Role of Pretreatment and Reaction Conditions in the Photocatalytic Efficiency, *Journal of Catalysis* **198**(1): 1–8.
- Zhao, J. and Yang, X. (2003). Photocatalytic oxidation for indoor air purification: A literature review, *Building and Environment* **38**(5): 645–654.
- Zhutovsky, S., Kovler, K. and Bentur, A. (2002). Efficiency of lightweight aggregates for internal curing of high strength concrete to eliminate autogenous shrinkage, *Materials and Structures* **35**(2): 97–101.

List of symbols and abbreviations

Abbreviations

CoA	Coenzyme A, pp. 142
COV	Coefficient of variation, pp. 24
CPM	Compressive packing model, pp. 49
EMC	Earth-moist concrete, pp. 1
GGBFS	Ground granulated blast furnace slag, pp. 28
hcp	Hexagonal close packing, pp. 42
HSC	High-strength concrete, pp. 99
LDA	Laser diffraction analysis, pp. 16
LOI	Loss on ignition, pp. 21
LPDM	Linear packing density model, pp. 49
LWC	Light-weight concrete, pp. 1
NWC	Normal strength, normal weight concrete, pp. 1
OPC	Ordinary Portland cement, pp. 7
PCO	Photocatalytic oxidation, pp. 139
PSD	Particle size distribution, pp. 16
RCA	Recycled concrete aggregates, pp. 12
RCC	Roller-compacted concrete, pp. 2
RCD	Roller-compacted concrete for dams, pp. 3
RCF	Recycled concrete fines, pp. 21
SAP	Super-absorbent polymers, pp. 100
sc	Simple cubic, pp. 41
SCC	Self-compacting concrete, pp. 1
SP	superplasticizer, pp. 112
SSM	Solid suspension model, pp. 49
UHPC	Ultra-high performance concrete, pp. 99
VOC	Volatile organic compound, pp. 140
XRD	X-Ray diffraction, pp. 24
XRF	X-Ray fluorescence, pp. 21

Roman

\dot{V}	Volume flow , pp. 150	[l/min]
$\hbar\omega$	Lifshitz-van der Waals constant , pp. 111	[eV]
\bar{D}	Mean particle diameter , pp. 16	[mm]
Δp	Capillary pressure , pp. 113	[bar]
A_F	Photocatalytic activity of NO _x reduction (UNI 11247:2007) , pp. 146	[m/h]
a_{spl}	Length of the splitting area , pp. 92	[mm]

c	Degree of compaction , pp. 31	[-]
C_g	Pollutant gas concentration , pp. 149	[ppm]
D	Diameter , pp. 51	[mm]
D_h	Hydraulic diameter , pp. 150	[mm]
E	Irradiance , pp. 140	[W/m ²]
E_g	Band gap , pp. 139	[eV]
F	Frequency , pp. 139	[Hz]
f	converted air-flow rate at standard state , pp. 145	[l/min]
$f_{ct,sp}$	Splitting tensile strength , pp. 91	[N/mm ²]
f_c	Compressive strength , pp. 55	[N/mm ²]
H	Height , pp. 31	[mm]
h	Planck constant , pp. 139	[eVs]
I	Non-dimensional intensity of the luminous flux (UNI 11247:2007) , pp. 146	[-]
I'	Experimentally measured intensity (UNI 11247:2007) , pp. 146	[W/m ²]
k	Reaction rate constant , pp. 174	[mg/m ³ s]
K_d	Adsorption equilibrium constant , pp. 174	[m ³ /mg]
L_d	Critical length , pp. 150	[mm]
M	Mass , pp. 18	[kg]
m	Number of ingredients that make up the total concrete volume , pp. 75	[-]
n_{NO}	Amount of NO removed (ISO 22197-1:2007) , pp. 145	[μ mol]
P	Cumulative finer fraction , pp. 47	[%]
PF	Packing fraction , pp. 40	[-]
Q	Sieve residue , pp. 75	[M.-%]
q	Distribution modulus , pp. 47	[-]
R	Radius , pp. 114	[m]
r	Reaction rate , pp. 174	[-]
R^2	Coefficient of determination , pp. 74	[-]
Re	Reynolds number , pp. 150	[-]
RSS	Sum of the squares of the residuals , pp. 74	[-]
s	Size ratio , pp. 42	[-]
S_w	Degree of saturation , pp. 40	[%]
T	Splitting tensile strength according to EN 1338 , pp. 92	[N/mm ²]
t	Time , pp. 152	[s]
u	Flow velocity , pp. 150	[m/s]
V	Volume , pp. 18	[m ³]
v	Volumetric proportion , pp. 75	[-]
w/c	Water cement ratio , pp. 3	[-]
w/p	Water powder ratio , pp. 4	[-]
W_c	Compaction work , pp. 36	[J/kg]
x_{cem}	Compressive strength per kg cement / m ³ concrete , pp. 62	[Nm ³ /kgmm ²]
Greek		
α	Angle , pp. 36	[$^\circ$]
α_i	Curve fitting parameter , pp. 154	[-]

ϵ_0	Electric constant , pp. 111	$[A^2s^4/kgm]$
ϵ_r	Relative static permittivity , pp. 111	[-]
η	Removal rate , pp. 152	[%]
γ	Surface tension , pp. 112	$[mN/m]$
κ	Stoichiometric coefficient , pp. 174	[-]
λ	Wavelength , pp. 153	$[nm]$
μ_{air}	Dynamic viscosity , pp. 150	$[Ns/m^2]$
ν_{air}	Kinematic viscosity , pp. 150	$[m^2/s]$
$\phi_{NO,in}$	NO volume fraction at the reactor inlet , pp. 145	$[\mu l/l]$
$\phi_{NO,out}$	NO volume fraction at the reactor outlet , pp. 145	$[\mu l/l]$
ψ	Electric surface charge density , pp. 111	$[e/\mu m^2]$
ψ_m	Mass based moisture content , pp. 19	$[M.-%]$
θ	Contact angle , pp. 114	$[^\circ]$
ϕ	Void fraction , pp. 40	[-]
Φ_{open}	Open porosity , pp. 19	$[Vol.-%]$
ρ	Density , pp. 18	$[g/cm^3]$
ξ	Shape factor , pp. 120	[-]

Superscripts

<i>den</i>	Densely packed, pp. 18
<i>dry</i>	Dry, pp. 19
<i>i + 1</i>	Fraction index of the upper sieve size, pp. 73
<i>loo</i>	Loosely packed, pp. 18
<i>sat</i>	Saturated, pp. 19
<i>spe</i>	Specific, pp. 18
<i>tot</i>	Total, pp. 75
<i>und</i>	Under water, pp. 19
<i>vib</i>	Vibrated, pp. 18
<i>wet</i>	Wet, pp. 19

Subscripts

<i>adm</i>	Admixture, pp. 76
<i>agg</i>	Aggregate, pp. 76
<i>air</i>	Air, pp. 40
<i>app</i>	Apparent, pp. 44
<i>cap</i>	Capillary, pp. 114
<i>cem</i>	Cement, pp. 62
<i>coa</i>	Coarse, pp. 44
<i>com</i>	Computed, pp. 32
<i>con</i>	Concrete, pp. 33
<i>fil</i>	Filler, pp. 76
<i>fin</i>	Fine, pp. 44
<i>i</i>	Fraction index of the lower sieve size, general counter, pp. 73
<i>ICT</i>	Intensive compaction test, pp. 36
<i>in</i>	Inlet, pp. 149

<i>k</i>	Counter variable for materials, pp. 75
<i>lar</i>	Large, pp. 43
<i>liq</i>	Liquid, pp. 18
<i>max</i>	Maximum, pp. 40
<i>med</i>	Medium, pp. 46
<i>min</i>	Minimum, pp. 40
<i>mix</i>	Composed mix, pp. 74
<i>n</i>	End value of the counter, pp. 73
<i>opt</i>	Optimum, pp. 44
<i>out</i>	Outlet, pp. 151
<i>pyc</i>	Pycnometer, pp. 18
<i>sli</i>	Slit, pp. 147
<i>sma</i>	Small, pp. 43
<i>sol</i>	Solid, pp. 18
<i>tar</i>	Target grading curve, pp. 74
<i>uni</i>	Unit cell, pp. 40
<i>vdW</i>	Van der Waals, pp. 111
<i>ves</i>	Vessel, pp. 33
<i>wat</i>	Water, pp. 76

Chemical compounds

Al_2O_3	Aluminium oxide, pp. 21
BrO_3^-	Bromate, pp. 141
C_2S	Dicalcium silicate, pp. 28
C_3S	Tricalcium silicate, pp. 28
CaO	Calcium oxide, pp. 21
Fe_2O_3	Iron(III) oxide, pp. 21
K_2CO_3	Potassium carbonate, pp. 105
K_2O	Potassium oxide, pp. 21
MnO	Manganese(II) oxide, pp. 21
N_2	Nitrogen, pp. 149
Na_2O	Sodium oxide, pp. 21
NO_3^-	Nitrate, pp. 139
NO_x	Nitrogen oxides, pp. 139
SiO_2	Silicon dioxide, pp. 21
SnO_2	Tin dioxide, pp. 137
SO_3	Sulfur trioxide, pp. 21
SO_x	Sulfur oxide, pp. 141
TiO_2	Titanium dioxide, pp. 137
CdS	Cadmium sulfide, pp. 137
CSH	Calcium silicate hydrate, pp. 28
ZnO	Zinc oxide, pp. 137
ZnS	Zinc sulfide, pp. 137

Material properties

A.1 Physical properties

Table A.1: Physical properties of materials used in this research.

Material	Type	ρ^{spe}	D_{max}	D_{50}	D_{min}	SSA
		[g/cm ³]	[mm]	[mm]	[mm]	[cm ² /g]
Cement	CEM I 32.5 R	3.138	0.1047	0.0071	3.63E-04	2800
Cement	CEM I 52.5 N	3.064	0.0525	0.0059	3.63E-04	4840
Cement	CEM III/B 42.5 N	2.962	0.0794	0.0081	3.63E-04	4820
Micro cement	CEM I 52.5 R	3.150	0.0199	0.0038	3.63E-04	22000
Filler	Fly ash	2.211	0.1380	0.0116	2.75E-04	3820
Filler	Micro silica	2.333	3.16E-04	1.75E-04	9.12E-05	
Recycled concrete fines	RCF1	2.580	0.1380	0.0176	3.16E-04	
Recycled concrete fines	RCF2	2.580	0.1585	0.0212	2.75E-04	
Quartz flour 1	Quartz	2.650	0.1202	0.0103	4.17E-04	4000
Quartz flour 2	Quartz	2.650	0.1202	0.0110	4.17E-04	3600
Quartz flour 3	Quartz	2.650	0.1380	0.0130	4.17E-04	2000
Photocatalyst	TiO ₂ A	3.900	0.0033	0.0012	3.16E-04	
Photocatalyst	TiO ₂ B	3.935	0.0199	0.0028	3.63E-04	
Photocatalyst	TiO ₂ C	3.900	0.0263	0.0021	1.59E-04	
Photocatalyst	TiO ₂ D	3.900	0.0263	0.0020	1.38E-04	
Photocatalyst	TiO ₂ E	3.900	0.0263	0.0021	1.59E-04	
Fine sand	Sand 0-1	2.636	1	–	0.125	
Medium Sand	Sand 0-2	2.650	2	–	0.125	
Coarse Sand	Sand 0-4	2.642	4	–	0.250	
Normsand	Normsand EN 196-1	2.650	2.0	–	0.08	
Premix sand	Premix 0-4	2.648	5.6	–	0.28	
Recycled concrete aggr.	RCA1	2.635	1.4	–	0.71	
Recycled concrete aggr.	RCA2	2.635	1.4	–	0.71	
Broken Granite	Granite 2-8	2.650	8	–	2	
Fine gravel	Gravel 2-8	2.620	8	–	2	
Medium Gravel	Gravel 4-16	2.650	16	–	4	
Medium Gravel	Gravel 8-16	2.650	16	–	8	

A.2 Chemical composition

Table A.2: Chemical composition of the analyzed recycled concrete fines (RCF), stone waste material, and selected cements. (Chen, 2007; Pöllmann, 2007, 2009).

Content [%]	RCF1	RCF2	Granite	CEM I
LOI	6.2	1.3	5.2	2.8
Na ₂ O	0.7	1.0	3.3	0.4
MgO	1.2	1.5	2.0	1.0
Al ₂ O ₃	5.9	10.8	14.0	4.5
SiO ₂	69.9	73.3	61.7	19.9
P ₂ O ₅	0.0	0.0	0.0	0.0
SO ₃	0.8	0.1	0.2	3.3
Cl	0.0	0.0	0.0	0.1
K ₂ O	1.2	2.3	3.7	0.6
CaO	11.6	5.1	5.8	63.8
TiO ₂	0.3	0.6	0.6	0.2
MnO	0.1	0.1	0.1	0.1
Fe ₂ O ₃	1.9	3.8	3.2	3.2
NiO	0.0	0.0	0.0	0.0
ZnO	0.0	0.0	0.0	0.1
SrO	0.0	0.0	0.0	0.1
ZrO ₂	0.1	0.0	0.0	0.0
BaO	0.0	0.0	0.2	0.0
Total	100.0	100.0	100.0	100.0

Sieve data

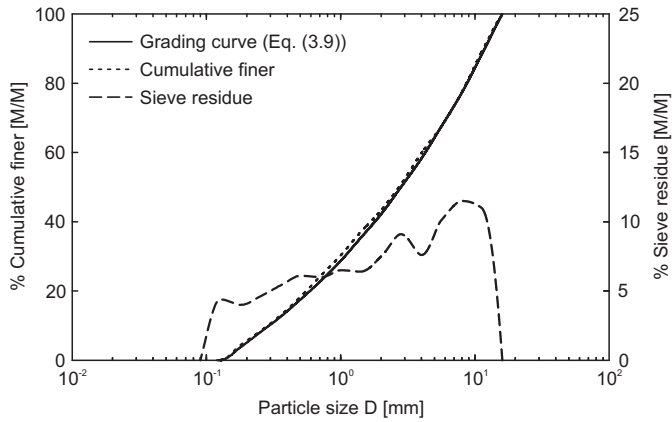


Figure B.1: Composed aggregate mix ($q = 0.25$, $D_{max} = 16$ mm, $D_{min} = 0.125$ mm).

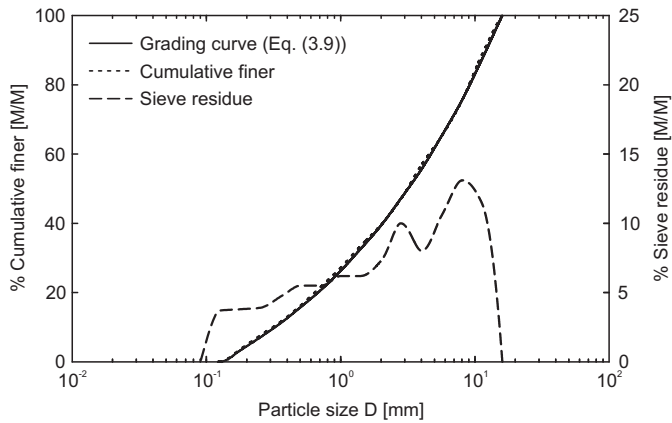


Figure B.2: Composed aggregate mix ($q = 0.30$, $D_{max} = 16$ mm, $D_{min} = 0.125$ mm).

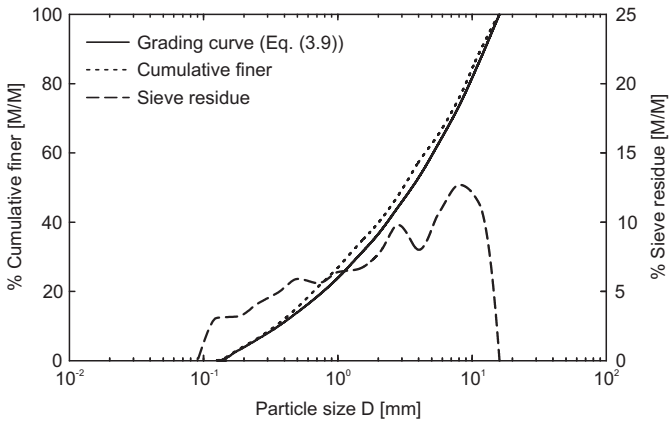


Figure B.3: Composed aggregate mix ($q = 0.35$, $D_{max} = 16$ mm, $D_{min} = 0.125$ mm).

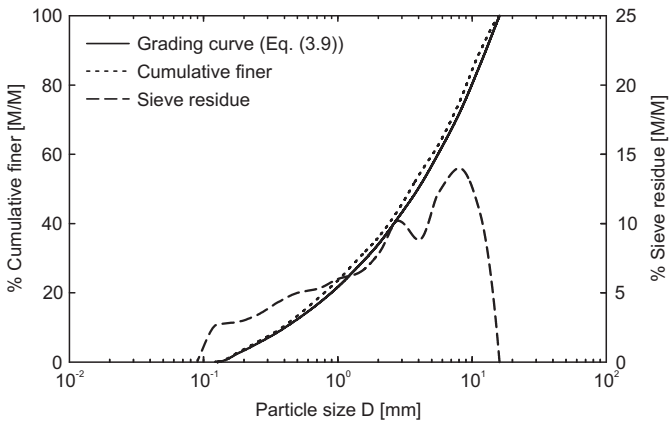


Figure B.4: Composed aggregate mix ($q = 0.40$, $D_{max} = 16$ mm, $D_{min} = 0.125$ mm).

Table B.1: ISO (EN) sieve sizes (ISO 3310), and ASTM (ASTM E11) and Tyler meshes in comparison. The shaded cells indicate sieves that have been used in the present study.

US sieve types		ISO sieve sizes		US sieve types		ISO sieve sizes	
ASTM	Tyler	[mm]	[inch]	ASTM	Tyler	[μm]	[inch]
		63.0	2.480	No. 25	24 Mesh	710	0.028
		31.5	1.240			630	0.025
		22.4	0.882	No. 30	28 Mesh	600	0.024
		20.0	0.787			560	0.022
5/8 in.		16.0	0.630	No. 35	32 Mesh	500	0.020
		14.0	0.551			450	0.018
0.53 in.		13.2	0.520	No. 40	35 Mesh	425	0.017
1/2 in.		12.5	0.492			400	0.016
7/16 in.		11.2	0.441	No. 45	42 Mesh	355	0.014
		10.0	0.394			315	0.012
3/8 in.		9.50	0.374	No. 50	48 Mesh	300	0.012
		9.00	0.354			280	0.011
5/16 in.	2 1/2 Mesh	8.00	0.315	No. 60	60 Mesh	250	0.010
		7.10	0.280			224	0.009
0.265 in.	3 Mesh	6.73	0.265	No. 70	65 Mesh	212	0.008
1/4 in.		6.30	0.248			200	0.008
No. 3 1/2	3 1/2 Mesh	5.60	0.220	No. 80	80 Mesh	180	0.007
		5.00	0.197			160	0.006
No. 4	4 Mesh	4.75	0.187	No. 100	100 Mesh	150	0.006
		4.50	0.177			140	0.006
No. 5	5 Mesh	4.00	0.157	No. 120	115 Mesh	125	0.005
		3.55	0.140			112	0.004
No. 6	6 Mesh	3.35	0.132	No. 140	150 Mesh	106	0.004
		3.15	0.124			100	0.004
No. 7	7 Mesh	2.80	0.110	No. 170	170 Mesh	90	0.004
		2.50	0.098			80	0.003
No. 8	8 Mesh	2.36	0.093	No. 200	200 Mesh	75	0.003
		2.24	0.088			71	0.003
No. 10	9 Mesh	2.00	0.079	No. 230	250 Mesh	63	0.002
		1.80	0.071			56	0.002
No. 12	10 Mesh	1.70	0.067	No. 270	270 Mesh	53	0.002
		1.60	0.063			50	0.002
No. 14	12 Mesh	1.40	0.055	No. 325	325 Mesh	45	0.002
		1.25	0.049			40	0.002
No. 16	14 Mesh	1.18	0.046	No. 400	400 Mesh	38	0.001
		1.12	0.044			36	0.001
No. 18	16 Mesh	1.00	0.039	No. 450		32	0.001
		0.90	0.035	No. 500		25	0.001
No. 19	20 Mesh	0.85	0.033	No. 635		20	0.001
		0.80	0.031				

Mix design concept

Optimization Algorithm

Proportioning per m³ concrete

Mix xx

Material	Supplier	Volume [dm ³]	Mass [kg]
CEM III/B 42.5N LH/HS	Supplier 1	109.7	325.0
Fly Ash	Supplier 2	70.9	156.8
Sand 0-1	Supplier 3	59.6	157.1
Sand 0-4	Supplier 3	260.8	689.1
Gravel 2-8	Supplier 3	166.1	435.2
Gravel 4-16	Supplier 3	140.3	365.6
Water		162.5	162.5
Air		30.0	
Total		1000.0	2291.3

Proportioning for batch of:

30 l

CEM III/B 42.5N LH/HS	Supplier 1	3.3	9.7500
Fly Ash	Supplier 2	2.1	4.7043
Sand 0-1	Supplier 3	1.8	4.7118
Sand 0-4	Supplier 3	7.8	20.6743
Gravel 2-8	Supplier 3	5.0	13.0546
Gravel 4-16	Supplier 3	4.2	10.9677
Water		4.9	4.8750
Air		0.9	
Total		30.0	68.7376

Water: 7.09 M-%
Air: 3.0 %

Binder Content: 110 l/m³
Binder Content: **325 kg/m³**

w/c Ratio: 0.500

Fines <250 µm: 232.1 l/m³
Fines <250 µm: 617.5 kg/m³
w/f <250 µm: 0.263
Fines <125 µm: 181.3 l/m³
Fines <125 µm: 483.6 kg/m³
w/f <125 µm: 0.336

comp. Surface 537220 m²/m³ (solids)
comp. Surface 433805 m²/m³ (concrete)

D_{max}: 18.931 mm
D_{min}: 0.224 micron
q: 0.250

Deviation: 122.1
R²: 0.995207

min. Binder Content: 325 kg/m³
max. Binder Content: 350 kg/m³

φ_{house}: 23.5 %
φ_{dense}: 5.2 %

Figure C.1: Composed concrete mix for an arbitrary selection of raw materials.

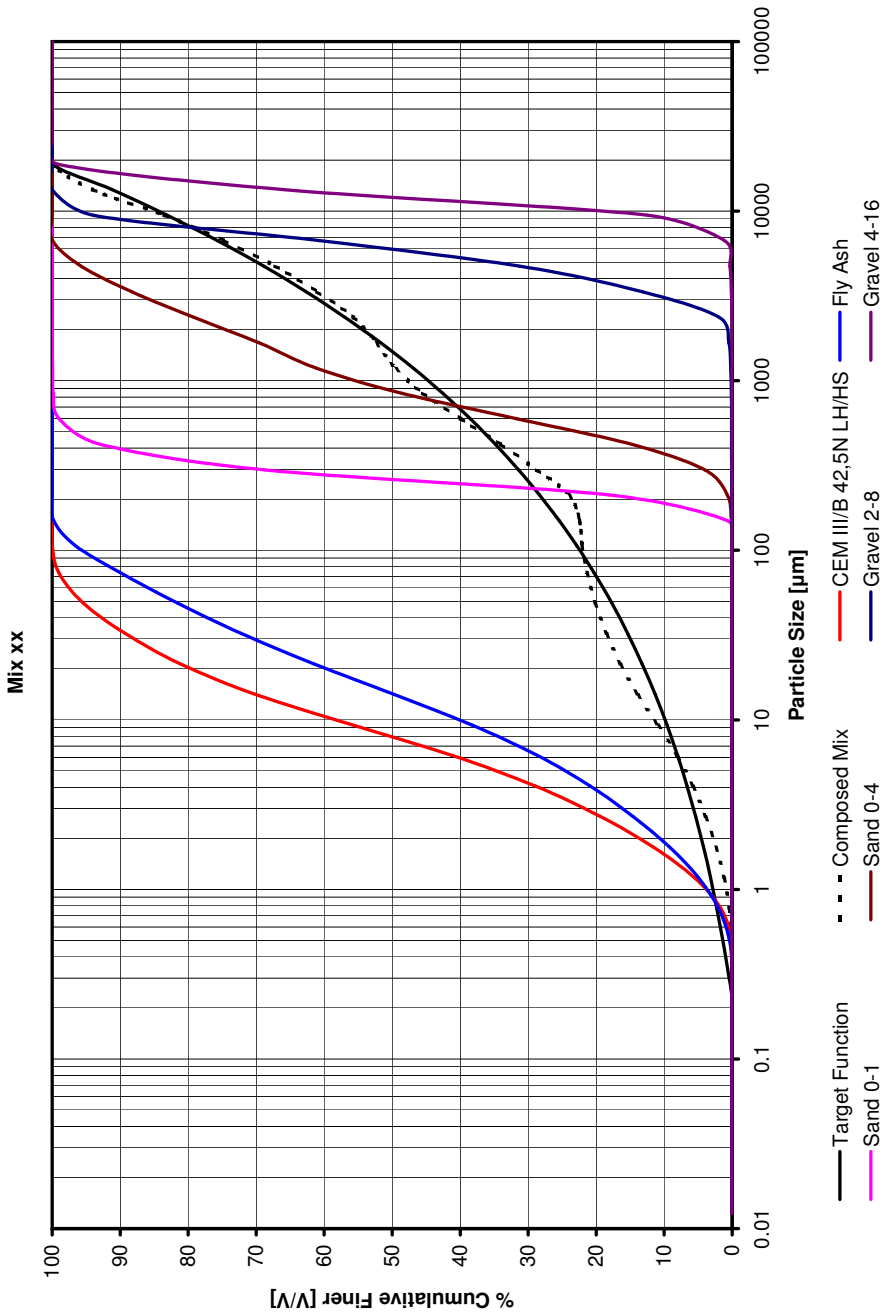


Figure C.2: PSD of the raw material and the composed concrete mix depicted in Figure C.1 (output of the mix design algorithm).

Mix designs

Table D.1: Proportioning of the designed aggregate mixes for varying distribution moduli q ($D_{max} = 16$ mm, $D_{min} = 0.125$ μ m).

Material class	Size	$q = 0.25$			$q = 0.30$			$q = 0.35$			$q = 0.40$		
		Frac. [V.-%]	Mass [g]	Vol. [cm ³]	Frac. V.-%	Mass [g]	Vol. [cm ³]	Frac. V.-%	Mass [g]	Vol. [cm ³]	Frac. V.-%	Mass [g]	Vol. [cm ³]
Grav. 4-16	11.2-16	11.8	1548.4	591.4	12.9	1688.1	644.8	14.0	1832.3	699.9	15.1	1980.5	756.5
	8-11.2	10.8	1419.9	542.3	11.6	1521.4	581.1	12.4	1623.0	619.9	13.2	1724.1	658.6
Grav. 2-8	5.6-8	9.9	1303.0	497.3	10.5	1372.2	523.7	11.0	1438.7	549.1	11.5	1502.1	573.3
	4-5.6	9.1	1194.9	456.1	9.4	1236.7	472.0	9.7	1274.3	486.4	10.0	1307.6	499.1
Sand 0-4	2.8-4	8.4	1095.7	418.2	8.5	1114.5	425.4	8.6	1128.8	430.8	8.7	1138.4	434.5
	2-2.8	7.7	1013.2	383.5	7.7	1012.9	383.4	7.6	1008.2	381.6	7.6	999.3	378.2
Sand 0-2	1.4-2	7.0	929.1	351.7	6.9	912.9	345.5	6.8	893.0	338.0	6.6	870.0	329.3
	0.71-1	6.4	852.0	322.5	6.2	822.7	311.4	6.0	791.0	299.4	5.7	757.3	286.7
Total	0.5-0.71	5.8	766.0	289.9	5.5	727.1	275.2	5.2	687.2	260.1	4.9	646.7	244.8
	0.355-0.5	5.4	717.7	271.7	5.1	669.7	253.5	4.7	622.2	235.5	4.4	575.6	217.9
Total	0.25-0.355	5.0	658.1	249.1	4.6	603.6	228.5	4.2	551.1	208.6	3.8	501.1	189.7
	0.18-0.255	4.6	603.3	228.4	4.1	543.8	205.9	3.7	488.0	184.8	3.3	436.0	165.1
	0.125-0.18	4.1	542.5	205.4	3.6	480.7	182.0	3.2	424.0	160.5	2.8	372.4	141.0
Total		3.8	508.2	192.4	3.4	442.6	167.6	2.9	383.8	145.3	2.5	331.4	125.5
		100.0	13152.0	5000.0	100.0	13148.8	5000.0	100.0	13145.6	5000.0	100.0	13142.5	5000.0

Table D.2: Recalculated mix proportioning of the tested mortar mixes listed in Table 3.5 (dosage per m³ mortar).

Material	EN 196-1		Mix 1		Mix 2		Mix 3		Mix 4	
	[dm ³]	[kg]	[dm ³]	[kg]	[dm ³]	[kg]	[dm ³]	[kg]	[dm ³]	[kg]
CEM I 32.5 R	162.8	512.9	82.0	257.3	82.0	257.3	—	—	—	—
CEM III/B 42.5 N	—	—	—	—	—	—	86.6	256.3	86.6	256.3
CEM I 52.5 R	—	—	44.2	139.4	—	—	44.1	138.8	—	—
Quarz powder	—	—	—	—	44.2	117.3	—	—	44.1	116.8
Norm sand	580.7	1538.8	—	—	—	—	—	—	—	—
Premix 0-4	—	—	654.4	1732.7	654.4	1732.7	651.9	1726.2	651.9	1726.2
Water	256.5	256.5	214.3	214.3	214.3	214.3	213.4	213.4	213.4	213.4
SP	—	—	5.1	5.6	5.1	5.6	4.1	4.5	4.1	4.5
Total	1000.0	2308.2	1000.0	2349.3	1000.0	2327.2	1000.0	2339.2	1000.0	2317.1

Table D.3: Mix proportioning of the designed EMC mixes discussed in Section 4.4.1 (dosage per m³ concrete).

Mix	CEM A* [kg]	CEM B# [kg]	Sand				Gravel				Water [kg]	SP [kg]	q [-]	w/c [-]	w/p [-]	Paste [‡] [l/m ³]
			0-1 [kg]	0-2 [kg]	0-4 [kg]	2-8 [kg]	4-16 [kg]	8-16 [kg]								
Mix 1	—	320.0	526.2	—	482.3	595.3	369.3	—	112.0	—	0.25	0.35	0.32	232.9		
Mix 2	—	310.0	482.8	—	475.4	584.8	366.0	—	139.5	—	0.25	0.45	0.41	256.1		
Mix 3	—	310.0	482.8	—	475.4	584.8	366.0	—	139.5	—	0.25	0.45	0.41	256.1		
Mix 4	—	310.0	88.6	—	594.1	818.7	448.8	—	124.0	—	0.35	0.40	0.39	232.1		
Mix 5	—	310.0	227.8	—	604.7	605.0	512.7	—	124.0	—	0.35	0.40	0.38	235.2		
Mix 6	—	310.0	92.0	—	599.5	826.2	452.9	—	116.2	—	0.35	0.38	0.37	224.5		
Mix 7	—	310.0	92.0	—	599.5	826.2	452.9	—	116.2	0.63	0.35	0.38	0.37	224.5		
Mix 8	—	310.0	92.0	—	599.5	826.2	452.9	—	116.2	0.94	0.35	0.38	0.37	224.5		
Mix 9	—	310.0	92.0	—	599.5	826.2	452.9	—	116.2	0.93	0.35	0.38	0.37	224.5		
Mix 10	—	290.0	120.1	—	655.7	628.1	585.3	—	116.0	—	0.40	0.40	0.39	218.1		
Mix 11	—	239.5	2.3	—	715.0	773.3	613.4	—	89.8	—	0.35	0.38	0.37	172.4		
Mix 12	—	310.0	400.2	—	522.7	599.2	448.6	—	116.3	0.63	0.30	0.38	0.35	231.1		
Mix 13	—	310.0	400.2	—	522.7	599.2	448.6	—	116.3	0.94	0.30	0.38	0.35	231.1		
Mix 14	—	235.0	2.3	—	701.2	668.8	740.4	—	88.1	—	—	0.38	0.35	169.1		
Blend 1	130.0	245.0	—	698.0	—	—	—	356.0	131.3	—	—	0.35	0.34	263.8		
Blend 2	112.7	212.3	—	602.0	—	—	—	396.9	113.7	—	0.35	0.35	0.34	228.6		
Blend 3	112.7	212.3	—	602.0	—	—	—	396.9	113.7	1.63	0.35	0.35	0.34	228.6		
Blend 4	112.7	212.3	—	602.0	—	—	—	396.9	113.7	0.98	0.35	0.35	0.34	228.6		

* CEM I 52.5 N

CEM III/B 42.5 N LH/HS

‡ based on particles smaller than 125 µm including water

SP: superplasticizer

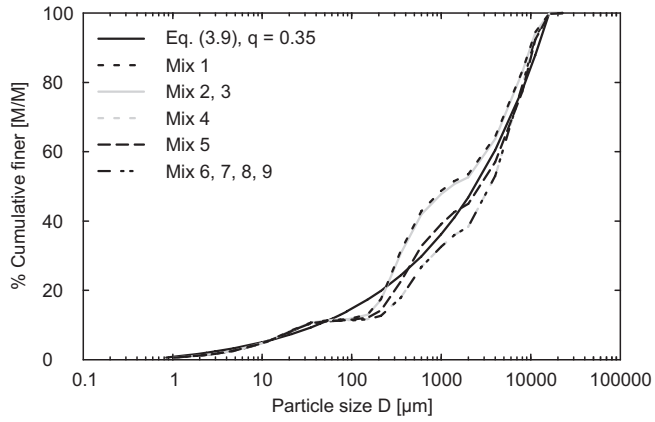


Figure D.1: PSD of tested trial mixes discussed in Section 4.4.1. The mix designs are given in Table D.3.

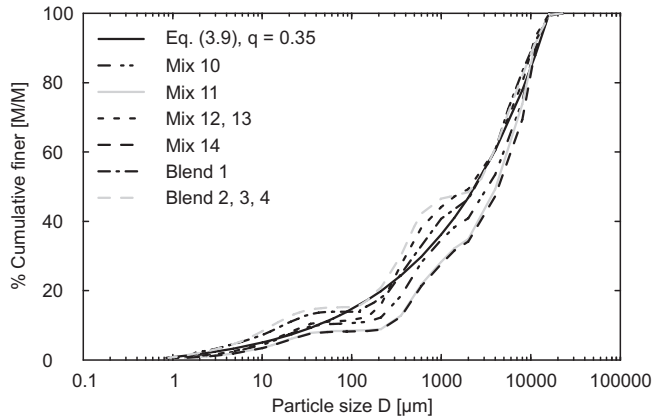


Figure D.2: PSD of tested trial mixes discussed in Section 4.4.1 The mix designs are given in Table D.3.

Test results

E.1 Fresh mortar properties

Table E.1: Spread flow values of the tested mortar mixes discussed in Section 3.3.3.

Mix	without impacts			with 15 impacts		
	D_1	D_2	Avg.	D_1	D_2	Avg.
	[mm]	[mm]	[mm]	[mm]	[mm]	[mm]
Blend 1	100	100	100	166	170	168
Blend 2	103	106	105	181	182	182
Blend 3	100	100	100	180	190	185
Blend 4	100	100	100	185	190	188
Mix 1	104	107	104	126	127	126
Mix 2	105	106	105	124	125	124
Mix 3	113	116	113	148	148	148
Mix 4	103	104	103	124	125	124

E.2 Hardened mortar properties

Table E.2: Compressive strength of tested mortar samples discussed in Section 3.3.3.

Mix	Compressive strength after days		
	1	7	28
	[N/mm ²]	[N/mm ²]	[N/mm ²]
Cem 1	14.4	32.8	44.3
Cem 2	3.7	30.5	51.6
Cem 3	36.9	51.5	61.5
Blend 1	13.4	39.7	49.2
Blend 2	3.2	15.4	19.5
Blend 3	12.5	30.4	53.1
Blend 4	1.2	16.8	29.6
Mix 1	26.9	47.4	57.8
Mix 2	5.0	22.4	31.9
Mix 3	15.6	39.5	60.6
Mix 4	4.2	28.6	43.1

Table E.3: Compressive strength of the designed mortars containing stone waste materials discussed in Section 5.2.2.

Mix	Compressive strength after days		
	3	7	28
	[N/mm ²]	[N/mm ²]	[N/mm ²]
C275	–	44.9	61.7
C250	28.7	36.8	63.9
C200	13.8	25.2	38.5
C175	16.0	34.6	52.0

Table E.4: Compressive strength of the designed mortars used for tests on cement replacement discussed in Section 5.3.2.

Mix	Compressive strength after days		
	3	7	28
	[N/mm ²]	[N/mm ²]	[N/mm ²]
EN 196-1	26.3	32.3	50.4
10% RCF1	22.7	30.3	47.4
20% RCF1	19.6	26.8	40.2
10% RCF2	22.4	27.2	40.1
20% RCF2	18.3	23.5	34.2
10% Quartz	21.1	26.1	46.7
20% Quartz	19.6	24.0	41.2

Table E.5: Compressive strength of the designed mortars used for the shrinkage tests discussed in Section 5.4.4.

Mix	Compressive strength after days		
	3	7	28
	[N/mm ²]	[N/mm ²]	[N/mm ²]
Reference mix [‡]	81.7	88.7	125.5
Reference mix [#]	92.7	114.6	151.6
10% RCA [‡]	81.9	94.0	128.3
10% RCA [#]	94.9	111.3	142.9
20% RCA [‡]	76.1	86.0	117.3
20% RCA [#]	86.2	104.8	135.5

[‡] tested on fracture halves obtained from the flexural strength test
prisms 40 × 40 × 160 mm

[#] tested on cubes 50 × 50 × 50 mm

Table E.6: Flexural strength of the designed mortars containing stone waste materials discussed in Section 5.2.2.

Mix	Flexural strength after days		
	3	7	28
	[N/mm ²]	[N/mm ²]	[N/mm ²]
C275	–	6.5	8.3
C250	5.8	6.7	7.9
C200	5.0	6.3	8.7
C175	3.6	5.3	8.1

Table E.7: Flexural strength of the designed mortars used for the shrinkage tests discussed in Section 5.4.4.

Mix	Flexural strength after days		
	3	7	28
	[N/mm ²]	[N/mm ²]	[N/mm ²]
Reference mix	9.9	10.8	13.6
10% RCA	9.3	9.6	11.9
20% RCA	8.4	9.7	12.0

Table E.8: Test results of the shrinkage measurements discussed in Section 5.4.5.

Mix	Condition	Strain after days		
		1	7	28
		[$\mu\text{m}/\text{m}$]	[$\mu\text{m}/\text{m}$]	[$\mu\text{m}/\text{m}$]
Reference mix	45% RH	6.7	380.0	582.3
	Sealed	-46.7	66.7	235.6
	Water	-96.7	-90.0	-61.5
10% RCA1 OD	45% RH	23.3	380.1	560.0
	Sealed	-30.0	81.0	182.0
	Water	-103.3	97.6	-80.7
10% RCA1 SSD	45% RH	26.7	403.3	640.0
	Sealed	-40.0	25.6	166.7
	Water	-106.7	-122.3	-100.0
20% RCA1 OD	45% RH	16.7	440.0	630.2
	Sealed	-13.3	113.3	210.0
	Water	-150.0	-120.1	131.3
20% RCA1 SSD	45% RH	33.3	523.3	713.3
	Sealed	-46.7	76.7	193.3
	Water	-106.6	156.7	-126.7
20% RCA1 ODW	45% RH	40.0	403.3	613.4
	Sealed	-6.7	70.0	173.3
	Water	-95.3	-91.4	-74.4

E.3 Fresh concrete properties

Table E.9: Fresh concrete properties of the tested trial mixes discussed in Section 4.4.2.

Mix	c_{DIN}	c_{com}	ρ_{con}^{loo}	ρ_{con}^{den}	PF^{loo}	PF^{den}	S_w^{loo}	S_w^{den}
	[-]	[-]	[g/cm ³]	[g/cm ³]	[V.-%]	[V.-%]	[%]	[%]
Mix 1	1.15	–	–	1.886	–	66.9	–	26.5
Mix 2	1.42	–	–	2.215	–	77.5	–	58.3
Mix 3	1.53	1.49	1.495	2.221	52.3	77.7	15.4	49.0
Mix 4	1.62	1.62	1.432	2.322	50.5	81.9	15.1	66.7
Mix 5	1.59	1.64	1.418	2.319	50.0	81.8	13.8	62.2
Mix 6	1.61	1.64	1.407	2.308	49.8	81.7	13.6	61.2
Mix 7	1.60	1.59	1.424	2.258	50.4	79.9	13.9	54.6
Mix 8	1.59	1.57	1.470	2.309	52.0	81.8	14.9	61.4
Mix 9	1.53	1.36	1.740	2.362	61.6	83.7	22.0	70.1
Mix 10	1.56	1.58	1.476	2.325	52.3	82.4	15.0	63.9
Mix 11	1.41	1.41	1.436	2.027	51.6	72.9	11.0	27.6
Mix 12	1.57	1.58	1.436	2.266	50.9	80.2	14.2	55.6
Mix 13	1.57	1.55	1.483	2.297	52.5	81.3	15.2	59.7
Mix 14	1.39	1.36	1.446	1.970	52.0	70.9	10.9	24.5
Blend 1	1.61	1.59	1.466	2.327	51.4	81.6	16.6	69.5
Blend 2	1.61	1.61	1.466	2.358	51.9	83.5	14.7	68.7
Blend 3	1.49	1.40	1.696	2.373	60.0	84.0	20.4	71.4
Blend 4	1.46	1.37	1.743	2.394	61.7	84.7	21.9	75.6

E.4 Hardened concrete properties

Table E.10: Hardened concrete properties of the tested trial mixes discussed in Section 4.4.3.

Mix	f_c	x	$f_{ct,sp}$
	[N/mm ²]	[Nm ³ /kgmm ²]	[N/mm ²]
Mix 1	–	–	–
Mix 2	41.1	0.133	–
Mix 3	36.9	0.119	–
Mix 4	48.8	0.157	–
Mix 5	52.3	0.169	–
Mix 6	48.2	0.156	–
Mix 7	47.3	0.153	–
Mix 8	49.9	0.161	–
Mix 9	63.7	0.205	–
Mix 10	51.6	0.178	–
Mix 11	14.1	0.059	–
Mix 12	43.0	0.139	–
Mix 13	48.0	0.155	–
Mix 14	14.4	0.061	–
Blend 1 (7d)	63.5	0.169	–
Blend 2 (7d)	66.9	0.206	–
Blend 3 (7d)	73.6	0.226	–
Blend 4 (7d)	75.9	0.234	–
Blend 1 (28d)	82.6	0.220	4.9
Blend 2 (28d)	83.5	0.257	5.0
Blend 3 (28d)	95.3	0.293	–
Blend 4 (28d)	100.2	0.308	–

E.5 IC-test

Table E.11: Test results of the IC-test on the influence of fines on the early-age behavior discussed in Section 6.4.2.

Sample	Ψ_m	PF	Air	S_w	ρ_{con}^{den}	Force	σ_{gre}
	[M.-%]	[V.-%]	[V.-%]	[%]	[g/cm ³]	[N]	[N/mm ²]
Quartz flour 2	9.6	53.1	32.0	31.7	1.556	731.1	0.093
	10.8	54.5	28.1	38.3	1.618	834.2	0.106
	12.9	55.9	22.1	50.0	1.702	998.1	0.127
	14.7	57.6	16.1	62.1	1.789	1188.8	0.151
	16.3	59.3	10.0	75.4	1.878	1144.9	0.146
	18.1	61.1	3.1	92.0	1.978	1357.3	0.173
Fly ash	4.8	62.0	31.1	18.1	1.440	502.4	0.064
	8.2	63.5	24.0	34.2	1.528	628.3	0.080
	12.3	64.5	15.5	56.4	1.626	722.4	0.092
	14.3	67.6	7.4	77.0	1.745	893.2	0.114
	16.2	69.7	0.5	98.3	1.839	950.1	0.121

Table E.12: Results of the IC-test on the influence of plasticizing admixtures on the early-age behavior of fines discussed in Section 6.4.3.

Sample	Ψ_m	SP	WC	PF	Air	S_w	ρ_{con}^{den}	Force	σ_{gre}
	[M.-%]	[M.-%]	[-]	[V.-%]	[V.-%]	[%]	[g/cm ³]	[N]	[N/mm ²]
Quartz flour 2	12.9	no SP	100	56.1	21.8	50.3	1.707	998.1	0.127
	12.9	0.25	71	55.9	22.1	50.0	1.702	800.1	0.102
	12.9	0.25	100	56.7	21.0	51.5	1.725	882.7	0.112
	12.9	1.00	41	55.9	22.1	50.0	1.702	750.0	0.095
	12.9	1.00	100	57.6	19.6	53.6	1.755	980.5	0.125
	Fly ash	8.2	no SP	100	63.5	24.0	34.2	1.528	628.3
8.2		0.25	83	63.5	24.0	34.2	1.528	489.4	0.062
8.2		0.25	100	64.0	23.4	35.1	1.542	594.0	0.076
8.2		1.00	62	63.6	23.9	34.5	1.532	518.4	0.066
8.2		1.00	100	64.3	23.1	35.5	1.548	591.4	0.075

WC: amount of working cycles

Table E.13: Results of the IC-test on the influence of the distribution modulus q on the early-age behavior of EMC mixes discussed in Section 6.4.4.

Mix	Ψ_m	PF	Air	S_w	ρ_{con}^{den}	Force	σ_{gre}
	[M.-%]	[V.-%]	[V.-%]	[%]	[g/cm ³]	[N]	[N/mm ²]
Quartz 1	3.34	75.4	17.7	28.0	2.066	627.2	0.080
	4.12	75.9	15.5	35.8	2.097	803.5	0.102
	4.83	77.0	12.6	45.1	2.145	869.2	0.111
	6.07	80.9	5.3	72.4	2.281	1404.7	0.179
	6.80	82.5	1.5	91.5	2.347	1573.3	0.200
Quartz 2	3.27	76.9	16.2	29.8	2.106	--	-
	3.50	78.2	14.3	34.4	2.147	386.2	0.049
	4.20	79.8	10.9	45.9	2.207	485.4	0.062
	5.02	82.9	5.5	67.9	2.313	667.8	0.085
	5.59	83.1	3.8	77.2	2.333	674.7	0.086
Fly ash 1	2.67	80.9	13.4	29.6	2.112	404.2	0.051
	3.19	81.3	11.8	36.5	2.134	484.3	0.062
	3.61	81.3	11.0	41.2	2.141	442.0	0.056
	4.34	83.7	6.7	59.1	2.222	610.9	0.078
	5.19	87.9	0.2	98.4	2.352	1096.6	0.140
Fly ash 2	2.19	80.5	14.8	24.0	2.140	105.8	0.013
	2.60	80.8	13.6	29.2	2.157	143.5	0.018
	3.01	82.3	11.1	37.5	2.206	214.4	0.027
	3.77	84.5	6.9	55.4	2.282	163.5	0.021
	4.71	85.8	3.2	77.7	2.341	165.3	0.021

Table E.14: Results of the IC-test on the early-age behavior of the tested EMC discussed in Section 6.5.2.

Mix	ψ_m	PF	Air	S_w	ρ_{con}^{den}	τ	W_c
	[M.-%]	[V.-%]	[V.-%]	[%]	[g/cm ³]	[kN/m ²]	[J/kg]
Original mix (OM)	4.79	76.4	13.8	41.5	2.142	71	1228.2
	5.26	78.2	10.2	53.2	2.217	73	1242.4
	5.73	79.7	8.0	60.6	2.256	75	1241.5
	5.97	80.0	7.3	63.5	2.268	76	1233.7
	6.40	79.7	6.6	67.5	2.271	76	1220.7
OM 0.13% SP	5.26	78.9	11.3	46.4	2.224	76	1251.9
OM 0.21% SP	5.26	79.9	9.3	53.7	2.250	76	1234.1
OM 0.21% SP. 7 min	5.26	79.9	8.9	55.7	2.250	76	1234.1
OM 0.21% SP. 12 min	5.26	79.5	9.3	54.6	2.240	78	1255.5
OM 0.21% SP. 18 min	5.26	79.1	9.8	53.1	2.228	74	1233.7
Optimization 1	5.20	77.8	11.8	46.8	2.186	72	1226.1
Optimization 2	5.95	81.8	4.6	74.7	2.299	76	1212.8
Optimization 3	6.48	83.2	3.3	80.4	2.352	74	905.5

[‡] The water content of the company mix amounts to 5.26 M.-%

Comparison of patents on photocatalytic concrete paving products

	Mitsubishi Materials Corporation (Murata et al., 1997)	Italcementi S.p.A. (Cassar and Pepe, 1997)
Patent name	NO _x -cleaning paving block	Paving tile comprising an hydraulic binder and photocatalyst particles
Field of the invention	NO _x -cleaning paving block with enhanced NO _x -cleaning capability due to an increased efficiency of fixing NO _x from the air and increased pluvial NO _x -cleaning efficiency and is provided with a non-slip property, wear resistance and decorative property.	Hydraulic binder, dry premix, cement composition having improved property to maintain the brilliance and color quantity and to prevent esthetic degradation.
Working principle	NO _x -cleaning paving block comprising a surface layer which contains TiO ₂ with or without adsorbing material in the surface layer and a concrete made base layer	Use of a photocatalyst or dry premix containing a hydraulic binder and a photocatalyst which is able to oxidize in the presence of light air and environmental polluting substances for the preparation of an hydraulic binder for manufacturing paving tiles that maintain after installation for a longer time brilliance and color quantity

	Mitsubishi Materials Corporation (Murata et al., 1997)	Italcementi S.p.A. (Cassar and Pepe, 1997)
Product requirements	<ul style="list-style-type: none"> - Replacement of the sand used by 10-50% of glass grains or silica sand having a particle size of 1-6 mm - Surface layer having a void fraction of 10-40% and water permeability of 0.01 cm/sec - NO_x-cleaning paving block roughened with a surface roughening tool 	
Binder	<ul style="list-style-type: none"> - Cement 	<ul style="list-style-type: none"> - Hydraulic binder - Cement (white, grey or pigmented) - Cement used for debris dams - Hydraulic lime
Photocatalyst	TiO ₂ without further requirements	<ul style="list-style-type: none"> - TiO₂ or a precursor thereof, mainly in the form of anatase - TiO₂ with anatase structure for at least 25, 50 and 70% - blend of anatase and rutile TiO₂ having a ratio 70:30 - TiO₂ doped with one or more atoms different from Ti - TiO₂ doped with one or more atoms selected from Fe(III), Mo(V), Ru(III), Os(III), Re(V), V(V), Rh(III) - Photocatalyst selected from the group consisting of tungstic oxide (WO₃), strontium titanate (SrTiO₃) and calcium titanate (CaTiO₃)
Amount of photocatalyst	<ul style="list-style-type: none"> - 0.6-20% by mass - 5-50% by mass of the binder 	<ul style="list-style-type: none"> - 0.01-10% by mass - 0.1% by mass of the binder - 0.5% by mass of the binder
Adsorbing materials	<ul style="list-style-type: none"> - Zeolite, magadiite, petalite and clay 	<ul style="list-style-type: none"> - none
Thickness of the surface layer	<ul style="list-style-type: none"> - 2-15 mm 	<ul style="list-style-type: none"> - not given

Experimental results of NO degradation measurements

Table G.1: Outlet concentrations $C_{g,out}$ of the reactor and resulting removal rates η for varying UV-A irradiance E discussed in Section 7.6.1. The measurements were performed on sample D2-2.

E	$C_{NO,in}$	$C_{NO,out}$	$C_{NO_2,in}$	$C_{NO_2,out}$	η_{NO}	η_{NO_2}	η_{NO_x}
[W/m ²]	[ppm]	[ppm]	[ppm]	[ppm]	[%]	[%]	[%]
0.31	1.016	0.964	0.009	0.007	5.1	19.9	5.2
1	1.016	0.929	0.009	0.007	8.5	21.5	8.6
2	1.016	0.898	0.009	0.007	11.6	19.1	11.7
3	1.016	0.875	0.009	0.007	13.9	22.1	13.9
4	1.016	0.850	0.009	0.008	16.3	13.2	16.2
5	1.016	0.840	0.009	0.008	17.3	14.3	17.2
6	1.016	0.826	0.009	0.008	18.7	5.8	18.6
7	1.016	0.813	0.009	0.009	20.0	0.7	19.8
8	1.016	0.802	0.009	0.009	21.0	-4.2	20.8
9	1.016	0.790	0.009	0.010	22.3	-14.9	21.9
10	1.016	0.781	0.009	0.011	23.1	-22.1	22.7
11	1.016	0.776	0.009	0.012	23.6	-30.4	23.1
13	1.016	0.760	0.009	0.013	25.1	-46.8	24.5

Table G.2: Outlet concentrations $C_{g,out}$ of the reactor and resulting removal rates η for varying NO inlet concentrations $C_{NO,in}$ discussed in Section 7.6.3. The measurements were performed on sample D2-2.

$C_{NO,in}$	$C_{NO,out}$	$C_{NO_2,in}$	$C_{NO_2,out}$	η_{NO}	η_{NO_2}	η_{NO_x}
[ppm]	[ppm]	[ppm]	[ppm]	[%]	[%]	[%]
0.096	0.030	0.002	0.005	68.4	-196.9	63.5
0.304	0.159	0.003	0.006	47.6	-87.6	46.1
0.505	0.312	0.004	0.008	38.3	-96.1	37.2
0.989	0.624	0.015	0.077	36.9	-420.0	30.1

Table G.3: Outlet concentrations $C_{g,out}$ of the reactor and resulting removal rates η for varying relative humidity RH discussed in Section 7.6.2. The measurements were performed on sample D2-2.

RH	$C_{NO,in}$	$C_{NO,out}$	$C_{NO_2,in}$	$C_{NO_2,out}$	η_{NO}	η_{NO_2}	η_{NO_x}
[%]	[ppm]	[ppm]	[ppm]	[ppm]	[%]	[%]	[%]
10	1.006	0.681	0.014	0.008	32.3	40.6	32.4
20	1.006	0.724	0.014	0.009	28.0	36.3	28.1
30	1.006	0.751	0.014	0.010	25.3	23.4	25.3
40	1.006	0.770	0.014	0.013	23.4	5.3	23.2
50	1.006	0.789	0.014	0.015	21.5	-8.1	21.1
60	1.006	0.812	0.014	0.016	19.2	-15.0	18.8
70	1.006	0.843	0.014	0.015	16.1	-10.0	15.8
80	1.006	0.869	0.014	0.013	13.6	1.8	13.4

Table G.4: Outlet concentrations $C_{g,out}$ of the reactor and resulting removal rates η for varying flow rates Q discussed in Section 7.6.4. The measurements were performed on sample D2-2.

Q	$C_{NO,in}$	$C_{NO,out}$	$C_{NO_2,in}$	$C_{NO_2,out}$	η_{NO}	η_{NO_2}	η_{NO_x}
[l/min]	[ppm]	[ppm]	[ppm]	[ppm]	[%]	[%]	[%]
1	0.997	0.333	0.046	0.035	66.6	23.7	64.8
3	0.989	0.624	0.015	0.077	36.9	-420.0	30.1
5	0.998	0.777	0.020	0.081	22.1	-313.7	15.6

Table G.5: Outlet concentrations $C_{g,out}$ of the reactor and resulting removal rates η for varying types of TiO_2 discussed in Section 7.6.5.

Material	$C_{NO,in}$	$C_{NO,out}$	$C_{NO_2,in}$	$C_{NO_2,out}$	η_{NO}	η_{NO_2}	η_{NO_x}
	[ppm]	[ppm]	[ppm]	[ppm]	[%]	[%]	[%]
TiO_2 A [‡]	0.999	0.895	0.024	0.040	10.5	-66.7	8.7
TiO_2 A [‡]	1.001	0.759	0.027	0.064	24.2	-137.0	19.9
TiO_2 B [‡]	1.004	0.928	0.026	0.021	7.6	19.2	7.9
TiO_2 B [‡]	0.999	0.888	0.026	0.021	11.2	19.2	11.4
TiO_2 C [‡]	1.000	0.724	0.023	0.086	27.6	-273.9	20.8
TiO_2 C [‡]	1.005	0.612	0.023	0.054	39.1	-134.8	35.2
TiO_2 D [‡]	1.006	0.935	0.017	0.023	7.0	-35.3	6.3
TiO_2 D [‡]	1.008	0.952	0.022	0.019	5.5	13.6	5.7
TiO_2 E [‡]	1.001	0.906	0.034	0.047	9.4	-38.2	7.9
TiO_2 E [‡]	1.003	0.808	0.012	0.034	19.5	-183.3	17.1

[‡] Ground surface

[‡] Sand blasted surface

Table G.6: Outlet concentrations $C_{g,out}$ of the reactor and resulting removal rates η for varying types of pigments and TiO_2 contents discussed in Section 8.3.3.

Sample	$C_{NO,in}$	$C_{NO,out}$	$C_{NO_2,in}$	$C_{NO_2,out}$	η_{NO}	η_{NO_2}	η_{NO_x}
	[ppm]	[ppm]	[ppm]	[ppm]	[%]	[%]	[%]
Reference	0.999	0.895	0.024	0.040	10.5	-66.7	8.7
Pig1	1.033	0.902	0.031	0.068	12.6	-122.5	8.7
Pig2	1.008	0.876	-	-	13.1	-	-
Pig3 [‡]	1.010	0.779	0.014	0.066	22.9	-374.5	17.5
Pig4 [‡]	1.013	0.617	0.018	0.118	39.1	-565.4	28.7

Table G.7: Data of the NO degradation of the produced paving blocks discussed in Section 8.3.3.

Sample	$C_{NO,in}$	$C_{NO,out}$	$C_{NO_2,in}$	$C_{NO_2,out}$	η_{NO}	η_{NO_2}	η_{NO_x}
	[ppm]	[ppm]	[ppm]	[ppm]	[%]	[%]	[%]
Pav1-1	1.018	0.861	0.025	0.032	15.4	-31.5	14.3
Pav1-2	1.013	0.856	0.029	0.043	15.5	-49.4	13.7
Pav1-3	1.015	0.882	0.033	0.040	13.1	-21.1	12.0
Pav1-4	1.017	0.885	0.034	0.035	12.9	-4.4	12.4
Pav1-5	1.004	0.808	0.011	0.049	19.5	-353.1	15.5
Pav1-6	1.002	0.834	0.010	0.041	16.8	-290.7	13.6
Pav1-7	1.000	0.853	0.013	0.038	14.7	-186.4	12.0
Pav1-8	1.000	0.875	0.018	0.037	12.5	-99.9	10.5
Average	-	-	-	-	15.1	-129.6	13.0
Pav1-1	1.027	0.914	0.009	0.011	10.9	-19.5	10.7
Pav1-2	1.013	0.875	0.007	0.018	13.6	-155.8	12.4
Pav1-5	1.015	0.819	0.013	0.061	19.3	-370.9	14.3
Pav1-6	1.005	0.839	0.021	0.041	16.5	-97.9	14.2
Average	-	-	-	-	15.1	-161.0	12.9
Pav2-1	1.016	0.521	-0.001	0.117	48.7	-21507.8	37.1
Pav2-2	1.013	0.597	-0.002	0.088	41.1	-5697.5	32.2
Pav2-3	1.003	0.528	0.002	0.099	47.4	-4317.9	37.6
Pav2-4	1.003	0.513	0.006	0.086	48.9	-1403.4	40.6
Avg	-	-	-	-	46.5	-8231.7	37.0
Pav4	1.007	0.920	0.008	0.027	8.6	-261.1	6.6

Table G.8: Data of the conducted measurements discussed in Section 8.4.2.

$C_{g,in}$	$C_{g,out}$ [ppm]			η_{NO} [%]			
	[ppm]	Flow rate Q [l/min]			Flow rate Q [l/min]		
		1	3	5	1	3	5
0.1	0.011	0.032	0.041	89.0	68.4	59.4	
0.3	0.039	0.157	0.197	87.1	47.6	34.3	
0.5	0.210	0.309	0.356	58.0	38.3	28.9	
1.0	0.334	0.729	0.779	66.6	27.1	22.1	

Table G.9: NO inlet concentrations and resulting NO and NO_x removal rates extracted from Mitsubishi (2005).

$C_{NO,in}$	NO removal	η_{NO_x}
[ppm]	[mmol/m ² 12h]	[%]
0.05	0.2	89.6
0.1	0.4	88.9
0.2	0.8	90.6
0.5	2.0	88.4
1.0	3.7	82.3
2.0	6.1	68.0
5.0	10.0	44.3

Table G.10: NO removal rates for varying UV-A irradiance and NO inlet concentrations of the measurements discussed in Section 8.4.3.

$C_{NO,in}$	η_{NO} for UV-A irradiance [W/m ²]											fit Eq. (7.16)		
	[ppm]	1	2	3	4	5	6	7	8	9	10	11	α_1	α_2
0.1	25.9	38.9	40.8	41.7	45.7	48.5	50.5	52.0	53.8	55.5	57.4	28.29	0.30	0.96
0.3	16.9	24.0	26.5	30.5	32.9	36.7	38.4	41.6	43.3	45.4	47.1	17.95	0.42	0.99
0.5	13.7	18.5	21.6	23.9	26.0	28.9	31.2	32.9	35.4	36.8	38.8	13.50	0.43	0.99
0.7	7.9	12.2	14.1	15.8	16.7	18.1	18.8	20.4	21.3	22.1	23.0	8.53	0.42	0.99
1.0	8.5	11.6	13.9	16.3	17.3	18.7	20.0	21.0	22.3	23.1	23.6	8.65	0.43	0.99

Table G.11: NO removal rates for varying relative humidity and NO inlet concentrations of the measurements discussed in Section 8.4.3.

$C_{NO,in}$ [ppm]	η_{NO} for relative humidity [%]							linear fit		
	10	20	30	40	50	60	70	m	n	R^2
0.1	67.5	64.3	61.3	57.0	51.7	44.2	35.5	-0.52	75.33	0.96
0.3	59.4	52.1	46.1	40.9	35.7	29.1	23.3	-0.59	64.47	0.99
0.5	51.3	43.5	37.7	33.2	28.2	23.5	19.3	-0.52	54.60	0.99
0.7	35.0	31.1	28.3	26.2	24.4	22.4	19.7	-0.24	36.33	0.98
1.0	32.3	28.0	25.3	23.4	21.5	19.2	16.1	-0.25	33.69	0.98

Table G.12: Fit parameter of the measurements discussed in Section 8.4.3 and corresponding values of the reaction rate constant k and the adsorption equilibrium constant K_d in dependence on the UV-A irradiance.

Irradiance [W/m ²]	Linear fit			k	K_d
	m	n	R^2	[mg/m ³ s]	[m ³ /mg]
1	2.28	14.85	0.64	0.07	6.50
2	1.39	9.95	0.75	0.10	7.15
3	1.44	8.25	0.82	0.12	5.73
4	1.56	6.38	0.92	0.16	4.09
5	1.38	5.82	0.95	0.17	4.22
6	1.29	5.18	0.96	0.19	4.02
7	1.24	4.81	0.96	0.21	3.89
8	1.20	4.38	0.97	0.23	3.64
9	1.16	4.12	0.97	0.24	3.56
10	1.11	3.91	0.97	0.26	3.53
11	1.05	3.75	0.97	0.27	3.56

Table G.13: Fit parameter of the measurements discussed in Section 8.4.3 and corresponding values of the reaction rate constant k and the adsorption equilibrium constant K_d in dependence on the relative humidity.

RH [%]	Linear fit			k	K_d
	m	n	R^2	[mg/m ³ s]	[m ³ /mg]
10	0.89	2.07	0.99	0.48	2.32
20	0.94	2.65	0.99	0.38	2.81
30	1.00	3.16	0.99	0.32	3.16
40	1.12	3.54	0.99	0.28	3.17
50	1.29	3.97	0.99	0.25	3.07
60	1.64	4.49	0.98	0.22	2.74
70	2.25	5.04	0.98	0.20	2.24

Summary

This thesis provides a multifunctional design approach for sustainable concrete, particularly earth-moist concrete (EMC), with application to concrete mass products. EMC is a concrete with low water content and stiff consistency that is used for the production of concrete mass products, such as paving blocks, curbstones, and sewage pipes. The stiff consistency allows for short processing times as the product can immediately be removed from the mold. The practical design of EMC mixes is based on experience and variations that are made during production, as an in-depth scientific description of the material is limited.

Within this thesis, a multifunctional design approach is proposed that is based on particle packing ideas derived from theories for geometric packings of polydisperse systems. This new approach for the mix design of EMC mixes considers the entire grading of all solid ingredients in order to compose a concrete mix that meets required performance criteria. A computer based optimization algorithm was developed that allows for the composition of a granular mix taking into account theories of continuous geometric particle packing. Using the algorithm, EMC mixes have been designed that are characterized by optimized and dense particle packing, lower cement content, and better workability in fresh state. Since the early-age behavior of EMC is one of the most relevant criteria for production, the formation of interparticle forces in the micro range has been studied, and relations to the granulometric properties of the concrete mix have been accounted for. This overall consideration of the granulometric properties and resulting effects on the concrete properties in fresh and hardened state results in EMC mixes that have higher mechanical strength compared to classical mix designs. In this way, cement is used more efficiently and cement content can be reduced.

The aspect of sustainability is further addressed by the incorporation of waste materials and industrial by-products in EMC and other types of concrete. To do this, the ideas of the new mix design concept have been used to replace primary filler materials, such as limestone powder or fly ash, by fine inert stone waste materials generated in the natural stone industry. This successful replacement of conventional raw materials lowers the environmental footprint of the produced concrete to a further extent. Adopting the ideas of a closed concrete life cycle, attention was also paid to the utilization of recycled materials in concrete used for the production of concrete mass products. Recycled aggregates have been applied to replace traditional aggregates, and fines that originate during the recycling process have been used as source to replace partly reactive filler materials.

Finally, photocatalytic materials have been investigated to give multifunctional properties to concrete mass products and enhance their contribution to sustainability. The photocatalytic properties of these semiconducting materials come along with air-purifying and self-cleaning abilities. The working principles of the photocatalytic oxidation (PCO) of nitrogen oxides (NO_x) in EMC have been studied under experimental conditions and the reaction kinetics of the PCO have been modeled. The experimental work on photocatalytic materials revealed that the performance of already available systems differs to a large extent and that improvements are achieved when the application techniques on industrial scale account for the specific properties of the photocatalysts. Furthermore, the NO degradation performance of a photocatalytic concrete paving block has been modeled by means of the Langmuir-Hinshelwood model. The validation of the model by experimental data revealed a good agreement between experimental results and predicted values of the model.

Thus, the new mix design concept allows for the performance based design of sustainable and multifunctional concrete mixes suitable for the production of concrete mass products.

Samenvatting

Dit proefschrift behandelt een multifunctionele ontwerpaanpak voor duurzaam beton, specifiek aardvochtig beton (AVB), toegepast op in massa geproduceerde betonwaren. AVB is een beton met een laag watergehalte en een slechte verwerkbaarheid dat wordt gebruikt voor het produceren van in massa geproduceerde betonwaren zoals straatstenen, stoepbanden en rioleringen. De lage consistentie zorgt voor een korte verwerkingstijd zodat de producten direct uit de mal kunnen worden verwijderd. In de praktijk is het ontwerp van AVB-samenstellingen voornamelijk gebaseerd op productieervaring omdat de wetenschappelijke onderbouwing van het materiaal beperkt is.

In dit proefschrift wordt een multifunctionele ontwerpaanpak voorgesteld welke gebaseerd is op theorieën over geometrische polydisperse korrelpakkingen. Deze nieuwe aanpak voor het ontwerp van de AVB-mengsels omvat de totale gradering van alle vaste stoffen om zo tot een mix te komen met de gewenste eigenschappen. Hiervoor is computer gebaseerd optimalisatiealgoritme ontwikkeld welke de korrelgrootteverdelingen van de ingrediënten zodanig combineert dat het mengsel een geometrische korrelopbouw heeft. Met dit algoritme zijn AVB-mengsels ontworpen die worden gekenmerkt door een optimalisatie van de korrelpakking, lagere cementgehalten en een betere verwerkbaarheid van het verse (groene) beton. Het gedrag van het groene AVB is belangrijk voor de productie en daarom is gekeken naar de ontwikkeling van krachten tussen de losse korrels op microschaal en haar relatie met de korrelopbouw. De integrale korrelopbouw is gerelateerd aan de eigenschappen van het beton in zowel de groene als de uitgeharde fase. Dit heeft geresulteerd in AVB-mengsels met betere mechanische eigenschappen vergeleken met een standaard mix. Op deze manier wordt het cement effectiever toegepast waardoor de hoeveelheid cement kan worden gereduceerd.

Het duurzaamheidsaspect is verder beïnvloed door de inzet van afvalmaterialen en industriële restproducten uit de industrie in AVB en andere betonsoorten. Het mengselontwerpconcept is gebruikt om primaire vulmaterialen, zoals kalksteenmeel en vliegas, te vervangen door fijn inert steenafval uit de steenindustrie. Deze succesvolle vervanging van standaard ingrediënten leidt tot een verdere verlaging van de CO₂ uitstoot van het geproduceerde beton. Om de materiaalcyclus te sluiten is er aandacht besteed aan het gebruik van gerecyclede bouwmaterialen voor de productie van AVB en ander beton. Met behulp van gerecyclede betongranulaten kunnen traditionele aggregaten en fijne stoffen worden vervangen.

Tenslotte zijn fotokatalytische materialen onderzocht om multifunctionele eigenschappen van massa betonwaren te bewerkstelligen. De fotokatalytische eigenschappen van deze halfgeleidermaterialen zorgen ook voor luchtverversing en zelfreinigende eigenschappen. Het werkingsprincipe van fotokatalytische oxidatie (FKO) van stikstofoxiden (NO_x) door AVB is experimenteel onderzocht en de kinetiek van FKO is gemodelleerd. In het experimenteel onderzoek kwam naar voren dat de prestaties van reeds beschikbare producten onderling significant variëren en dat verbeteringen worden bereikt wanneer de toepassing op industriële schaal wordt afgestemd op de specifieke eigenschappen van de gebruikte fotokatalysator. De NO afbraak van een fotokatalytische betonklinker is gemodelleerd door gebruik van het Langmuir-Hinshelwood model. Dit model is gevalideerd met behulp van experimenten en een goede overeenstemming is bereikt.

Het nieuwe concept voor mengselontwerp is geschikt voor het prestatiegericht ontwerpen van duurzame en multifunctionele betonmengsels en voor het produceren van massa betonproducten.

Relevant publications

Publications generated within this PhD project are listed below:

Journals

1. Ballari, M.M., Hunger, M., Hüskén, G. and Brouwers, H.J.H. (2010) Modelling and Experimental Study of the NO_x Photocatalytic Degradation Employing Concrete Pavement with Titanium Dioxide, *Catalysis Today*, **151**(1-2): 71-76.
2. Ballari, M.M., Hunger, M., Hüskén, G. and Brouwers, H.J.H. (2010) NO_x Photocatalytic degradation employing concrete pavement containing titanium dioxide, *Applied Catalysis B: Environmental*, **95**(3-4): 245-254.
3. Hunger, M., Hüskén, G. and Brouwers, H.J.H. (2010). Photocatalytic degradation of air pollutants – From modeling to large scale application, *Cement and Concrete Research* **40**(2): 313-320.
4. Hüskén, G., Hunger, M. and Brouwers, H.J.H. (2009). Experimental study of photocatalytic concrete products for air purification, *Building and Environment* **44**(12): 2463-2474.
5. Hüskén, G. and Brouwers, H.J.H. (2008). A new mix design concept for earth-moist concrete: A theoretical and experimental study, *Cement and Concrete Research* **38**(10): 1246-1259.

Non-refereed journal papers

1. Hüskén, G., Hunger, M. and Brouwers, H.J.H. (2009). Photocatalytic concrete products - Practical application and modeling, *Betonwerk + Fertigteil-Technik / Concrete Plant + Precast Technology* **75**(12): 24-33.
2. Hunger, M., Hüskén, G. and Brouwers, H.J.H. (2009). Photocatalysis applied to concrete products – Part 3: Practical relevance and modeling of the degradation process, *ZKG international Vol.* **62**(2): 63-70.
3. Hüskén, G., Hunger, M. and Brouwers, H.J.H. (2008). Comparative study on air-purifying concrete products – Eine vergleichende Untersuchung von luftreinigenden Betonprodukten, *Betonwerk + Fertigteil-Technik / Concrete Plant + Precast Technology* **74**(4): 12-18.
4. Hüskén, G., Hunger, M. and Brouwers, H.J.H. (2008) Estudio comparativo entre productos de hormigón para purificación de aire / Estudo comparativo de produtos de betão com purificação de ar, *BFT International - BFT Edición española/Edição portuguesa* (3): 38–43.
5. Hunger, M., Hüskén, G. and Brouwers, H.J.H. (2008). Photocatalysis applied to concrete products – Part 1: Principles and test procedure, *ZKG international* **61**(8): 77-85
6. Hunger, M., Hüskén, G. and Brouwers, H.J.H. (2008). Photocatalysis applied to concrete products – Part 2: Influencing factors and product performance, *ZKG international* **61**(10): 76-84.

Conferences

1. Hüskén, G. and Brouwers, H.J.H. (2010). Eco-SCC: From Theory to Practical Application, Proceedings 1st International Conference on Sustainable Construction Materials: Design, Performance and Application, 10-12 August 2010, Wuhan, Hubei province, China, pp. 720-732.

2. Hüsken, G. and Brouwers, H.J.H. (2009). On the Early Age Behavior of Earth-Moist Concrete, Proceedings 17th Ibausil, International Conference on Building Materials (Internationale Baustofftagung), 23-26 September 2009, Weimar, Germany, Ed. H.B. Fischer, F.A. Finger-Institut für Baustoffkunde, pp. 2:0531-2:0536.
3. Ballari, M.M., Hunger, M., Hüsken, G. and Brouwers, H.J.H. (2009) Photocatalytic Concrete Stones containing TiO₂ for Atmospheric NO_x Removal, Proceedings 17th Ibausil, International Conference on Building Materials (Internationale Baustofftagung), 23-26 September 2009, Weimar, Germany, Ed. H.B. Fischer, F.A. Finger-Institut für Baustoffkunde, pp. 2:0537-2:0542.
4. Ballari, M.M., Hunger, M., Hüsken, G. and Brouwers, H.J.H. (2009) Eco Concrete Stones with TiO₂ for Atmospheric Decontamination, Proceedings CMS 2009 conference on life-cycle design of buildings, systems and materials, CIB W115 construction materials stewardship, Ed. E. Durmisevic, 12-15 June 2009, Enschede, The Netherlands, pp. 126-130.
5. Hüsken, G., Hunger, M., Ballari M. M. and Brouwers, H.J.H. (2009). The effect of various process conditions on the photocatalytic degradation of NO, Proceedings 3rd International Symposium on Nanotechnology in Construction NICOM3, 31 May - 2 June 2009, Prague, Czech Republic, Eds. Z. Bittnar, P.J.M. Bartos, J. Němecěk, V. Šmilauer, J. Zeman, pp. 223-229.
6. Ballari, M.M., Hunger, M., Hüsken, G., and Brouwers, H.J.H. (2009) Heterogeneous Photocatalysis Applied to Concrete Pavement for Air Remediation, Proceedings 3rd International Symposium on Nanotechnology in Construction NICOM3, 31 May - 2 June 2009, Prague, Czech Republic, Eds. Z. Bittnar, P.J.M. Bartos, J. Němecěk, V. Šmilauer, J. Zeman, pp. 409-414.
7. Hüsken, G. and Brouwers, H.J.H. (2008). Concrete containing TiO₂: Properties and Evaluation of Air Purifying Abilities, 7th International PhD Symposium in Civil Engineering. 11-13 September 2008, Stuttgart, Germany, pp. 25-34.
8. Hüsken, G. and Brouwers, H.J.H. (2008). Development of eco earth-moist concrete, International Conference Excellence in Concrete Construction through Innovation, 9-10 September 2008, London, United Kingdom, pp. 97-105.
9. Hüsken, G. and Brouwers, H.J.H. (2008). Air purification by cementitious materials: evaluation of air purifying properties, International Conference on Construction and Building Technology, 16-20 June 2008, Kuala Lumpur, Malaysia, pp. 263-274.
10. Hüsken, G., Hunger, M. and Brouwers, H.J.H. (2007). Comparative study on cementitious products containing titanium dioxide as photo-catalyst. Proceedings International RILEM Symposium on Photocatalysis, Environment and Construction Materials-TDP 2007, 8-9 October 2007, Florence, Italy, Eds. P. Baglioni and L. Cassar, RILEM Publications, Bagneux, France, pp. 147-154.
11. Hüsken, G. and Brouwers, H.J.H. (2006). Theoretical and experimental study of earth-moist concrete, Proceedings 16th Ibausil, International Conference on Building Materials (Internationale Baustofftagung), 20-23 September 2006, Weimar, Germany, Ed. H.B. Fischer, F.A. Finger-Institut für Baustoffkunde, pp. 1:1143-1:1152.

Curriculum Vitae

Personal data

Name: Götz Hüsken
Date of birth: 3 September 1978
Place of birth: Eisenach, Germany

Education

1998-2005 Bauhaus-Universität Weimar, Germany
Faculty of Civil Engineering
Master thesis: The non-linear load bearing behavior of timber under longitudinal compression beyond the proportional limit (in German), supervised by Prof. Dr.-Ing. K. Rautenstrauch

1997-1998 Military service
Training as fire-control soldier at the 1st mobile artillery battalion 355, Wildflecken, Germany

1991-1997 Ernst-Abbe Gymnasium (secondary school), Eisenach, Germany
Intensive courses in mathematics and physics

PhD research / Work

2009-present Eindhoven University of Technology, The Netherlands
Faculty of Architecture, Building and Planning
Unit Building Physics & Systems
Researcher in the field of concrete technology

2005-2009 University of Twente, Enschede, The Netherlands
Faculty of Engineering Technology
Department of Construction Management & Engineering
PhD student

2004 Bauhaus-Universität Weimar, Germany
Faculty of Civil Engineering
Department of Masonry and Timber Structures
Student assistant

This thesis provides a multifunctional design approach for sustainable concrete, particularly earth-moist concrete (EMC), with application to concrete mass products. EMC is a concrete with low water content and stiff consistency that is widely used for the production of concrete mass products, such as paving blocks, curbstones, and sewage pipes. As an in-depth scientific description of the material is limited, the practical design of EMC mixes is based on experience and variations that are made during production.

The multifunctional design approach proposed in this thesis is based on ideas derived from particle packing models. This new approach considers the entire grading of all solid ingredients to compose a concrete mix that meets required performance criteria and has been implemented in a computer based optimization algorithm. The developed algorithm allows for the design of EMC mixes that are characterized by optimized and dense particle packing, lower cement content, and better workability in fresh state.

The aspect of sustainability is addressed by the incorporation of stone waste materials and industrial by-products to replace primary filler materials. Adopting the ideas of a closed concrete life cycle, attention was also paid to material recycling. Recycled aggregates and fines have been used to replace traditional raw materials. Finally, photocatalytic materials have been investigated to give multifunctional properties to concrete mass products and enhance their sustainability. In brief, the new mix design concept allows for the performance based design of sustainable and multifunctional concrete mixes suitable for the production of concrete mass products.

F A C

B W H

E H U

/ faculty of architecture building and planning